DESIGN OF NOVEL GAS VELOCITY SENSORS FOR FLOTATION SYSTEMS

by

Jorge Agustin Torrealba Vargas

A thesis submitted to the Faculty of Graduate Studies and Research of McGill University in partial fulfillment of the requirements for the degree of Doctor of Philosophy

Department of Mining, Metals and Materials Engineering
McGill University,
Montreal, Quebec, Canada
August 2004

"In my life, I have triumphed because I have learned to fail"

Alejandro Jodorowski

ABSTRACT

Gas dispersion properties of flotation systems, such as: bubble size (d_b), gas holdup (ε_g) and gas velocity (J_g) are became increasingly relevant in the past 10 years for optimization of flotation systems. Flotation system kinetics have been related to the bubble surface area flux (S_b), which is known to be derived from gas dispersion properties (J_g, d_b). Modeling of flotation systems and in particular flotation kinetics requires reliable measurements of J_g and to do this, two novel sensors were developed. The sensors collect bubbles by natural buoyancy, and relate gas flow to either accumulation of the gas bubbles (discontinuous technique) or the pressure drop across an orifice (continuous technique). Fundamental flow equations were derived to relate those properties to J_g.

Experiments range from laboratory scale (column of 15.24 cm diameter and 4 m high) to industrial flotation systems (up to 130 m^3 flotation cells) were performed to validate the sensing principles and reliability of the sensor measurements. Over the range of J_g from 0.20 to 3.00 (cm/s) the continuous sensor accuracy ranges from –2.40 to –4.20 % and –0.90 to –1.93 % for tubes of 7.62 and 10.16 (cm) diameter respectively. Sampling tests indicate that tubes of 7.62 and 10.16 (cm) diameter gave same results for discontinuous and continuous techniques. In contrast, for tubes smaller than 7.62 (cm) a bias occurs between the two techniques, being the continuous always higher than the discontinuous, for example the difference between the on-off J_g sensor with a 0.5 (inch) diameter tube (1.27 cm) and the continuous 4 (inch) (10.16 cm) diameter tube is as high as 45 %.

Analysis of the sensitivity of the relationship between sensors measurements and process parameters, for example bulk density, were performed.

Both sensors were used in industrial applications to set the gas profiles across banks of flotation cells and, along with metallurgical analysis, allowed the industrial operators, to improved performance.

The time taken to set a profile of gas distribution in a bank of flotation cells, using a multi unit continuous sensor compared to a single on-off sensor, is reduced from about a shift to half an hour.

The continuous sensor measurements were found to be stable for periods up to 15 minutes after modifications were made to control operational issues as sensors froth build up. This time was sufficient to balance a bank of flotation cells.

RÉSUMÉ

Les propriétés des systèmes de flottation ayant rapport à la dispersion de gaz, par exemple: la taille des bulles (d_b), la charge gazeuse (ε_g), et la vélocité de gaz (J_g), sont devenues de plus en plus importantes les vingt dernières années dans l'optimisation de ces systèmes. Une relation a été établie entre la cinétique des systèmes de flottation et le flux superficiel des bulles (S_b), dérivée des propriétés de la dispersion de gaz J_g et d_b. La modélisation des systèmes de flottation et particulièrment de la cinétique requiert des mesures exactes de J_g et pour cette raison, deux nouvelles sondes ont été développées. Ces sondes recueillent les bulles par flottabilité naturelle et font le lien entre la circulation gazeuse et ou l'accumulation des bulles (technique en discontinu) ou le changement de pression à travers un orifice (technique en continu). Des équations de bases pour la circulation ont été dérivées afin de relier ces propriétés à J_g.

Des expériences en laboratoire (colonne de 15.24 cm de diamètre et 4 m de hauteur) et en industrie (volumes cellulaires jusqu'à 130m^3) ont été complétées afin de valider les principes de précision et de fiabilité des mesures des sondes. Pour des valeurs de J_g entre 0.20 et 3.00 (cm/s) la précision de la sonde a été variée entre –2.40 et 4.20 % et entre –0.90 et –1.93 % pour des diamètres de tubes de 7.62 et 10.16 (cm) respectivement. Des tests par prélèvement ont indiqué que les tubes avec un diamètre entre 7.62 et 10.16 (cm) ont donné les mêmes résultats pour les techniques en continu et en discontinu. Par contraste, pour les tubes de diamètre de moins de 7.62 (cm), la tendance de la sonde en continu était de donner une mesure plus élevée que celui en discontinu. Par exemple, la différence entre une sonde en discontinu avec un diamètre de 1.27 (cm) et celui en continu avec un diamètre de 10.16 (cm) peut atteindre 45%.

L'analyse de la précision de la relation entre les mesures des sondes et les paramètres du procédé, par exemple la densité de masse (ρ_{bulk}), a été complétée.

Les deux sondes ont été utilisées dans des applications industrielles pour construire des profils de gaz à travers des rangées de cellules de flottation. Ces profils, á l'aide d'analyses métallurgiques, ont rendu possible l'amélioration de la performance métallurgique par les opérateurs industriels.

Le temps nécessaire pour compléter un profil de la distribution de gaz dans une série de cellules de flottation a été réduit de 8 heures, dans le cas d'une seule sonde en discontinu, à 30 minutes en utilisant un système de plusieurs sondes en continus.

Après avoir fait des changements pour contrôler des problèmes opérationnels, comme l'accumulation de mousse, la sonde en continu s'est révélée stable jusqu'à 15 minutes, ce qui est une période suffisante pour construire un profil complet.

ACKNOWLEDGEMENTS

I would like to thank my Mother: Maria Eugenia Vargas, Sister: Carolina Torrealba and Grandfather: Agustin Vargas for all the support during my time away from Chile.

I would like to thank my fiancé: Kimberley Smith for her support and patience.

I would like to thank the following people for their contributions to my work and experiences at McGill University:

Professor Jim Finch for his support, ideas and encourage provided throughout this work.

Professor Ralph Harris for his ideas and interesting conversations.

Cesar Gomez, Hugo Hernandez, Jose Hernandez, Marta Bailey, Helin Girgin, Grant McSorley, Luis Calzado, Jan Nesset, Pamela Moyo and the other members of The McGill's Flotation Group, Paul Voigt from University of New Castle and Kim Runge and Dave Seaman from University of Queensland, for their ideas, support and friendship.

I would like to thank the following organizations for their contributions to my work:

The Programa de Perfeccionamiento Académico de la Universidad de Santiago de Chile (USACH) for financial contribution.

The Natural Sciences and Engineering Research Council of Canada (NSERC), INCO, Falconbridge, Teck Cominco, Noranda, and now Corem and SGS-Lakefield Research, and since January 2001 under an NSERC Collaborative Research and Development grant co-sponsored by the Australian Mineral Industry Research Association (AMIRA) for financial contribution.

The enthusiastic assistance of operators and engineers at the various sites was much appreciated and is gratefully acknowledged.

TABLE OF CONTENTS

GLOSSARY

Accuracy: Qualitative term refers to whether there is agreement between the measured value and the true value [14]. It is a measure of the quality of the measurement. For example, if an instrument has an accuracy of 1%, it means that the readings will lie within an envelope of 1% of the true value. It must be understood that the readings have individual errors, but we are interested in the relation of the population of readings to the true value.

Since accuracy relates readings with the true value, they must be measured using a national standard document or facility. Also, because it is a statistical term, a confidence level must be defined for how frequently the reading does lie within the envelope.

For the flowmeters used here uncertainty is reported as a percentage of the full-scale flow using the following term: upper range value (URV) [14].

Bias: Quantitative term defined as the difference between the true value and the average value of a distribution. This can be reduced or eliminated by calibration. Calibrations can be conducted by third parties in dedicated laboratory rigs or in-house based on comparisons to standard instruments or artifacts.

Confidence level: Is a statement of probability. Usually, for flow measurement it is 95% [14].

Flow meter: Defined by ANSI/ISA 51.1 [55] as a device that measures the rate of flow or quantity of a moving fluid in an open or closed conduit. Consists of a primary and secondary device.

Flow meter primary device: A device mounted internally or externally to the fluid conduit which produces a signal with a defined relationship to the fluid flow in accordance with known physical laws relating the interaction of the fluid to the presence of the primary device.

Flow meter secondary device: A device that responds to the signal from the primary device and converts its to a display or to an output signal that can be translated relative to flow rate or quantity.

Pressure:

Gauge Pressure: The pressure difference of a system and the surrounding atmosphere measured using a pressure gauge.

Absolute Pressure: The total pressure exerted on a system, is equal to the gauge pressure plus atmospheric pressure.

Precision: It is the statistical measurement of repeatability. It should not be used as a synonym for accuracy [14]. Can be divided in a short-term (repeatability) or long-term variation (reproducibility).

Range and Rangeability: Interval (lower and upper range) of performance where an instrument can be trusted. The rangeability (turndown ratio) is the ratio of the upper range value and lower range.

Repeatability: Defined as the value below which the difference between any two test measurements, taken under the same conditions by the same observer and with a short elapsed time, are expected to lie within 95% confidence [14].

Span: Defined as the difference between upper and lower or negative range values.

LIST OF SYMBOLS

Symbol	Description	Units
a, a^{*2}	: Redlich-Kwong constants.	$(m^6PaK^{0.5}/mol^2, Pa^{-1})$
a_C	: Cubic regression coefficient.	$(kg^{5/2}/s\sqrt{(1/(m^3kPa))^3})$
a_L	: Linear regression coefficient.	$(kg^{3/2}/s\sqrt{(1/(m^3kPa))})$
a_Q	: Quadratic regression coefficient.	$(kg^2/(sm^3kPa))$
a_{SCMS}	: Orifice calibration slope.	$(SCMS\sqrt{kg/(m^3kPa)})$
A	: Internal area of J_g sensor tube.	(m^2)
A_1, A_2	: Cross sectional area at plane 1 and 2.	(m^2)
b, b^{*2}	: Redlich-Kwong constants.	$(m^3/mol, Pa^{-1})$
b_C	: Cubic regression coefficient.	$(kg^2/(sm^3kPa))$
b_L	: Linear regression coefficient.	(kg/s)
b_Q	: Quadratic regression coefficient.	$(kg^{3/2}/s\sqrt{(1/(m^3kPa))})$
b_{SCMS}	: Orifice calibration intercept.	(SCMS)
B	: Magnitude of $q_{KPS,in}$ step change.	(dimensionless)
c_C	: Cubic regression coefficient.	$(kg^{3/2}/s\sqrt{(1/(m^3kPa))})$
c_Q	: Quadratic regression coefficient.	(kg/s)
C_e	: Constant.	(kg/Pa)
C_p	: Specific heat at constant pressure.	(J/mol/K)
C_v	: Specific heat at constant volume.	(J/mol/K)
d	: Orifice diameter.	(mm)
d_b	: Bubble size.	(mm)
d_{b32}	: Bubble size Sauter mean.	(mm)
d_C	: Cubic regression coefficient.	(dimensionless)
D	: Pipe diameter.	(mm)
F	: Sensor constant.	(dimensionless)
g	: Gravity acceleration = 9.8.	(m/s^2)
h	: Redlich-Kwong constant.	(m^3)
h, h_1, h_2	: Enthalpy at plane 1 and 2.	(J)
H	: Distance from the top of the sensor to the level inside the tube at the time t.	(m)

Symbol	Description	Units
$\bar{H}$	: Average Distance from the top of the sensor to the level inside the tube at the time t.	(m)
H_l	: Total length of the sensor.	(m)
H_p	: Distance from the top of the sensor to the froth – pulp interface. In the case of the JK sensor is the distance from the bottom of the sensor to the top of the froth.	(m)
H_w	: Distance from the bottom of the tube to the second mark.	(m)
H_1, H_2	: Distance from the top of the tube to the first and second mark.	(m)
J_g	: Superficial gas velocity.	(cm/s)
$J_{g\text{-}exp}$	: J_g Rate of change of H in time (cm/s).	(cm/s)
$J_{g\ Pl}$	: J_g calculated at bubble collection conditions of pressure (P_l) and Temperature (air temperature).	(cm/s)
$J_{g\ STD}$	: J_g calculated at standard conditions of pressure (101325 Pa) and Temperature (273.15 K).	(cm/s)
k	: Flotation rate constant.	(1/s)
K_p	: Steady state gain.	(Pa)
l	: Length of orifice tip depth.	(cm)
L	: Length of orifice tip.	(cm)
ΔL	: Distance between the ends of the tubes.	(m)
n	: Moles at time t.	(mol)
P	: Pressure inside the sensor at time t.	(Pa)
P	: Flotability.	(dimensionless)
$\bar{P}$	: Average Pressure inside the sensor at time t.	(Pa)
P_{atm}	: Atmospheric pressure.	(Pa)
P_c	: Critical pressure.	(Pa)
P_{calc}	: Pressure in Function P calculated at (Hl-Hp)/2 of the tube or half distance between the marks.	(Pa)
P_l	: Pressure at the bottom of the tube.	(Pa)
P_o	: Pressure inside of the sensor at time =0.	(Pa)
P_{out1}	: Pressure in the sensor generated by the flow leaving the control volume through orifice 1.	(Pa)
P_{out2}	: Pressure in the column generated by the flow leaving the control volume through orifice 2.	(Pa)
P_{pc}	: Pseudo critical pressure.	(Pa)
P_r	: Reduced pressure.	(dimensionless)
P_1, P_2	: Pressure at plane 1 and 2.	(Pa)

Symbol	Description	Units
ΔP	: Pressure drop.	(kPa)
dP/dt	: Pressure variation rate in the tube.	(Pa/s)
$q_{KPS,in}$	: Mass flow entering the control volume.	(kg/s)
$q_{KPS,out1}$	: Mass flow leaving the control volume through orifice 1.	(kg/s)
$q_{KPS,out2}$	: Mass flow entering the control volume through orifice 2.	(kg/s)
$q_{KPS,1}$	: Mass flow entering the control volume at plane 1.	(kg/s)
$q_{KPS,2}$	: Mass flow leaving the control volume at plane 2.	(kg/s)
q_{SCMS}	: Volumetric flow at standard conditions.	(m3/s)
Q	: Heat transfer.	(J/s)
Q_f, Q_g	: Volumetric pumping rate of pulp and gas.	(m^3/s)
R	: Ideal gases constant = 8.314.	(m^3Pa/mol/K)
R_f	: Recovery in the froth zone.	(dimensionless)
R_s	: Orifice resistance.	($Pa^{0.5}$s/kg)
s, s_1, s_2	: Entropy at plane 1 and 2.	(J/K)
S	: Variance.	(dimensionless)
S_b	: Bubble surface area flux.	(m/m/s)
t	: Time.	(s)
T	: Temperature.	(K)
T_c	: Critical temperature.	(K)
T_{pc}	: Pseudo critical temperature.	(K)
T_r	: Reduced temperature.	(dimensionless)
T_1, T_2	: Temperature at plane 1 and 2.	(K)
ΔT	: Temperature change.	(K)
v_1, v_2	: Velocity at plane 1 and 2.	(m/s)
V	: Gas volume at time t.	(m^3)
$\bar{V}$	: Average gas volume at time t.	(m^3)
W	: Work.	(J/s)
x_i	: Mole fraction of gas *i*.	*(dimensionless)*
X_i	: Sensitivity coefficient for variable i.	(dimensionless)
Y_1	: Adiabatic gas expansion factor.	(dimensionless)
z_1, z_2	: Elevation plane 1 and 2.	(m)
Z	: Compressibility factor.	(dimensionless)

GREEK SYMBOLS

Symbol	Description	Units
β	: Orifice beta ratio.	(dimensionless)
δ	: Constant.	$(Pa*(m^3/kg)^{\gamma}$
γ	: Isentropic exponent.	(dimensionless)
ρ	: Air density.	(kg/m^3)
$\overline{\rho}$	: Average air density.	(kg/m^3)
ρ_b	: Bulk density.	(kg/m^3)
ρ_p	: Density of the aerated pulp.	(kg/m^3)
ρ_s	: Density of the sample inside of the sensor tube.	(kg/m^3)
ρ_w	: Density of the aerated water inside of the J_g probe.	(kg/m^3)
ρ_{out1}	: Density of gas estimated by P_{out1}.	(kg/m^3)
ρ_{out2}	: Density of gas estimated by P_{out2}.	(kg/m^3)
ρ_1, ρ_2	: Air density at plane 1 and 2.	(kg/m^3)
τ_p	: Time constant.	(s)
ω	: Accentricity.	(dimensionless)

LIST OF ACRONYMS

Avg: Average.

LPM: Liter per minute.

NCMS: Normal (273.15 K and 101325 Pa) cubic meter per second.

SCMS: Standard (298.15 K and 101325 Pa) cubic meter per second.

SLPM: Standard (298.15 K and 101325 Pa) liter per minute.

Stdev: Standard deviation.

URV: Upper range value.

LIST OF FIGURES

LIST OF TABLES

CHAPTER 1
INTRODUCTION

1.1 The problem

Flotation is conducted in machines of various designs, currently dominated by two types, mechanically agitated (i.e., mechanical) cells and flotation columns. Key is the introduction and dispersion of air (usually) into bubbles typically 0.5 – 2.5 (mm) (diameter). The bubbles encounter particles in the pulp (slurry) and collect those sufficiently hydrophobic to attach. These bubble/particle aggregates rise to form a froth zone.

Various parameters have been used to characterize air dispersion (Harris [41]); Gorain [30] introduced the term "gas dispersion parameters" to refer to bubble size (D_b), gas holdup (ε_g) and superficial gas rate (J_g), in particular. Measurements can be global (cell average) or, importantly local (mapping) to define gas distribution throughout a cell.

Gorain et al. [32 to 36 and 37] conducted extensive work to relate the gas dispersion properties to the flotation rate constant (k) in the pulp phase. They found that individually the gas dispersion parameters did not relate to k readily. A derived parameter, bubble surface area flux (S_b), however, did. The bubble surface area flux was introduced by Finch and Dobby [26] as the bubble surface area rate per unit time per unit cell cross-section. Taking a mean bubble size and assuming spherical bubbles then $S_b = 6\ J_g/D_b$. In summary, therefore, Gorain et al [36] concluded $k \propto S_b$ and introduced P as the proportionality constant. Thus a model of the pulp phase is,

$$k = PS_b \qquad \text{Eq. (1.1)}$$

where P summarises ore properties (particle size, hydrophobicity, etc).

To include the froth phase, Gorain et al [36] (and others [26]) introduced a global froth zone recovery factor R_f. The model then became,

$$k = PS_bR_f \qquad \text{Eq. (1.2)}$$

Figure 1.1 shows schematically this interactive system.

The model has attracted considerable attention, largely became the parameters that appear tractable to measurement [27]. This is not to claim that the model does not have its critics. Duan et al. [21] continue to develop models more closely dependent on the sub-processes in flotation (collision, attachment, etc). Heiskanen [42] has challenged the validity of some of the measurements used by Gorain, noting some discrepancies.

Heiskanen's observations raise the need for high quality measurement: without accurate measurements the science of flotation (or, indeed, any science) will not progress. This thesis takes on the task of reliable superficial gas velocity measurement to determine gas distribution in cells and banks of cells.

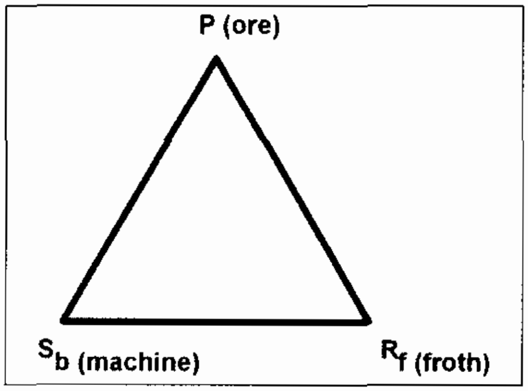

Figure 1.1: The flotation system (after Gorain et al. [31])

1.2 Objectives and organization of the thesis

1.2.1 Objectives

The overall objective is the design of a reliable sensor for superficial gas velocity, J_g, for both single and continuous measurements.

Specific objectives include:

- Establish and validate the flow equation for the J_g sensors.
- Establish design criteria for the sensor.
- Develop a multi sensor unit.
- Evaluate laboratory and, importantly, plant results.
- Establish the benefits of the proposed technique(s).

1.2.2 Organization

The thesis work is broken down as follows:

A **Glossary** is included to help understand some terms and concepts.

Chapter 1 Gives an introduction to the thesis work.

Chapter 2 Describes briefly the different types of flotation cells, the state of the art of current J_g sensors, and introduces the flow meters used in the thesis and one for scaling down the sensor for possible laboratory cell applications.

Chapter 3 Covers the important characteristics of compressible flow.

Chapter 4 Derives the flow equation for the discontinuous and continuous J_g sensors.

Chapter 5 Discusses validation of the sensors.

Chapter 6 Gives field work experiences from troubleshooting to settling J_g profiles to a bank of cells.

Chapter 7 Summarises the conclusions, future work and claims to original research.

Appendix A. Illustrates some calculations with examples.

Appendix B. Gives a JTACQ30 software manual.

Appendix C. Gives a general information about the equipment.

Appendix D. Shows two algorithms for the data filtering.

Appendix E. Discusses for the frothing problem.

Appendix F. Gives the experimental data.

The following is a manuscript written by the author and was used in preparation of this thesis. The manuscript comprises Chapter 6 and was published as indicated:

Torrealba-Vargas, J.A., Gomez, C.O. and Finch, J.A. (2004) "Continuous Air Rate Measurement in Flotation Cells: a Step Towards Gas Distribution Management". Minerals Engineering 17 (6), pp. 761-765.

The manuscript presented is co-authored by Dr. James Finch in his capacity as research supervisor.

CHAPTER 2
BACKGROUND

2.1 Introduction

In the first part of this chapter, the most common flotation machines are briefly described. Since the superficial gas rate measuring devices described in this thesis must be inserted in the cell (i.e., they are "invasive") then the machine design and operating characteristics may become a factor. This point will be returned to in Chapter 6.

Several discontinuous methods to measure superficial velocity of gas dispersed in a flotation cell are reported in the literature. These techniques are reviewed later in this chapter. One technique is based on pumping an aerated pulp sample, while the others rely on bubble buoyancy. Only two continuous techniques applicable to bubble dispersions were found. There was no indication of a multi-sensor unit (several sensors measuring at the same time).

At the end of this chapter a review of Flow Meter instrumentation related with this work is included.

2.2 Review of flotation machines

Flotation is used in a variety of industries from mineral processing to oil/water separation and de-inking recycled paper. The machines described here are those common to the mineral industry.

The dominant flotation machines today are mechanical cells and flotation columns. The two are distinguished on several fronts. One is the generation of bubbles. Mechanical cells produce bubbles by shear over the surface of the volume of air carried behind rotating blades as they sweep through the slurry; in columns, bubbles are generated through porous materials (filter cloth, rubber, etc), or breaking a flow of air through a nozzle (Jet spargers).

2.3 Mechanical cells

In general, mechanical cells have a rectangular or circular cross section. Fallenius [22] describes the requirements for the mechanism as:

1. Ensure the part of the rotor surface from which air is dispersed is large enough for the volume of air injected.
2. Distribute the air-slurry mixture efficiently over the cell cross sectional area.
3. Maintain sufficiently intensive turbulence over the entire air dispersion surface.

4. The rotor to function as an efficient pump to maintain the suspension.

Finch [25] describes the two basic functions of flotation as collection of particles by bubbles, then separation of these bubble-particle aggregates from the slurry. The two functions can be distinguished in the design of mechanical cells: a zone with intense mixing around the impeller and a quiescent region above followed by the froth zone. The design of mechanical cells involves compromise between these two functions which may limit the overall performance. This is leading to new designs, here referred to as "feed aeration".

2.3.1 Outokumpu

Modern Outokumpu cells, designated "tanks", currently range up to 200 (m^3). Since the 1960's the trend has been towards ever larger flotation machines [22]. The reasons are both economic (to drive down unit operating costs) and technical (to treat ever larger throughputs). These cells are found in all parts of a circuit as roughers, cleaners and scavengers.

Outokumpu cells use a conventional rotor-stator [32] (Figure 2.1) near the bottom of the tank, which is either flat or U-shaped (Figure 2.2). Air is introduced from a blower. The level control system may be a float with angle transmitter or ultrasonic transmitter connected with a local controller and dart valve. The cells have internal and external launders. The metal plates that cover the top of the cell often become walkways (Figure 2.3).

There are two types of stator, the standard design (multi-mix) and free flow. The selection will depend on the particle size to be floated. The most popular is the multi-mix (Figure 2.1).

The principal changes in cell design over the years focused on enhancing the ability to float coarse particles and improve froth recovery in scavenger banks. Low grade products are characteristic of scavenging and through froth crowding, it is anticipated deeper froths can be built to give higher grade products. Foreman [28] disputes this concept and does not recommend the use of froth crowders, because in his experience, froth crowders promote coalescence and limit gas rate by reducing the surface area of the cell.

2.3.2 Dorr-Oliver

Dorr-Oliver cells (Figure 2.4) are similar to Outokumpu in the rotor–stator assembly. The size of the rotor is smaller than Outokumpu for an equivalent tank volume. Air is again delivered by a blower. Level control is through weirs or automatic control similar to the Outokumpu.

Dorr-Oliver has a patented design of rotor. As seen in Figure 2.5, the rotor is curved in DA-DB to blend with the angle of the stator and to deflect the slurry horizontally across the cell. Dorr-Oliver claim that this design “eliminates short circuiting and extends the air dispersion operating range” [3].

Another difference with Outokumpu cell is that the Dorr-Oliver cell is designed to deliver air between the rotor vanes (D1 in Figure 2.5) instead of through the vanes as in the Outokumpu rotor design (Figure 2.1).

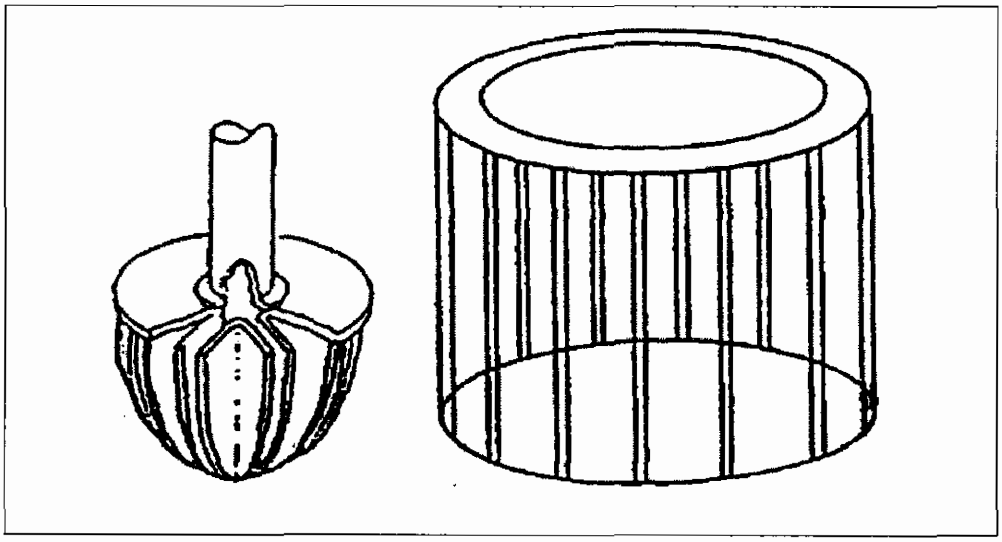

Figure 2.1: Rotor-stator (multi-mix) for an Outokumpu cell [32].

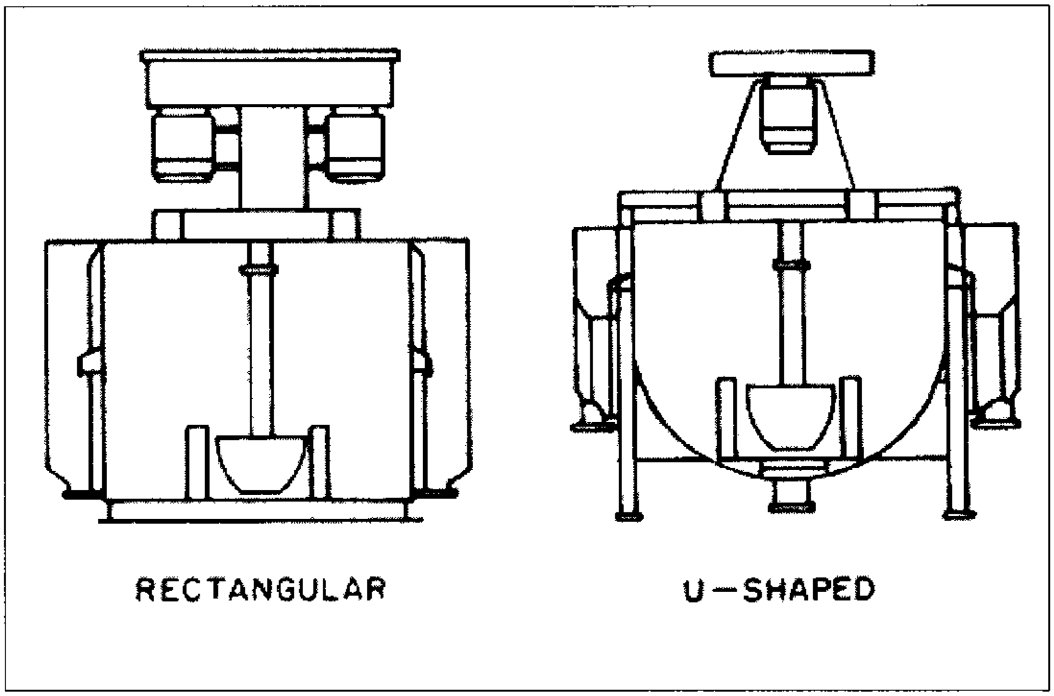

Figure 2.2: Outokumpu cell shapes [17].

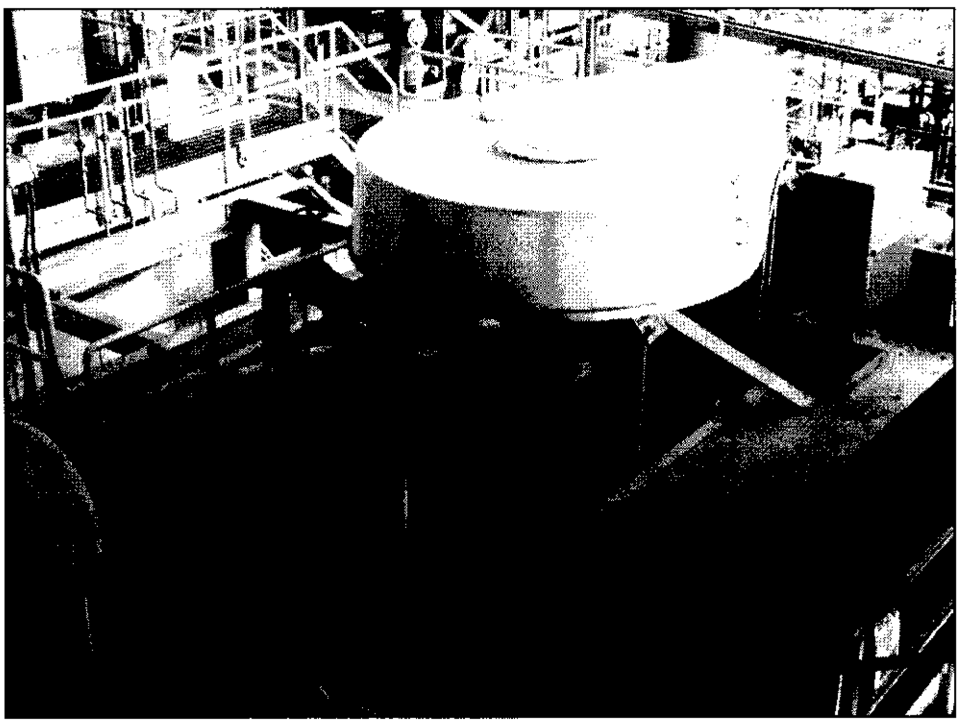

Figure 2.3: Top view of an Outokumpu OK 130 flotation cell.

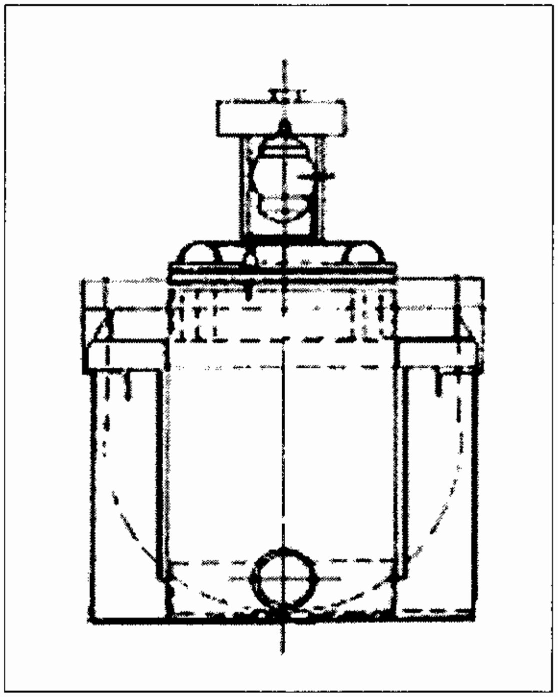

Figure 2.4: Dorr-Oliver cell [3].

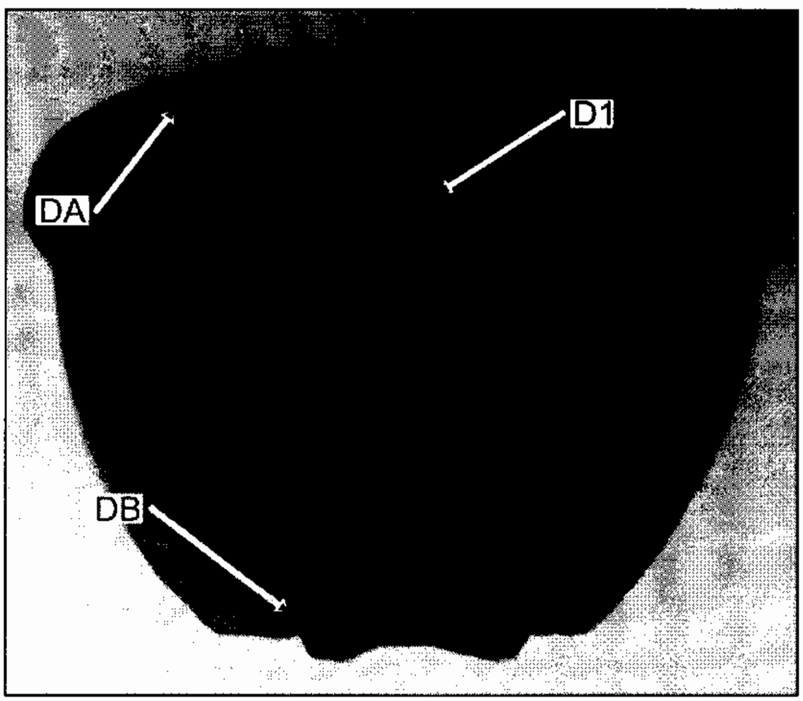

Figure 2.5: Dorr-Oliver rotor [3].

2.3.3 Wemco

The Wemco (Figure 2.6) approach is different from the previous designs being a self-aspiration machine. The cells are popular with large concentrators, partly due to the following features [5]:

1. The self-aspiration capability eliminates the need for a blower.
2. Low wear due to a large distance between rotor and stator.
3. Low wear due to the large distance between the rotor-stator and bottom of the cell.
4. Use of a disperser and hood assembly to baffle and control the turbulence throughout cell.

The air intake flow can be increased or decreased by varying the motor speed and froth depth (i.e., changes in pulp head). It is claimed by Wemco [5] that a minimum of seven cells in a bank is required to prevent what is termed a "troughing phenomena" (presumably referring to backmixing between cells in a bank).

Compared to most other designs, Wemco cells are shallow, which is believed helps explain the good performance on coarse material [5]. A negative point is that they are generally the highest power consumers among competing cells for a given application and do not readily provide independent air control [5].

Figure 2.6: Wemco cell [17].

2.3.4 Denver

Denver cells (Figure 2.7) use an impeller (De1) instead of a rotor-stator. It acts as a pump to mix the slurry-air and suspend the solids. The use of a recirculation well (De2) produces a down flow of slurry that mixes with the air in the rotating impeller: "This slurry-air mixture is then ejected by the impeller through a diffuser (De3) over the entire bottom of the cell. This action then lifts and suspends solids" [5]. The Denver cell has a flat bottom.

Denver, like the Wemco cells, are shallow and perform well with coarse material [5].

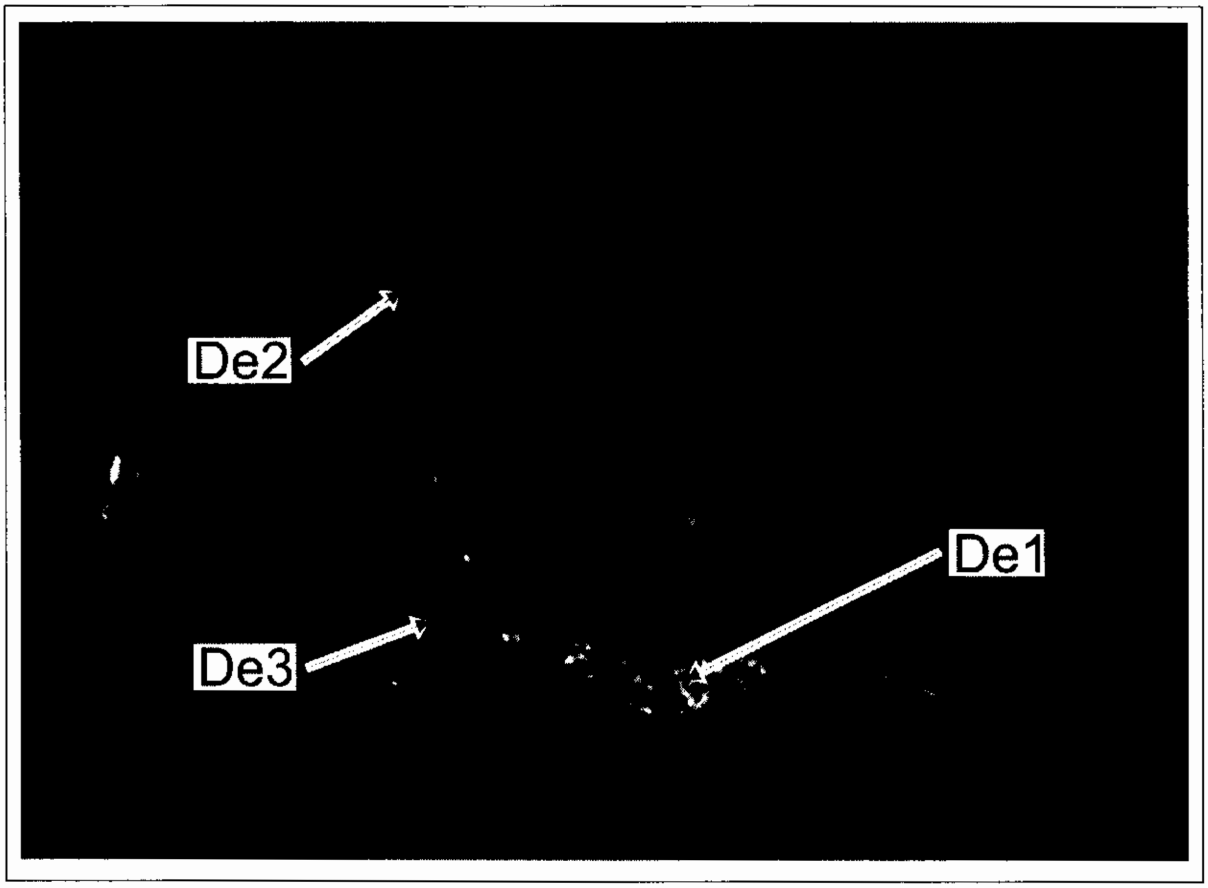

Figure 2.7: Denver cell details of the mechanism.

2.3.5 Sala

The Sala (Figure 2.8) is similar to the Denver design, using likewise an impeller and having a flat bottom, but no recirculation well. The largest cell found in the literature is 16 m^3. The Sala cells are designed with a “stabilizer system” (similar to a stator) around the impeller along the lines of the diffuser assembly [5].

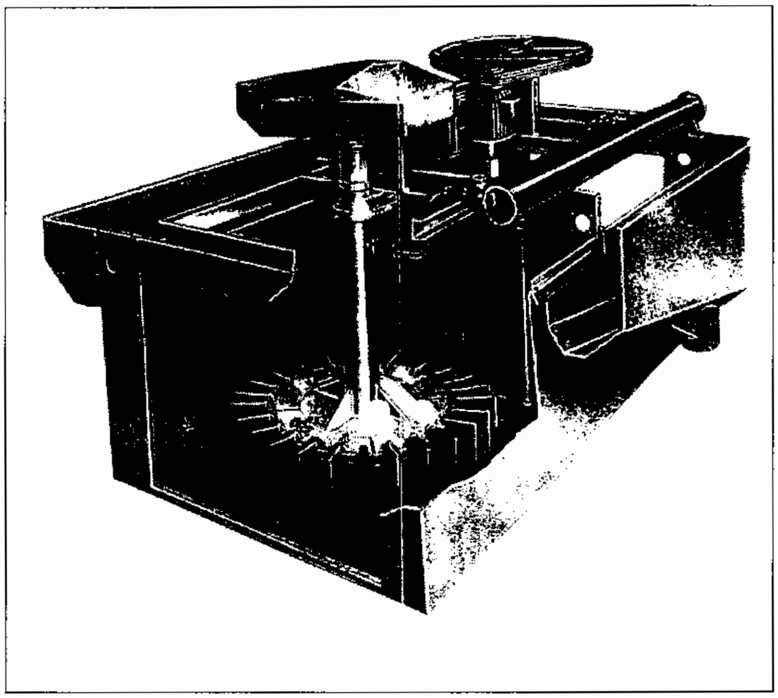

Figure 2.8: Sala cell [5].

2.3.6 Agitair

According to Claridge [17], the slurry flow in an Agitar cell is downward throughout the central area. Air is delivered through a hollow shaft and mixes on the underside of the impeller with slurry which is then displaced out toward the cell walls (Figure 2.9). A "stationary stabilizer" eliminates rotational movement of the aerated pulp and directs it outward in a rising motion.

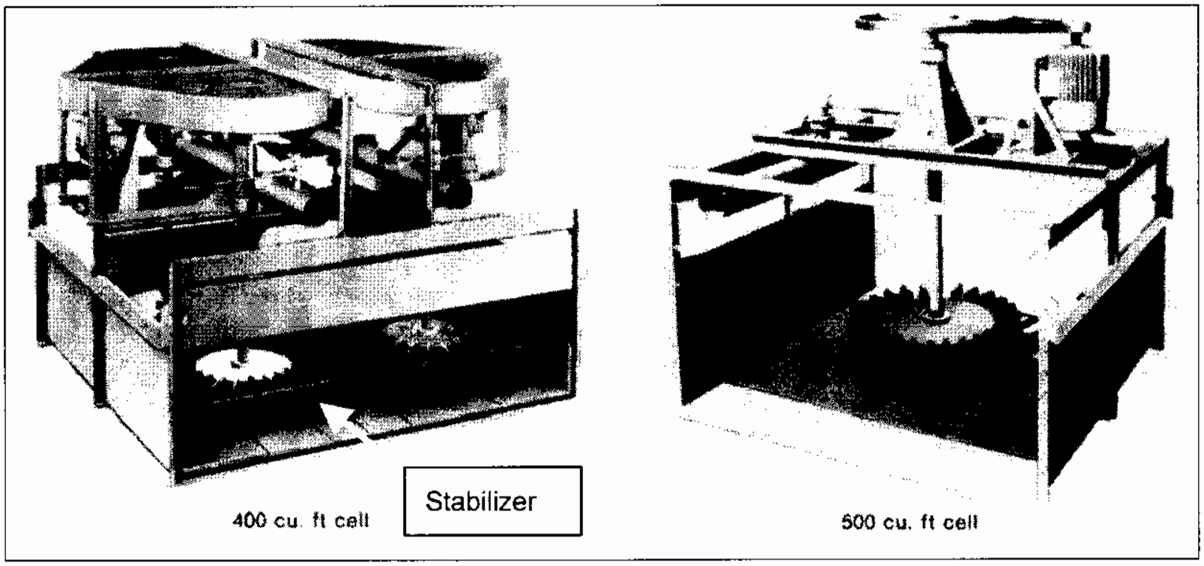

Figure 2.9: Agitar cell [17].

2.3.7 Metso and Bateman

Metso and Bateman are members of the new generation of cells. They are used principally in South Africa.

The Metso flotation machine RCS^{TM} (Figure 2.10) [9] has a circular tank and a unique mechanism claimed to maximize flotation performance for rougher, cleaner and scavenger duties. Currently tanks range up to 200 (m^3). Metso cells use the DV^{TM} (Deep Vane) mechanism, which comprises a series of vertical vanes with shaped lower edges and air dispersion shelf. This design produces a radial slurry pumping action (eliminating slurry rotation) and reduces sanding due to the strong return flow under the impeller [9]. Also, the mechanism is designed to minimize local high velocity zones to extend impeller and diffuser wear life.

Bateman cells are designed with a mechanism that disperses bubbles radially after the interaction of downwardly forced air and upwardly pumped slurry. Bezuidenhout [15] describes that “during operation a zone of low pressure exists within the impeller. The upper impeller volume is then taken up by slurry and air vortices form behind the blades. Rotation of the impeller edges sheds a broad cavitation tail of fine bubbles which are radially dispersed through the stator vanes”.

Bateman cells are designed as square or circular tanks. The circular design eliminates possible corner dead zones and has the advantage that froth transport distance is the same in all directions. Cells can be provided with froth crowders [7]. The cost of manufacturing square cells is lower than for circular tanks and they are recommended for small plants.

The Outokumpu and Dorr-Oliver designs use a hollow shaft, where the Metso and Bateman cells use a solid shaft, surrounded by a pipe (i.e., air flows in through the annulus). This is claimed to reduce wear and plugging of the holes in the mechanism where the air enters the cell [57]. A solid shaft does make it difficult to remove the mechanism. A notable feature of the Bateman mechanism is the top-hung stator. This has the advantage that the entire mechanism can be removed from the tank without the need to drain and wash out [7].

The size of the mechanism is also larger than the competing designs with the idea to increase the capacity of the cell. Bezuidenhout describes the “upward characteristics of the impeller are the result of the pressure drop upwards along the height of the impeller and the air dispersion capacity is determined by the proportion of the impeller volume occupied by the forced air. The height of the parabolic impeller governs the pressure drop between lower tip and the upper horizontal impeller edges".

Metso and Bateman cells are provided with baffles (Figure 2.10) to create a zone of high mixing at the bottom of the cell and leave a calm zone at the top of the cell [25]. Bezuidenhout describes the function of the horizontal hood of the stator on the Bateman mechanism is to create a horizontal baffling effect on turbulent pulp flows emanating from the mixing zone. This is designed to "enhance the relative tranquility in the quiescent zone above the hood plane improving the separation of the hydrophillic particles from the bubble attached hydrophobic particles". In addition, the tank must be designed with the hydrodynamic constraint of maintaining particles in suspension.

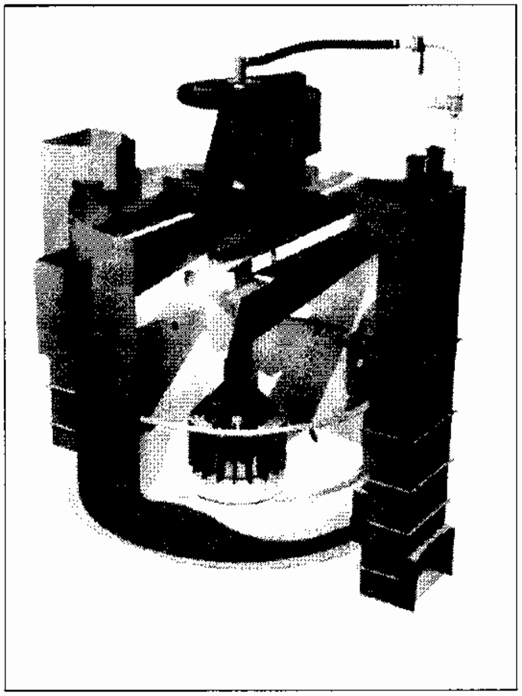

Figure 2.10: Metso RCS cell [9].

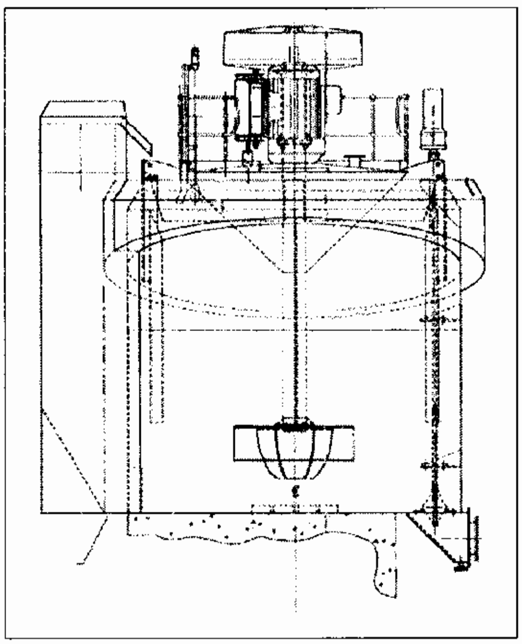

Figure 2.11: Bateman cell [57].

2.4 Flotation columns

The first obvious difference from mechanical cells is the geometry; flotation columns (Figure 2.12) are typically tall relative to their cross section (commercially 9-15 m high and 0.5 to 3.0 m in diameter [26]). The cross section may be square, rectangular or circular.

Other notable features are the bubble generation system and the use of wash water (A, Figure 2.12). Bubble generators are divided in two classes: Internal (were the bubbles are generated inside the column, B Figure 2.12) and External (were the contact and shear of gas with water or slurry is outside the column).

Internal spargers are fabricated from porous material (e.g., filter cloth, perforated rubber, stainless steel) or are Jet action spargers (e.g., Minnovex variable gap, CPT Slamjet). An example of external sparger is the Microcell™ described by Brake et al. [16].

Wash water is added into the froth, usually from an array of perforated pipes located just above or below the overflow lip [26]. This feature is described by Finch and Dobby [26] as the “key factor which permits high upgrading”.

A common internal bubble generator for flotation columns is the Jet-type, illustrated by the Slamjet sparger in Figures 2.13 and 2.14. It is described in the

CPT catalog [6] as "an automatic, self regulating gas injection system". It has a single orifice with a wear resistant injection nozzle. The system is designed to reduce scaling (with precipitates) and fouling (with particles).

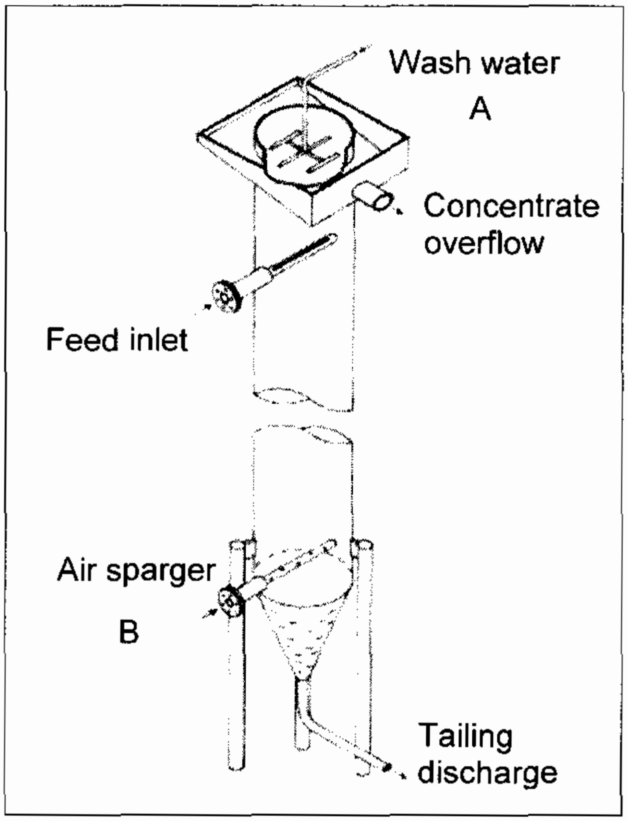

Figure 2.12: Flotation column [17].

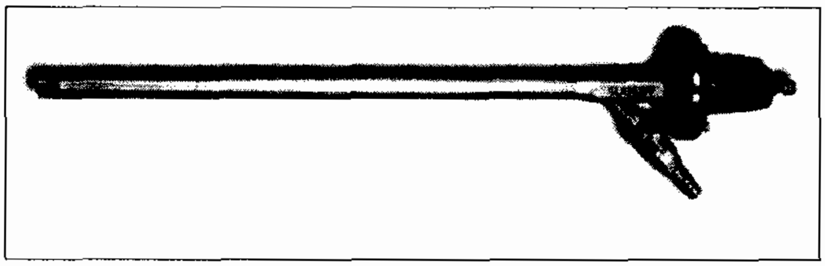

Figure 2.13: Slamjet [6].

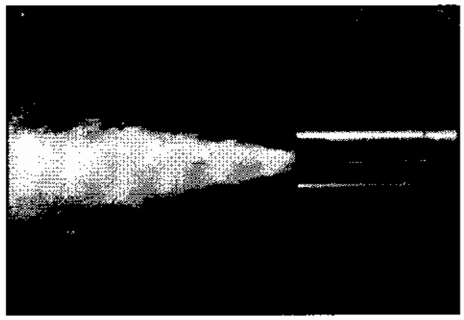

Figure 2.14: Slamjet tip showing jet [6].

2.5 "Feed-aeration" cells

2.5.1 Jameson Cell

Jameson cells have been widely used in the minerals industry for applications from Copper to Coal. A Jameson cell is shown in Figure 2.15. Slurry (Feed) and air are introduced at the top of a pipe (or downcomer) and this mixture travels downwards. The slurry enters through a feed line, where an orifice plate generates a liquid jet. The plunging jet of slurry entrains air as it shears. Harbort et al. [39] describe that: "due to a high mixing and large interfacial area (in the downcomer) there is rapid contact and collection of particles". The Voith Sulzer-Ecocell, common in de-inking recycled paper, has a similar aeration/downcomer arrangement (Figure 2.16) [40].

2.5.2 Contact cell

The Contact cell (Figure 2.17) is a trade mark of Minnovex. Typical applications are rougher or scavenger operations. It is claimed by Minnovex that a "contact cell can provide the same output as a mechanical flotation device, while taking up as little as one quarter the space. The contact cell has fast flotation kinetics and uses minimal air which results in an efficient, selective flotation machine" [12].

The Jameson and Contact cell are also classified as reactor-separator designs [25]. The reactor is the downcomer (Jameson) or contactor (Contact) and the separator is the cell (Jameson) or column (Contact).

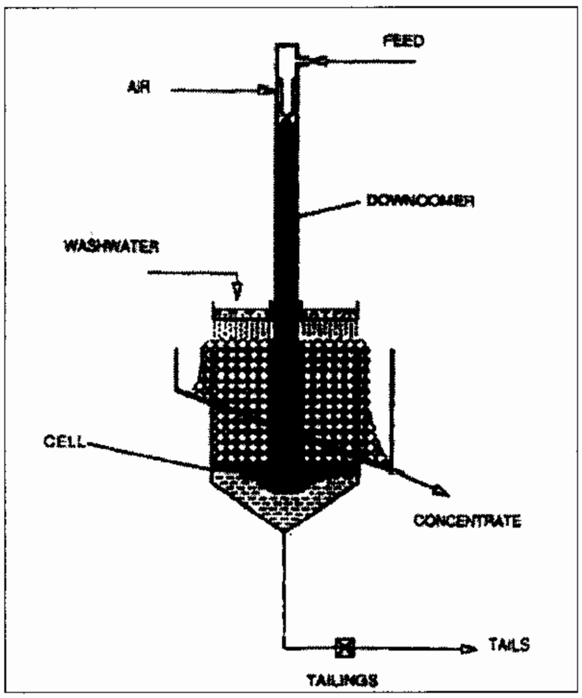

Figure 2.15: Jameson cell [18].

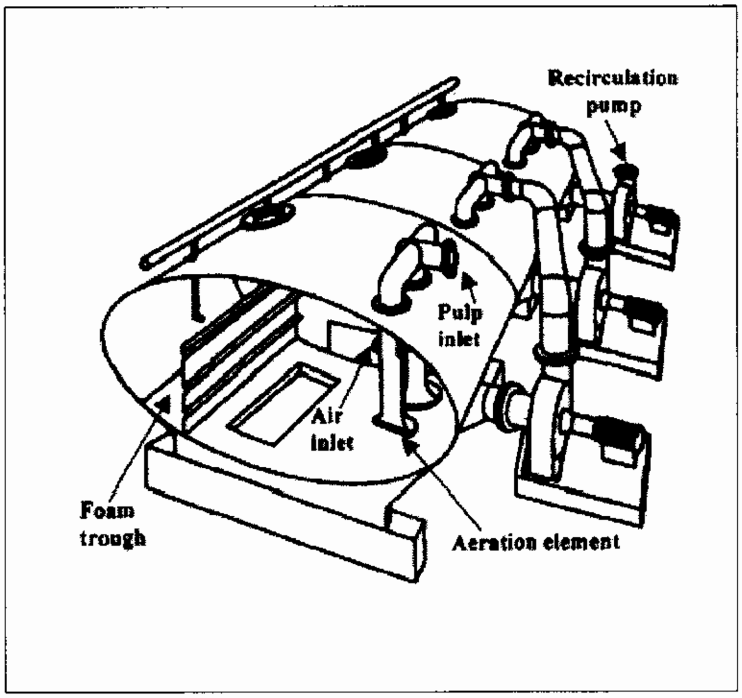

Figure 2.16: Voith Sulzer EcoCell [24].

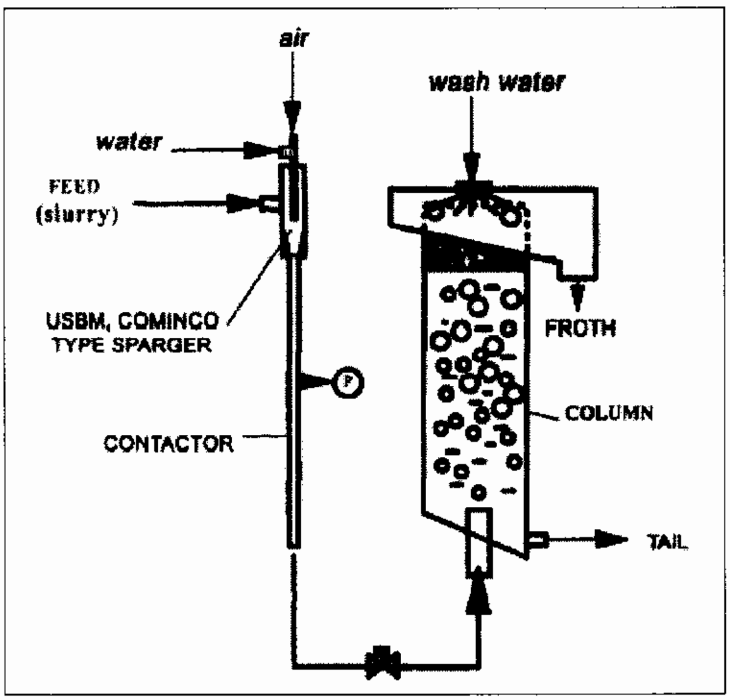

Figure 2.17: Contact cell [25].

2.6 Review of techniques to measure superficial gas velocity J_g

2.6.1 Pumping of aerated pulp sample; the Falutsu J_g sensor

This sensor [23] comprises a transparent tube connected to a peristaltic pump (Figure 2.18). Aerated slurry is pumped from the flotation cell pulp zone. The volumetric pulp pumping rate (Q_f) is measured by means of a cylinder and the volumetric gas pumping rate (Q_g) is measured by water displacement in an inverted cylinder. The pulp density (% solids) is also measured. Depending on the range of % solids, the appropriate empirical equation is applied to estimate gas velocity.

2.6.2 Techniques based on natural bubble buoyancy

2.6.2.1 Denver methodology

For this technique just a graduated transparent cylinder and a stopwatch are needed [1]. The cylinder is filled with water and, with one hand sealing the top, the cylinder is inverted and submerged into the cell, typically to a depth of a few centimeters below the froth. The gas is allowed in to displace the water. At the end of a predetermined time the cylinder is re-closed (by hand), the displaced volume of water is recorded and, dividing by the cylinder cross-section area, J_g is calculated.

2.6.2.2 The Jameson J_g sensor

The Jameson sensor [45] comprises a transparent tube, connected to a valve and a manometer (Figure 2.19). Initially the valve is open; when the valve is closed, the pressure increases, and the time for the meniscus (level) to travel between two reference marks is taken. The rate of pressure change is related with J_g.

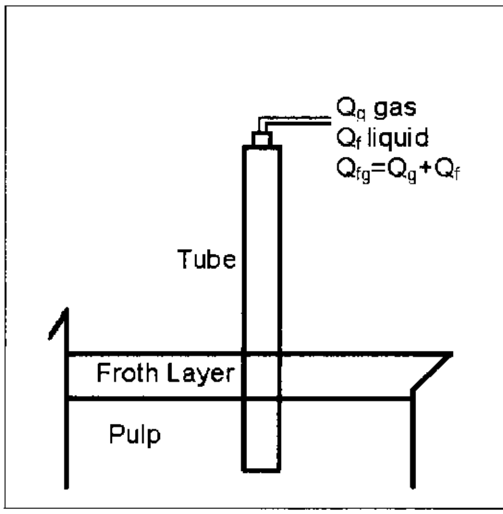

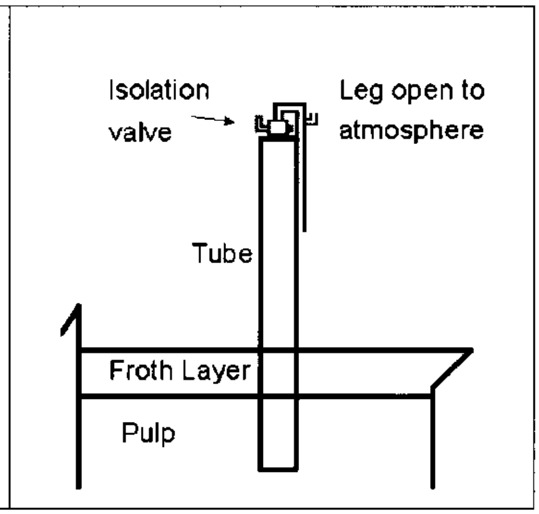

Figure 2.18: Falutsu J_g sensor. **Figure 2.19: Jameson J_g sensor.**

2.6.2.3 The JKMRC (or JK) J_g sensor

The JK sensor [60] is a transparent tube, connected to a pinch valve (P) and a nozzle (N) (Figure 2.20). The rate of displacement of water is measured by the time taken for the level to travel between two marks, M_1 to M_n. The displacement rate is related to J_g (see section 4.3.1.2).

2.6.2.4 The McGill conductivity J_g sensor

This was an adaptation of the open cell in the McGill gas holdup sensor [27]. That sensor (Figure 2.21) is a tube with a valve housing a conductivity cell in the form of ring electrodes. On closing the valve (manually), the aerated pulp inside the tube is pushed down. When the level reaches the first ring, this is recorded by a change in the slope of the conductivity versus time curve; when the level reaches the second ring a second change in slope is reported. The time to pass through the cell is thus determined, and knowing the ring spacing the mean rate of displacement was calculated and equated with J_g.

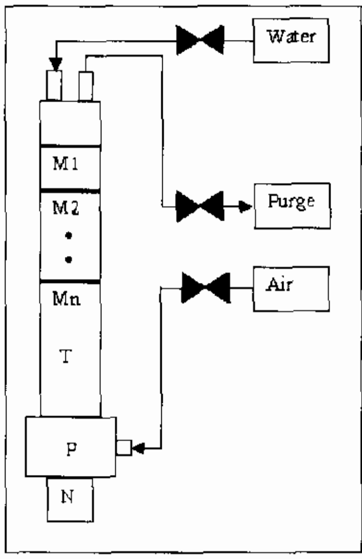

Figure 2.20: The JK J_g sensor.

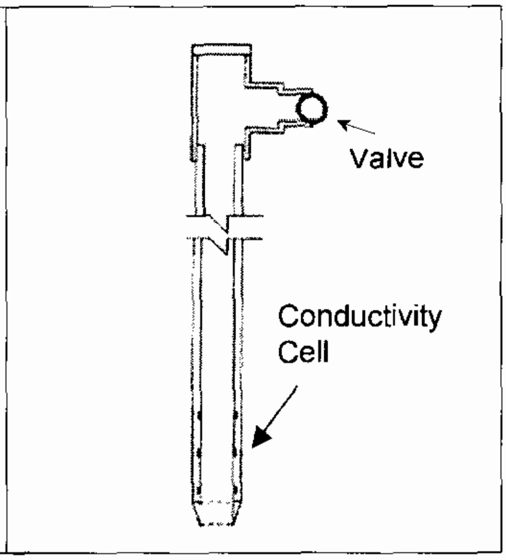

Figure 2.21: McGill conduct. J_g sensor.

2.6.2.5 The McGill on-off pressure J_g sensor

This device one of two J_g sensors which are the subject of this thesis, is an automated version of the Jameson device. Made of PVC or ABS, the tube has a pressure transmitter and globe valve (Figure 2.22). The system is completed with an acquisition electronics (Dutec BIO4) and software (JTACQ V30.0). As soon as the valve is closed, the aerated pulp inside the tube is pushed down as the pressure begins to increase. When the level reaches the bottom of the tube, the pressure becomes constant. The resulting plot is called the "pressure variation curve" (Figure 2.23), and the slope can be related to the J_g [62] (see section 4.3.1.1). This technique has been used to troubleshoot gas dispersion in flotation circuits [20] and to set profiles down a bank [19].

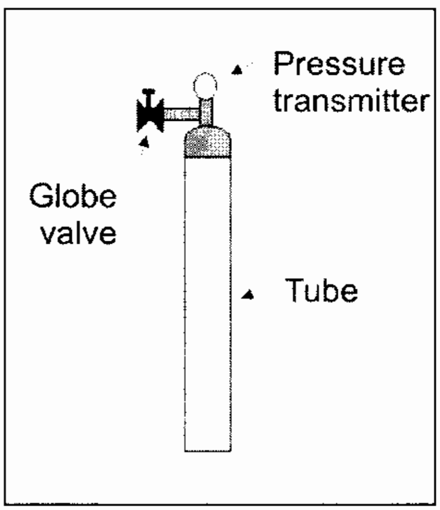

Figure 2.22: McGill on-off (pressure) J_g sensor.

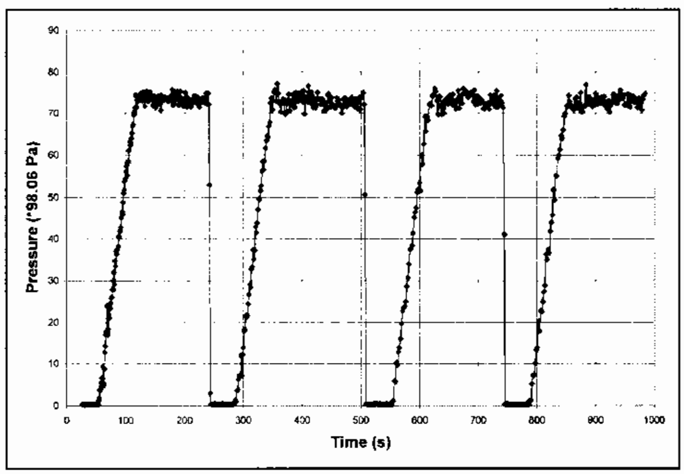

Figure 2.23: Typical pressure variation curve from McGill on-off J_g sensor.

The full potential of the technique was exploited for the first time (June 2001) with a multi on-off J_g sensor unit used during the Northparkes campaign [63].

Table 2.1 gives a summary of the important features of each of the techniques based on collecting bubbles by buoyancy. Techniques based on the visual reading of level displacement require the tube extend above the froth (and be transparent). For the techniques based on pressure (or conductivity), this is not necessary, meaning shorter non-transparent tubes can be used.

These natural buoyancy techniques share a common theory. This has not been formally derived before, which is done in this thesis in Chapter 4.

Table 2.1: Working principle summary for methods to measured J_g based on natural buoyancy.

Method	Position of measurement	Measurement
Denver (graduate cylinder)	Over the top of the froth	$\Delta V/\Delta A/\Delta t$
Jameson	Under the froth	$\Delta P/\Delta t$
JK	Over the top of the froth	$\Delta H/\Delta t$
McGill conductivity	Under the froth	$\Delta H/\Delta t$
McGill on-off (pressure)	Under the froth	dP/dt

2.6.3 Continuous Techniques

There are only two continuous techniques to measure J_g found in the literature (other than the one design from this thesis [64]): The USM (Yianatos et al.) [68] and the HUT (Grau and Heiskanen) [38]. They share the same design: A tube with continuous vacuum control to equalize the gas entering and leaving and a flow meter to monitor the gas rate.

2.6.3.1 The USM[1] J_g sensor

The sensor (Figure 2.24) comprises a tube, a rotameter flowmeter, a manometer and a vacuum system. The flow meter is connected to the top of the sensor with the manometer and the vacuum system. A continuous flow of gas can be established keeping a low vacuum.

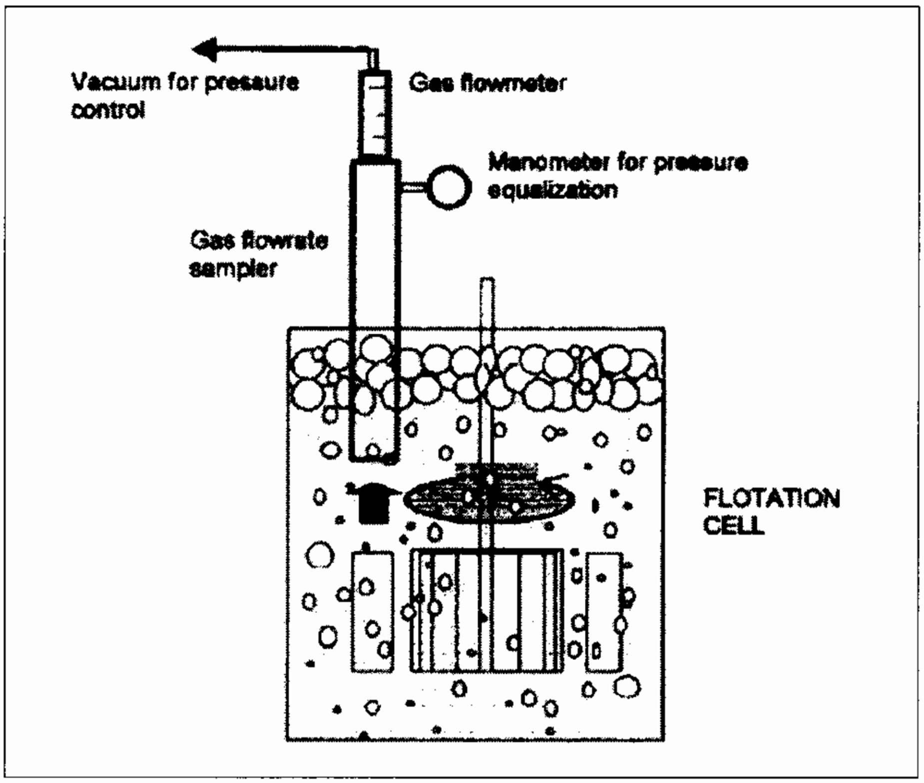

Figure 2.24: The USM sensor [68].

[1] USM: Santa Maria University.

2.6.3.2 The HUT[2] J_g sensor

An adaptation of the USM device (Figure 2.25), it comprises a transparent cylindrical tube (44 mm inner diameter), a mass flowmeter (with a gas drying and particle filter system), a digital vacuum pressure gauge, a vacuum system and a data acquisition system. Automation is the major advantage compared to the parent device.

Grau and Heiskanen describe the operation of the sensor as follows: "The probe is partially immersed into the flotation cell. The water-froth interface is shifted into the vertical tube by means of controlled vacuum level system. As a result a continuous gas flow is produced, which is measured using a mass flow meter". The authors claim monitoring of gas flow for a period of at least 20 minutes.

Grau and Heiskanen found that a stable froth could degrade sensor performance. This is a significant disadvantage in a plant environment (it is noted that they give no industrial-scale experimental data). Based on experience in this thesis, a stable froth is common in plant test work. (If a vacuum pump is used, turbulence is increased which may encourage rapid froth growth, i.e., the problem may be exacerbated.) It seems unlikely that this sensor can be considered a practical basis for a user-friendly device.

---

[2] HUT: Helsinki University of Technology.

This thesis will describe a J_g sensor that meets the challenge.

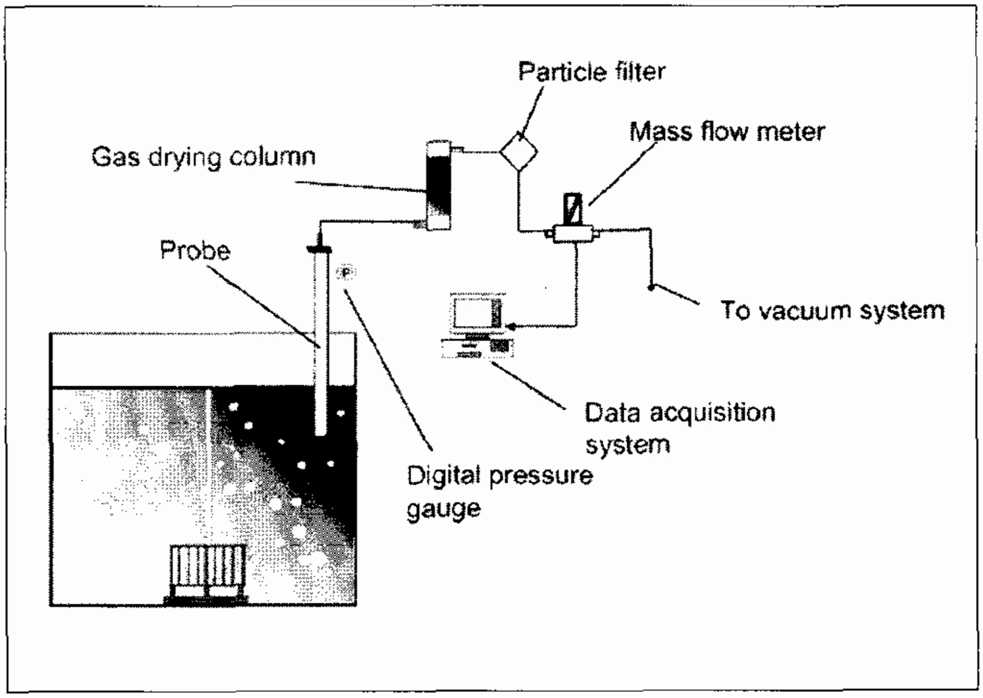

Figure 2.25: HUT J_g sensor [38].

2.7 Review of flow meter instrumentation

Flow meters can be classified by their applied theory (differential pressure, velocity, area, etc.), or by their applied technology (orifice, turbine, vortex, etc.). [14]. The applied technology classification will be used and three meters will be described, the first two being used in the present work and the last being selected as it has a potential use.

2.7.1 Orifice meter

The orifice plate flowmeter, a differential pressure device, is the most common industrial flow measurement instrument. The construction is simple and the device reliable, as evident from the many years of operational experience.

Figure 2.26 shows an illustration of fluid flow through an orifice plate. The abrupt change in cross section area generates a pressure drop that is proportional to the flow rate. The pressure drop can be tracked by a differential pressure gauge. Using a calibration for the orifice (flow versus pressure drop), the flow rate can be derived the from pressure measurement.

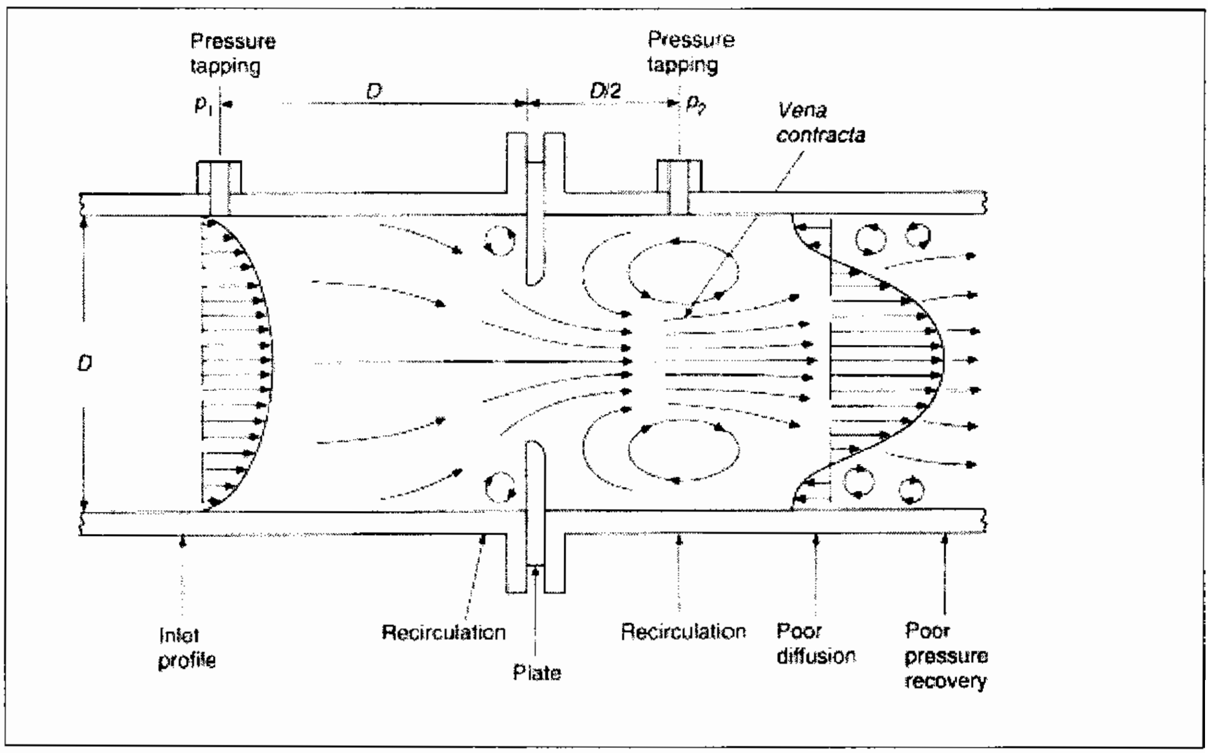

Figure 2.26: Orifice plate flow meter [14].

2.7.2 Thermal mass flow meter

The instrument used in the present work was a capillary thermal mass flowmeter (CTMF). The operation of a CTMF is described as follows: "Heat is supplied to the gas passing through a capillary tube so that the temperature of the gas rises and the change in temperature between two points provides a measure of the flowrate" [14]. The relationship between the mass flowrate, q_{KPS}, and temperature change, ΔT , is

$$q_{KPS} = \frac{Q}{FC_p\Delta T} \qquad \text{Eq. (2.1)}$$

where F is the sensor constant, C_p is specific heat of the fluid at constant pressure, and Q is the heat transferred.

Figure 2.27 is a schematic of the capillary tube of the instrument and shows the source passing heat to the tube via a collar. Two thermocouples, to yield ΔT, are located one either side of the source. Outside these are two heat sink collars which ensure that the gas temperature is negligibly affected by the presence of the flowmeter [14].

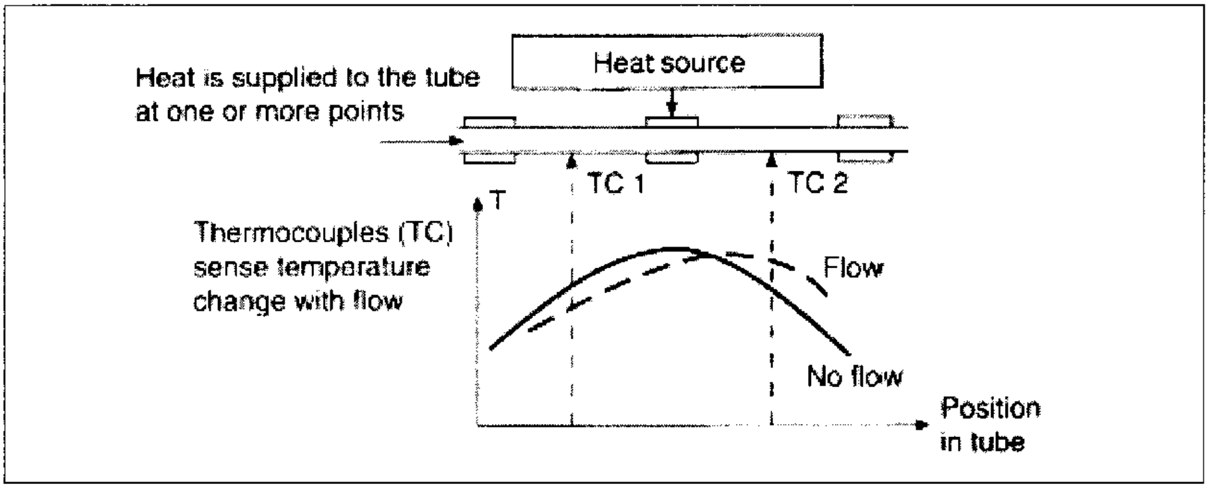

Figure 2.27: Thermal mass flow meter [14].

2.7.3 Film flow meter

This meter is based on the generation of a film of soap and tracking the time taken for the film to travel (due to the flow of gas) between two marks. The meter is designed for very low flows. A high precision film flow meter was found in the literature (Figure 2.28) [11] that comprises electronics for continuous tracking of the flow.

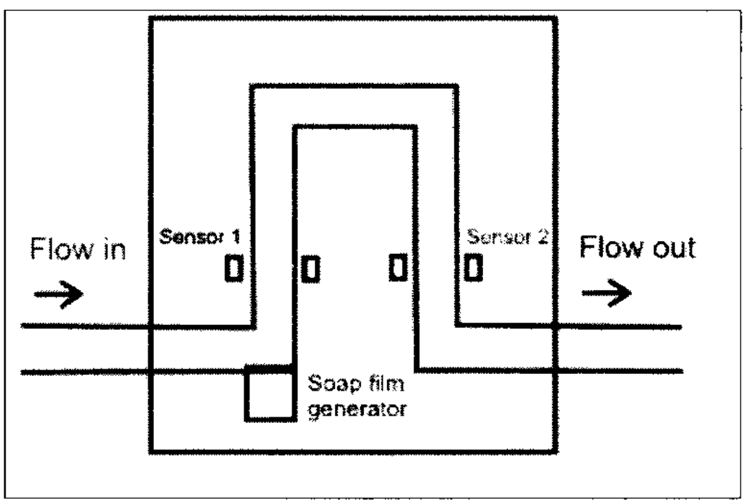

Figure 2.28: High precision flow meter [11].

CHAPTER 3
BACKGROUND: FLOW OF COMPRESSIBLE FLUIDS

3.1 Introduction

Prior to developing the model for the measurement of air flow using the sensors described in Chapter 4, it is necessary to explore one of the properties of a real gas: Compressibility. The term compressibility describes the ability of molecules in a fluid to be pressed together, i.e., gas is made more dense, and their ability to rebound to their original density. Compressibility expresses how much a gas is behaving like an ideal gas under any condition. If the compressibility equals one, then the gas is behaving exactly like an ideal gas. If the compressibility deviates much from one, then the ideal gas equation will not accurately model the real gas under those conditions. Compressibility can be estimated from temperature and pressure.

The basis is the theoretical adiabatic mass flow equation described by Miller [56], derived from an energy balance [66] and applied to the flow of gas through an orifice.

3.2 Fluid properties

3.2.1 The PVT gas-density equation

The pressure, temperature, and volume relationship for a real (non-ideal) gas can be expressed by the equation of state:

$$PV = nZRT \qquad \text{Eq. (3.1)}$$

where Z is the compressibility factor, which corrects for real-gas behaviour.

3.2.2 Compressibility and density estimation

Equations of state can calculate compressibility either from pressure and temperature or directly from density. Miller [53] called the two options, Generalized and Specific. He pointed out that the equation in the Generalized approach may have two or three parameters. Pressure and temperature are ratioed to a particular gas critical temperature T_c and pressure P_c, and two reduced parameters P_r and T_r are used to predict the compressibility factor Z. A third parameter, the acentric factor ω, is introduced to improve the prediction accuracy by accounting for the non spherical nature of the molecules [53].

In the case of Specific equations of state, Miller describes these as the equations used where metering accuracy and other thermodynamic properties, such as enthalpy or the velocity of sound, require that the state equation be exact. Miller mentioned that the most widely used Specific equations are NX-19 (Manual for the Determination of Supercompressibility for Natural Gas, 1962) and the 1967 ASME Steam Tables (1967 IFC Formulation for Industrial Use Steam Tables).

Finally, Miller introduces new equations that have been proposed (AGA-8 1986 and the NBS formulation, 1984). These equations require iterative solution, while the earlier forms were analytical.

3.2.3 Virial equation

Analytical state equations are derived using statistical mechanics and considerations of the intermolecular forces between gas molecules [53]. The solution, representing the PVT surface, is presented in terms of temperature-dependent virial coefficients and may be developed to solve for density ρ or compressibility Z. These equations are called virial equations and are written in the form:

$$P = RT\rho + RT\rho^2 + RT\rho^3 + \ldots \qquad \text{Eq. (3.2)}$$

3.2.4 Method of Pitzer

Liley et al. [51] describe the corresponding states method of Pitzer for prediction of vapor density of pure hydrocarbon and non polar gases as the most accurate method with errors less than 1%, except in the critical region[3] (where errors can be up to 30%).

Compressibility can be calculated using Equation 3.3,

$$Z = Z^{(0)} + \omega Z^{(1)} \qquad \text{Eq. (3.3)}$$

where $Z^{(0)}$ is the compressibility factor for a simple fluid and $Z^{(1)}$ is the correction term for molecular accentricity, both being functions of T_r and P_r. Charts and tabulated data are available in the literature [51]. Critical temperature and pressure and the accentric factor are required.

If P_r is in the range from 0 to 0.2, Liley et al. present a more accurate and practical equation,

$$Z=1+\frac{P_r}{T_r}[(0.1445+0.073\omega)-(0.330-0.46\omega)T_r^{-1}-(0.1385+0.50\omega)T_r^{-2}-(0.0121+0.097\omega)T_r^{-3}-0.0073\omega T_r^{-8}] \qquad \text{Eq. (3. 4)}$$

[3] In a phase diagram, the phase boundary between liquid and gas does not continue indefinitely. Instead, it terminates at a point called the critical point. This reflects the fact that, at high temperatures and pressures, the liquid and gaseous phases become indistinguishable. For air, the critical point occurs at around 309.7 K and 3.8 MPa.

For hydrocarbon and non polar gas mixtures, Liley et al. consider that the Pitzer pure component method can be used to predict vapor density by replacing the true critical properties with pseudo critical properties, namely:

$$T_{pc} = \sum_{i=1}^{n} x_i T_{c_i} \qquad \text{Eq. (3. 5)}$$

$$P_{pc} = \sum_{i=1}^{n} x_i P_{c_i} \qquad \text{Eq. (3. 6)}$$

$$\omega = \sum_{i=1}^{n} x_i \omega_i \qquad \text{Eq. (3. 7)}$$

3.2.5. Redlich-Kwong equation of state

The Redlich-Kwong equation of state [58,59] has the form (where a and b are constants):

$$P = \frac{RT}{(V-b)} - \frac{a}{(T^{1/2}V(V+b))} \qquad \text{Eq. (3. 8)}$$

$$Z = \frac{1}{1-\frac{b}{V}} - \frac{a}{RT^{3/2}V(1+\frac{b}{V})} \qquad \text{Eq. (3. 9)}$$

$$Z = \frac{1}{(1-h)} - (\frac{a^{*2}}{b^{*}})\frac{h}{(1+h)} \qquad \text{Eq. (3. 10)}$$

where $a^{*2} = \frac{a}{R^2T^{2.5}}, b^* = \frac{b}{RT}$ and $h = \frac{b}{V}$

From thermodynamic considerations [58], a and b in Equation 3.9 can be expressed in terms of the critical properties. Redlich-Kwong have shown that substitution of the critical properties, T_c and P_c, and rearrangement, leads to the following equalities:

$$a^{*2} = \frac{a}{R^2T^{2.5}} = \frac{0.4278T_c^{2.5}}{P_cT^{2.5}} \qquad \text{Eq. (3. 11)}$$

$$b^* = \frac{b}{RT} = 0.0867\frac{T_c}{P_cT} \qquad \text{Eq. (3. 12)}$$

$$h = \frac{b}{V} = \frac{bP}{Z} \qquad \text{Eq. (3. 13)}$$

Z can be determined by first substituting the values for T, P, V, T_c and P_c and solving the resulting expression by trial and error. It should be noted that since the equation is cubic, three roots are possible, but only one of the solutions will be physically meaningful and represent the correct value.

3.2.6 Compressibility factor of gas mixtures

Gas mixtures that display significant deviation from ideal gas behavior can be modeled by using an average Z factor that is defined by the following relationship:

$$\bar{Z} = Z_1x_1 + Z_2x_2 + \ldots + Z_nx_n \qquad \text{Eq. (3. 14)}$$

where Z_1 and Z_2 and Z_n represent the Z factors for each component contained in the mixture, and x_1, x_2 and x_n represent the respective mole fraction of each gas in the mixture.

3.3 Orifice theory

Gases are compressible, i.e., the fluid density changes with pressure and temperature. Figure 3.1 illustrates the components of the Bernoulli equation for flow of a fluid through an orifice. If the fluid is a gas, the fluid density is not constant between planes 1 and 2. Miller [56] describes this process as a "decrease in pressure to accommodate the increase in kinetic energy (the velocity increases at the orifice), [thus] the density decreases, and the assumption of constant density no longer applies. Only for a very low differential pressures can the density change be neglected with any degree of accuracy".

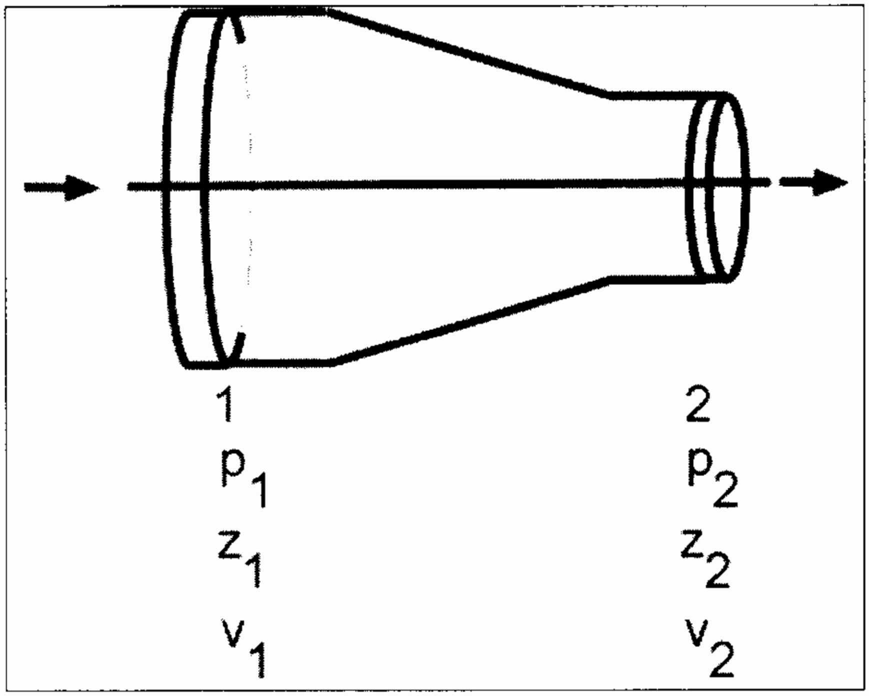

Figure 3.1: Setting up the Bernoulli equation.

Equation 3.15 expresses the energy balance between planes 1 and 2 (ignoring friction losses).

$$Q\text{-}W = -q_{KPS,1}(h_1 + \frac{1}{2}v_1^2 + gz_1) + q_{KPS,2}(h_2 + \frac{1}{2}v_2^2 + gz_2) \qquad \text{Eq. (3. 15)}$$

An adiabatic process is assumed because gas flowing through an orifice at high velocity cannot maintain a constant temperature and, therefore, it should not be treated as an isothermal process. The effect of acceleration due to changes in flow cross-sectional area and the effect of friction cause changes in temperature. High velocities and insulation prevent the compressible fluid from coming to thermal equilibrium with its surroundings. When heat cannot be exchanged, as in compressible-flow situations, it may be assumed to be an essentially adiabatic process.

For an adiabatic process, with no work W entering or leaving the system, no elevation difference, and from continuity $q_{KPS,1} = q_{KPS,2} = q_{KPS}$, Equation 3.15 reduces to:

$$\frac{v_2^2 - v_1^2}{2} = h_1 - h_2 = -\int_{P_1}^{P_2} \frac{dP}{\rho} \qquad \text{Eq. (3. 16)}$$

where h_1 - h_2 is the enthalpy difference between measuring planes. To solve this integral, we compute the entropy change from the first and second laws of thermodynamics for a pure substance,

$$Tds = dh - \frac{dP}{\rho} \qquad \text{Eq. (3. 17)}$$

Introducing $dh=C_pdT$ for an ideal gas and solving for ds, we substitute $\rho = \frac{P}{RT}$ from the ideal gas law and obtain,

$$\int_1^2 ds = \int_1^2 C_p \frac{dT}{T} - R\int_1^2 \frac{dP}{P} \qquad \text{Eq. (3. 18)}$$

$$s_2 - s_1 = c_p \ln\frac{T_2}{T_1} - R\ln\frac{P_2}{P_1} = c_v \ln\frac{T_2}{T_1} - R\ln\frac{\rho_2}{\rho_1} \qquad \text{Eq. (3. 19)}$$

For an isentropic flow (s_1=s_2), the following relation holds for an ideal gas:

$$P\left(\frac{1}{\rho}\right)^{\gamma} = \text{constant} = \delta \qquad \text{Eq. (3. 20)}$$

Substituting Equation 3.20 in 3.16 and solving the integral yields,

$$h_1 - h_2 = \int_{P_1}^{P_2} \frac{dP}{\rho} = \frac{P_1}{\rho_1} \frac{\gamma}{\gamma - 1}\left[1 - \left(\frac{P_2}{P_1}\right)^{(\gamma-1)/\gamma}\right] \qquad \text{Eq. (3. 21)}$$

and, from mass flow continuity we know that,

$$q_{KPS} = \rho_1 A_1 \bar{v}_1 = \rho_2 A_2 \bar{v}_2 \qquad \text{Eq. (3. 22)}$$

$$\bar{v}_1 = \frac{\rho_2 A_2 \bar{v}_2}{\rho_1 A_1} \qquad \text{Eq. (3. 23)}$$

Substituting Eq. 3.21, 3.23 into 3.16 yields,

$$\frac{P_1}{\rho_1} \frac{\gamma}{\gamma - 1}\left[1 - \left(\frac{P_2}{P_1}\right)^{(\gamma-1)/\gamma}\right] = \frac{[1 - (\rho_2 A_2 / \rho_1 A_1)^2]}{2} \bar{v}_2^2 \qquad \text{Eq. (3. 24)}$$

If we consider the case that 1 and 2 are circular planes, Equation 3.24 can be rearranged as,

$$\frac{P_1}{\rho_1} \frac{\gamma}{\gamma - 1}\left[1 - \left(\frac{P_2}{P_1}\right)^{(\gamma-1)/\gamma}\right] = \frac{[1 - (\rho_2 / \rho_1)^2 (d/D)^4]}{2} \bar{v}_2^2 \qquad \text{Eq. (3. 25)}$$

Using Equation 3.22 to solve at plane 2,

$$\bar{v}_2 = \frac{q_{KPS}}{\rho_2 \frac{\pi}{4} d^2} \qquad \text{Eq. (3. 26)}$$

$$q_{KPS} = (\frac{\pi}{4} d^2 \rho_2) \sqrt{\frac{\frac{\gamma}{\gamma-1}\left[1-(\frac{P_2}{P_1})^{(\gamma-1)/\gamma}\right]}{\frac{[1-(\rho_2/\rho_1)^2 (d/D)^4]}{2}}} \sqrt{\frac{P_1}{\rho_1}} \qquad \text{Eq. (3. 27)}$$

Using Equation 3.20 as,

$$\rho_2 = \rho_1 (\frac{P_2}{P_1})^{1/\gamma} \qquad \text{Eq. (3. 28)}$$

and, substituting Equation 3.28 in 3.27, we get,

$$q_{KPS} = (\frac{\pi}{4} d^2) \sqrt{2} \sqrt{\frac{\frac{\gamma}{\gamma-1}\left[1-(\frac{P_2}{P_1})^{(\gamma-1)/\gamma}\right]}{[1-(P_2/P_1)^{2/\gamma}(d/D)^4]}} \sqrt{(\rho_1 (\frac{P_2}{P_1})^{1/\gamma})^2} \sqrt{\frac{P_1}{\rho_1}} \frac{\sqrt{P_1-P_2}}{\sqrt{P_1-P_2}}$$

Eq. (3. 29)

Ordering and simplifying Equation 3.29,

$$q_{KPS} = (\frac{\pi}{4} d^2) \frac{\sqrt{2}}{\sqrt{1000}} \sqrt{\frac{\frac{\gamma}{\gamma-1}(\frac{P_2}{P_1})^{2/\gamma}\left[1-(\frac{P_2}{P_1})^{(\gamma-1)/\gamma}\right]}{[1-(\frac{P_2}{P_1})^{2/\gamma}(\frac{d}{D})^4](1-\frac{P_2}{P_1})}} \sqrt{\Delta P \rho_1} \qquad \text{Eq. (3. 30)}$$

$$q_{KPS} = \frac{(\frac{\pi}{4}d^2)\frac{\sqrt{2}}{\sqrt{1000}}}{\sqrt{1-(d/D)^4}} \underbrace{\sqrt{\frac{[1-(d/D)^4]\frac{\gamma}{\gamma-1}(\frac{P_2}{P_1})^{2/\gamma}\left[1-(\frac{P_2}{P_1})^{(\gamma-1)/\gamma}\right]}{[1-(\frac{P_2}{P_1})^{2/\gamma}(\frac{d}{D})^4](1-\frac{P_2}{P_1})}}}_{Y_1} \sqrt{\Delta P \rho_1} \qquad \text{Eq. (3.31)}$$

where Y_1 is defined by Miller as the adiabatic gas expansion factor. Equation 3.31 is more conveniently written[4],

$$q_{KPS} = \frac{\pi}{4}\frac{\sqrt{2}}{\sqrt{1000}}\frac{Y_1 d^2}{\sqrt{1-(d/D)^4}}\sqrt{\Delta P \rho_1} \qquad \text{Eq. (3.32)}$$

where Equation 3.32 is called the "theoretical adiabatic mass flow equation" [56]. For volumetric units in standard cubic meters per second (SCMS), the equation becomes,

$$q_{scms} = \frac{\pi}{4}\frac{\sqrt{2}}{\sqrt{1000}}\frac{Y_1 d^2}{\sqrt{1-(d/D)^4}}\sqrt{\frac{\Delta P}{\rho_1}} \qquad \text{Eq. (3. 33)}$$

Miller indicates that "the equation requires the determination of the upstream density (at plane 1); hence, when the PVT relationship is used to calculate density, the assumption is that the pressure, temperature, and compressibility are determined as well".

---

[4] a) The ratio (d/D) is named β in some references. b) The coefficient $\frac{\pi}{4}\sqrt{2}\frac{Y_1 d^2}{\sqrt{1-(d/D)^4}}$ in Equation 3.33 is generally called Discharge Coefficient.

CHAPTER 4
MODEL FOR THE GAS VELOCITY SENSORS

4.1 Introduction

For the last decade, intensive work has been conducted to develop sensors to measure the superficial gas velocity (J_g) of air dispersed as bubbles in a flotation machine. The most popular J_g sensors, as judged by their use in industrial campaigns, are the JK, On-off McGill, and the Continuous McGill. They exploit the same principle but to date a common theory has not been formally derived. This chapter introduces the principles that govern each sensor and derives the theory.

4.2 Description of the J_g sensors

All the sensors share a common component: A tube to collect bubbles by natural buoyancy. The sensors are inserted in the flotation cell with the bottom of the tube below the froth-pulp interface.

4.2.1 Discontinuous techniques: On-off McGill and JK

These techniques are based on collection of air bubbles in a closed vessel. The accumulation of air pushes down the level of water (JK) or slurry (On-off McGill). Tracking the change in level can be visual (JK) or by means of a pressure transmitter (On-off McGill). The rate of change of level is related to the superficial gas velocity, J_g.

Figure 4.1 shows a typical On-off McGill sensor. It comprises: A, a cylinder or tube (PVC, ABS, etc); B, a globe valve; and, C, a pressure transmitter. Typical dimensions are: D, between 2 and 3 (m); and, E, 7.5 to 10 (cm) (3 to 4 inch).

The sampling process can be divided into three steps:

I) Figure 4.2: At the beginning of bubble collection, the globe valve (F) is open. The levels inside and outside the sensor are the same.

II) Figure 4.3: As soon as the valve is closed, the level (G) is pushed down due to the accumulation of gas. The accumulation is tracked by the pressure transmitter as the pressure inside the tube increases (H).

III) Figure 4.4: When the level reaches the bottom of the sensor, the pressure becomes constant (I) and the system can be readied for another cycle.

The resulting curve is called "pressure variation curve". The slope of this curve between t1 and t2 is used to estimate J_g.

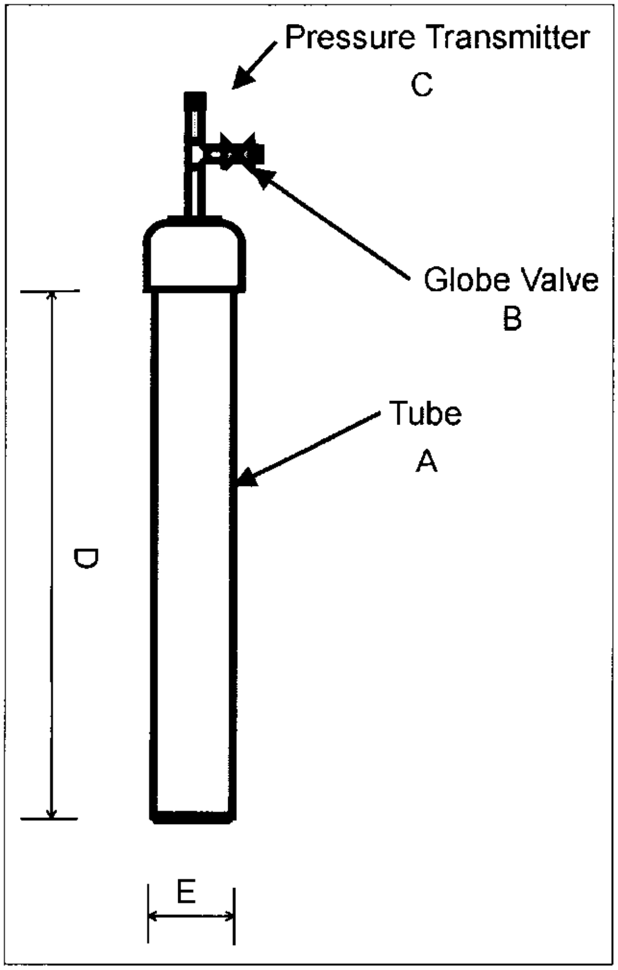

Figure 4.1: On-off McGill J_g sensor.

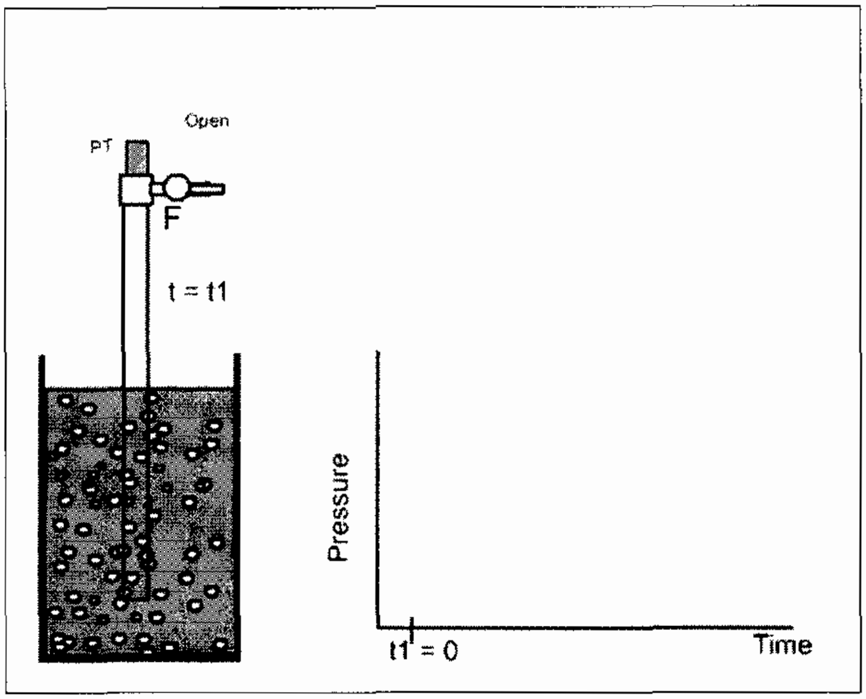

Figure 4.2: Step 1.

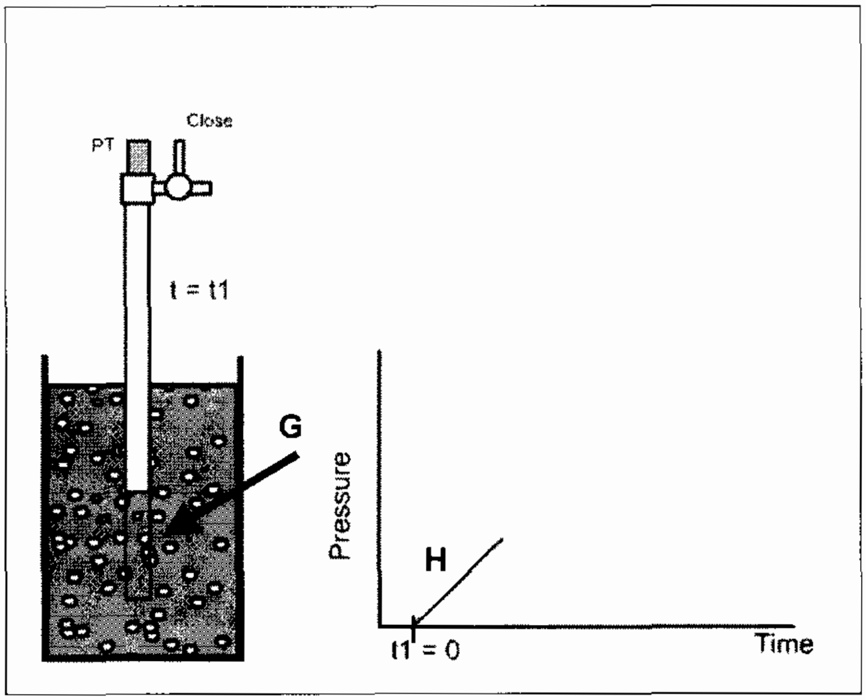

Figure 4.3: Step 2.

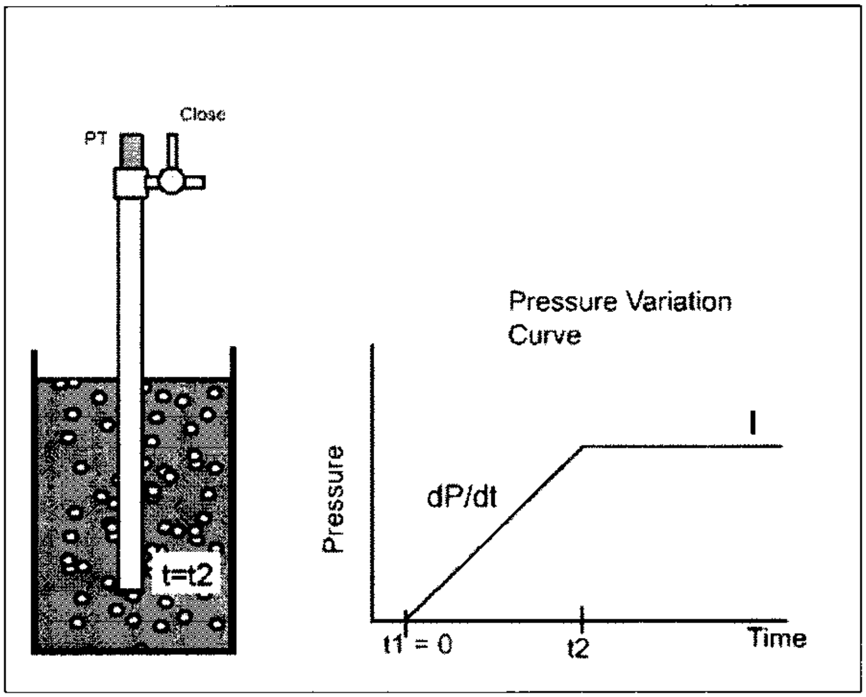

Figure 4.4: Step 3.

Figure 4.5 shows a typical JK sensor [69]. It comprises a transparent cylinder (J) and a pinch valve (K). A coupling is shown on the end of the tube which allows the length to be increased (if required) by attaching another section of pipe. The pinch valve likewise has a coupling.

The sampling process for this sensor can also be divided into three steps:

I) Figure 4.6: At the beginning, the pinch valve at the bottom of the sensor is closed and the tube contains just water. The level inside the tube is at the top (L). The level is tracked between two marks (M1 and M2) separated by a fixed distance N.

II) Figure 4.7: As soon as the valve is opened, the level is pushed down due to the accumulation of gas. The stopwatch is started when the level reaches the first mark (M1).

III) Figure 4.8: When the level reaches the second mark (M2) the stopwatch is stopped; the sensor is ready to be filled again with water for another measurement.

The distance between the two marks divided by the time that it takes the level to travel between the two marks is a "raw" J_g ($J_{g\text{-}exp}$). This value is processed by means of a hydrostatic balance to calculate the actual J_g.

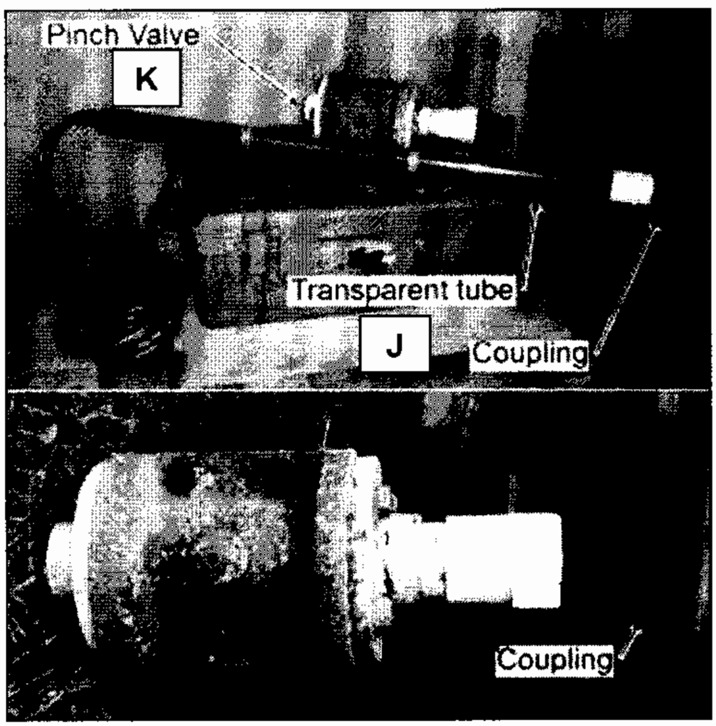

Figure 4.5: JK sensor (photo courtesy of Dave Seaman).

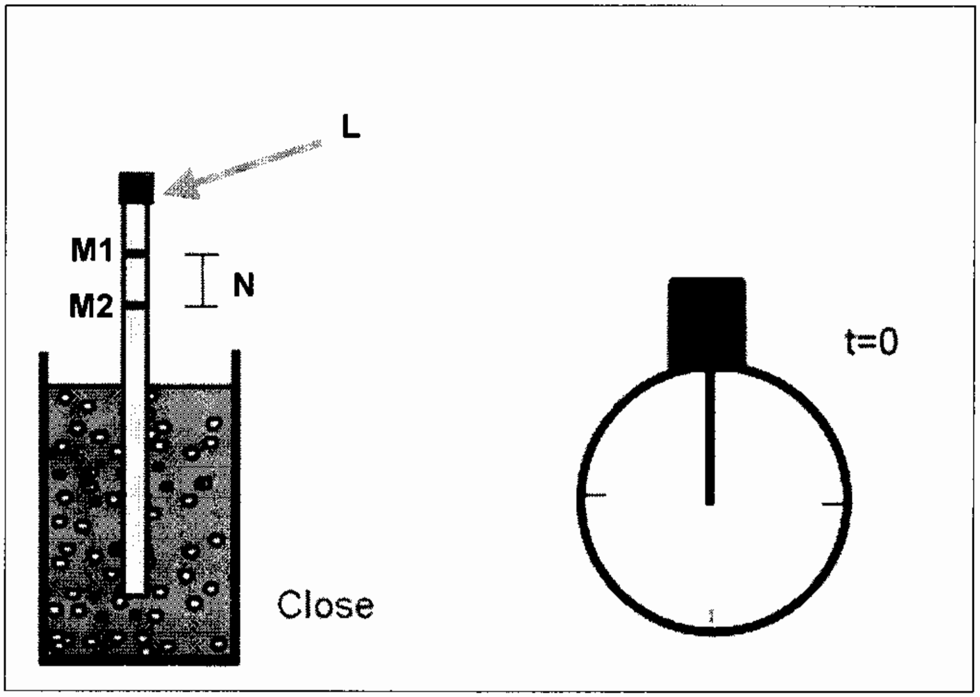

Figure 4.6: Step 1.

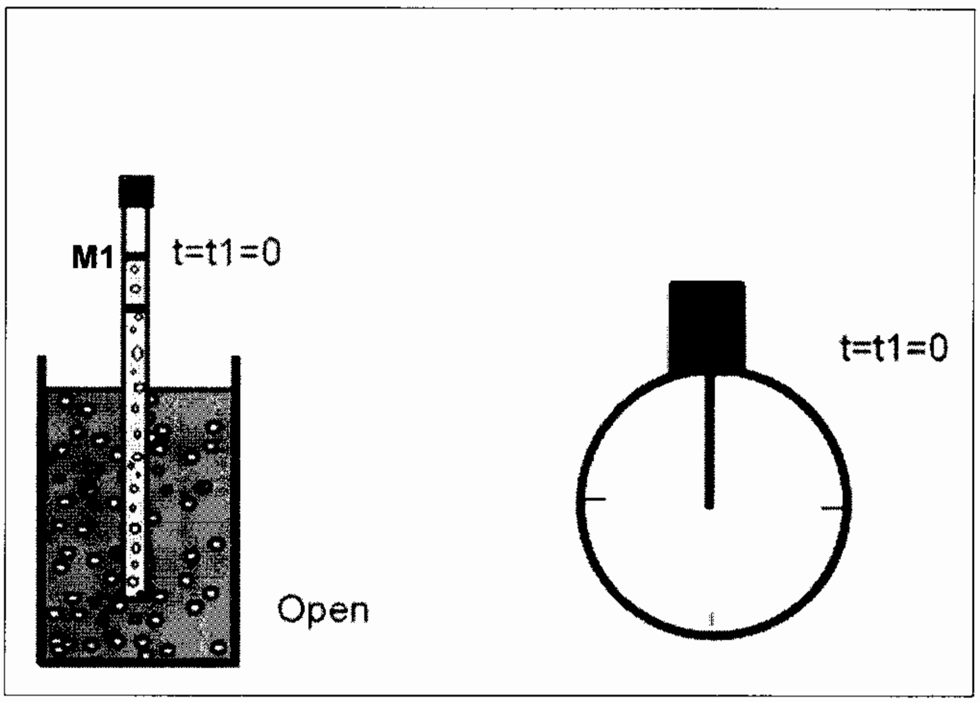

Figure 4.7: Step 2.

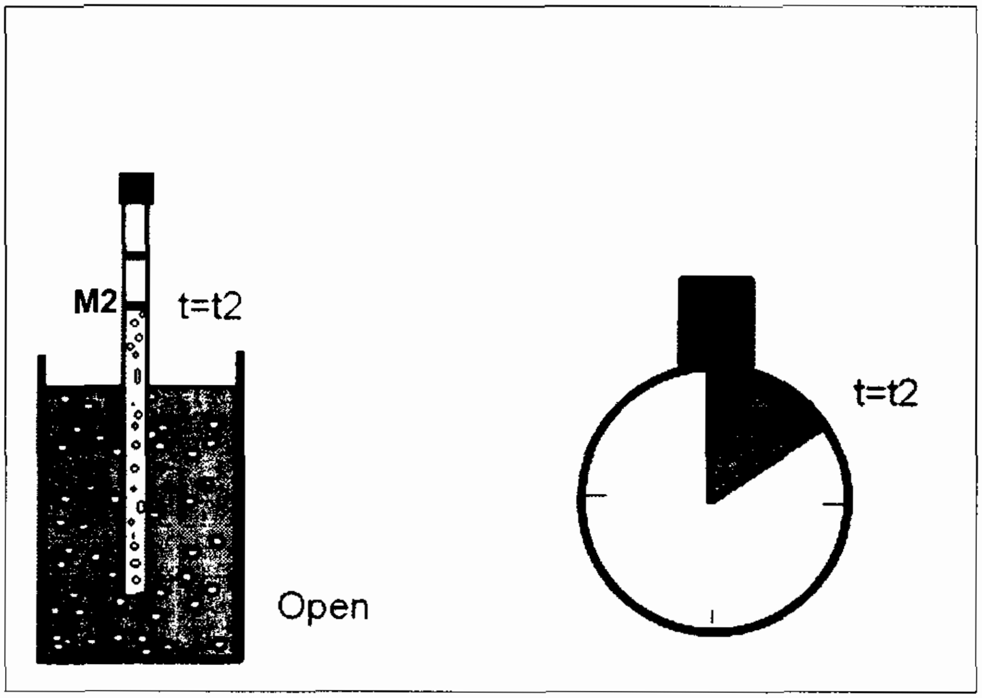

Figure 4.8: Step 3.

4.2.2 McGill continuous

The continuous technique shares the same "tube sampling bubbles by natural buoyancy" design of the discontinuous devices but now estimates J_g from the pressure drop across an orifice as gas exits from the tube. Once steady state is reached, the pressure drop is related to air flow rate by a calibration. Dividing volumetric air flow rate by tube cross-section area gives the J_g related to the sampling location.

Figure 4.9 shows a schematic. The sensor comprises: O, a tube (PVC, ABC, etc); P, two globe valves; Q, a pressure transmitter; and, R, a calibrated orifice. Typical dimensions are: S, between 2 and 3 (m); and, T, 7.5 to 10 (cm) (3 to 4 inch).

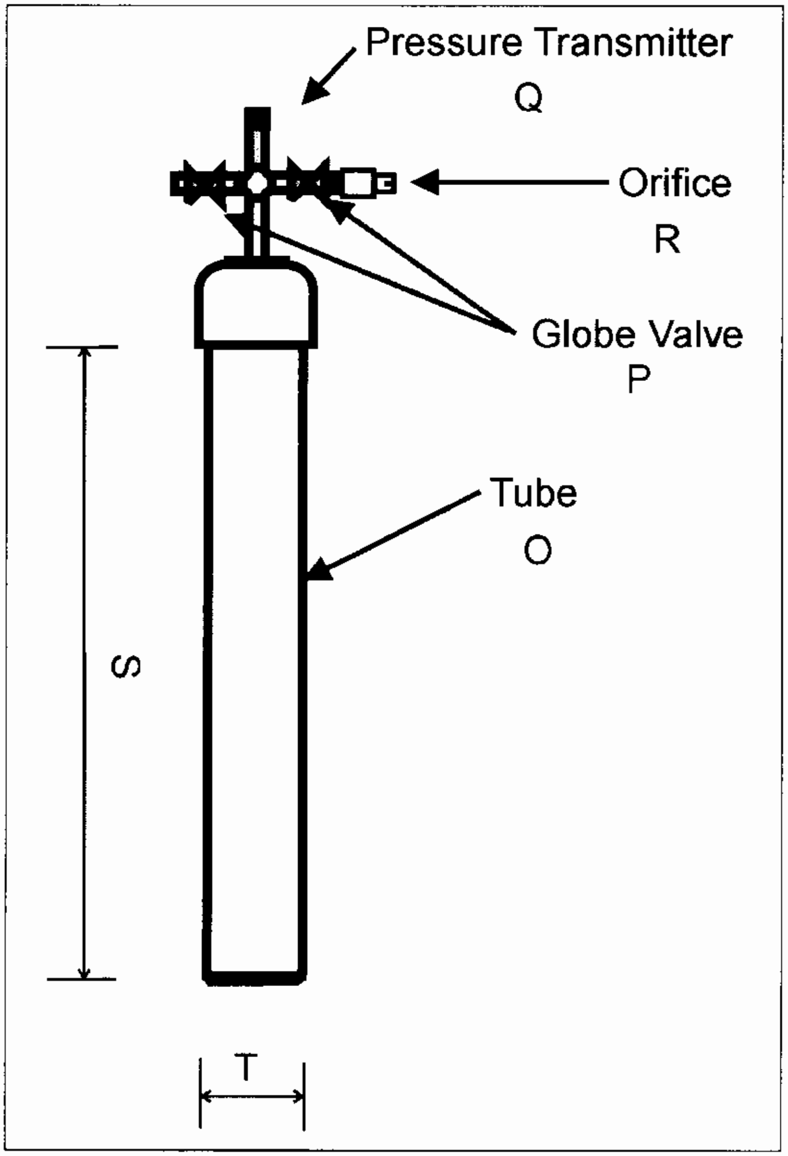

Figure 4.9: Continuous sensor.

The sampling process conveniently divides into three steps:

I) Figure 4.10: The tube is inserted with globe valves U and V closed, i.e., the tube is full of air and the pressure signal after a peak reaches a steady state (W).

II) Figure 4.11: As soon as valve V is opened, the level rises until a hydrostatic equilibrium (steady state) is reached. The pressure signal drops until the flow of gas entering and leaving equalizes.

III) Figure 4.12: When steady state is reached (X), the pressure signal remains stable and using the calibration equation for this orifice the flow rate of gas can be estimated. The flow of gas divided by the cross-section area of the tube is the measured J_g.

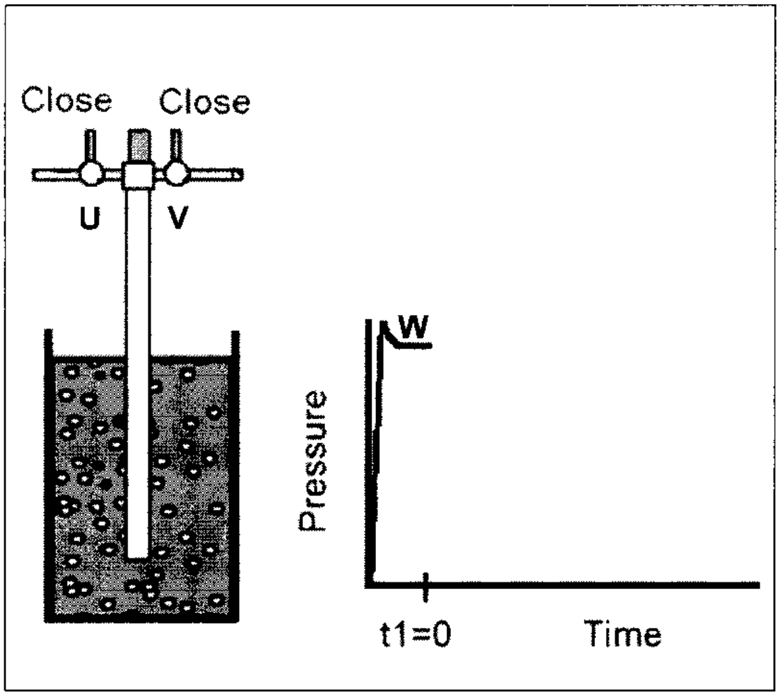

Figure 4.10: Step 1.

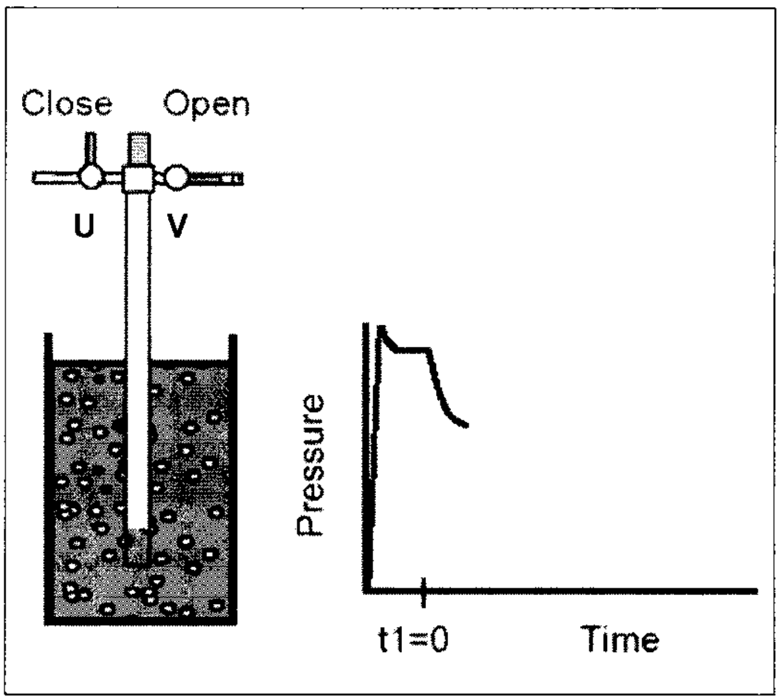

Figure 4.11: Step 2.

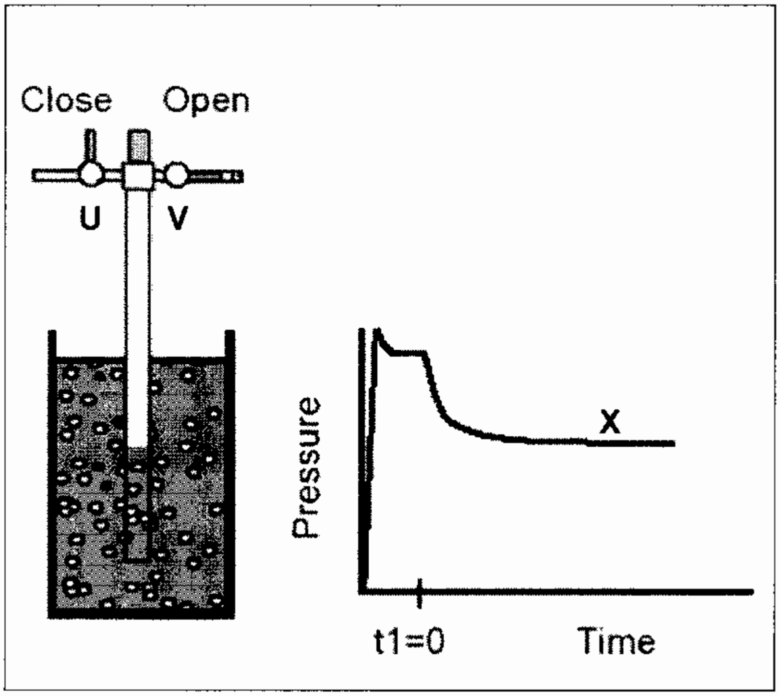

Figure 4.12: Step 3.

4.3 Flow calculation equation for the J_g sensors

The starting point is the general mass balance for a system with variable volume and pressure, and no chemical reaction (4.13):

$$q_{KPS,in} - q_{KPS,out} = \text{Rate of accumulation} \qquad \text{Eq. (4.1)}$$

where $q_{KPS,in}$ and $q_{KPS,out}$ are the in and out mass flow rates, respectively.

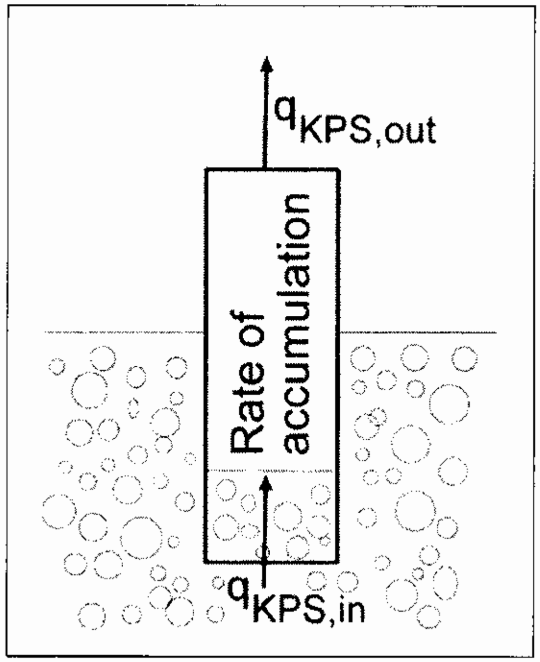

Figure 4.13: Mass balance over the sensor.

4.3.1 Discontinuous techniques

These constitute the case with no gas exiting the system, i.e., the on-off McGill (Figure 4.14) and JK (Figure 4.15) sensors.

Consider $q_{KPS,in} > 0$ and $q_{KPS,out} = 0$, then

$$q_{KPS,in} = \frac{d}{dt}(\rho V) \qquad \text{Eq. (4.2)}$$

Applying the chain rule,

$$q_{KPS,in} = \frac{d}{dP}(\rho V)\frac{dP}{dt} \qquad \text{Eq. (4.3)}$$

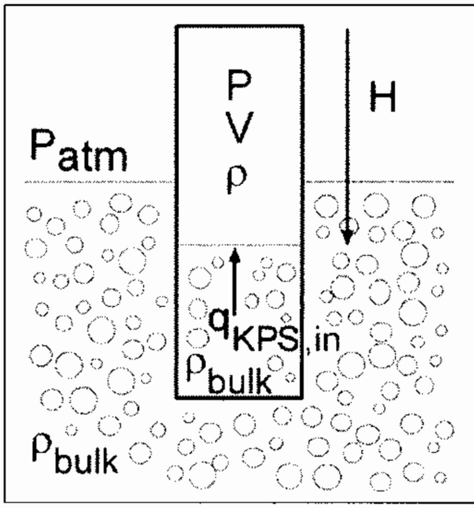

Figure 4.14: On-off McGill sensor variables.

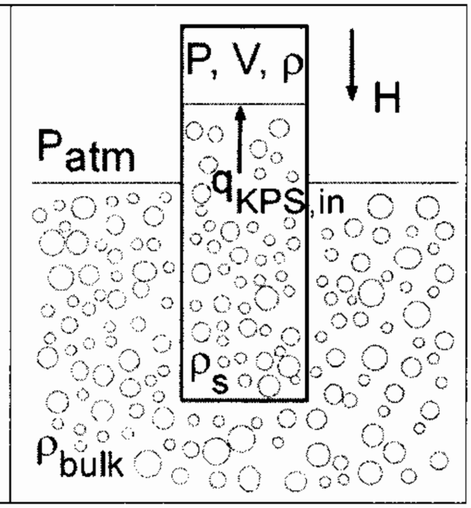

Figure 4.15: JK sensor variables.

Substituting Equation 3.20 in the first term of 4.3,

$$\frac{d}{dP}(\rho V) = \frac{d(\frac{P^{1/\gamma}V}{\delta^{1/\gamma}})}{dP} \qquad \text{Eq. (4.4)}$$

$$\frac{d}{dP}(\rho V) = \frac{1}{\delta^{1/\gamma}}(\frac{1}{\gamma}P^{(1/\gamma-1)}\bar{V} + P^{1/\gamma}\frac{dV}{dH}\frac{dH}{dP}) \qquad \text{Eq. (4.5)}$$

To solve this differential we know that the volume of air in the tube is related to the cross sectional area and the height (Figure 4.16) as follows

$$V = Vo + A(H - H_p) \qquad \text{Eq. (4.6)}$$

Is important to mention that in the case of the JK technique, V_o is zero.

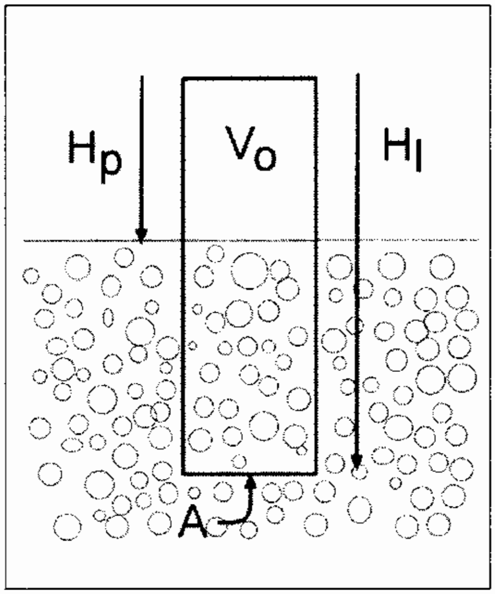

Figure 4.16: Sensor dimensions.

Differentiating Equation 4.6,

$$\frac{dV}{dH} = A \qquad \text{Eq. (4.7)}$$

also the pressure in the tube is,

$$P = P_{atm} + \rho_s g(H - H_p) \qquad \text{Eq. (4.8)}$$

Is important to mention that H is lower than H_p in the JK technique; and is higher than H_p in the on-off McGill technique (illustrated in Figures 4.15 and 4.16).

Differentiating Equation 4.8:

$$\frac{dH}{dP} = \frac{1}{\rho_s g} \qquad \text{Eq. (4.9)}$$

Using Equations 4.7 and 4.9 in 4.5,

$$\frac{d}{dP}(\rho V) = \frac{\rho}{P^{1/\gamma}}\left(\frac{1}{k}P^{(1/\gamma-1)}V + P^{1/\gamma}A\frac{1}{\rho_s g}\right) \qquad \text{Eq. (4.10)}$$

$$\frac{d}{dP}(\rho V) = \frac{\rho V}{kP} + \frac{\rho A}{\rho_s g} \approx \frac{\bar{\rho}\bar{V}}{k\bar{P}} + \frac{\bar{\rho}A}{\rho_s g} \qquad \text{Eq. (4.11)}$$

$$\frac{d}{dP}(\rho V) = \frac{28.8\bar{P}}{RTZ}\left(\frac{A\bar{H}}{k\bar{P}} + \frac{A}{\rho_s g}\right) \qquad \text{Eq. (4.12)}$$

And, using Equation 4.12 in 4.3

$$q_{KPS,in} = \frac{28.8A}{RTZ}\left(\frac{\bar{H}}{\gamma} + \frac{\bar{P}}{\rho_s g}\right)\frac{dP}{dt} \qquad \text{Eq. (4.13)}$$

$$q_{KPS,in} = \frac{28.8A}{RTZ}\left(\frac{\rho_s g\bar{H} + \gamma\bar{P}}{\gamma\rho_s g}\right)\frac{dP}{dt} \qquad \text{Eq. (4.14)}$$

that is,

$$q_{KPS,in} = \text{mass}/t = \rho Q \qquad \text{Eq. (4.15)}$$

$$q_{KPS,in} = \rho J_g A \qquad \text{Eq. (4.16)}$$

The J_g at the bottom of the tube is,

$$q_{KPS,in} = J_g \frac{28.8P_lA}{RTZ} \qquad \text{Eq. (4.17)}$$

Using Equation 4.17 in 4.14,

$$J_g \frac{28.8P_lA}{RTZ} = \frac{28.8A}{RTZ}\left(\frac{\rho_s g\bar{H} + \gamma\bar{P}}{\gamma\rho_s g}\right)\frac{dP}{dt} \qquad \text{Eq. (4.18)}$$

$$J_g = \left(\frac{\rho_s g\bar{H} + \gamma\bar{P}}{\gamma P_l \rho_s g}\right)\frac{dP}{dt} \qquad \text{Eq. (4.19)}$$

Equation 4.19 describes the relation between J_g and dP/dt for discontinuous techniques. The following analyzes the two sensors in that category.

4.3.1.1 On-off McGill

Figure 4.17 shows a schematic illustration of the specific variables for the McGill sensor to solve Equation 4.19:

$$\bar{H} = \frac{H_l + H_p}{2} \qquad \text{Eq. (4.20)}$$

$$\bar{P} = P_{atm} + \rho_{bulk} g\left(\frac{H_l - H_p}{2}\right) \qquad \text{Eq. (4.21)}$$

$$J_g = \left(\frac{\rho_s g\frac{(H_l + H_p)}{2} + \gamma\left(P_{atm} + \rho_{bulk} g\frac{(H_l - H_p)}{2}\right)}{\gamma(P_{atm} + \rho_{bulk} g(H_l - H_p))\rho_s g}\right)\frac{dP}{dt} \qquad \text{Eq. (4.22)}$$

And since $\rho_s = \rho_{bulk}$, finally

$$J_g = \underbrace{\left(\frac{\rho_{bulk} g \dfrac{(H_l + H_p)}{2} + \gamma\left(P_{atm} + \rho_{bulk} g \dfrac{(H_l - H_p)}{2} \right)}{\gamma(P_{atm} + \rho_{bulk} g (H_l - H_p))\rho_{bulk} g} \right)}_{FP_{McGill}} \frac{dP}{dt} \qquad \text{Eq. (4.23)}$$

where FP_{McGill} (Function P for the on-off McGill J_g sensor) is defined as the factor correlating the J_g with the slope of the pressure variation curve (dP/dt). Solving Equation 4.23 gives J_g from FP_{McGill} and dP/dt. For an adiabatical gas flow γ = 1.4; for an isothermical gas flow γ = 1 and Equation 4.23 becomes,

$$J_g = \left(\frac{\rho_{bulk} g \dfrac{(H_l + H_p)}{2} + \left(P_{atm} + \rho_{bulk} g \dfrac{(H_l - H_p)}{2} \right)}{(P_{atm} + \rho_{bulk} g (H_l - H_p))\rho_{bulk} g} \right) \frac{dP}{dt} \qquad \text{Eq. (4.24)}$$

Finally,

$$J_g = \left(\frac{P_{atm} + \rho_{bulk} g H_l}{(P_{atm} + \rho_{bulk} g (H_l - H_p))\rho_{bulk} g} \right) \frac{dP}{dt} \qquad \text{Eq. (4.25)}$$

An example of J_g calculation is shown in Appendix A.1

4.3.1.2 JK

Figure 4.18 shows a schematic of the specific variables for the JK sensor to solve Equation 4.19:

$$\bar{H} = \frac{H_1 + H_2}{2} \qquad \text{Eq. (4.26)}$$

$$P_1 = P_{atm} - \rho_s g(H_l - H_1) + \rho_{bulk} g(H_l - H_p) \qquad \text{Eq. (4.27)}$$

$$P_2 = P_{atm} - \rho_s g(H_l - H_2) + \rho_{bulk} g(H_l - H_p) \qquad \text{Eq. (4.28)}$$

$$\bar{P} = P_{atm} - \rho_s g\left(H_l - \frac{H_2 + H_1}{2}\right) + \rho_{bulk} g(H_l - H_p) \qquad \text{Eq. (4.29)}$$

$$J_g = \underbrace{\left(\frac{\rho_s g \dfrac{(H_2 + H_1)}{2} + \gamma\left(P_{atm} - \rho_s g\left(H_l - \dfrac{H_2 + H_1}{2}\right) + \rho_{bulk} g(H_l - H_p)\right)}{\gamma(P_{atm} + \rho_{bulk} g(H_l - H_p))\rho_s g} \right)}_{FP_{JK}} \rho_s g \frac{dH}{dt} \qquad \text{Eq. (4.30)}$$

where FP_{JK} (Function P for the JK J_g sensor) is defined as the factor correlating the J_g with the rate of level descent (dH/dt). Solving Equation 4.30 gives J_g from FP_{JK} and dH/dt. For adiabatic gas flow γ =1.4; for isothermical gas flow γ =1 and Equation 4.30 becomes,

$$J_g = \left(\frac{\rho_s g \frac{(H_2 + H_1)}{2} + \left(P_{atm} - \rho_s g \left(H_l - \frac{H_2 + H_1}{2} \right) + \rho_{bulk} g (H_l - H_p) \right)}{(P_{atm} + \rho_{bulk} g (H_l - H_p)) \rho_s g} \right) \rho_s g \frac{dH}{dt}$$
Eq. (4.31)

Finally,

$$J_g = \left(\frac{P_{atm} + \rho_s g (H_2 + H_1) + H_l g (\rho_{bulk} - \rho_s) - \rho_{bulk} g H_p}{P_{atm} + \rho_{bulk} g (H_l - H_p)} \right) \frac{dH}{dt} \qquad \text{Eq. (4.32)}$$

In the literature [69], the following Equation is given for the JK device,

$$J_g = \left(\frac{P_{atm} + \rho_p g H_p - \rho_w g H_w}{P_{atm} + \rho_p g H_p} \right) J_{g-exp} \qquad \text{Eq. (4.33)}$$

To compare with the present derivation, first the nomenclature must be understood (Figure 4.19):

$J_{g\text{-}exp}$: Rate of change of H in time (cm/s).

ρ_p : Density of the aerated pulp (ρ_{bulk} in Equation 4.32).

ρ_w : Density of the aerated water inside the J_g probe (ρ_s in Equation 4.32).

H_w : Distance from the bottom part of the sensor to the second mark (H_l-H_2 in Figure 4.19).

H_l : Total length of the sensor.

H_p : Distance from the bottom part to the top of the froth (H_l-H_p in Figure 4.19).

If we express Equation (4.33) using the present nomenclature:

$$J_g = \left(\frac{P_{atm} + \rho_{bulk} g (H_l - H_p) - \rho_s g (H_l - H_2)}{P_{atm} + \rho_{bulk} g (H_l - H_p)} \right) \frac{\Delta H}{\Delta t} \qquad \text{Eq. (4.33b)}$$

A test of Equations 4.23, 4.30 and 4.33b is described in section 5.3.

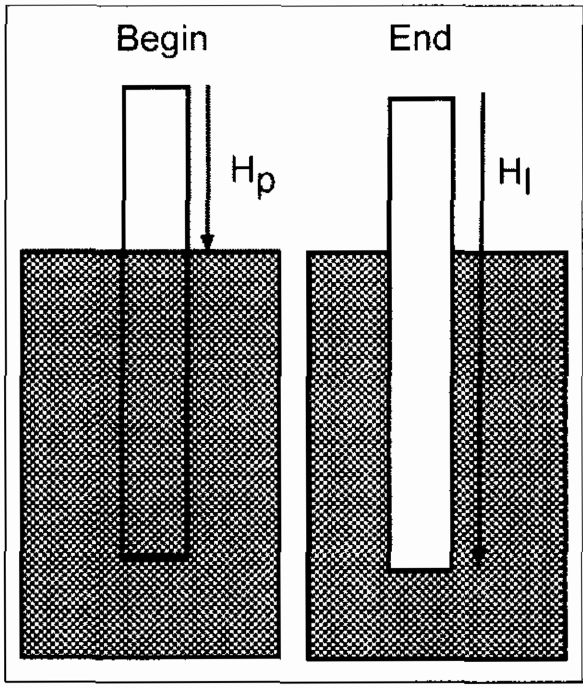

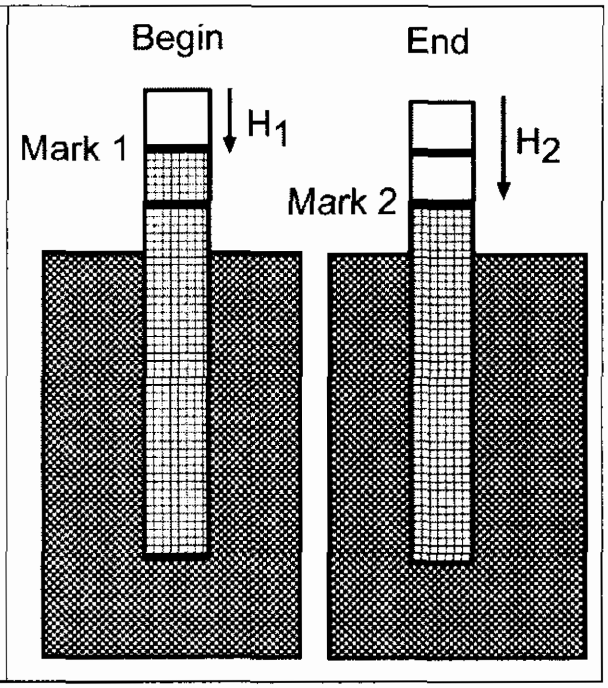

Figure 4.17: On-off McGill sensor.

Figure 4.18: JK sensor.

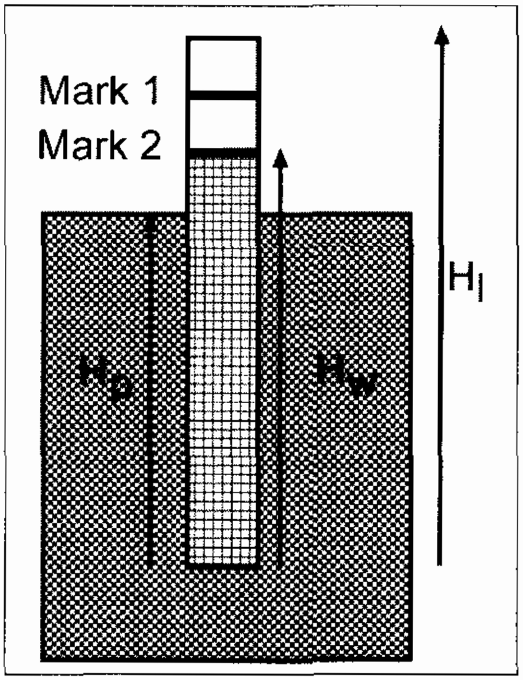

Figure 4.19: Components used to derive "JK Equation".

4.3.2 Continuous technique

4.3.2.1 McGill continuous

This constitutes an open vessel steady state gas flow case, i.e., the McGill continuous sensor (Figure 4.20).

Consider $q_{KPS,in}$ and $q_{KPS,out} \neq 0$. Then the general mass balance, Equation 4.34,

$$q_{KPS,in} - q_{KPS,out} = \frac{d}{dt}(\rho V) \qquad \text{Eq. (4.34)}$$

becomes Equation 4.35,

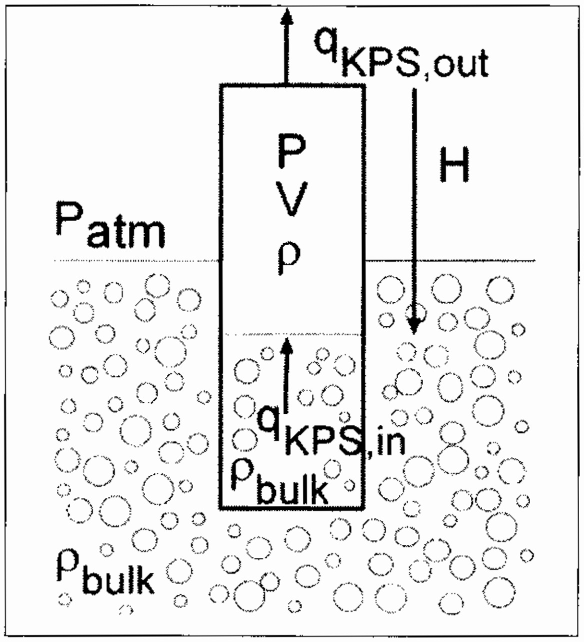

Figure 4.20: Continuous McGill sensor.

$$q_{KPS,in} = q_{KPS,out} \qquad \text{Eq. (4.35)}$$

The flow of gas leaving the sensor can be calculated from the pressure drop, ΔP (steady state pressure, P_s minus atmospheric pressure, P_{atm}, in kPa), using the calibration equation[5],

$$q_{SCMS,out} = a_{SCMS}\sqrt{\frac{\Delta P}{\rho}} + b_{SCMS} \qquad \text{Eq. (4.36)}$$

where a_{SCMS} and b_{SCMS} are the coefficients from the calibration of the orifice and is calculated at P_S as,

[5] Equation 3.33 does not consider an intercept coefficient (b), but it is necessary to include one because the linear fit of the orifice calibration data does not cross the intercept at zero, due to growing inaccuracy as pressure drop approaches zero.

$$\rho = \frac{28.8P_s}{R(273.15+T)0.9996} \qquad \text{Eq. (4.37)}$$

Thus,

$$q_{SCMS,in} = a_{SCMS}\sqrt{\frac{\Delta P}{\rho}} + b_{SCMS} \qquad \text{Eq. (4.38)}$$

$$q_{SCMS,in} = J_{gSTD}A \qquad \text{Eq. (4.39)}$$

Thus,

$$J_{g,STD} = \frac{a_{SCMS}\sqrt{\frac{\Delta P}{\rho}} + b_{SCMS}}{A} \qquad \text{Eq. (4.40)}$$

Solving Equation 4.40 gives J_g at standard conditions ($J_{g,STD}$) from the steady state pressure P_s. The J_g at the bottom of the tube ($J_{g,Pl}$) is,

$$J_{g,P_l} = J_{g,STD}\frac{(101325)T}{P_l(273.15)} \qquad \text{Eq. (4.41)}$$

An example of J_g calculation is shown in Appendix A.2.

4.3.2.2 Dynamic response for the McGill continuous sensor to a step change

This constitutes the case were the rate of accumulation differs from zero. Applying the chain rule to Equation 4.34,

$$q_{KPS,in} - q_{KPS,out} = \frac{d}{dP}(\rho V)\frac{dP}{dt} \qquad \text{Eq. (4.42)}$$

using $\rho_s = \rho_{bulk}$ and Equation 4.11 as follows,

$$\frac{d}{dP}(\rho V) = \frac{\rho V}{\gamma P} + \frac{\rho A}{\rho_{bulk} g} \approx A\overline{\rho}\left(\frac{\overline{H}}{\gamma \overline{P}} + \frac{1}{\rho_{bulk} g}\right) = C_e \qquad \text{Eq. (4.43)}$$

and, substituting Equation 4.43 in 4.42, derives :

$$q_{KPS,in} - q_{KPS,out} = C_e \frac{dP}{dt} \qquad \text{Eq. (4.44)}$$

The flow of gas leaving the sensor is again expressed as follows,

$$q_{KPS,out} \approx \frac{1}{R_s}\sqrt{P - P_{atm}} \qquad \text{Eq. (4.45)}$$

Substituting Equation 4.45 in 4.44 yields,

$$q_{KPS,in} - \frac{\sqrt{P - P_{atm}}}{R_s} = C_e \frac{d(P - P_{atm})}{dt} \qquad \text{Eq. (4.46)}$$

And, ordering,

$$C_e \frac{d}{dt}(P - P_{atm}) = q_{KPS,in} - \frac{\sqrt{P - P_{atm}}}{R_s} \qquad \text{Eq. (4.47)}$$

This is a non-linear dynamic system. A standard approach to solving is to linearize over limited ranges [61]. In the present case the typical step change is J_g = 1 to 1.30 (cm/s), equivalent to a pressure drop of 1177 to 2942 (Pa) (12 to 30 cm of Water). This is a sufficiently narrow range for linearization. (The consequences are explored later in the Section 5.7.3.) To linearize Equation 4.47 it is necessary to introduce a deviation variable [48,61].

$$\frac{1}{R_s}\sqrt{P} = \frac{1}{R_s}\sqrt{P_0} + \left[\frac{d}{dP}\left(\frac{1}{R_s}\sqrt{P}\right)\right]_{P=P_0}(P-P_0) + \left[\frac{d^2}{dP^2}\left(\frac{1}{R_s}\sqrt{P}\right)\right]_{P=P_0}\frac{(P-P_0)^2}{2!} + \ldots$$

Eq. (4.48)

$$\frac{1}{R_s}\sqrt{P} = \frac{1}{R_s}\sqrt{P_0} + \frac{1}{R_s 2\sqrt{P_0}}(P-P_0) - \frac{1}{8R_s\sqrt[3]{P_0^{\,2}}}(P-P_0)^2 \ldots \quad \text{Eq. (4.49)}$$

Neglecting terms of order two and higher, substituting P by $P-P_{atm}$ and P_0 by P_0-P_{atm}.

$$\frac{1}{R_s}\sqrt{P-P_{atm}} \approx \frac{1}{R_s}\sqrt{P_0-P_{atm}} + \frac{1}{R_s 2\sqrt{P_0-P_{atm}}}(P-P_0) \qquad \text{Eq. (4.50)}$$

then, substituting Equation 4.50 in 4.47 gives,

$$C_e\frac{d(P-P_{atm})}{dt} + \frac{P-P_o}{2R_s\sqrt{P_0-P_{atm}}} = q_{KPS,in} - \frac{1}{R_s}\sqrt{P_0-P_{atm}} \qquad \text{Eq. (4.51)}$$

Letting P_s be the steady-state pressure for a given value of $q_{KPS,in,s}$ (inlet flow rate), then linealization around P_s-P_{atm} gives,

$$C_e\frac{d(P-P_{atm})}{dt} + \frac{P-P_s}{2R_s\sqrt{P_s-P_{atm}}} = q_{KPS,in} - \frac{1}{R_s}\sqrt{P_s-P_{atm}} \qquad \text{Eq. (4.52)}$$

and at steady-state, Equation 4.47 becomes,

$$C_e \frac{d(P_s - P_{atm})}{dt} = q_{KPS,in,s} - \frac{\sqrt{P_s - P_{atm}}}{R_s} \qquad \text{Eq. (4.53)}$$

Subtracting Equation 4.53 from 4.52 yields,

$$C_e \frac{d(P - P_s)}{dt} + \frac{(P - P_s)}{2R_s\sqrt{P_s - P_{atm}}} = q_{KPS,in} - q_{KPS,in,s} \qquad \text{Eq. (4.54)}$$

Defining the deviation variables

$$P^* = P - P_s \text{ and } q^*_{KPS,in} = q_{KPS,in} - q_{KPS,in,s} \qquad \text{Eq. (4.55)}$$

we find the following linearized form in terms of deviation variables:

$$C_e \frac{dP^*}{dt} + \frac{P^*}{2R_s\sqrt{P_s - P_{atm}}} = q^*_{KPS,in} \qquad \text{Eq. (4.56)}$$

Ordering the equation yields the following transfer function:

$$\underbrace{2\sqrt{P_s - P_{atm}}R_sC_e}_{\tau_p} \frac{dP^*}{dt} + P^* = \underbrace{2\sqrt{P_s - P_{atm}}R_s}_{K_p} q^*_{KPS,in} \qquad \text{Eq. (4.57)}$$

where K_p and τ_p are defined as the steady state or static gain and the time constant, respectively [61].

If $P^*(t)$ and $q^*_{in}(t)$ are the terms of deviation variables around steady state, the initial conditions are:

$$P^*(0) = 0 \text{ and } q^*_{KPS,\,in}(0) = 0 \qquad \text{Eq. (4.58)}$$

Finally, the transfer function of Equation 4.57 is given by,

$$G(s) = \frac{\bar{P}^*(s)}{\bar{q}^*_{KPS,in}(s)} = \frac{K_p}{\tau_p s + 1} \qquad \text{Eq. (4.59)}$$

Let us examine the response to a unit step change in $q_{KPS,in}$, since $\bar{q}^*_{KPS,in}(s) = 1/s$

$$\bar{P}^*(s) = \frac{K_p}{s(\tau_p s + 1)} = \frac{K_p}{s} - \frac{K_p \tau_p}{\tau_p s + 1} \qquad \text{Eq. (4.60)}$$

Inverting Equation 4.60,

$$P^*(t) = K_p\left(1 - e^{(-t/\tau_p)}\right) \qquad \text{Eq. (4.61)}$$

If the step change in $q_{KPS,in}$ was of magnitude B, then the response is,

$$P^*(t) = BK_p\left(1 - e^{(-t/\tau_p)}\right) \qquad \text{Eq. (4.62)}$$

and, finally,

$$P^*(t) = 2B\sqrt{P_s - P_{atm}}R_s(1 - e^{(-t/2\sqrt{P_s - P_{atm}}R_s C_e)}) \qquad \text{Eq. (4.63)}$$

Equation 4.63 relates the pressure with time for gas flowing through an orifice of resistance R_s, steady-state pressure P_s and sensor setup characteristics C_e [65].

4.4 Error propagation analysis for the J_g sensors

It is important to determine the effect of error in the measurements (Pressure, H_p, H_l, etc) on the estimated J_g. The assumption is that the measured variables are accurate.

The variance of the estimated J_g is calculated by expanding each function as a Taylor series about the mean. If only the zero and first order terms of the expansion are considered and the covariances between the variables are assumed to be zero, the variance will be as follows.

4.4.1 On-off McGill

a) Equation 4.23

$$J_g = \left(\frac{\rho_{bulk} g \frac{(H_l + H_p)}{2} + \gamma \left(P_{atm} + \rho_{bulk} g \frac{(H_l - H_p)}{2} \right)}{\gamma (P_{atm} + \rho_{bulk} g (H_l - H_p)) \rho_{bulk} g} \right) \frac{dP}{dt}$$

$$S_{J_g}^2 = \left(\frac{\partial J_g}{\partial \rho_b} \right)^2 S_{\rho_b}^2 + \left(\frac{\partial J_g}{\partial \frac{dP}{dt}} \right)^2 S_{\frac{dP}{dt}}^2 \qquad \text{Eq. (4.64)}$$

Table 4.1: Derivatives.

$\left(\frac{\partial J_g}{\partial \rho_b}\right)$	$\left(-\frac{\frac{dP}{dt}\left(g^2(H_l^2-H_p^2)\rho_{bulk}{}^2+\gamma(2P_{atm}^2+4g(H_l-H_p)P_{atm}\rho_{bulk}+g^2(H_l-H_p)^2\rho_{bulk}^2)\right)}{2g\gamma\rho_{bulk}^2(P_{atm}+g(H_l-H_p)\rho_{bulk})^2}\right)$ Eq. (4.65)
$\left(\frac{\partial J_g}{\partial \frac{dP}{dt}}\right)$	$\left(\frac{\rho_{bulk}g\frac{(H_l+H_p)}{2}+\gamma\left(P_{atm}+\rho_{bulk}g\frac{(H_l-H_p)}{2}\right)}{\gamma(P_{atm}+\rho_{bulk}g(H_l-H_p))\rho_{bulk}g}\right)$ Eq. (4.66)

An example of calculating J_g using Equations 4.65 and 4.66 is presented in Appendix A.3.

b) Equation 4.25

$$J_g=\left(\frac{P_{atm}+\rho_{bulk}gH_l}{(P_{atm}+\rho_{bulk}g(H_l-H_p))\rho_{bulk}g}\right)\frac{dP}{dt}$$

$$S_{J_g}^2=\left(\frac{\partial J_g}{\partial \rho_b}\right)^2 S_{\rho_b}^2+\left(\frac{\partial J_g}{\partial \frac{dP}{dt}}\right)^2 S_{\frac{dP}{dt}}^2 \qquad \text{Eq. (4.67)}$$

Table 4.2: Derivatives.

$\left(\dfrac{\partial J_g}{\partial \rho_b}\right)$	$\left(-\dfrac{\dfrac{dP}{dt}(P_{atm}^2+2g(H_l-H_p)P_{atm}\rho_{bulk}+g^2H_l(H_l-H_p)\rho_{bulk}^2}{g\rho_{bulk}^2(P_{atm}+g(H_l-H_p)\rho_{bulk})^2}\right)$ Eq. (4.68)
$\left(\dfrac{\partial J_g}{\partial \dfrac{dP}{dt}}\right)$	$\left(\dfrac{P_{atm}+\rho_{bulk}gH_l}{(P_{atm}+\rho_{bulk}g(H_l-H_p))\rho_{bulk}g}\right)$ Eq. (4.69)

4.4.2 JK

a) Equation 4.30

$$J_g=\left(\frac{\rho_s g\dfrac{(H_2+H_1)}{2}+\gamma\left(P_{atm}-\rho_s g\left(Hp-\dfrac{(H_1+H_2)}{2}\right)+\rho_{bulk}g(H_l-H_p)\right)}{\gamma(P_{atm}+\rho_{bulk}g(H_l-H_p))\rho_s g}\right)\rho_s g\frac{dH}{dt}$$

$$S_{J_g}^2=\left(\frac{\partial J_g}{\partial \rho_b}\right)^2 S_{\rho_b}^2+\left(\frac{\partial J_g}{\partial \rho_s}\right)^2 S_{\rho_s}^2+\left(\frac{\partial J_g}{\partial \dfrac{dH}{dt}}\right)^2 S_{\frac{dH}{dt}}^2 \qquad \text{Eq. (4.70)}$$

Table 4.3: Derivatives.

$\left(\dfrac{\partial J_g}{\partial \rho_b}\right)$	$\left(-\dfrac{g^2(H_l - H_p)(H_1 + H_2 + \gamma H_1 + \gamma H_2 - 2\gamma H_p)\rho_s \dfrac{dH}{dt}}{2\gamma(P_{atm} + g(H_l - H_p)\rho_{bulk})^2}\right)$ Eq. (4.71)
$\left(\dfrac{\partial J_g}{\partial \rho_s}\right)$	$\left(\dfrac{g(H_1 + H_2 + H_1\gamma + H_2\gamma - 2H_p\gamma)\dfrac{dH}{dt}}{2\gamma(P_{atm} + g(H_l - H_p)\rho_{bulk})}\right)$ Eq. (4.72)
$\left(\dfrac{\partial J_g}{\partial \frac{dH}{dt}}\right)$	$\left(\dfrac{\rho_s g\dfrac{(H_2 + H_1)}{2} + \gamma\left(P_{atm} + g\left(H_l\rho_{bulk} + \dfrac{(H_1 + H_2)}{2}\rho_s - H_p(\rho_{bulk} + \rho_s)\right)\right)}{\gamma(P_{atm} + \rho_{bulk} g(H_l - H_p))}\right)$ Eq. (4.73)

b) Equation 4.32

$$J_g = \left(\frac{P_{atm} + \rho_s g(H_2 + H_1) - \rho_s g H_p}{P_{atm} + \rho_{bulk} g(H_l - H_p)}\right)\frac{dH}{dt}$$

$$S_{J_g}^2 = \left(\frac{\partial J_g}{\partial \rho_b}\right)^2 S_{\rho_b}^2 + \left(\frac{\partial J_g}{\partial \rho_s}\right)^2 S_{\rho_s}^2 + \left(\frac{\partial J_g}{\partial \frac{dH}{dt}}\right)^2 S_{\frac{dH}{dt}}^2 \qquad \text{Eq. (4.74)}$$

Table 4.4: Derivatives.

$\left(\frac{\partial J_g}{\partial \rho_b}\right)$	$\left(\frac{g^2(H_1+H_2-H_p)(-H_l+H_p)\rho_s \frac{dH}{dt}}{(P_{atm}+g(H_l-H_p)\rho_{bulk})^2}\right)$ Eq. (4.75)
$\left(\frac{\partial J_g}{\partial \rho_s}\right)$	$\left(-\frac{g(H_1+H_2-H_p)\frac{dH}{dt}}{-P_{atm}-g(H_l+H_p)\rho_{bulk}}\right)$ Eq. (4.76)
$\left(\frac{\partial J_g}{\partial \frac{dH}{dt}}\right)$	$\left(\frac{P_{atm}+g(H_l\rho_{bulk}+(H_2+H_1)\rho_s-H_p(\rho_{bulk}+\rho_s))}{P_{atm}+\rho_{bulk}g(H_l-H_p)}\right)$ Eq. (4.77)

4.4.3 McGill continuous

Equation 4.40

$$J_{g,STD}=\frac{a_{SCMS}\sqrt{\frac{P_s-P_{atm}}{\rho}}+b_{SCMS}}{A}$$

$$S_{J_g}^2=\left(\frac{\partial J_g}{\partial a_{SCMS}}\right)^2 S_{a_{SCMS}}^2+\left(\frac{\partial J_g}{\partial b_{SCMS}}\right)^2 S_{b_{SCMS}}^2+\left(\frac{\partial J_g}{\partial P_s}\right)^2 S_{P_s}^2+\left(\frac{\partial J_g}{\partial A}\right)^2 S_A^2$$

Eq. (4.78)

Table 4.5: Derivatives.

$\left(\dfrac{\partial P}{\partial a_{SCMS}}\right)$	$\dfrac{280.75\sqrt{1-\dfrac{P_{atm}}{P_s}}}{A}$	Eq. (4.79)
$\left(\dfrac{\partial P}{\partial b_{SCMS}}\right)$	$\dfrac{1}{A}$	Eq. (4.80)
$\left(\dfrac{\partial P}{\partial P_s}\right)$	$\dfrac{140.38a_{SCMS}P_{atm}}{A\sqrt{1-\dfrac{P_{atm}}{P_s}}P_s^{\ 2}}$	Eq. (4.81)
$\left(\dfrac{\partial J_g}{\partial P_{atm}}\right)$	$-\dfrac{140.38a_{SCMS}}{A\sqrt{1-\dfrac{P_{atm}}{P_s}}P_s}$	Eq. (4.82)
$\left(\dfrac{\partial J_g}{\partial A}\right)$	$-\dfrac{b_{SCMS}+280.75a_{SCMS}\sqrt{1-\dfrac{P_{atm}}{P_s}}}{A^2}$	Eq. (4.83)

4.5 Sensitivity coefficients for the J_g sensors

A total differential can be used to study the individual effect of a measured variable on a function of two or more variables [54]. If the variables are independent then, for example, FP is,

$$FP = (\rho_{bulk}, H_l, H_p) \qquad \text{Eq. (4.84)}$$

The total differential is the sum of the partial differential of the independent variables:

$$dFP = \frac{\partial FP}{\partial \rho_{bulk}} d\rho_{bulk} + \frac{\partial FP}{\partial H_p} dH_p + \frac{\partial FP}{\partial H_l} dH_l \qquad \text{Eq. (4.85)}$$

Dividing Equation 4.85 by FP yields,

$$\frac{dFP}{FP} = X_{\rho_{bulk}} \frac{d\rho_{bulk}}{\rho_{bulk}} + X_{H_p} \frac{dH_p}{H_p} + X_{H_l} \frac{dH_l}{H_l} \qquad \text{Eq. (4.86)}$$

where $X_{\rho_{bulk}}$, X_{H_p} and X_{H_l} are the sensitivity coefficients for the variables.

Miller noted that the terms associated with each sensitivity coefficient represent relative changes in the variables, thus the percentage change in FP can be calculated as the sum of products formed when each sensitivity coefficient is multiplied by the percentage change in its associated variable.

The sensitivity coefficients for the model described in this thesis are presented for the three techniques. The sensitivity coefficients for the discontinuous techniques are derived from the respective FP, i.e., for the on-off McGill and JK, (Equations 4.23 and 4.30) respectively, and for the continuous McGill, by Equation 4.40.

4.5.1 On-off McGill

Table 4.6: Sensitivity coefficients for the on-off McGill sensor.

X_{ρ_b}	$$\left(-\frac{\rho_{bulk}(g^2(H_l^2-H_p^2)\rho_{bulk}{}^2+\gamma(2P_{atm}^2+4g(H_l-H_p)P_{atm}\rho_{bulk}+g^2(H_l-H_p)^2\rho_{bulk}^2)}{2g\gamma\rho_{bulk}^2(P_{atm}+g(H_l-H_p)\rho_{bulk})^2}\right)$$ Eq. (4.87)
X_{H_p}	$$\left(\frac{(g\rho_{bulk}(P_{atm}(\gamma+1)+2gH_l\rho_{bulk}))H_p}{(P_{atm}+g(H_l-H_p)\rho_{bulk})(g(H_l+H_p)\rho_{bulk}+\gamma(2P_{atm}+g(H_l-H_p)\rho_{bulk}))}\right)$$ Eq. (4.88)
X_{H_l}	$$\left(-\frac{(g\rho_{bulk}(P_{atm}(\gamma-1)+2gH_p\rho_{bulk}))H_l}{(P_{atm}+g(H_l-H_p)\rho_{bulk})(g(H_l+H_p)\rho_{bulk}+\gamma(P_{atm}+g(H_l-H_p)\rho_{bulk}))}\right)$$ Eq. (4.89)

An example of sensitivity coefficient calculations using Equations 4.87, 4.88 and 4.89 is presented in Appendix A.4.

4.5.2 JK

Table 4.7: Sensitivity coefficients for the JK sensor.

X_{ρ_b}	$$\left(\begin{array}{l}-\dfrac{g^2(H_l-H_p)(H_1+H_2+\gamma H_1+\gamma H_2-2\gamma H_p)\rho_s\rho_{bulk}}{(P_{atm}+g(H_l-H_p)\rho_{bulk})(g(H_1+H_2)\rho_s+\gamma(2P_{atm}+..} \\ \\ +g(2H_l\rho_{bulk}+(H_1+H_2)\rho_s-2Hp(\rho_{bulk}-\rho_s))))\end{array}\right)$$ Eq. (4.90)

Table 4.7: Sensitivity coefficients for the JK sensor (cont.).

X_{ρ_s}	$\left(\frac{g(H_1+H_2+H_1\gamma+H_2\gamma-2H_p\gamma)\rho_s}{\begin{array}{l} g(H_1+H_2)\rho_s+\gamma(2P_{atm}+.. \\ +g(2H_l\rho_{bulk}+(H_1+H_2)\rho_s-2H_p(\rho_{bulk}+\rho_s))) \end{array}}\right)$ Eq. (4.91)
X_{H_l}	$\left(-\frac{g^2(H_1+H_2+\gamma H_1+\gamma H_2-2\gamma H_p)\rho_s\rho_{bulk}H_l}{\begin{array}{l} (P_{atm}+g(H_l-H_p)\rho_{bulk})(g(H_1+H_2)\rho_s+.. \\ +\gamma(2P_{atm}+g(2H_l\rho_{bulk}+(H_1+H_2)\rho_s-2H_p(\rho_{bulk}+\rho_s)))) \end{array}}\right)$ Eq. (4.92)
X_{H_p}	$\left(-\frac{g(g(H_1+H_2)\rho_{bulk}+\gamma(-2P_{atm}+g(H_1+H_2-2H_l)\rho_{bulk}))\rho_s H_p}{\begin{array}{l} (P_{atm}+g(H_l-H_p)\rho_{bulk})(g(H_1+H_2)\rho_s+.. \\ +\gamma(2P_{atm}+g(2H_l\rho_{bulk}+(H_1+H_2)\rho_s-2H_p(\rho_{bulk}+\rho_s)))) \end{array}}\right)$ Eq. (4.93)
X_{H_1}	$\left(\frac{g(1+\gamma)\rho_s H_1}{\begin{array}{l} g(H_1+H_2)\rho_s+\gamma(2P_{atm}+.. \\ +g(2H_l\rho_{bulk}+(H_1+H_2)\rho_s-2H_p(\rho_{bulk}+\rho_s))) \end{array}}\right)$ Eq. (4.94)
X_{H_2}	$\left(\frac{g(1+\gamma)\rho_s H_2}{\begin{array}{l} g(H_1+H_2)\rho_s+\gamma(2P_{atm}+.. \\ +g(2H_l\rho_{bulk}+(H_1+H_2)\rho_s-2H_p(\rho_{bulk}+\rho_s))) \end{array}}\right)$ Eq. (4.95)
$X_{H_1+H_2}$	$\left(\frac{g(1+\gamma)\rho_s(H_1+H_2)}{\begin{array}{l} g(H_1+H_2)\rho_s+\gamma(2P_{atm}+.. \\ +g(2H_l\rho_{bulk}+(H_1+H_2)\rho_s-2H_p(\rho_{bulk}+\rho_s))) \end{array}}\right)$ Eq. (4.96)

4.5.3 McGill continuous

Table 4.8: Sensitivity coefficients.

$X_{a_{SCMS}}$	$\left(\dfrac{280.75\sqrt{1-\dfrac{P_{atm}}{P_s}}}{b_{SCMS}+280.75a_{SCMS}\sqrt{1-\dfrac{P_{atm}}{P_s}}} \right)$ Eq. (4.97)
$X_{b_{SCMS}}$	$\left(\dfrac{1}{b_{SCMS}+280.75a_{SCMS}\sqrt{1-\dfrac{P_{atm}}{P_s}}} \right)$ Eq. (4.98)
X_{P_s}	$\dfrac{0.5a_{SCMS}P_{atm}}{(0.00356187b_{SCMS}+a_{SCMS}\sqrt{1-\dfrac{P_{atm}}{P_s}})(\sqrt{1-\dfrac{P_{atm}}{P_s}}P_s^{\,2})}$ Eq. (4.99)
$X_{P_{atm}}$	$-\dfrac{140.38a_{SCMS}}{(b_{SCMS}+280.75a_{SCMS}\sqrt{1-\dfrac{P_{atm}}{P_s}})(\sqrt{1-\dfrac{P_{atm}}{P_s}}P_s)}$ Eq. (4.100)
X_A	$\left(-\dfrac{1}{A}\right)$ Eq. (4.101)

4.6 Computer derived sensitivity coefficients for the J_g sensors

Miller [54] notes that sensitivity coefficients derived by neglecting second and higher order derivatives are approximate and the complete solution for the J_g case should be programmed (i.e., for example in Microsoft Excel™) and the sensitivity coefficients for the different variables (ρ_{bulk}, ρ_s, H_p, H_l, etc), determined by, for example, incrementing each variable by 1 percent and calculating the percentage change in flow-rate when all the other variables remain fixed at the selected evaluation point.

An example of sensitivity coefficient calculations using this technique is presented Appendix A.5.

It can be observed in Appendices A.4 and A.5 that there is good agreement between the two sensitivity analysis techniques (data in Appendix F, Table F.8).

Error and sensitivity analysis will be performed in Chapter 5.

CHAPTER 5
SENSOR VALIDATION

5.1 Introduction

A series of experiments were designed to validate the discontinuous and continuous J_g sensors. Validation requires study of accuracy (how close is the value to an accepted independent measure) and sampling (how well does the value represent the system).

To test accuracy requires a standard measurement. The two major problems in testing the accuracy of the J_g sensor are: a) bubbles do not evenly distribute over a flotation cell or column [67], meaning the volumetric flow of gas into the cell cannot be used as standard, and b) There is no non-intrusive instrument to measure J_g in a dispersed system that may avoid this sampling issue. A rig (15.24 cm x 400 cm column) was setup to create a closed environment to conduct a mass balance as a way to study the accuracy. Tubes of 3 (7.62 cm) and 4 inch (10.16 cm) were used to conduct the tests.

The sampling tests used a 50 (cm) x 400 (cm) column and sensor tubes of different diameter. The on-off and continuous techniques shown a consistent agreement for 3 and 4 (inch) tubes. For tubes of diameter lower than 3, there is a difference between the techniques. The two major reasons are assumed to be, the cross sectional area of the sensor (in order to collect a representative sample) and the flow of liquid displaced downwards by the accumulating gas in the on-off technique, that excludes bubbles below a certain size from entering the sensor.

5.2 Calibrations

5.2.1 Mass flow meter calibration

A “wet test” was adapted based on literature [14]. The mass flow meter models were all MKS (Table 5.1). (The mass flow meter working principle was described in Chapter 3 Section 4.2). Figure 5.1 shows the experimental setup.

Table 5.1: MKS Mass flow meter.

Model	5 LPM	30 LPM	200 LPM	400 LPM*
Range (SCMS)	0-8.33 E-5	0-5E-4	0-3.33E-3	0-6.67E-3
* Flow meter was not calibrated.				

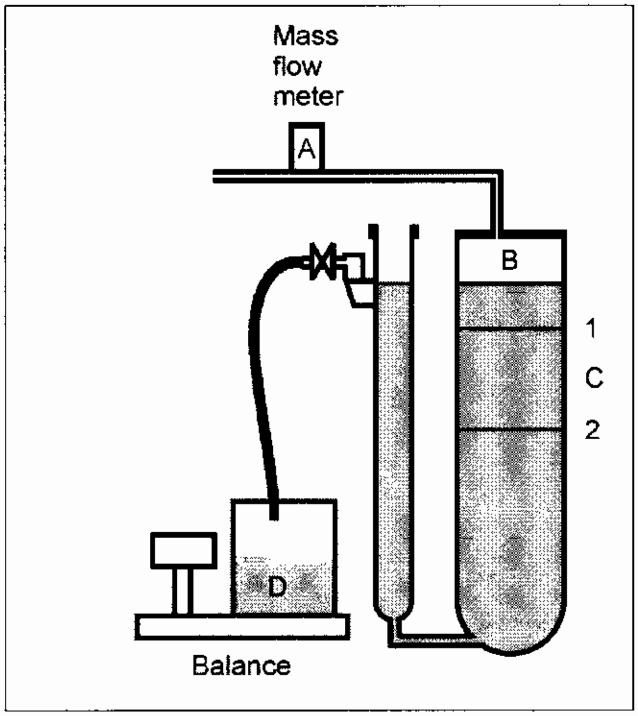

Figure 5.1: Setup for mass flow meter calibration.

The technique is as follows: air is introduced via the mass flow meter (A), which displaces the water (B), and the time taken for the level to travel between two marks is recorded while the displaced water (C) between the two marks is collected in a bucket and weighed (D).

The data for the mass flow meter calibrations are presented in Appendix F, Table F.1. The calibrations are given in Figures 5.2, 5.3 and 5.4 with the 95% confidence interval included (evident in Figure 5.4). The 400 LPM flow meter was not calibrated because the setup was not designed for such high flow. The raw data were fitted with second order polynomials (Appendix F, Table F.1). An example of the calculations is given in Appendix A.6.

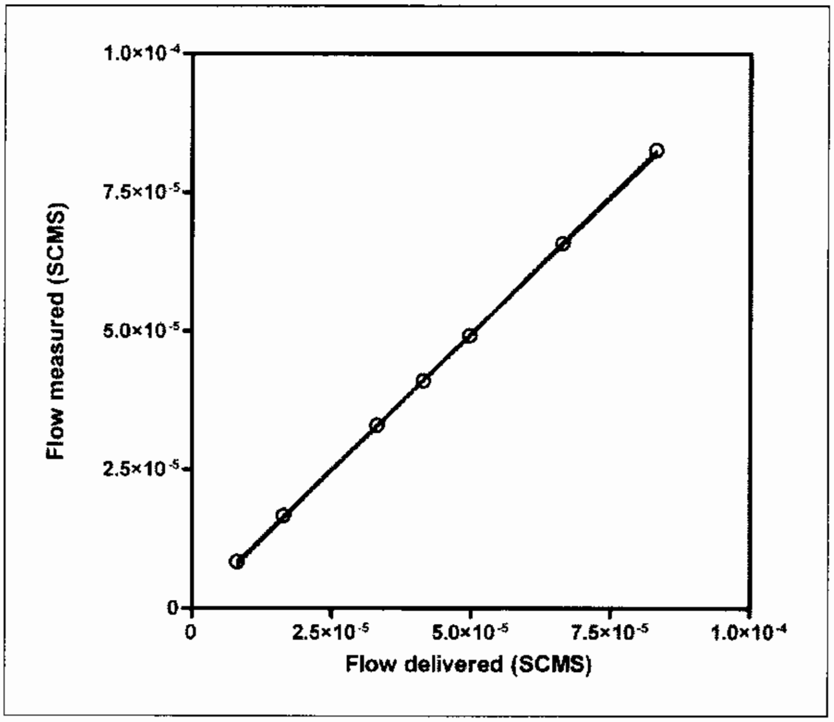

Figure 5.2: Calibration for the 5 LPM flow meter.

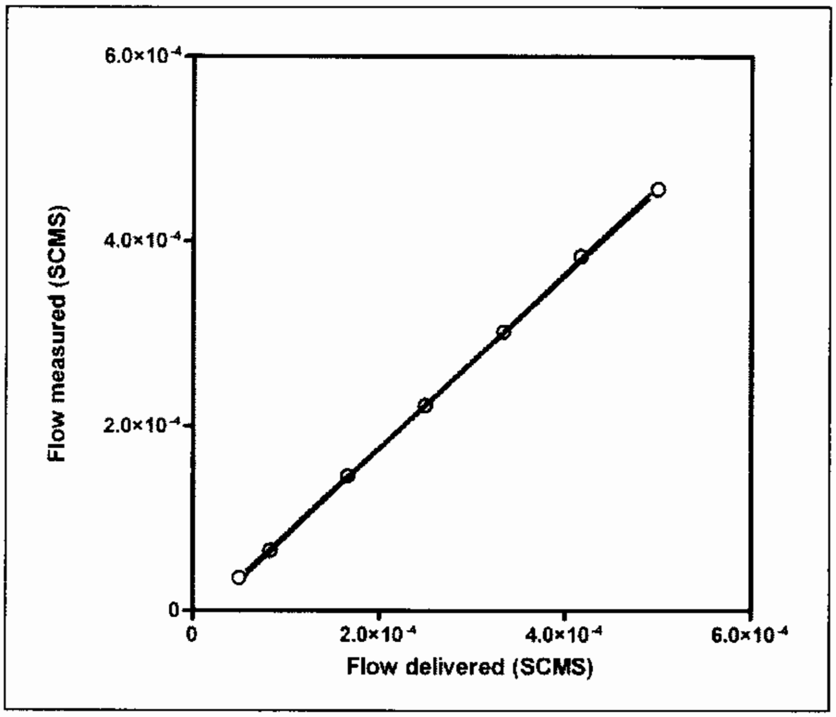

Figure 5.3: Calibration for the 30LPM flow meter.

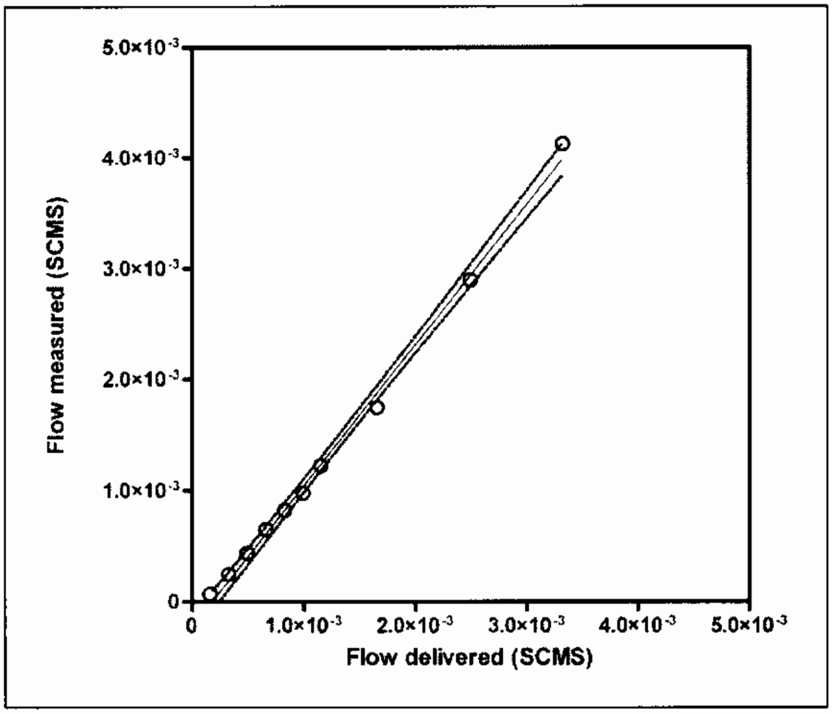

Figure 5.4: Calibration for the 200LPM flow meter.

5.2.2 Pressure transmitter calibration

The pressure transmitters were WIKA (model S-10) range 0 - 12442 (Pa) (0- 127 cm of water), serial numbers 6A and 4A. They were incorporated in a closed 6 (inch) (15.24 cm) diameter 4 m high column (Figure 5.5). The water displacement was measured using a ruler fixed to the column wall.

The technique is as follows: air is introduced through the mass flow meter (A), the flow of air (B) displaces the water a previously fixed distance and when the level reaches the bottom mark, the flow of air is stopped and the pressure is recorded.

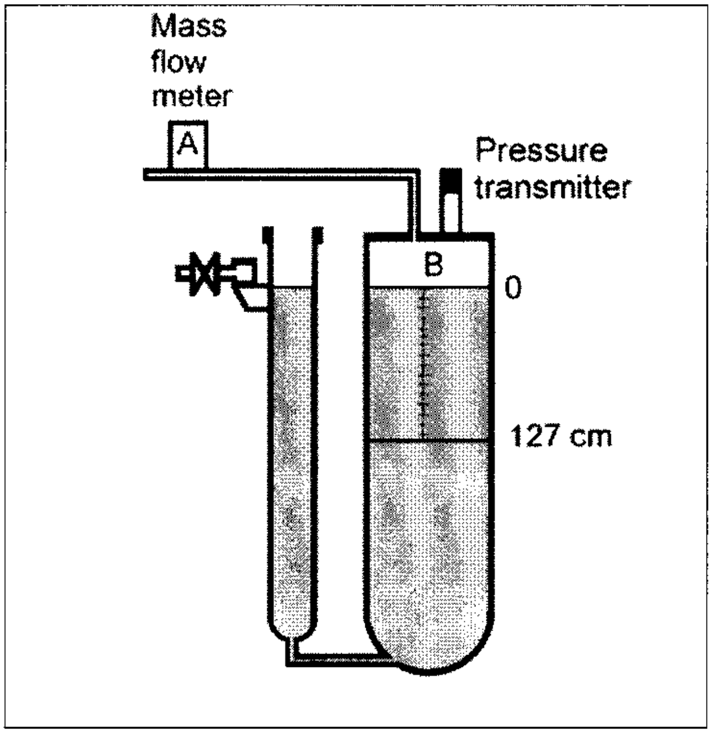

Figure 5.5: Pressure transmitter calibration.

The data for the pressure transmitter calibration are presented in Appendix F, Table F.2. The calibrations are given in Figure 5.6

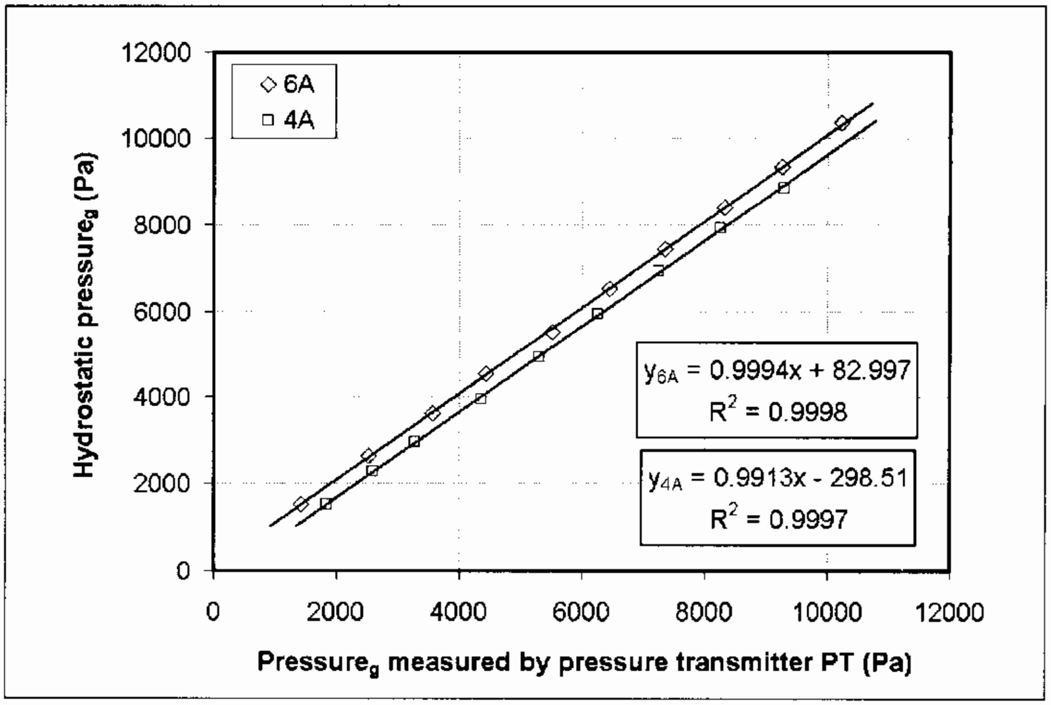

Figure 5.6: Pressure transmitter calibration. Note, subscript "g" stands for gauge.

5.3 Verification of flow calculation equation for discontinuous J_g sensor techniques

5.3.1 Laboratory test

The objective of the test was to verify Equations 4.23 (4.25), 4.30 (4.32) and 4.33b. As described in the Introduction of this chapter, the distribution of bubbles across the column diameter is not known, thus the real value of J_g at the sensor sampling location is unknown. To overcome this problem, air was introduced from the top of the sensor (Figures 5.7 and 5.8) through the 5 LPM mass flow meter.

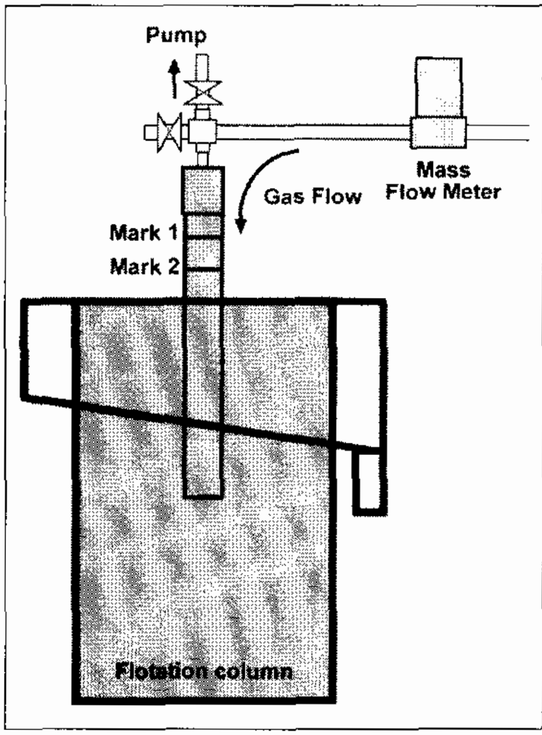

Figure 5.7: JK sensor.

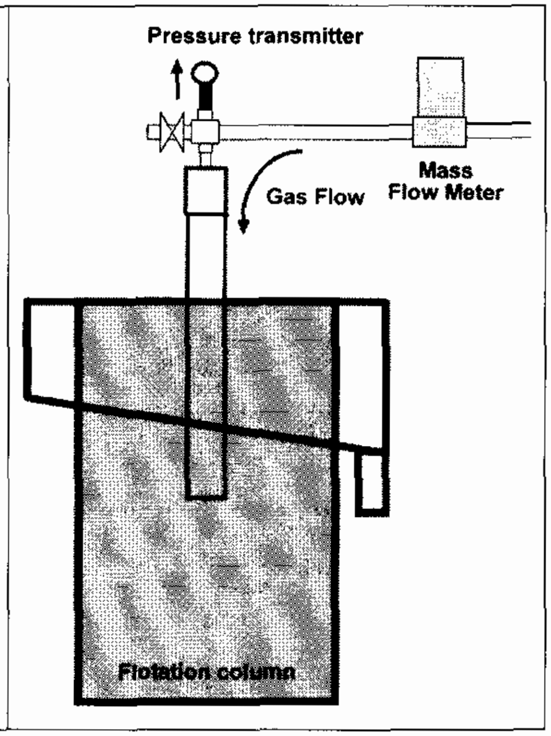

Figure 5.8: On-off McGill sensor.

The volumetric flow of gas (SCMS) and $J_{g\ STD}$[6] (cm/s) delivered to the sensor is presented in Table 5.2. Table 5.3 describes the characteristics of the two sensors.

Figure 5.9 illustrates the results for the verification test for on-off McGill and JK sensors. The data are presented in Appendix F, Table F.3. It was found that Equation 4.23 (adiabatic) fitted better than 4.25 (isothermic) for J_g higher than ca. 1.5 (cm/s) (4.23: error up to 1.2%, compared to 4.25: 3%), but for lower values the opposite was the case implying more isothermic behavior of the gas. Equation 4.30 shows a similar trend compared to 4.25 (4.30: error up to 0.6%,

[6] J_g calculated at standard conditions.

compared to 4.32: 3%). Equation 4.33b shows a bias over the range studied (error up to 7%).

Table 5.2: $J_{g\ STD}$ (cm/s) delivered to the sensor.

Q (SCMS)	1.56E-05	2.06E-05	2.56E-05	3.06E-05	3.57E-05	4.05E-05
J_g	0.5	0.75	1.00	1.25	1.75	2.00

Table 5.3: Characteristics of the two sensors tested.

	McGill	JK
H_l (m)	2.01	1.83
H_p (m)	1.24	1.055
H_1 (m)	-	0.68
H_2 (m)	-	0.98
ρ_b (kg/m^3)	1000	1000
ρ_s (kg/m^3)	1000	1000
Tube diameter (cm)	5.06	5.06
Distance Between marks (m)		0.30
Function P (m/Pa, dimensionless), Eq. 4.23 and 4.30	1.17E-4	1.04
Function P (m/Pa, dimensionless), Eq. 4.25 and 4.32 (4.33b)	1.22E-4	1.06 (0.99)

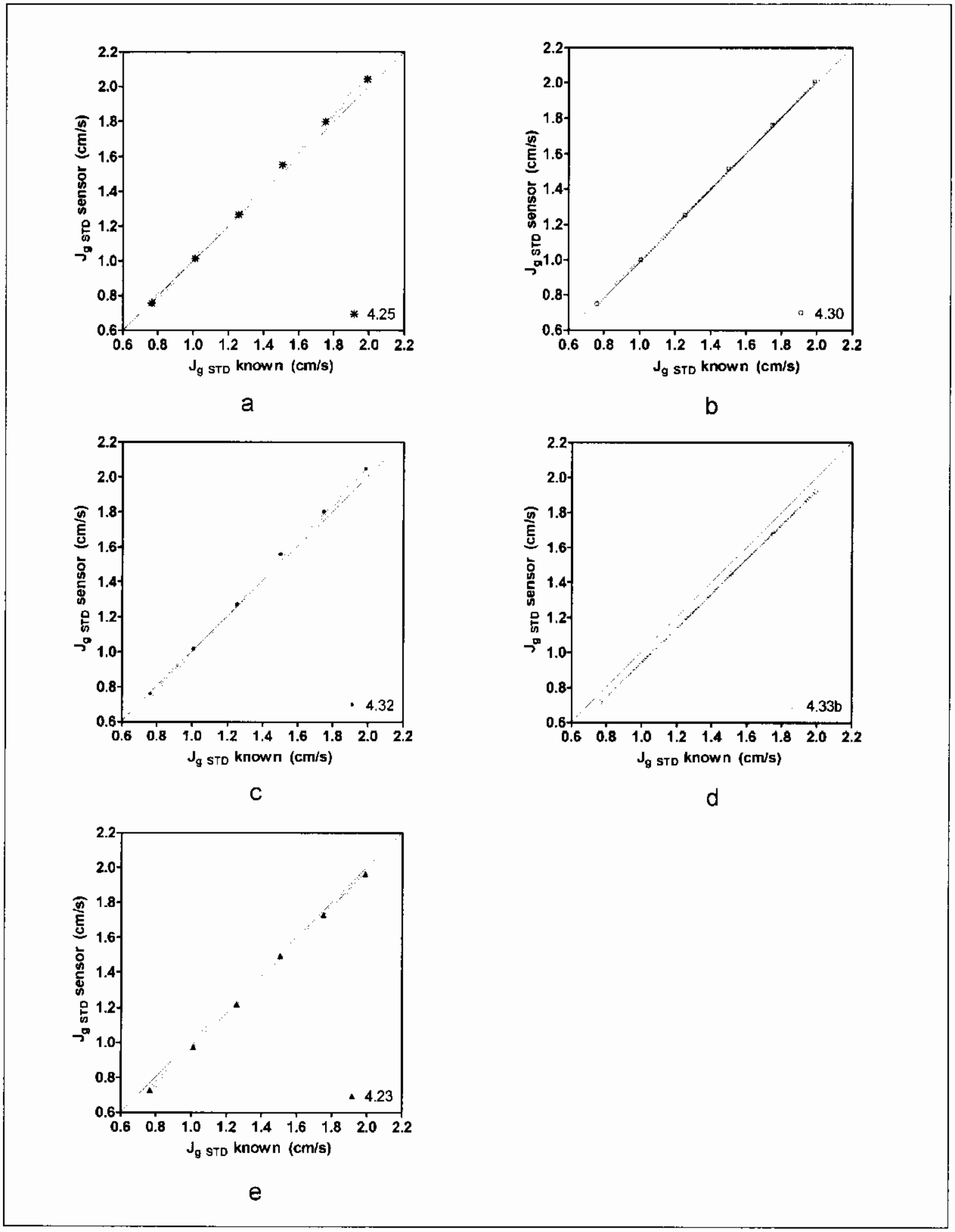

Figure 5.9: Verification plot for Equations a: 4.23, b: 4.25, c: 4.30, d: 4.32 and e: 4.33b.

5.3.2 Plant test (Northparkes and Red Dog Mine)

During the plant test at Northparkes (Australia), observed discrepancies between the on-off McGill and JK J_g techniques (data presented in Appendix F, Table F.4) prompted development of the general equation.

There was an opportunity to verify and compare the JK and on-off McGill techniques during the campaign at Red Dog (Alaska, USA). Testing in an OK50 flotation cell, a total of four gas flows were used. The data are presented in Appendix F, Table F.5. Figure 5.10 shows the setup: (Note, the JK sensor needs an operator, while the on-off McGill is logging data automatically.) Figure 5.11 gives the results and Appendix A.3 an example of calculation.

Over the mid–J_g range agreement is good among all candidate equations, considering that the sensors, while located close, are not at exactly the same spot. At the lowest gas rate, the McGill result is below the JK while the opposite is true at the highest gas rate. In 3 out of 4, the JK equation derived here gives a better agreement with McGill J_g results than the former JK equation, 4.33b, but in general terms the former and current JK versions are within experimental error.

It must be noted that all the data for the JK sensor needed to calculate the standard deviation for bulk density and sensor contents density were not available and the calculation of standard deviation for the JK measurement was only from the level displacement rate data ($\frac{\Delta H}{\Delta t}$).

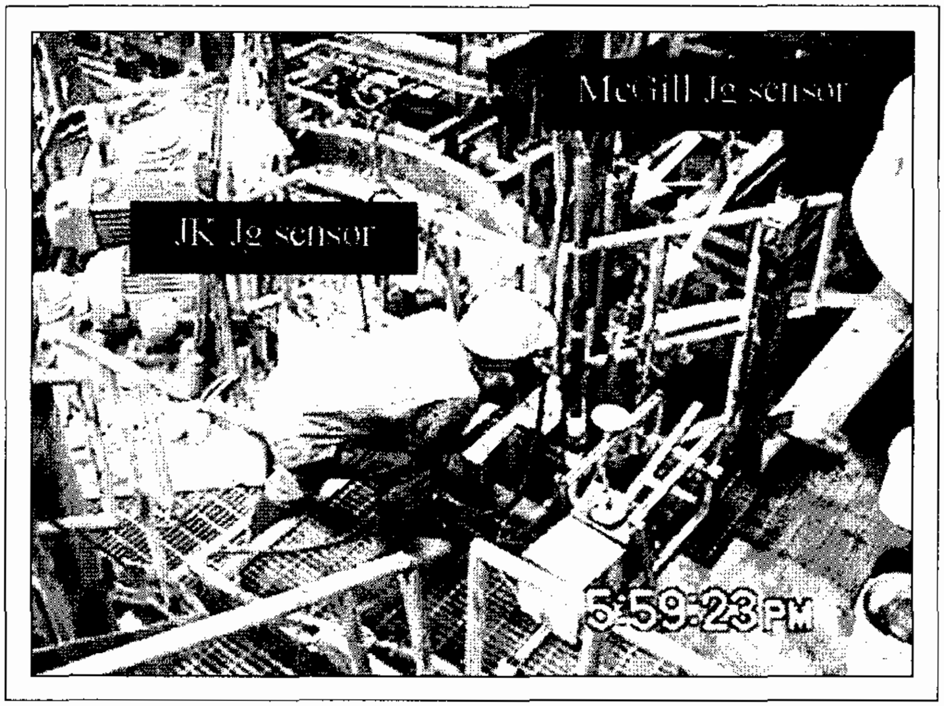

Figure 5.10: Sensor setup on top of an OK-50 flotation cell.

5.4 Bulk density measurement

Equation 4.23 introduced a variable that must be measured: Bulk density, the density of the aerated slurry. This can be estimated from two pressure signals (Figure 5.12), i.e.:

$$P_1 = \rho_{bulk} g H_1 \qquad \text{Eq. (5.1)}$$

$$P_2 = \rho_{bulk} g H_2 \qquad \text{Eq. (5.2)}$$

$$\bar{\rho}_{bulk} = \frac{P_2 - P_1}{g\Delta H} \qquad \text{Eq. (5.3)}$$

and, the variance can be estimated from:

$$S^2_{\rho_{bulk}} = \left(\frac{\partial \rho_{bulk}}{\partial (P_2 - P_1)}\right)^2 S^2_{\Delta P} \qquad \text{Eq. (5.4)}$$

Figure 5.13 shows the results of continuous measurement of bulk density over 5 days (Northparkes, Appendix F, Table F.6). It can be observed that the values are stable with the exception of day C when the mill was down; the origin of the "noisy" data, case e, was not identified, but the average follows the trend of previous days.

From Figure 5.13, it may be concluded that bulk density remains fairly constant over "normal" operating conditions (% solids, air rate). Thus periodic checking of bulk density for incorporation in the "J_g equation" should be sufficient most of the time.

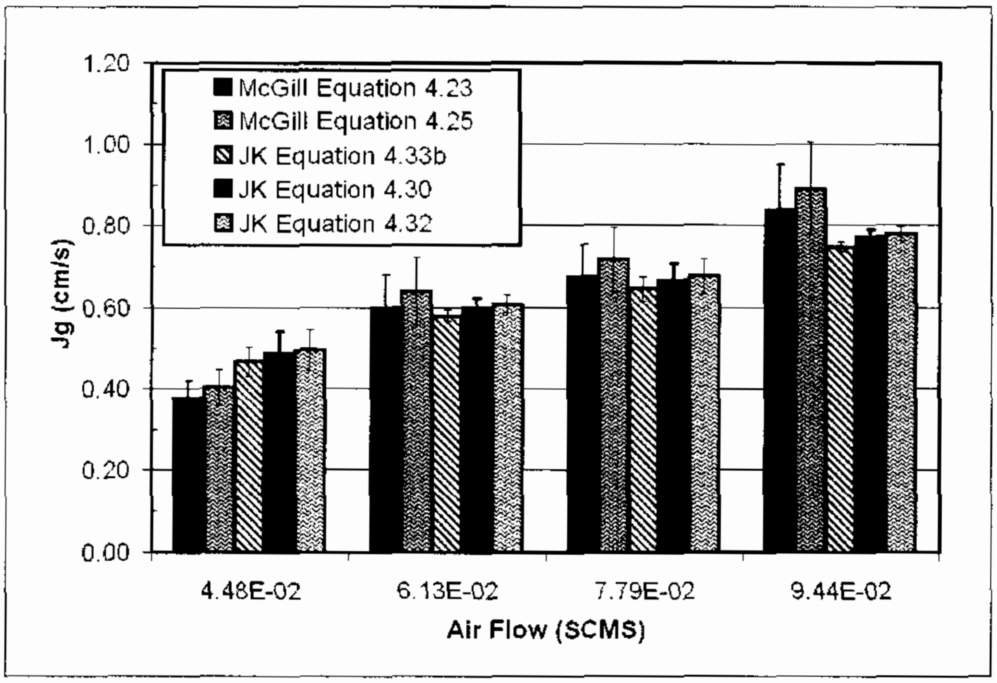

Figure 5.11: JK and on-off McGill J_g comparison, (J_g at 60 cm depth). Bars are standard deviation.

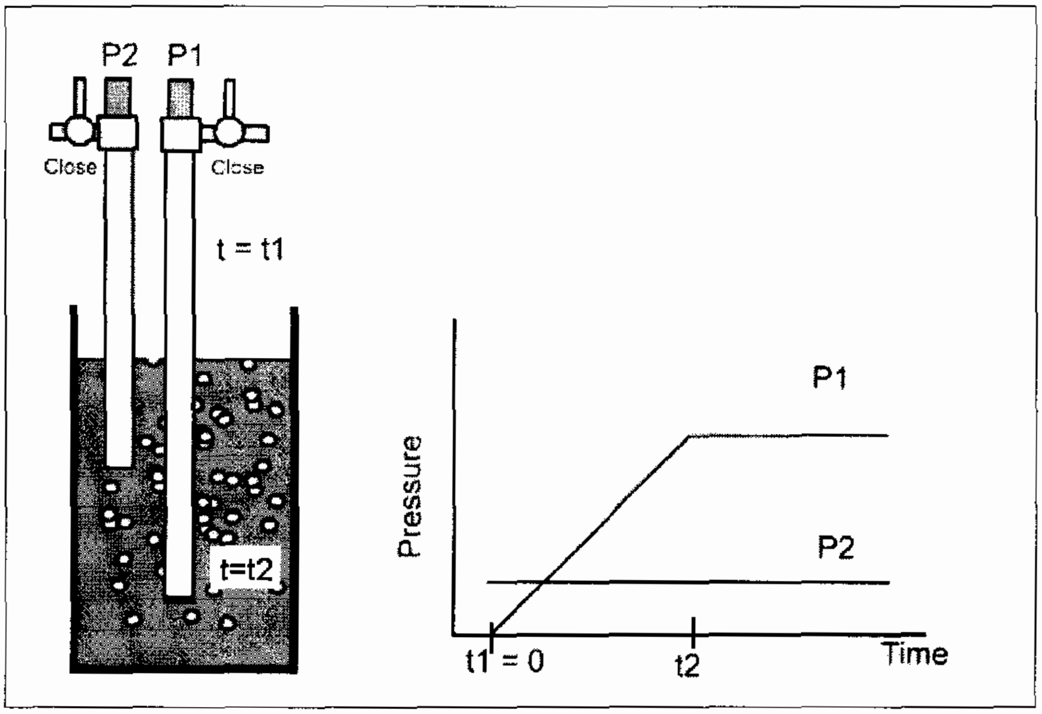

Figure 5.12: Bulk density measurement.

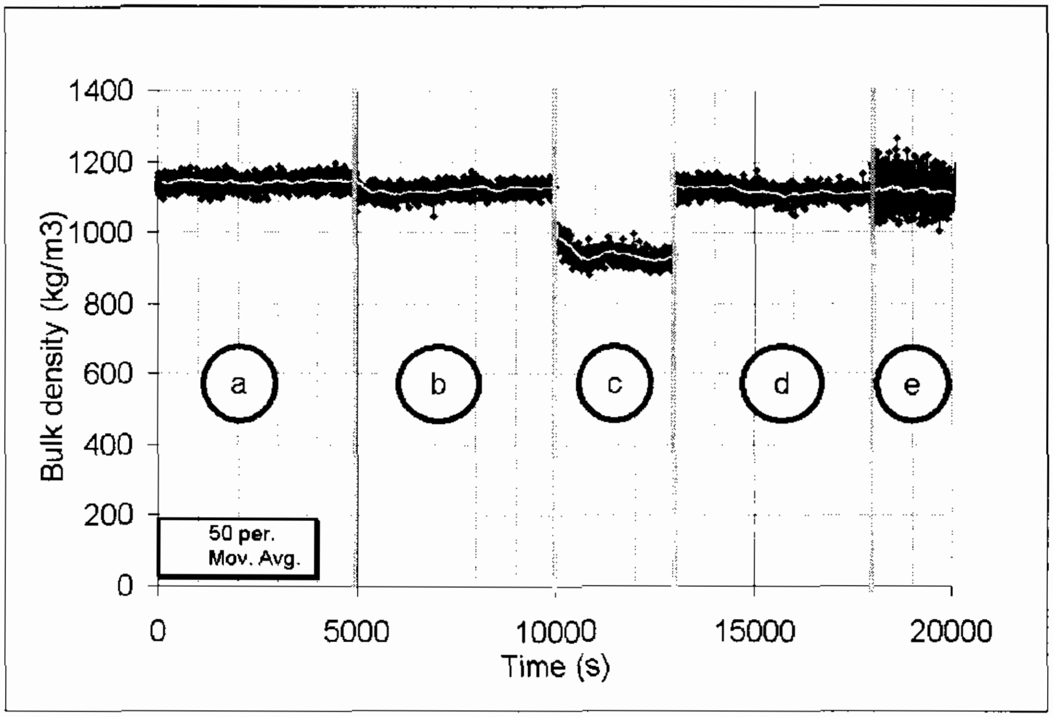

Figure 5.13: Rougher cell bulk density estimation at (date): a: 23-07-2001, b: 24-07-2001, c: 25-07-2001, d: 26-07-2001 and e: 30-07-2001.

5.5 Analysis of function P (FP)

It is useful to have both a qualitative (i.e., relative effect) and quantitative measure of how FP is affected by associated variables (since FP links measurement to J_g this is the key function to analyze). Figures 5.14 and 5.15 introduce FP nomographs for the McGill and JK sensors, respectively (see also Appendix F, Table F.7). The nomograph is constructed fixing the dimensions of the sensors (i.e., H_l and H_p) for a given gas holdup (in this case ε_g = 8,10,12%), and plotting FP against bulk density.

Figures 5.14 and 5.15 were plotted for three different tube lengths (H_l) at the same depth (ca. 1 m, close to upper limit of the current pressure transmitters), i.e., giving different H_l/H_p ratios. It can be observed for the McGill sensor (Figure 5.14) that at the same bulk density, the longer the tube the higher the FP. For the same tube, the higher the ε_g (same slurry density), the larger the FP, and the larger the ρ_{bulk} the smaller the FP. (In an early version, the slope dP/dt with dP measured in cm of water yielded units of cm of water per second which was mistaken as cm/s, which led to taking the slope directly as J_g [20]).

For the JK sensor, the important variable is tube length; gas holdup and slurry density (i.e., bulk density) have little impact. This is because the tube is filled with water and not slurry (as in the on-off McGill sensor). Examples of reading the FP for the McGill and JK sensors are illustrated in Appendix A, Example A.7.

The FP nomograph gives a useful and fast estimation of the function P for given experimental conditions, but the most important characteristic is that the nomograph synthesizes the influence of the associated variables in FP.

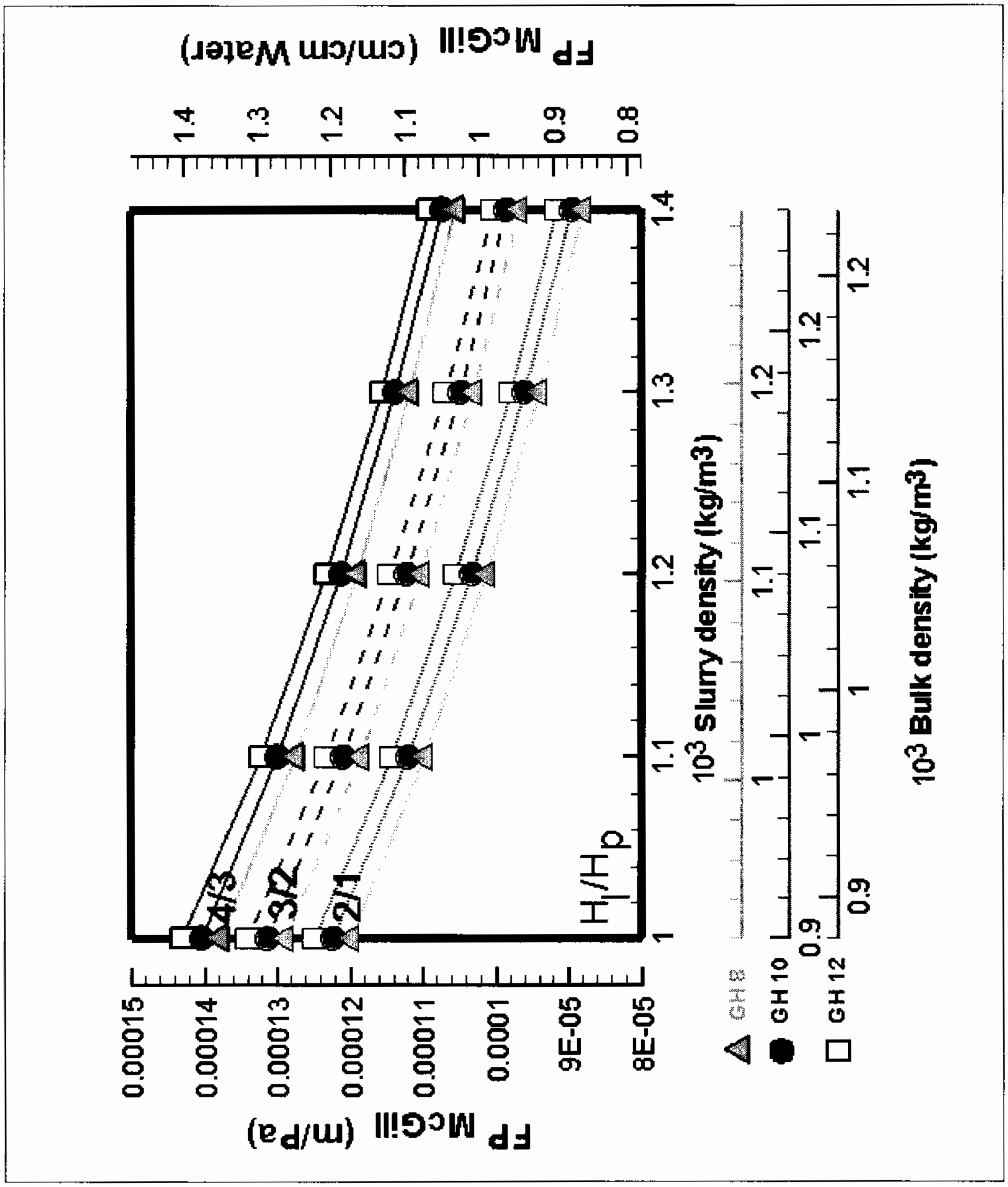

Figure 5.14: FP Nomograph for the on-off McGill sensor for tubes of different lengths at same depth (G.H. stands for gas holdup).

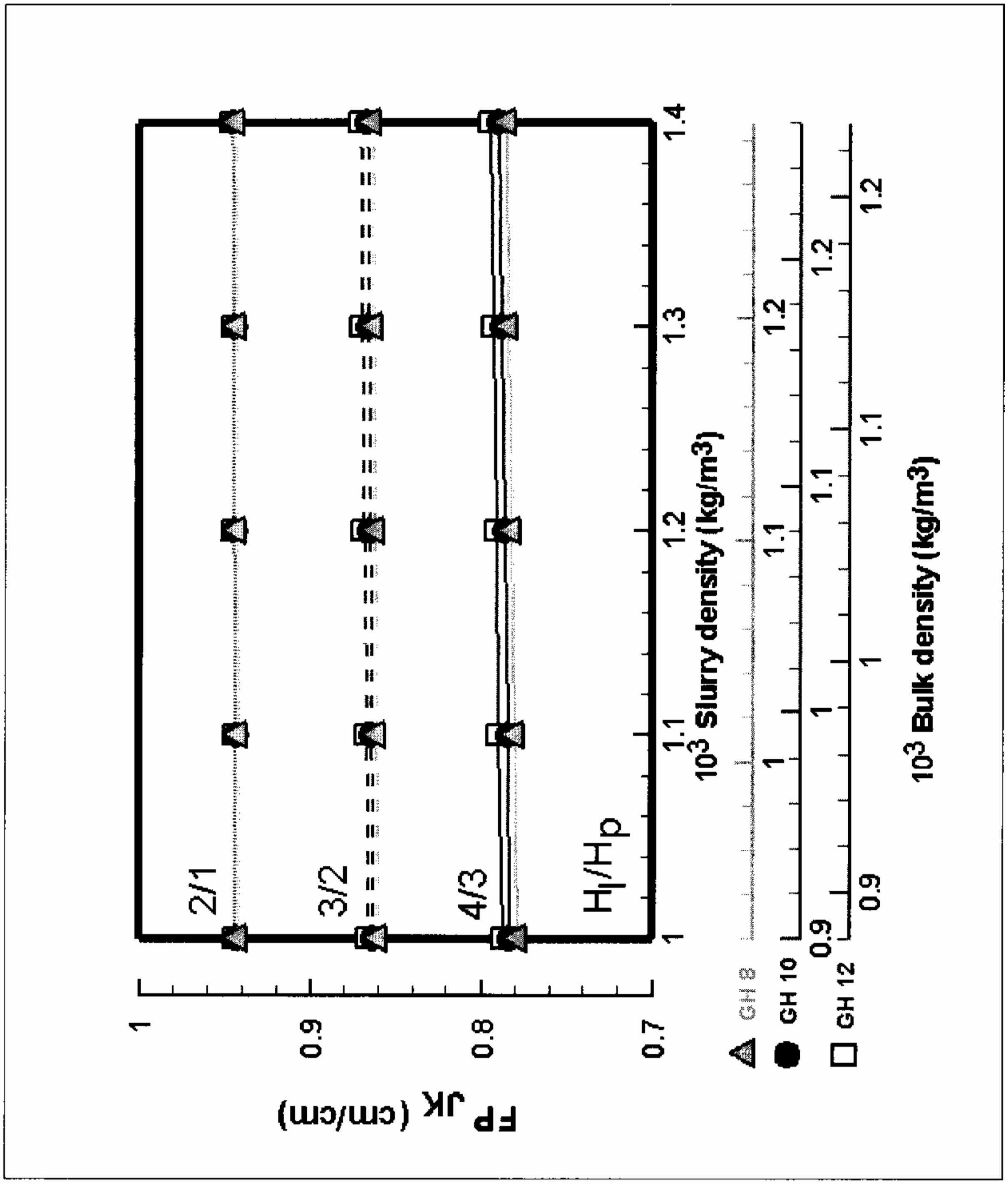

Figure 5.15: FP Nomograph for the JK sensor for tubes of different lengths at same depth (G.H. stands for gas holdup).

5.5.1 Sensitivity analysis for the on-off McGill sensor

A computer sensitivity analysis for the on-off McGill sensor Equation (4.23) was conducted. Figures 5.16 and 5.17 were constructed (data in Appendix F, Table F.8) using the parameters described in Tables 5.4 and 5.5. An example of calculations is shown in Appendix A, Example A.5.

Table 5.4: Parameters for sensitivity analysis.

Test	ρ_{bulk} (kg/m^3)	H_l (m)	H_p(m)
1	1000	3	2
2	1200	3	2
3	800	3	2

Table 5.5: Parameters for sensitivity analysis.

Test	ρ_{bulk} (kg/m^3)	H_l(m)	H_p(m)
1	1000	2	1
2	1200	2	1
3	800	2	1

Figures 5.16 and 5.17 show the high sensitivity of FP to ρ_{bulk} (as an example, in Figure 5.16 a 5% change in ρ_{bulk} gives almost 5% impact on FP), and the limited influence of a change in H_p (as an example, in Figure 5.16 a 50 % change in H_p gives only 10% impact on FP).

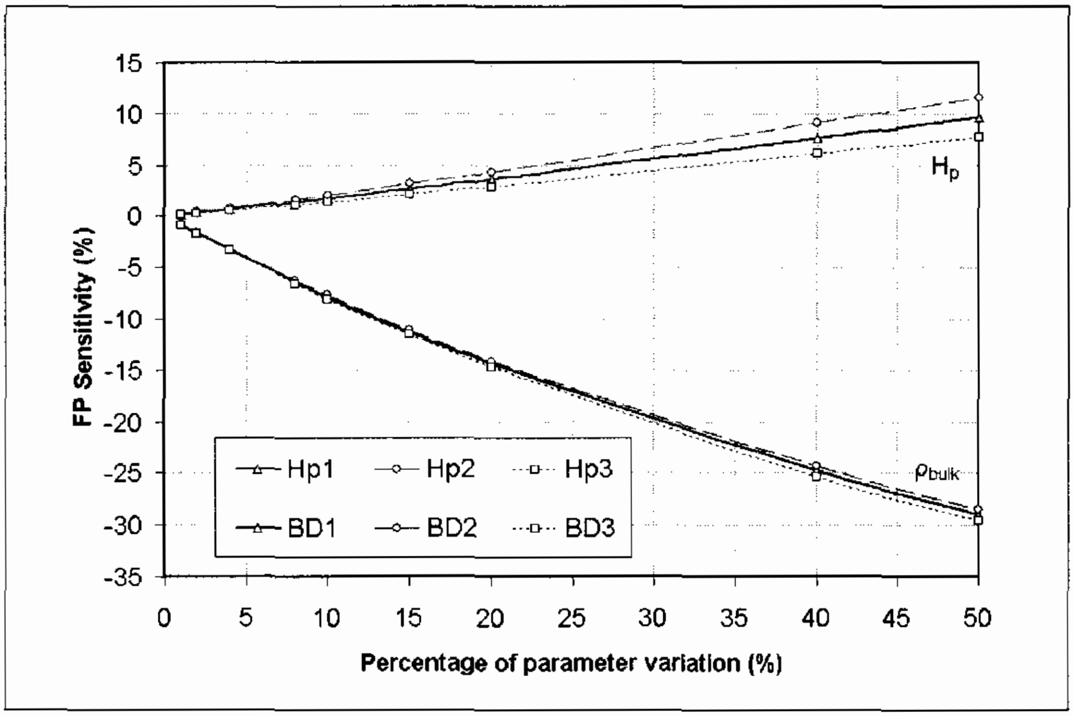

Figure 5.16: FP sensitivity graph. BD stands for bulk density and the number is the test in Table 5.4.

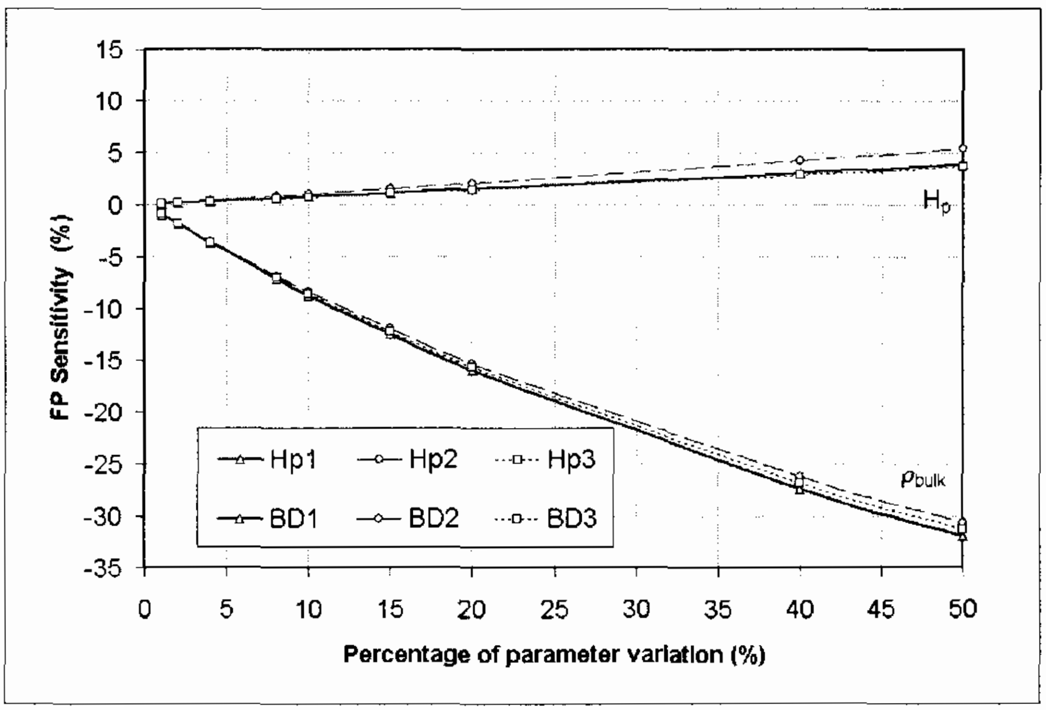

Figure 5.17: FP sensitivity graph. BD stands for bulk density and the number is the test in Table 5.5.

5.6 Continuous sensor

5.6.1 Introduction

An orifice plate (Chapter 2.6.1), is the most popular industrial gas flowmeter. The McGill continuous J_g sensor is based on the same principle of pressure drop (resistance) created by an orifice.

5.6.2 Adiabatic gas expansion

Equation 3.31 introduced the adiabatic gas expansion factor, Y_1. Figure 5.18 shows the plot of Y_1 (see Section 3.3) versus pressure gauge for the parameters shown in Table 5.6 (data, Appendix F, Table F.9).

Table 5.6: Parameters for Figure 5.18.

Isentropic exponent γ	Orifice diameter d (mm)	Pipe diameter D (mm)
1.40	0.7 to 3.0	12.7

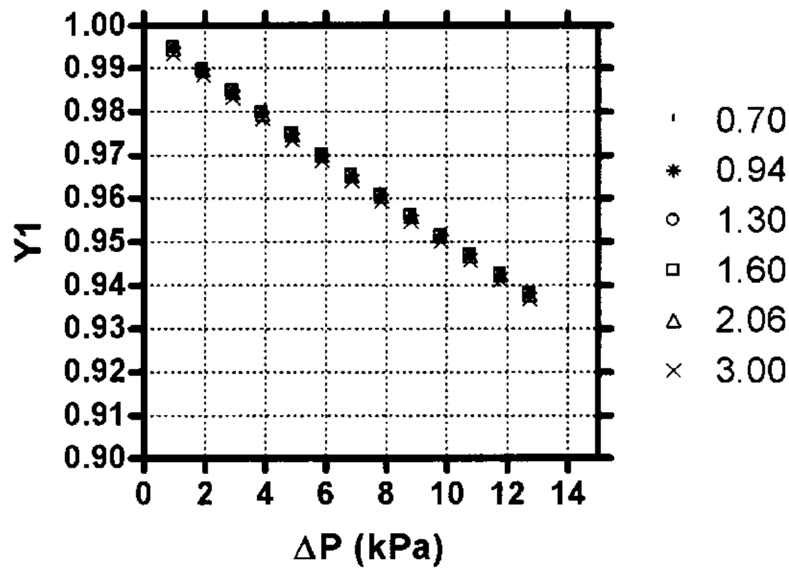

Figure 5.18: Adiabatic gas expansion Y_1 factor calculated for the range of the pressure transmitter and the orifice diameter from 0.7 to 3.00 (mm).

Figure 5.18 enables Y_1 to be included in the design and calibration of orifices.

5.6.3 Compressibility

The Pitzer and Redligh-Kwong methods of estimating compressibility Z were described in Section 3.2.3. The Redligh-Kwong method did not converge within the range of operation of the pressure transmitter (0-127 cm of water) but the Pitzer method was successful.

The critical parameters for the estimation of compressibility using the Pitzer method are indicated in Table 5.7 and examples of estimation are shown in Table 5.8.

Table 5.7: Critical parameters [51].

	Tc (K)	Pc (kPa)	Accentricity
O_2	154.58	5066.250	
N_2	126.2	3394.3875	
Air	132.13	3745.924	0
Volumetric fraction of 20.9% O_2 and 79.1 N_2.			

Table 5.8 shows the results of estimation of compressibility using Equation 3.4 for the low and high values of the pressure transmitter measuring range.

Table 5.8: Compressibility (Z) for air under the experimental conditions.

	T_r	P_r	Z
Air T=293.15 (K) P = 10 (cm of Water), (980.638 Pa)	2.22	0.027311	0.9996
Air T=293.15 (K) P = 100 (cm of Water), (9806.38 Pa)	2.22	0.029667	0.9996

The compressibility will be considered equal to 0.9996 over the sensor's operating range.

5.6.4 Orifice design

Baker [14] comments that international standards allow design of a flowmeter of known measurement uncertainty, provided the standard procedures [2] are rigorously followed. Baker notes that the "attainment of high accuracy is only as a result of careful observation of the correct design procedure and manufacturing requirements".

The first attempt in the present work focused on something easy to machine in a plastic material with a low thermal expansion coefficient. The literature [14] teaches that one of the most important design parameters is the angle of the bevel of the orifice, because a poor design of the orifice edge is likely to affect the development of the vena contracta and contribute to high pressure losses. Pressure losses can be minimized (i.e., with a sharp edge) but not eliminated. An orifice meter is installed directly in a fluid line and pressure losses are higher than with other types of pressure differential meters (e.g., a nozzle meter). Pressure loss is not a problem for this design of continuous J_g sensor, because the orifice discharges directly to atmosphere.

Figure 5.19 is a drawing of an orifice tip (from now on orifice tip is "orifice"). Figure 5.20 shows a set of orifices, made from Delrin[7]. The orifices are machined with a nominal ½ (inch) NPT[8] thread. The diameter D = ½ (inch) (12.7 mm) and length L = 3 (cm) were chosen as fittings of 0.5 (inch) are available in any hardware store (an important consideration for field work) and E is 17 (mm) (for a 11/16 A/F[9] spanner). Table 5.9 shows the orifice nominal diameter d (from now on the orifice nominal diameter identifies each orifice) used during the experimental work.

---

[7] Delrin: DuPont's trade name for Polyoxymethylene

[8] NPT: National pipe thread.

[9] Across flats.

The dimension l (ca. 2 cm) shown in Figure 5.19 was based in the length of the usual tool (ca. 1 cm) used to drill the orifices.

Table 5.9: Nominal orifice diameter.

Diameter (mm)	0.70	0.94	1.00	1.08	1.18	1.30
Diameter (mm)	1.40	1.45	1.60	1.80	2.06	3.00

Based on plant experience, it was found that to avoid excessive wear of the thread and deformation of the orifice hole (d), it was best to install the orifice in a coupling, Figure 5.21.

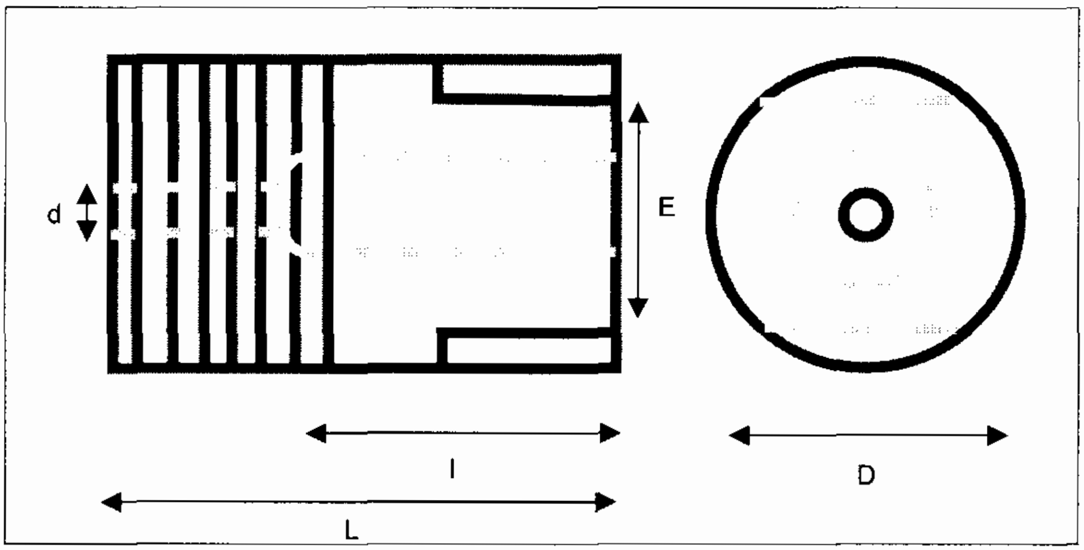

Figure 5.19: Drawing of orifice.

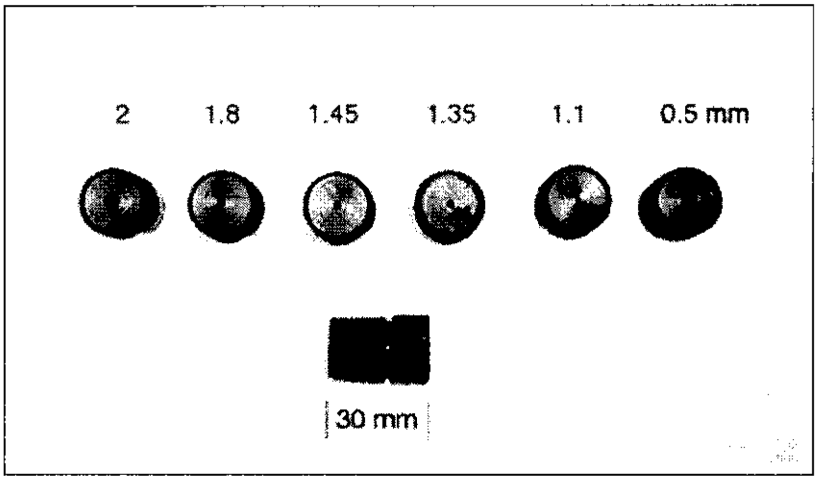

Figure 5.20: Orifices (nominal diameters).

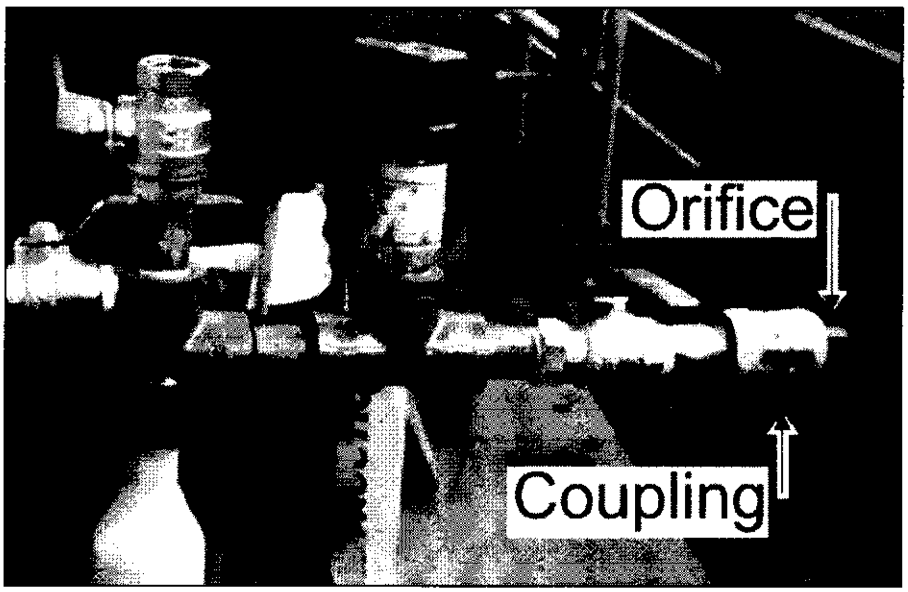

Figure 5.21: Plant sensor configuration.

5.6.5 Orifice calibration

A setup was designed to calibrate the orifices (Figure 5.22). The experimental procedure was as follows: Air was delivered from the top through a mass flow meter (A); the pressure was measured by a transmitter (B) (corrected for temperature, sensor (C)) as the air leaves through orifice (D). Once the steady state was reached (based on a moving average of 60 seconds), data was collected for 180 seconds.

Figures 5.22 (horizontal position), 5.23 (horizontal and short nipple), 5.24 (vertical and short nipple) and 5.25 (horizontal and long nipple) show different setups to study the influence of the orifice orientation and the nipple length (distance between D-E in Figure 5.22).

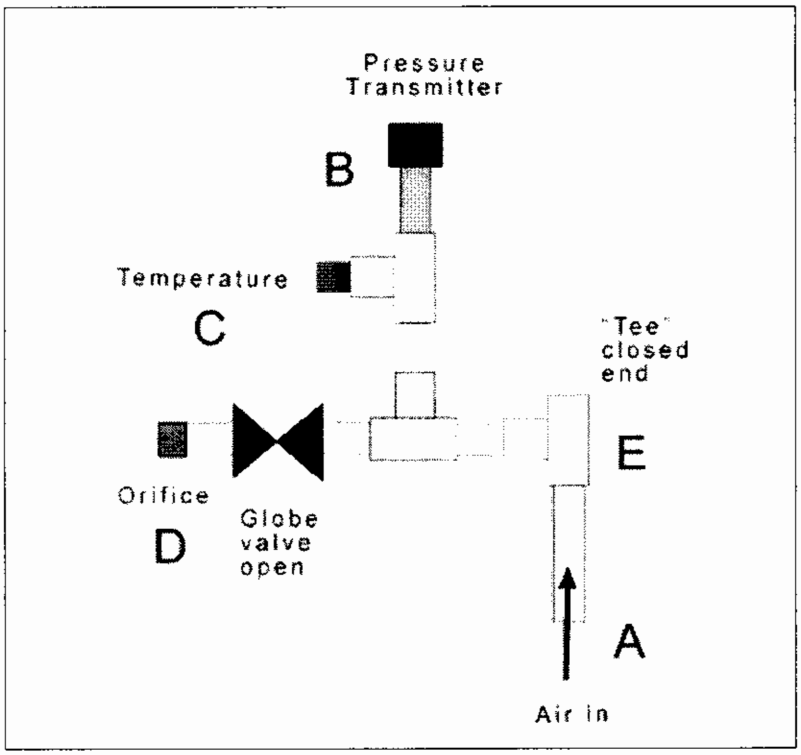

Figure 5.22: Orifice calibration setup.

Figure 5.26 shows two orientations for calibration of orifice 1.30, horizontal and vertical. The results of the calibrations are presented in Appendix F, Table F.10.

Figure 5.27 shows a comparison between the calibration for two orifices (1.60 and 3.00) for a short and long nipple. The results of the calibrations are presented in Appendix F, Table F.11.

It can be observed from Figures 5.26 and 5.27 that for the given design and flow range, the orientation and length of the nipple do not influence the measurement. The horizontal setup was chosen and a set of three calibrations for each orifice (Table 5.9) was conducted (data are in Appendix F, Table F.12). Figure 5.28 shows the results plotted around the operating range of the pressure transmitter, 0 - 12442 (Pa) (0-127 cm of water).

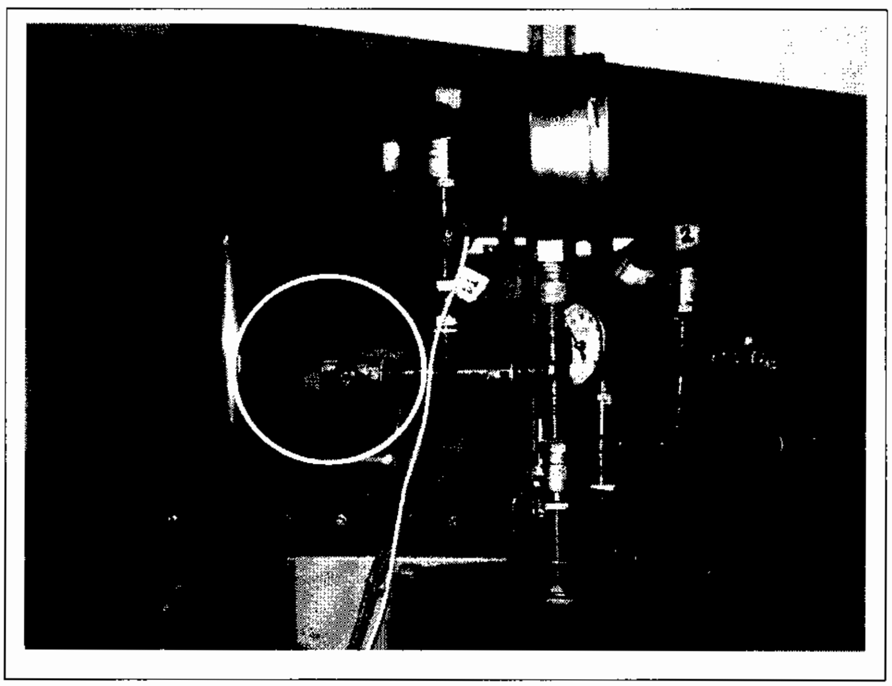

Figure 5.23: Orifice: horizontal setup.

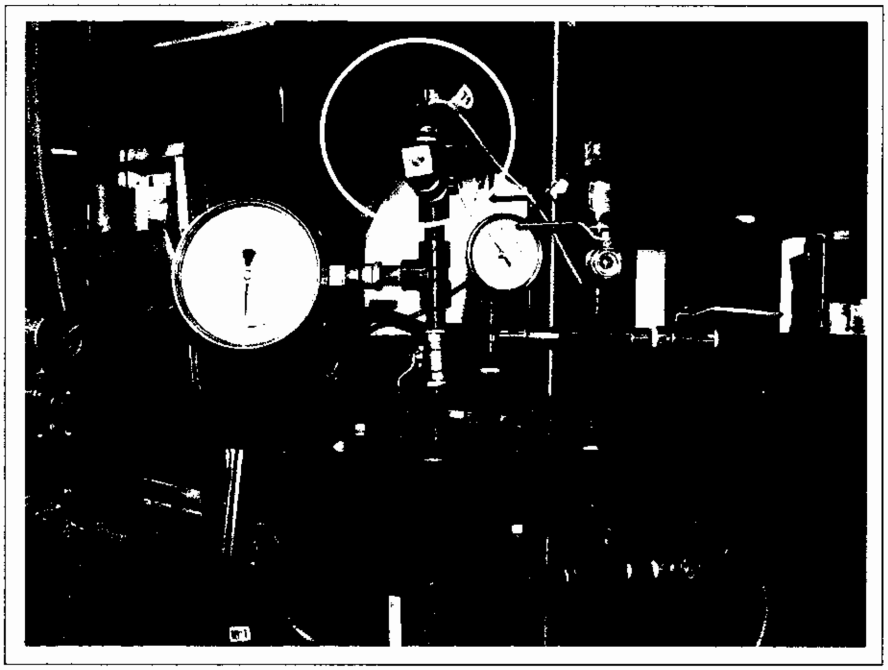

Figure 5.24: Orifice: vertical setup.

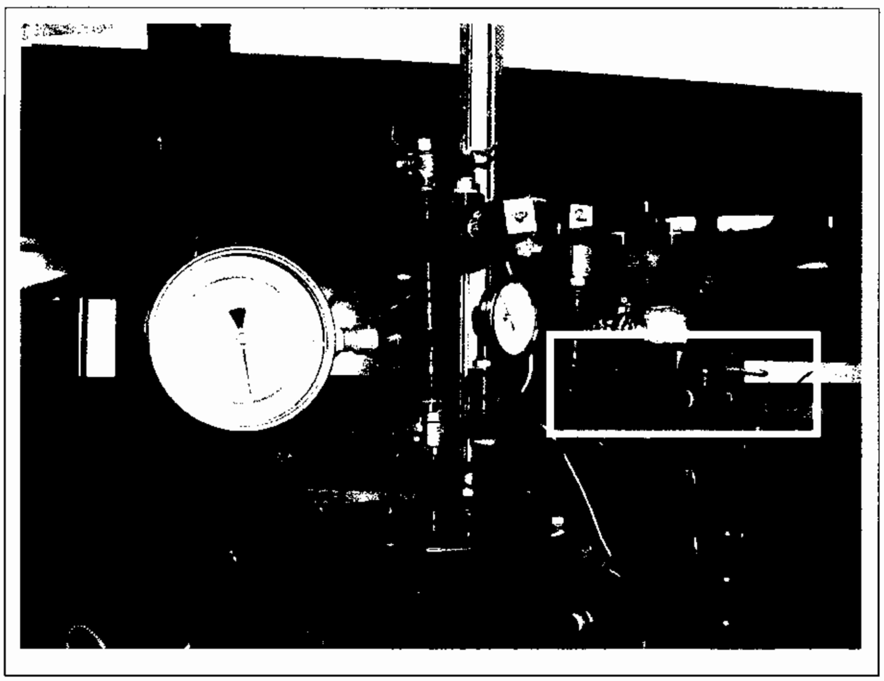

Figure 5.25: Orifice: long nipple.

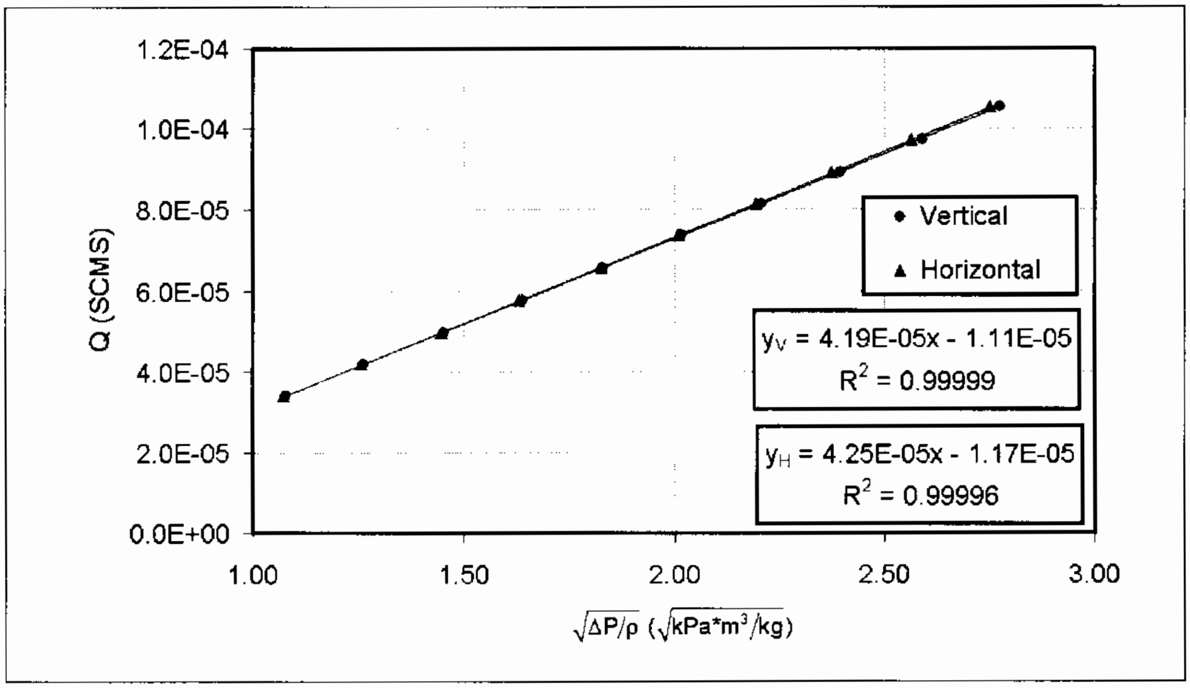

Figure 5.26: Calibration of a 1.30 (mm) orifice in horizontal (H) and vertical (V) configurations.

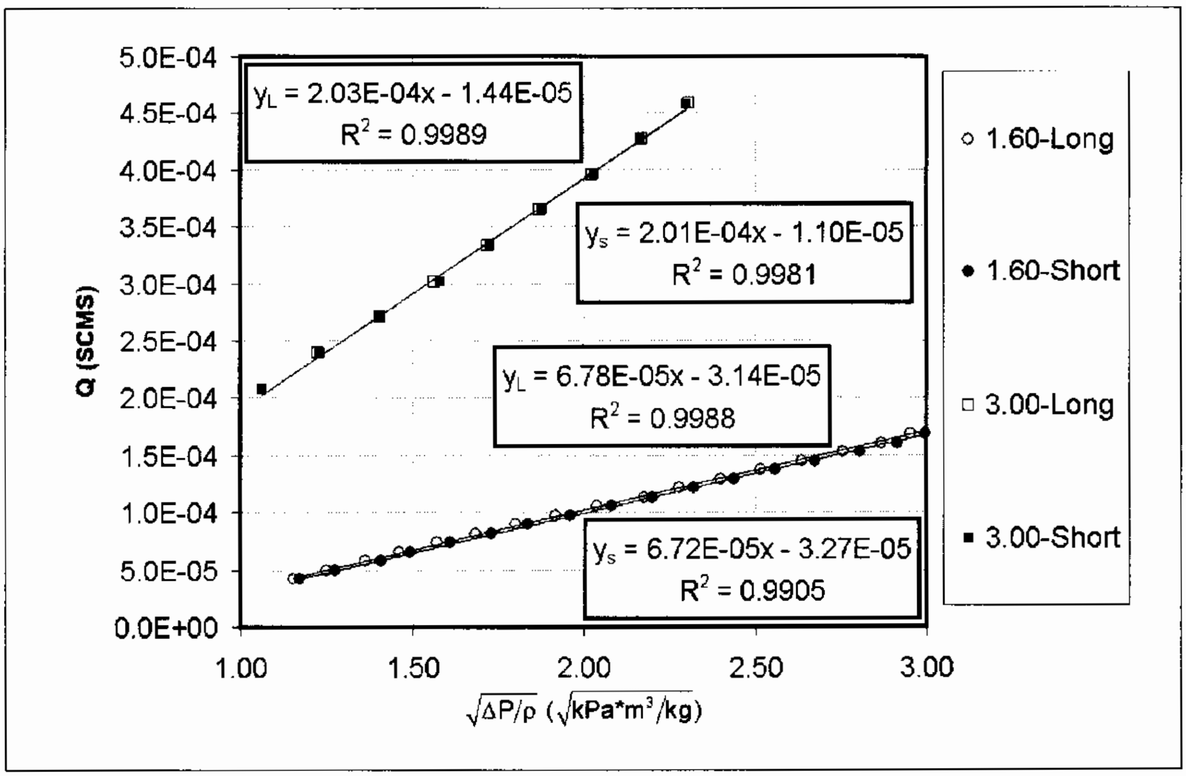

Figure 5.27: Comparison of two orifices for short (S) and long (L) nipple length.

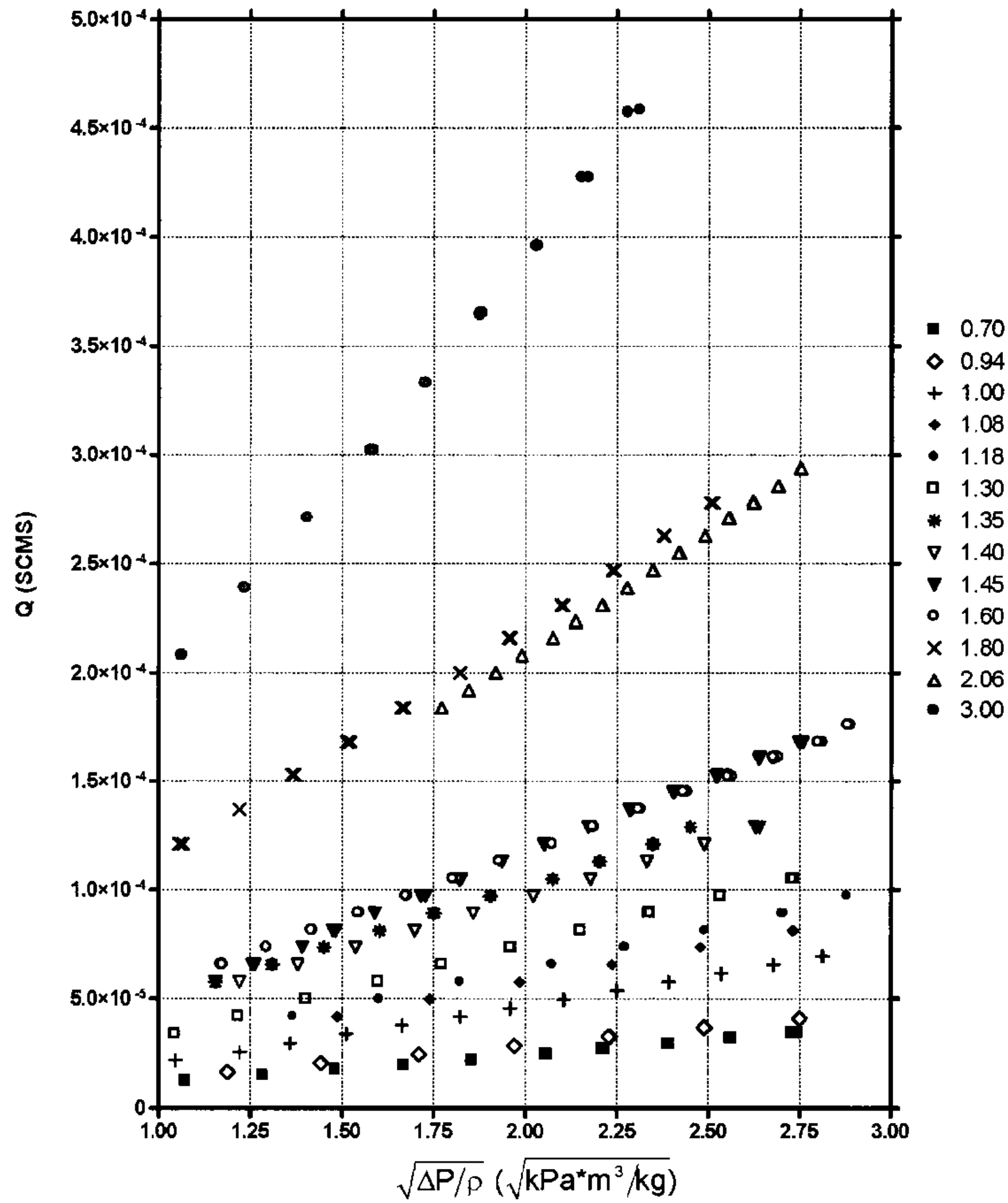

Figure 5.28: Orifice calibration. Symbols represent nominal orifice diameter (reading from the bottom up).

Appendix F, Table F.13 indicates the fitting of candidate equations to the data. They can be divided in categories:

13-1. Mass flow rate in kg per second versus square root of pressure drop: q_{KPS} versus $\sqrt{\Delta P}$.

13-2. Mass flow rate in kg per second versus square root of pressure drop multiplied by air density: q_{KPS} versus $\sqrt{\Delta P \rho}$.

13-3. Volumetric rate in SCMS (standard cubic meter per second) versus square root of pressure drop divided by air density: q_{SCMS} versus $\sqrt{\Delta P / \rho}$.

The first group will be used in modeling the orifice response time; the second will be used in the accuracy test (mass balance); and the third will be used in the calculation of $J_{g\ STD}$.

In Figure 5.28, the calibration curve reveals some discrepancies based on the nominal diameter. For example, the calibration curve for 1.80 and 2.06, shows no clear difference to resolve which value is correct (same for 1.45 and 1.60). Direct measurement of orifice diameter is given in Section 5.6.7.

Candidate orifices for field and laboratory work were selected using the data in Figure 5.28. Figures 5.29 and 5.30 show the J_g calibration charts for J_g sensors with 3 and 4 (inch) tubes (7.62 and 10 cm). The selection was made based on the orifice that gave the highest pressure drop ΔP for the range of J_g from 0 to 1, 1 to 2 and 2 to 3 (cm/s). The orifices selected were 0.94, 1.30 and 1.60 for the 3.00 (inch) tube and 1.30, 1.60 and 2.06 for the 4 (inch) tube.

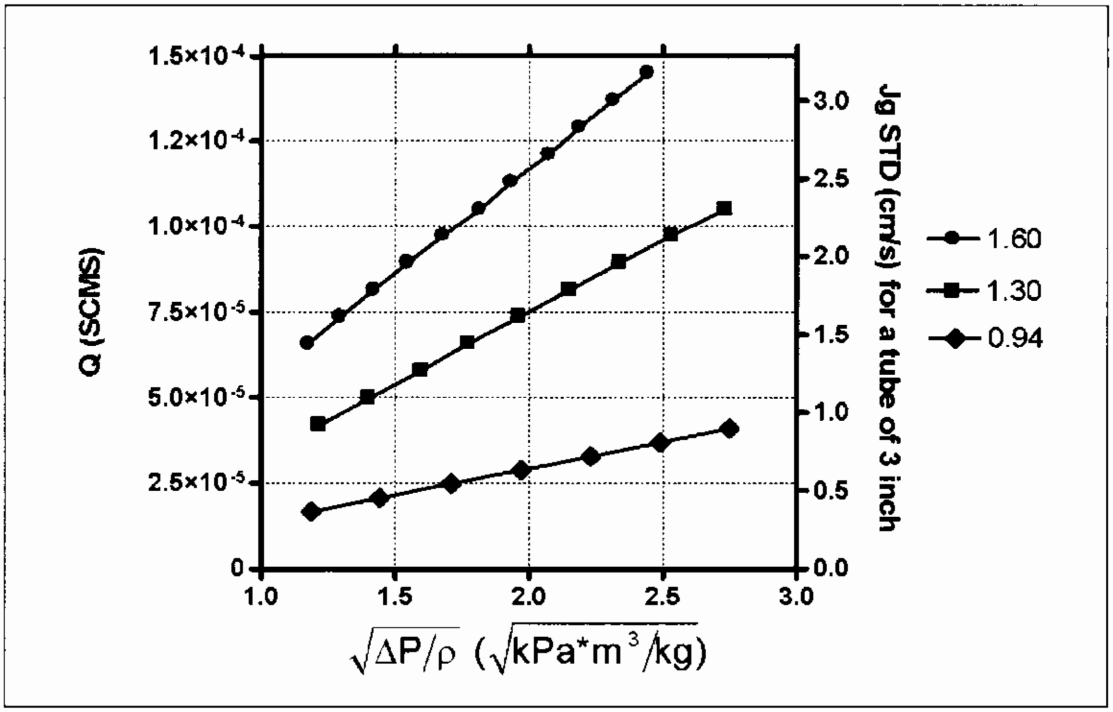

Figure 5.29: Orifice calibration chart for a J_g sensor with 3 (inch) tube.

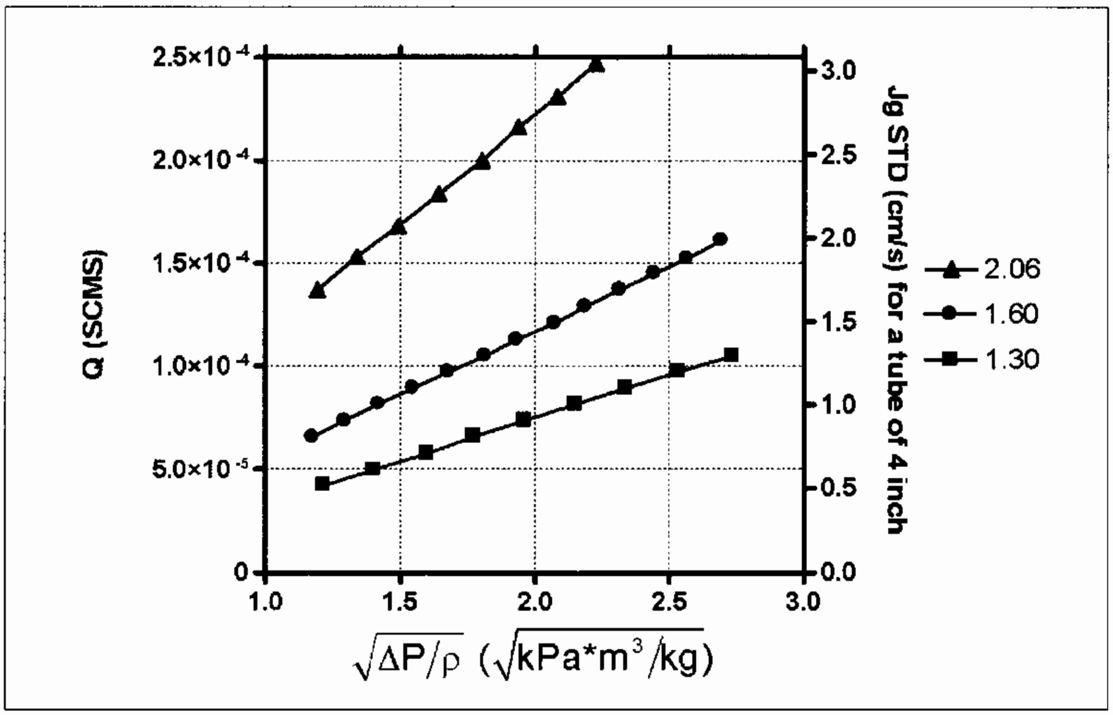

Figure 5.30: Orifice calibration chart for a J_g sensor with 4 (inch) tube.

5.6.6 Reproducibility

An advantage of the McGill continuous J_g technique, is the ready implementation of a multi-sensor unit. This requires the construction of sets of orifices to cover the working range of J_g in plant campaigns. Orifices were calibrated as described in Section 5.6.5. Figures 5.31, 5.32, 5.33 and 5.34 show the results for calibrations of sets of orifices of nominally 0.94, 1.30, 1.60 and 2.06 (mm), respectively. The orifices classified as "laboratory" (used for laboratory tests) and "industrial" (used for industrial work). The industrial orifices are indicated with a number, the laboratory ones with the letter "X" and in some cases "Y" (for the second laboratory orifice). A different design "L" (length of the orifice = 3) is included in Figure 5.32. Data is presented in Appendix F, Table F.14, and also statistical tests were conducted to characterize the significance of the results.

It can be observed that orifice 1.30-L, produces a higher pressure drop than the set of laboratory and industrial orifices, because the length of the orifice L is higher (3 compared to 1 cm) and offers more resistant to the flow of gas.

Reproducibility was not satisfactory, indicating an alternative manufacturing route was needed. The material (plastic) was thought to be the main culprit. Images of orifices, Section 5.6.7, show irregularities that support the contention.

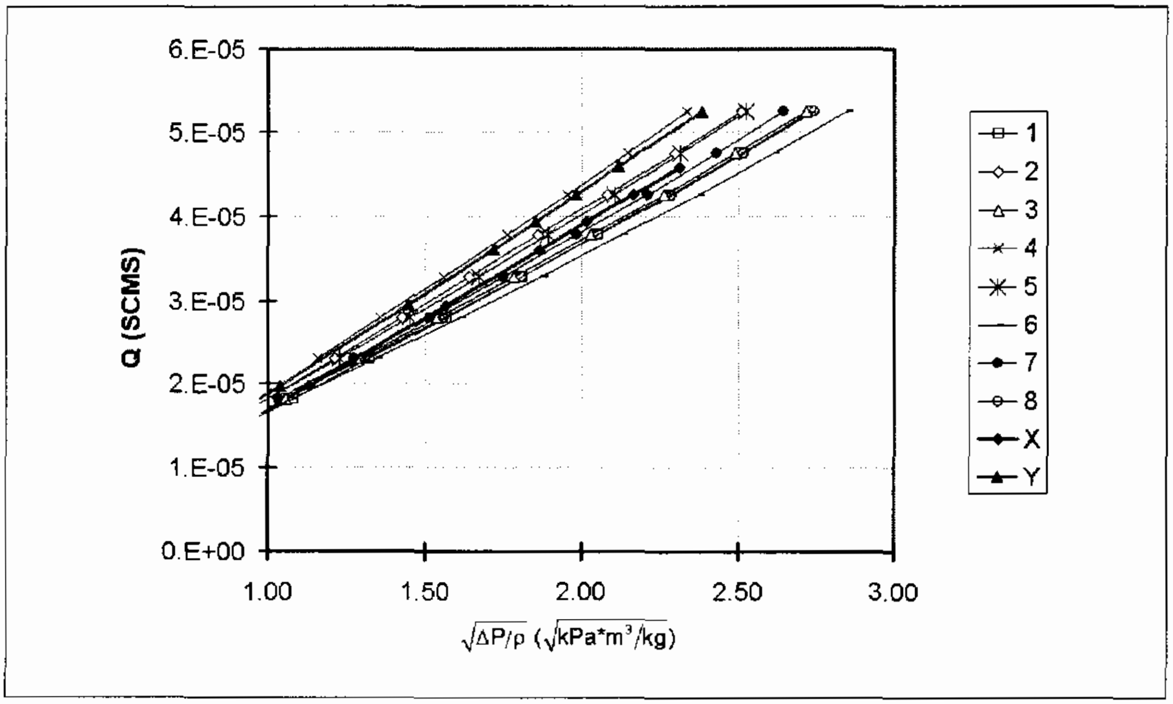

Figure 5.31: Calibrations comparison between the laboratory (X and Y) and industrial (1 to 10) sets for a series of nominally 0.94 (mm) orifices.

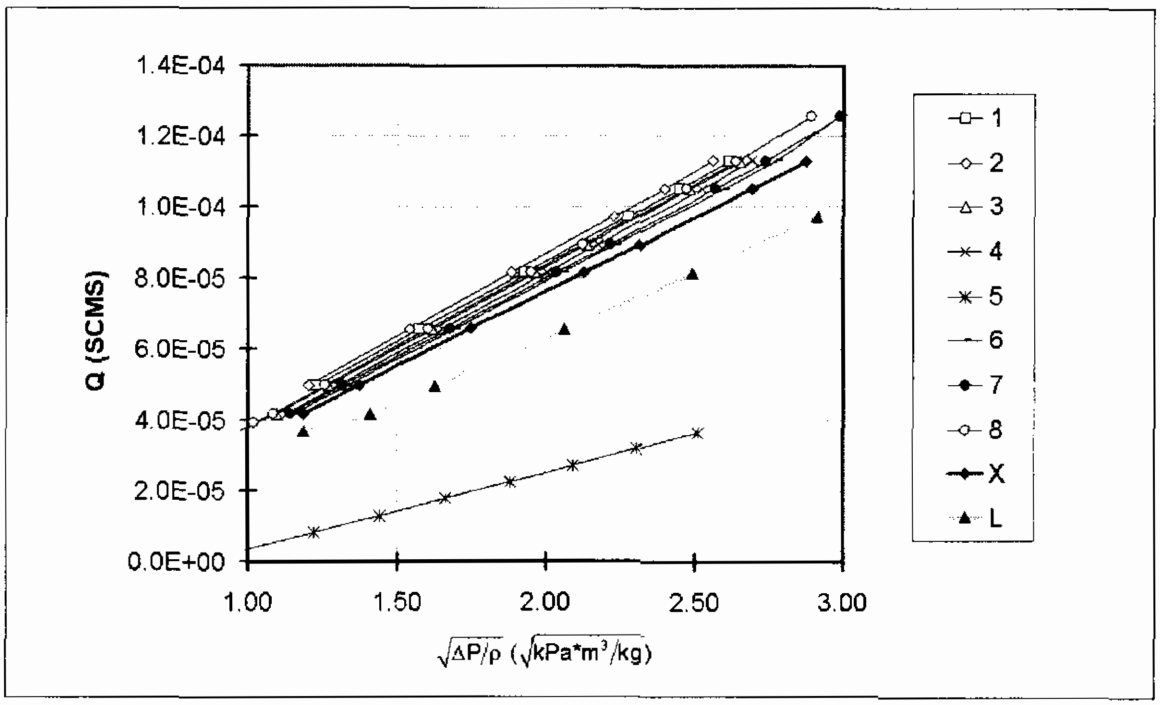

Figure 5.32: Calibrations comparison between laboratory (X and L) and industrial (1 to 8) sets for a series of nominally 1.30 (mm) orifices.

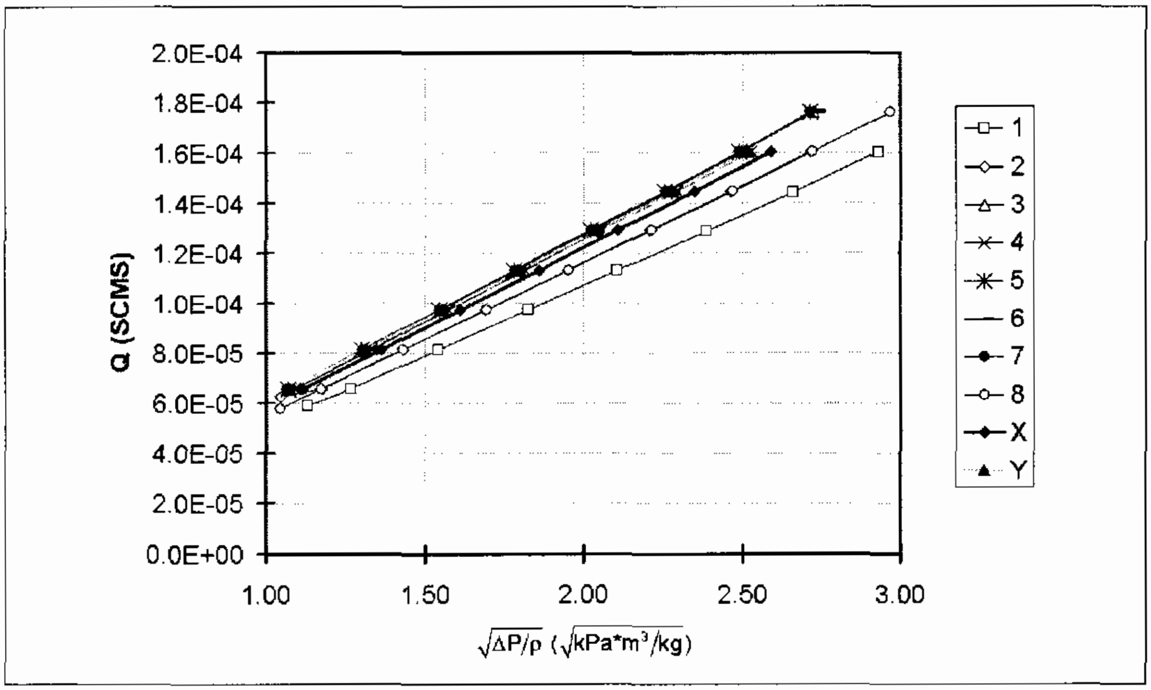

Figure 5.33: Calibrations comparison between laboratory (X and Y) and industrial (1 to 10) sets for a series of nominally 1.60 (mm) orifices.

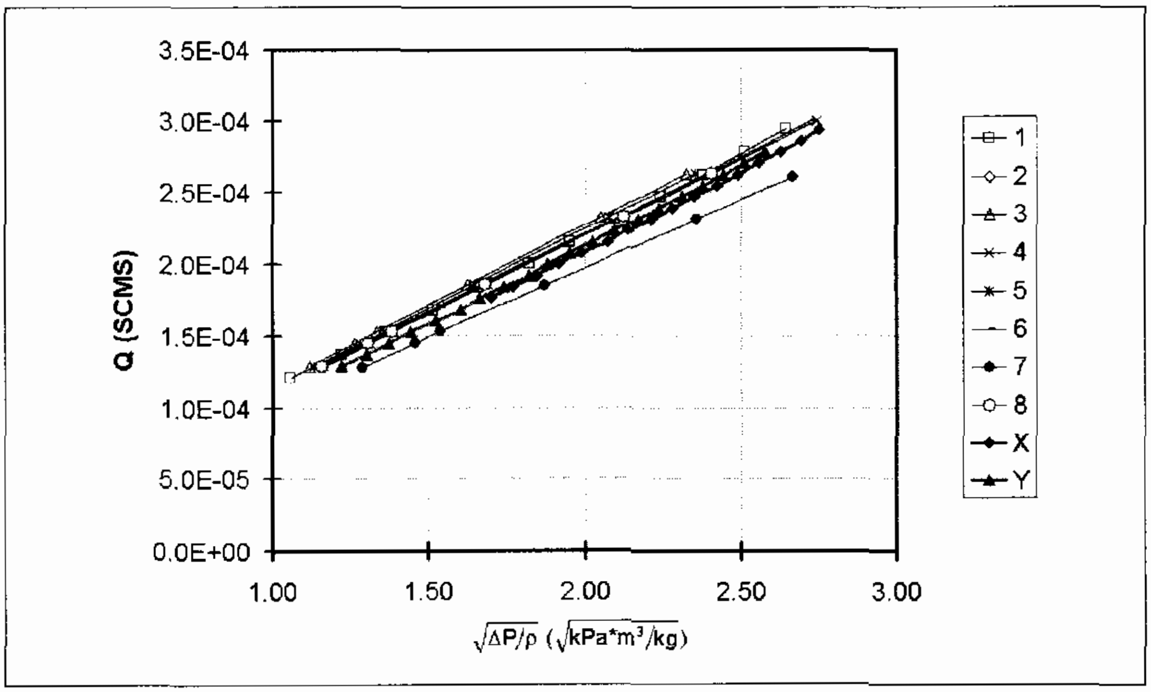

Figure 5.34: Calibrations comparison between laboratory (X and Y) and industrial (1 to 10) sets for a series of nominally 2.06 (mm) orifices.

5.6.7 Orifice diameter measurements

Figure 5.35 shows the measured diameter versus the nominal diameter for the orifices in Table 5.9, and Figure 5.36 shows the measured diameter for four sets of 10 orifices of nominally 0.94, 1.30, 1.60 and 2.06 (mm). The data are presented in Appendix F, Table F.15.

It can be observed in Figure 5.35 that there is a difference between the nominal and the measured diameter; in most cases the real value is lower.

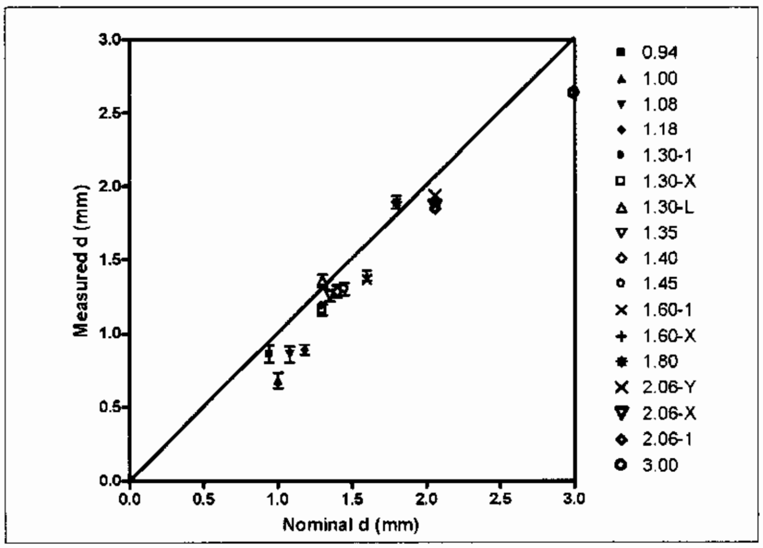

Figure 5.35: Measured diameter versus nominal diameter for the orifices in Table 5.9.

Figure 5.36a shows a similar trend: There is a large difference between the nominal and measured values and Figure 5.36b shows a plot of orifice diameter versus orifice length (L-l). It can be observed that the data in plot 5.36b (data presented in Appendix F, Table F.15) does not follow a consistent trend as it was expected from the calibrations in Figures 5.31 to 5.34. It was expected that when two orifices were compared, the smallest diameter and largest orifice length will generate a higher the pressure in the orifice (at the same gas flow).

For example, in Figure 5.36b for the orifice 1.60 orifices 1 and 8 have the same diameter and length; but in Figure 5.33 they show a different slope. In contrast orifice 2.06 7 and 8, because 7 is located in Figure 5.36b at the bottom right of 8, we can expected that a higher pressure drop is generated in 7 than 8, and this can be observed in Figure 5.34.

It can be observed in Figure 5.36a, that orifice 5 is not a 1.30 and this explains why the calibration for this orifice is out of the family of calibration curves in Figure 5.32.

It was also evident that there were differences in the sharpness of the orifice edge: Figures 5.37 and 5.38 show two examples of a sharp and irregular edge, respectively. An irregular orifice has a different cross section area and offers a different resistance to the flow (generating another slope in the calibration curve).

Finally, the objective of this section was to study the reproducibility of the orifices with the visualization of using a generic equation (calibration curve) for each orifice without conducting a calibration (for time and cost reasons). More emphasis should be focused on the machining of the orifices. The next section explores one of the next steps: A more robust material.

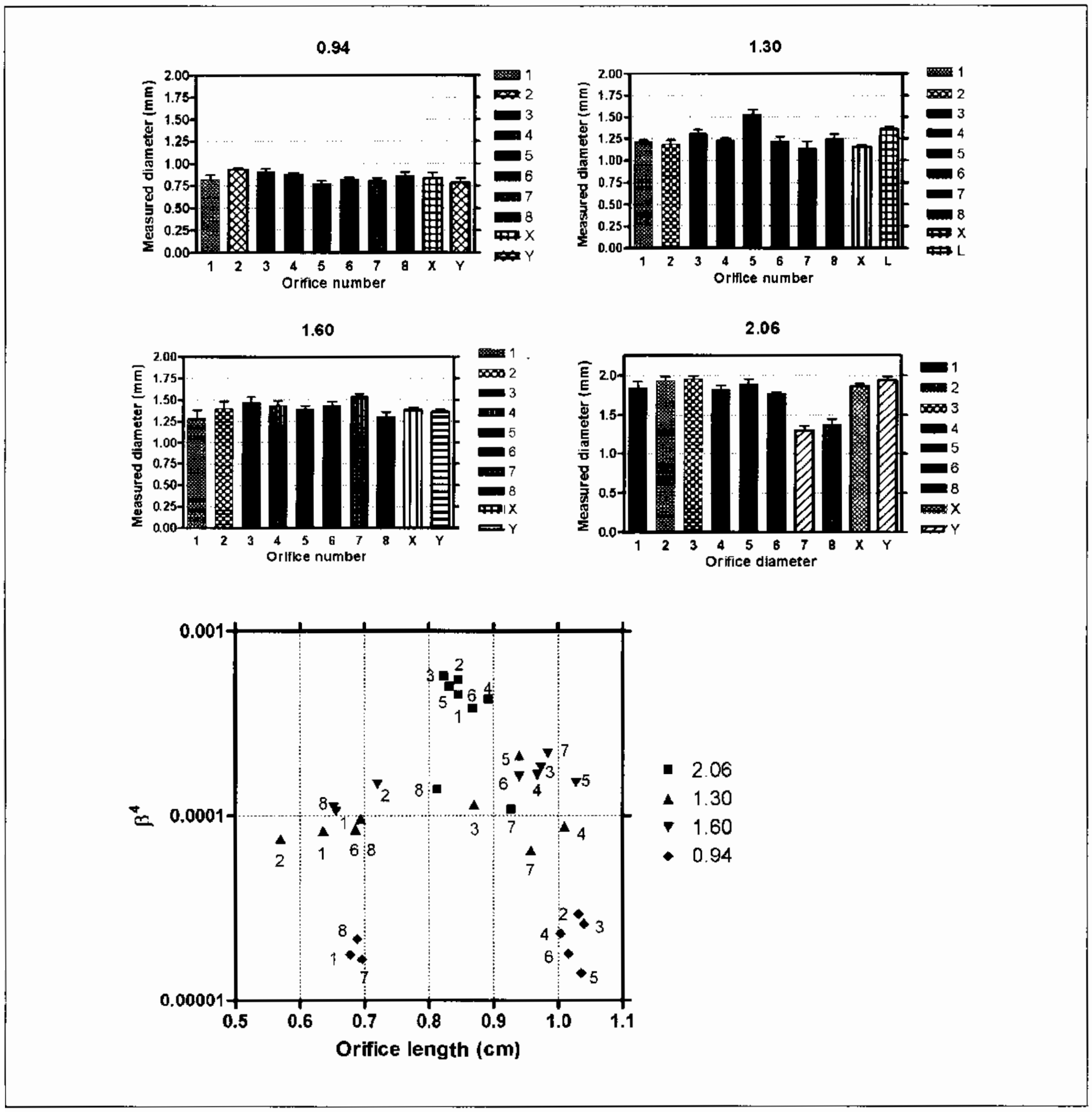

Figure 5.36: a) Orifice diameter measurement for 4 sets of orifices. b) β^4 versus orifice length (L- l).

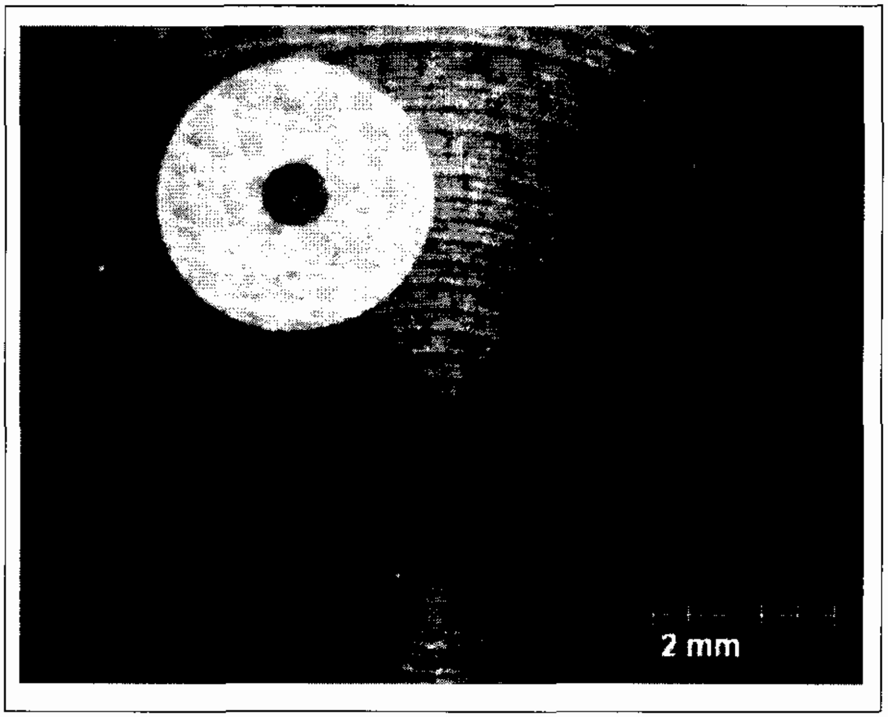

Figure 5.37: Orifice (2.06 mm, # Y) with a sharp edge. The golden disc is a 3.05 (mm).

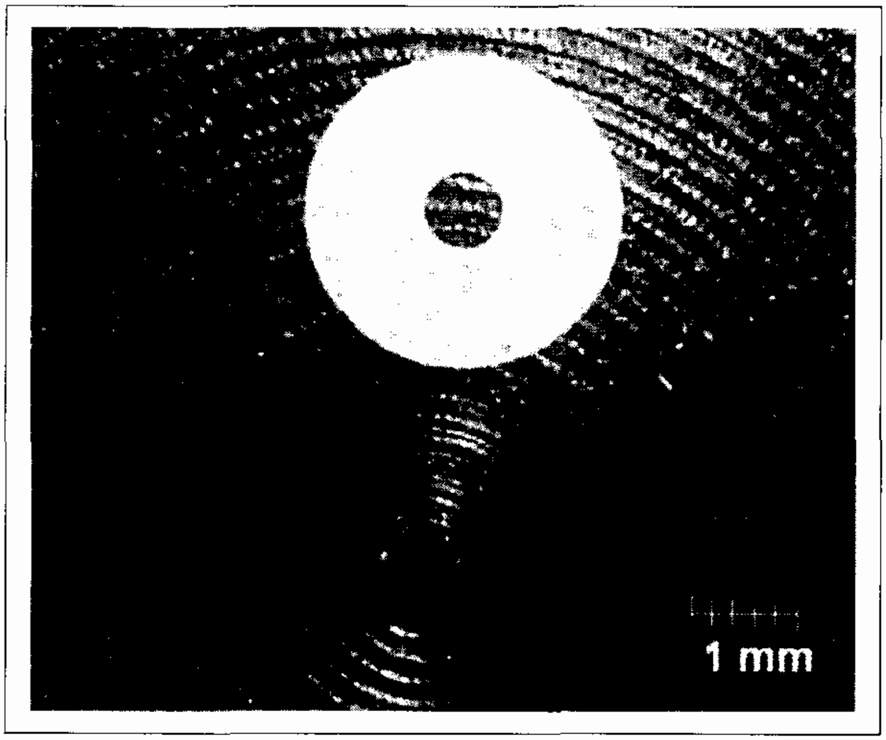

Figure 5.38: Orifice (0.94 mm, # 8) with a irregular edge. The golden disc is a 3.05 (mm).

5.6.8 Orifice material

A more robust material than plastic, brass, was used to build a new set of orifices (orifice-B) to try to improve reproducibility. Orifices are made from a Brass plug of half (inch) nominal NPT thread. Orifices were calibrated as described in Section 5.6.5. Figure 5.39 shows a set of calibrations for orifice-B compared to the former design (X). The data are presented in Appendix F, Table F.16.

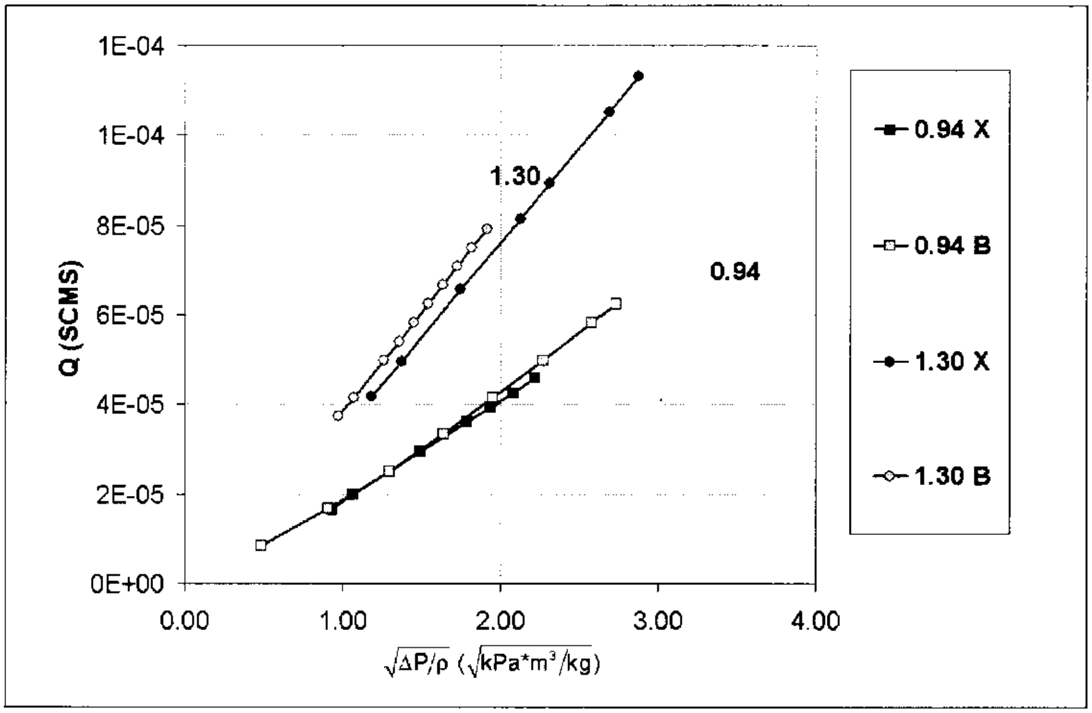

Figure 5.39: Orifice-B calibration (Data courtesy of Jose Hernandez).

Figure 5.39 shows that the calibration is similar but experience shows the new design is more robust.

5.6.9 Orifice location

The continuous McGill J_g sensor measurements can be biased by condensation in tubing ahead of the orifice. This can be overcome using an eccentric (i.e., off-centre) orifice [55]. Figure 5.40 shows the present design where the location of the orifice in the tip was modified to allow any accumulation of liquid to be expelled.

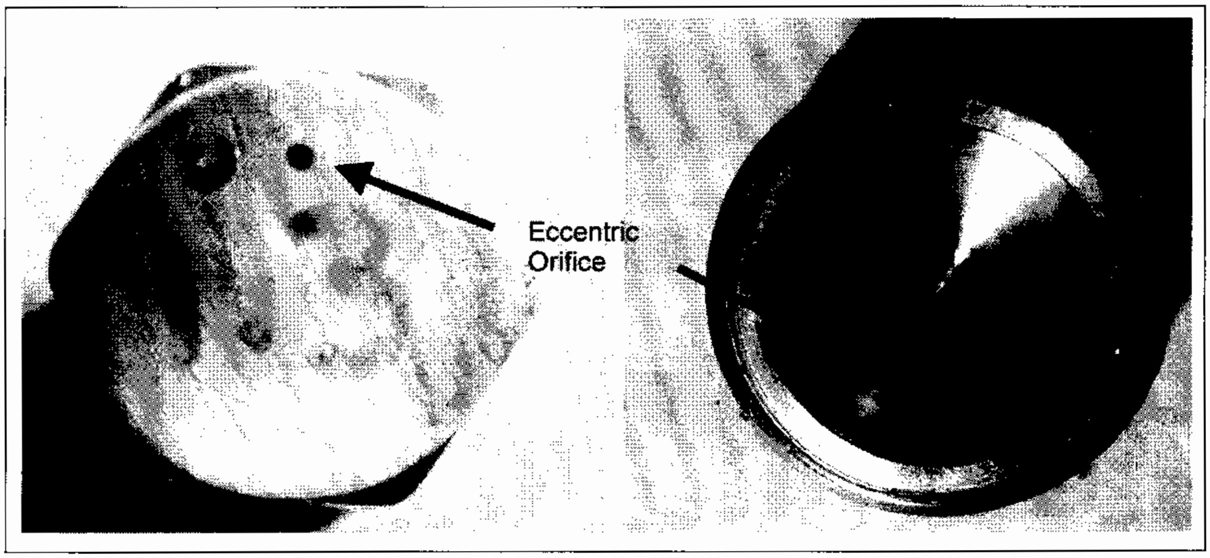

Figure 5.40: New orifice design, left front-external and right back-interior.

5.7 Test of accuracy for the continuous J_g sensor

As discussed in the Introduction of this Chapter, a standard technique is required to study the accuracy of the sensor. The two major problems are: a) bubbles do not evenly distribute over a flotation cell or column, meaning the volumetric flow of gas into the cell cannot be used as standard and b) there is no non-intrusive instrument to measure J_g in a dispersed system that may avoid this sampling issue. This chapter proposes a setup to overcome those problems.

5.7.1 Experimental setup

To try to address the problem a setup was specially designed. A 4 (m) high, 15.24 (cm) diameter acrylic transparent column was used (Figure 5.41). A rigid porous sparger (5 μm nominal pore diameter) was installed to generate bubbles. Five ppm of frother (MIBC) was used.

The column was transformed into a closed vessel using a flat flange with the idea of tracking continuously the gas fed to the column (A) and the gas that leaves the column via two exits: a) the fraction collected by the sensor (B), and b) that escaping at the top through a second orifice (C). Once the steady state was reached (based on a moving average of 120 seconds), data was collected for 360 seconds. Combinations of two orifices were used to cover the typical range of J_g: 0 - 3 (cm/s).

Using the continuous data collected from the mass flow meter and the two orifices, a mass balance was conducted as follows,

$$q_{KPS,in} = q_{KPS,out1} + q_{KPS,out2} \qquad \text{Eq. (5.5)}$$

Where $q_{KPS,\ in}$ is the mass flow of gas entering the control volume and $q_{KPS,out1}$ and $q_{KPS,out2}$ are the mass flow of gas leaving the control volume via orifice 1 and 2.

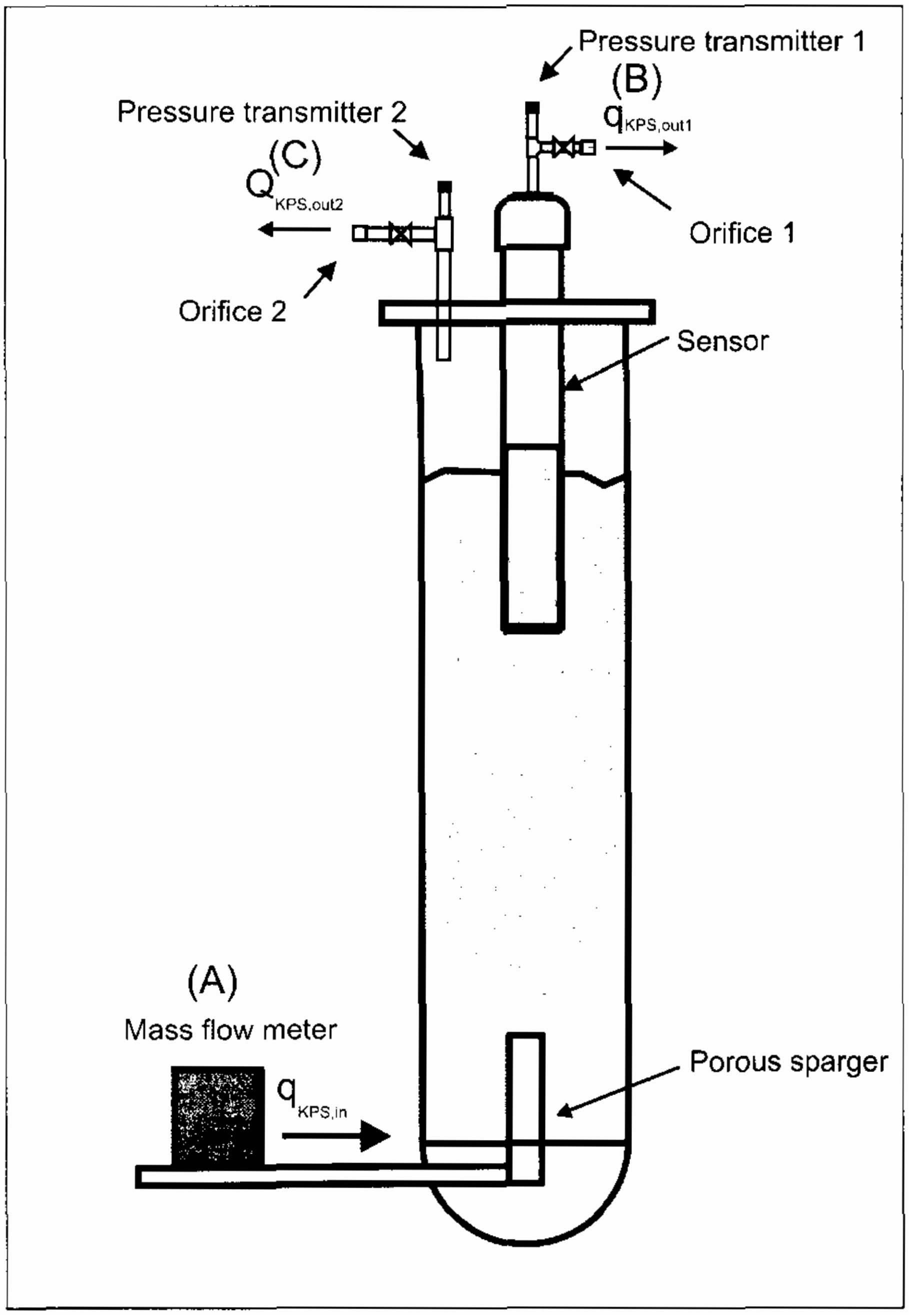

Figure 5.41: Setup designed to test continuous J_g measurement accuracy.

The accuracy test was based on the assumption that $q_{KPS,in}$ - $q_{KPS,out2}$ has small error and can be used as a standard, because the mass flow meters, pressure transmitters and orifices were calibrated using fundamental principles.

5.7.2 Results

Table 5.10 shows the tests and Figures 5.42 and 5.43 show the results of mass balancing for the 3 and 4 (inch) tubes, respectively. The data are presented in Appendix F, Table F.17.

Table 5.10: Accuracy test conducted.

	Low				Med				High			
Tube Diameter	**J_g STD (cm/s)**		**O1**	**O2**	**J_g STD (cm/s)**		**O1**	**O2**	**J_g STD (cm/s)**		**O1**	**O2**
4 (10.16 cm)	0.20	0.40	0.70	0.94	0.60	1.20	1.30	1.60	1.70	2.75	2.06-X	2.06-Y
3 (7.62 cm)	0.27	0.35	0.70	0.94	0.60	0.80	0.70	1.60	1.90	2.50	1.60	2.06
					1.30	1.80	1.30	2.06				
Note: O1 and O2 are orifices 1 and 2.												

It is important to note that the actual setup is not applicable to the discontinuous technique, because the displacement of water during data collection will affect the level in the column and this will introduce a bias in the readings of the second orifice. A second chamber to collect the water displaced by the discontinuous sensor is required and the level in the column will not be affected by the water displacement.

Figures 5.42 and 5.43 show that all the data fell into an envelope of 5 % of bias error.

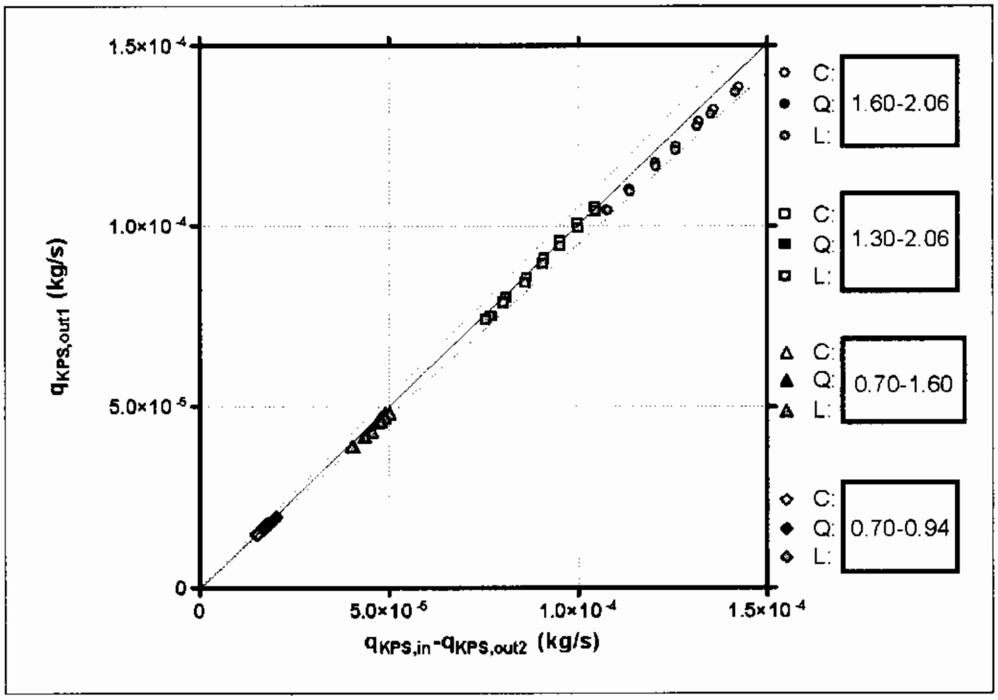

Figure 5.42: Mass balance results, 3 (inch) tube.

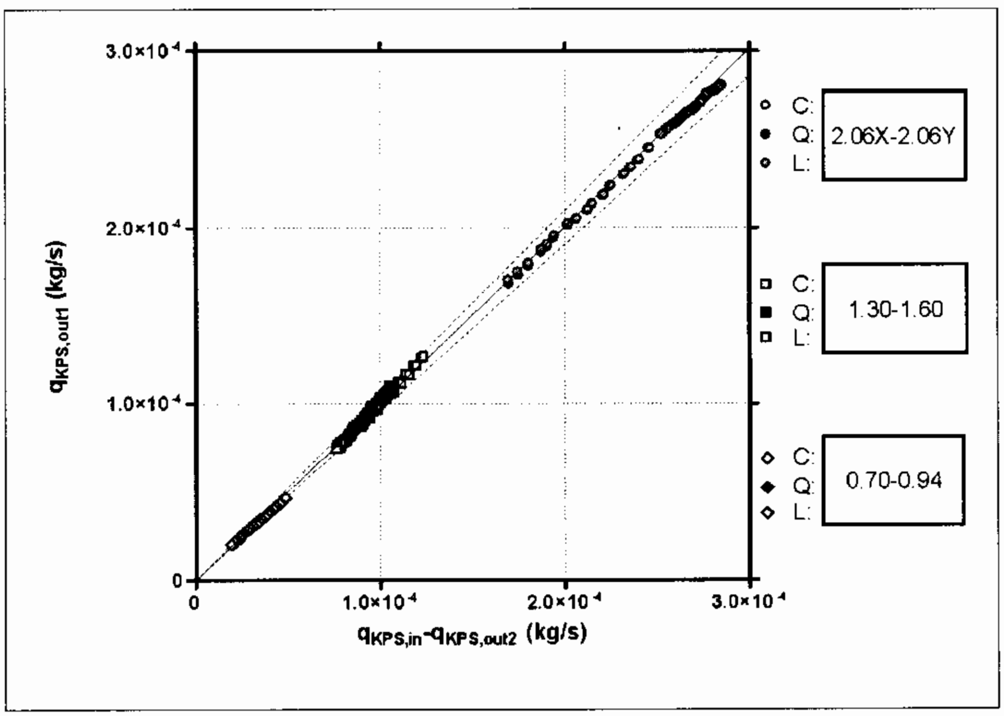

Figure 5.43: Mass balance results, 4 (inch) tube.

One source of error is thought to be because the air injected is dry and on passing through the column is subject to different levels of saturation with respect to water. The air in the test is at high pressure and when it passes through the column it expands and absorbs water, approaching saturation point (around 4.24 kPa at 101325 Pa).

Based on pressure transmitter catalog, it was expected to have less linearity at the extremes of the pressure transmitter range (pressure gauge range from 0 to 12454 Pa), but Figure 5.6 shows a linear trend over the range studied (1510-10345 Pa).

Another source of error is that the orifice calibrations are less linear at the low and high extremes of the pressure transmitter range (e.g. Figure 5.33 orifice 1 at the lower range), and thus have higher error than the middle range is expected: This will be discussed in the next section.

5.7.2.1 Directional bias error (bias) calculation

Using the test results (Appendix F, Table F.17) bias (in percentage) was calculated for the candidate equations: linear (Equation 5.6), quadratic (Equation 5.7) and cubic (Equation 5.8) as follows:

$$q_{KPS,out} = a_L \sqrt{\Delta P_{out} \rho_{out}} + b_L \qquad \text{Eq. (5.6)}$$

$$q_{KPS,out} = a_Q(\sqrt{\Delta P_{out}\rho_{out}})^2 + b_Q(\sqrt{\Delta P_{out}\rho_{out}}) + c_Q \qquad \text{Eq. (5.7)}$$

$$q_{KPS,out} = a_C(\sqrt{\Delta P_{out}\rho_{out}})^3 + b_C(\sqrt{\Delta P_{out}\rho_{out}})^2 + c_C(\sqrt{\Delta P_{out}\rho_{out}}) + d_C \qquad \text{Eq. (5.8)}$$

Regression coefficients indicated in Appendix F, Table F.13-2.

Each value has an individual bias, but for practical reasons it is better to define a mean value with a confidence interval (CI). Table 5.11 shows the results of statistical calculations.

Table 5.11: Mean bias for tubes 3 and 4.

	Linear	Quadratic	Cubic
Mean bias (%) for tube 3	-3.30	-2.42	-2.07
Lower 95% CI of mean	-3.71	-2.95	-2.61
Upper 95% CI of mean	-2.90	-1.90	-1.52
Mean bias (%) for tube 4	-1.42	-0.97	-0.93
Lower 95% CI of mean	-1.72	-1.8	-1.26
Upper 95% CI of mean	-1.11	-0.67	-0.61

Statistical tests were conducted for tubes 3 (t test, with 30 samples) and 4 (Z test, with 113 samples). The results (Appendix F, Table F.18) show that the difference, between the mean bias for the quadratic and cubic equations was not significant, but between the mean bias for linear and quadratic, there is a significant difference.

5.7.2.2 Calculation of accuracy

Figure 5.44 shows the results of tests conducted for the accuracy of the calibration curves: Accuracy versus the percentage of the continuous J_g sensor

URV[10]. Appendix F, Table F.18, shows the data and Appendix A.8 gives an example of accuracy calculation.

It can be observed in Figure 5.44 for tubes 3 and 4 that all tests show a different trend along the range of percentages of URV. This prevents the derivation of an accuracy calculation as a function of the percentage of URV and due to this reason calculation of an accuracy calibration curve for each combination of orifices is unjustified (and will be difficult to understand). However, all the results fall in a –5 % bias. Using this characteristic it is possible to define a reference accuracy envelope [54]. Using this approach, the accuracy was calculated from the results of Table 5.11 and Appendix F, Table F.18. Table 5.12 shows the results.

Analysis of Table 5.11 for tubes 3 and 4 shows that the quadratic and cubic equations gave smaller mean bias results than the linear. For practical purposes (i.e., plant work), a mean bias of –3.30 % (with a 95% CI of –2.90% and –3.71%) for a 3 (inch) tube and –1.42 % (with a 95% of CI of –1.11% and –1.72%) for a 4 (inch) tube, obtained with the linear model are satisfactory. For the remainder of the thesis, a linear fit for orifice calibration will be used.

[10] URV: Upper range value

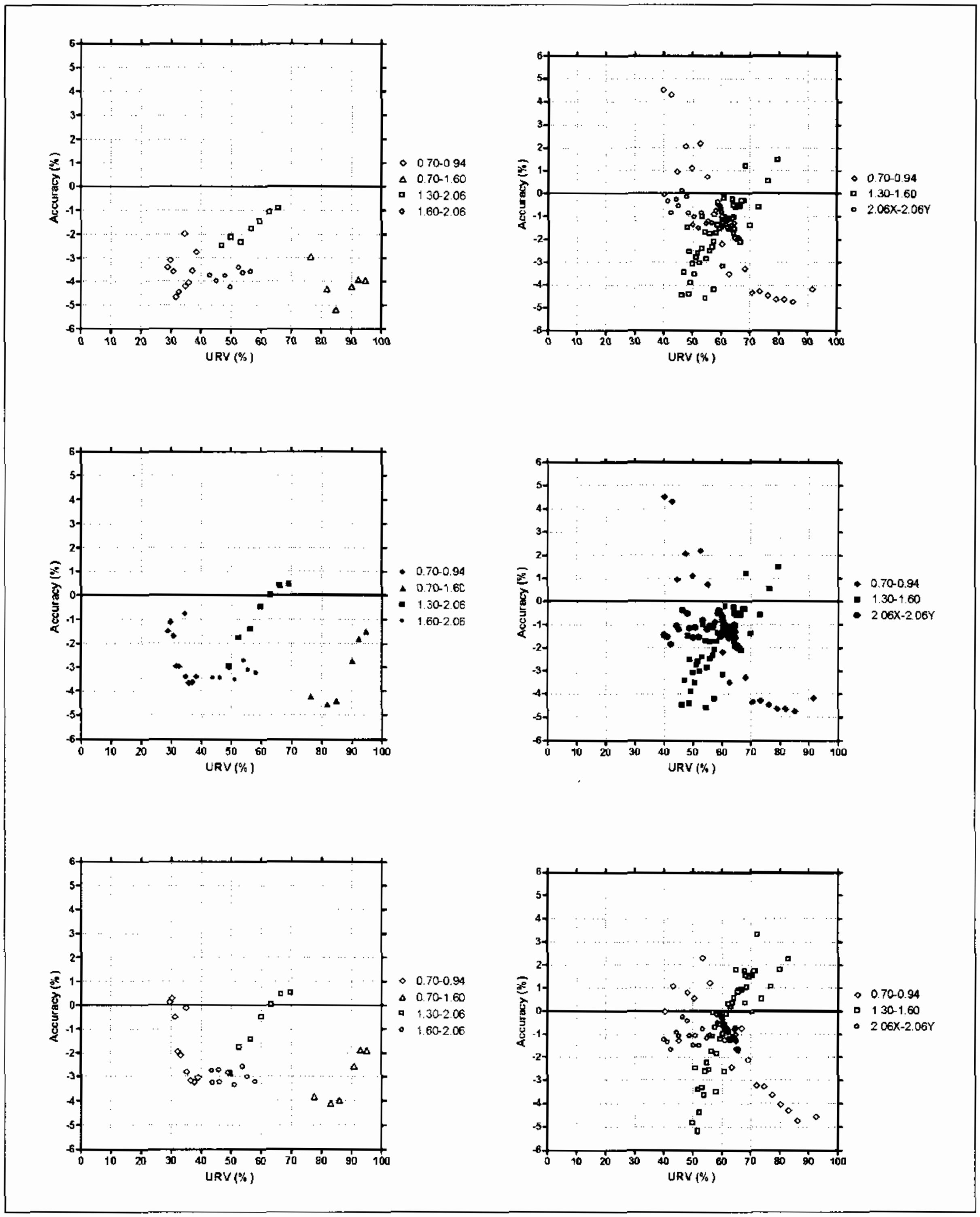

Figure 5.44: Accuracy calibration curves versus the percentage of the continuous J_g sensor URV (upper range value) for tubes 3 (left column) and 4 (right column).

Table 5.12: Accuracy calculation for tubes 3 and 4

Tube 3		
Std. Deviation (%)	0.45	
Precision (%)	0.90	
Mean correction factor	1.03	
Accuracy calculation (%)	**-2.40**	**-4.20**
Tube 4		
Std. Deviation (%)	0.26	
Precision (%)	0.52	
Mean correction factor	1.01	
Accuracy calculation (%)	**-0.90**	**-1.93**

From Table 5.12 we conclude that the accuracy envelope for a J_g sensor is: -2.40 to –4.20 % for a 3 (inch) tube and –0.90 to –1.93 % for a 4 (inch) tube for the range.

5.7.2.3 Discussion

Figure 5.44 shows that data of low bias are located in the 50 - 60 % of URV. To investigate this characteristic, Figure 5.45 was plotted: the x-axis in Figure 5.44 was modified from J_g sensor percentage of URV to pressure transmitter's percentage of URV (PT-URV). It was found that the low bias values are shifted to the range of 30 – 50 % PT-URV. This reinforces the practical conclusion that can be inferred from this analysis: namely, for a given flow delivered to a flotation cell, a linear trend gives acceptable accuracy (compared to the quadratic and cubic), only if the orifice is selected to produce a pressure drop around the half PT-URV.

It can be seen that the bias is minimum (c.a. –3%) at the half range scale for most of the tests. If possible, orifices should be selected to have an operating range that produces a pressure drop around half the scale of the pressure transmitter's percentage of URV. If this is not possible, i.e., shallow flotation cell where the maximum pressure that can be achieved (at the bottom of the sensor) is less than 2941 (Pa) (30 cm of water), the bias can be as high as 5%.

In conclusion, for a given gas flow rate delivered to a flotation cell and a given tube diameter, if an orifice is selected to generate a pressure drop that is ca. half the PT-URV, then the accuracy of the J_g measurement will be ca. –4 % and -2 for an 3 and 4 (inch) tubes respectively. If this is not possible the accuracy can be consider as the range presented in Table 5.12.

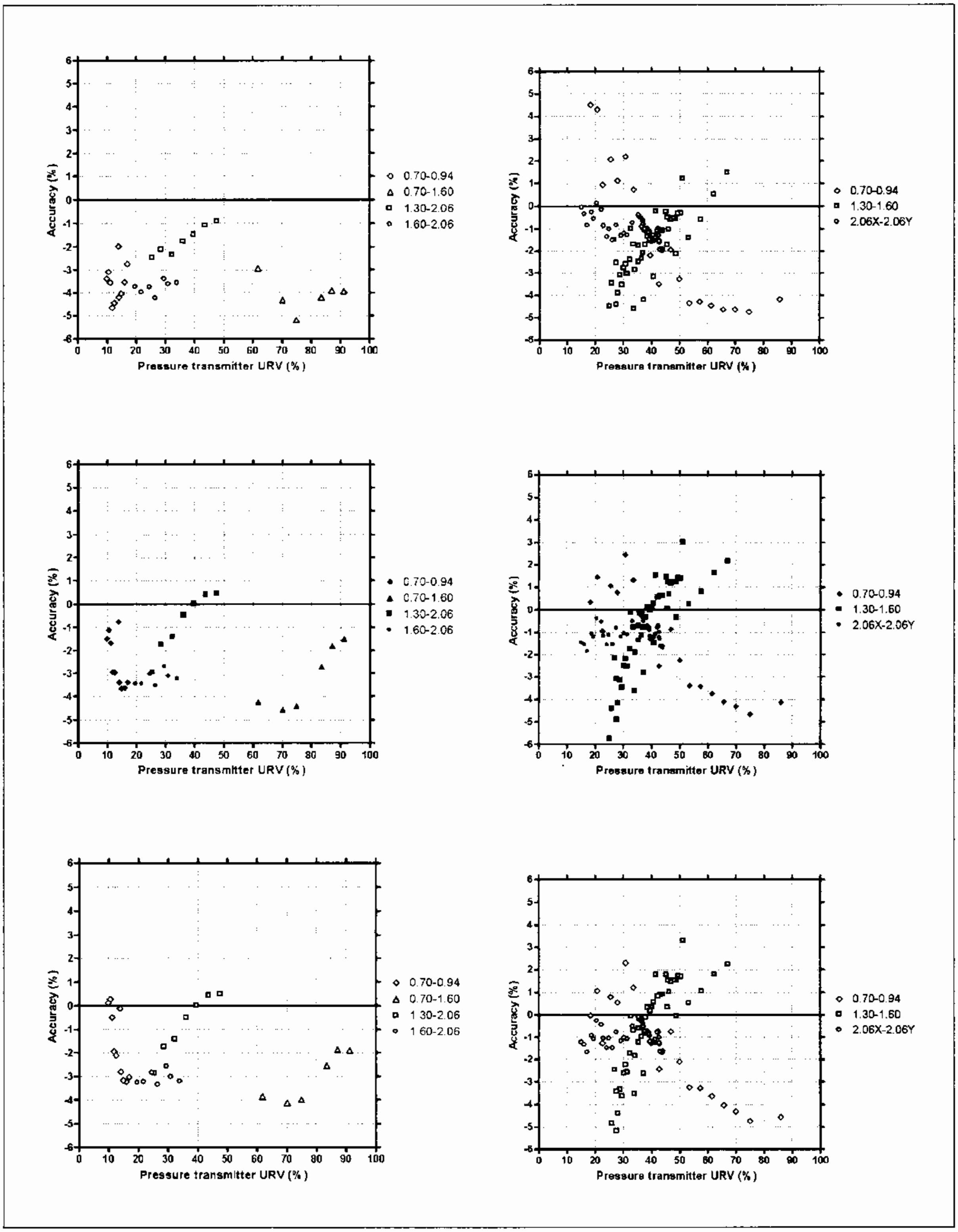

Figure 5.45: Accuracy calibration curves versus the percentage of Pressure transmitter URV for tubes 3 (left column) and 4 (right column).

5.7.3 Dynamic response of a first order lag system

A test was designed to study the response time of the sensor to a step change in the flow. Table 5.13 shows the sensor characteristics. Orifices 0.94 and 1.30 were used. (The explanation for the use of a 3 (inch) (7.62 cm) diameter tube is given in Section 5.8.)

Table 5.13: Sensor characteristics.

H_p (m)	H_l (m)	Tube diameter (cm)
0.76	1.76	7.62 (3 inch)

The first test used orifice 0.94. To execute the step change, the flow delivered to the column was set on 1.64E-3 (SCMS) (ca. $J_{g\ STD}$ = 0.83 cm/s) and after steady state was reached, the flow was increased to 2.00 E-3 (ca. $J_{g\ STD}$ = 1.00 cm/s), defining time zero. Data was collected for 350 seconds. Figure 5.46 shows the result. (Data are in Appendix F, Table F.19.)

A similar procedure was applied to orifice 1.30: The flow delivered to the column was set on 2.00 E-3 (SCMS) (ca. $J_{g\ STD}$ = 1.00 cm/s) and after steady state was reached, the flow was increased to 2.67 E-3 (ca. $J_{g\ STD}$ = 1.30 cm/s). Data was collected between 200 and 350 seconds. Figure 5.47 shows the result. (Data are in Appendix F, Table F.19.)

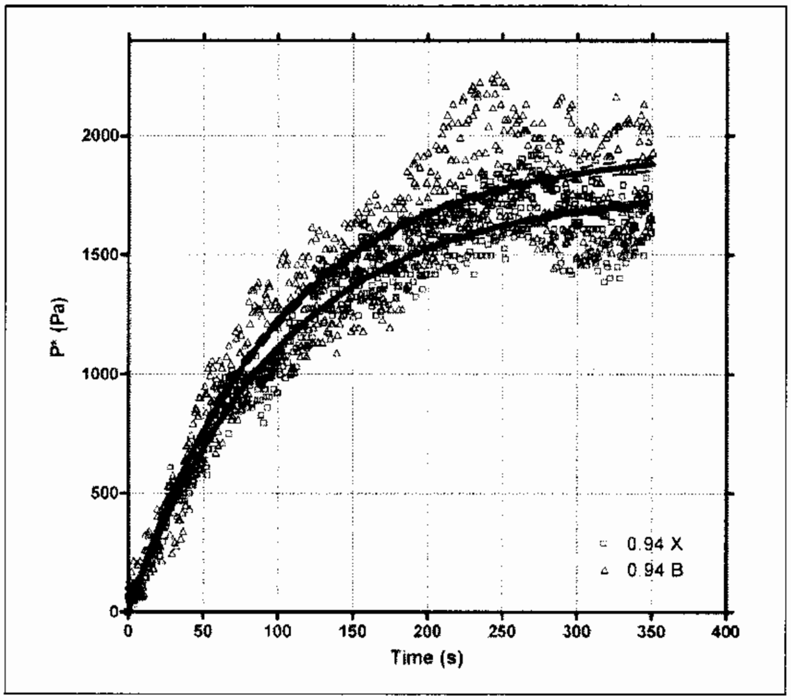

Figure 5.46: Response time curve for a 0.94 orifice, to a step increase in $J_{g\ STD}$ (0.83 to 1.00 cm/s). Solid line is Equation 5.5 fit.

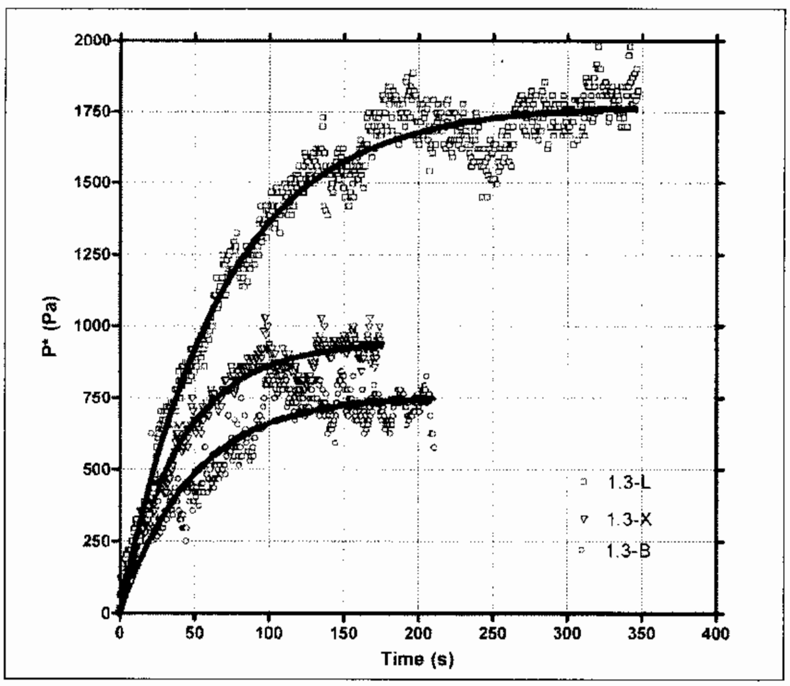

Figure 5.47: Response time curve for a 1.30 orifice, to a step increase in $J_{g\ STD}$ (1.00 to 1.30 cm/s). Solid line is Equation 5.5 fit.

5.7.3.1 Modeling response time to a step change

The governing Equation 4.63 was derived in Section 4.3.2.2:

$$P^{*}(t) = 2B\sqrt{P_s - P_{atm}}R_s(1 - e^{(-t/2\sqrt{P_s - P_{atm}}R_s C_e)}) \qquad \text{Eq. (4.63)}$$

It is one of a family called "one phase exponential association" [10], namely,

$$P^{*}(t) = BK_p * (1 - \exp(-t/\tau_p)) \qquad \text{Eq. (5.9)}$$

Table 5.14 shows the coefficients τ_p and K_p estimated from the non-linear fitting of Equation 5.5 using the data in Figures 5.46 and 5.47. (The raw data are presented in Appendix F, Table F.19.)

Table 5.14: K_p and τ_p coefficients from non-linear fitting of Equation 5.5.

Orifice	1.3-X	1.3-L	1.3-B	0.94-X	0.94-B
BK_p (Pa)	946	1774	759	1771	1940
τ_p (s)	41.05	68.40	48.69	101.10	100.60

The analysis assumes τ_p is constant. This derives from Equation 4.43, which assumes C_e is constant, leading to the conclusion that τ_p is constant (Equation 4.57). However, for a large step change in flow delivered to a flotation cell (higher than 50%) measured with a sensor tube more than 2 (m) long, C_e cannot be considered constant (i.e. the linearization assumption would be violated). In the present case, the tube is short (less that 1 m) and changes in the flow delivered to a flotation cell higher than 10% are rare. Probably a constant C_e, therefore, is reasonable.

The fluctuations at the longer times in Figures 5.46 and 5.47 may suggest higher order terms, but the variations could also be the result of sampling bubbles from a swarm. At this stage a first order approximation seems sufficient.

Table 5.15 shows the results of modeling using Equation 4.63. The data are presented in Appendix F, Table F.19.

Table 5.15: K_p and τ_p coefficients from Equation 4.63. Average values calculated at $(H_l-H_P)/2$.

Orifice	1.3-X	1.3-L	1.3-B	0.94-X	0.94-B
BK_p (Pa)	1067	1502	802	1774	1991
τ_p (s)	44.50	70.32	42.33	111.32	112.64

Having this in mind, we can study the dynamic response of a first order lag system, with the help of a plot $\frac{P^*(t)}{BK_p}$ versus $\frac{t}{\tau_p}$ (Figure 5.48).

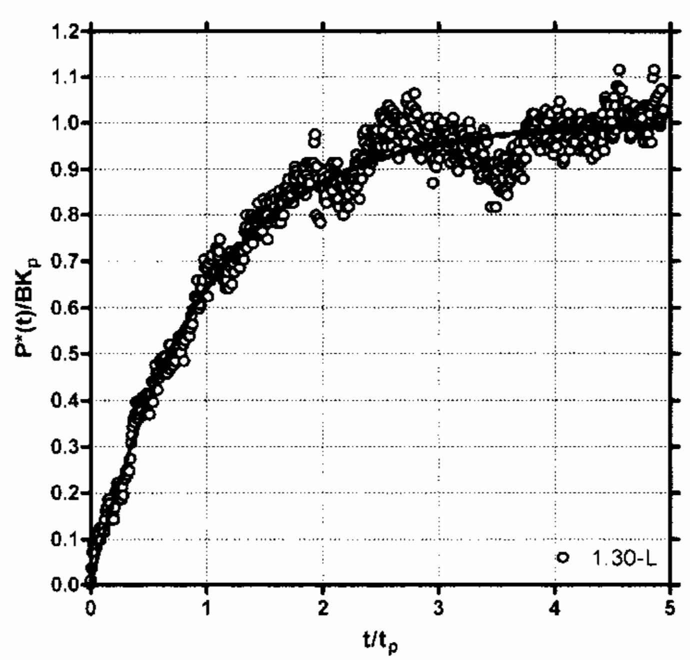

Figure 5.48: Example of dimensionless response of first order lag to step input change (orifice 1.30-L).

5.7.3.2 Model characteristics analysis

Stephanopoulos [61] describes the important characteristics of the plot in Figure 5.48. They are listed below (a, b, c, and d) followed by the implications for the continuous McGill J_g sensor:

a) A first order lag system is self-regulating, i.e., the process reaches a new steady state.

In our system this means that when the inlet flow increases by a unit step, the slurry level in the sensor goes down, as a result of the increase in pressure inside the tube, which in turn increases the flow rate $q_{KPS,out}$. "This action works towards the restoration of an equilibrium state".

b) The slope of the response at t=0 is equal to 1. The implication is that "if the initial rate of change of P*(t) were to be maintained, the response would reach its final value in one time constant". A practical conclusion is that: "The time constant τ_p of a system is a measure of the time necessary for the process to adjust to a change in its input".

In the present subject, for a given tube diameter, τ_p is independent of the magnitude of the step change B. In other words, τ_p is characteristic of the sensor primary device (tube diameter, orifice diameter). This is because τ_p is a function of C_e (C_e is a function of diameter of the tube, Equation 4.39).

c) In the plot, the value of the response P*(t) reaches 63.2 % of its final value when the time elapsed is equal to one time constant τ_p. It can be calculated from the plot that for two, three and four time constants, the values reached by P*(t) as a percentage of its final value are 86.5, 95 and 98.

For practical purposes here, after four time constants P*(t) reaches its final value.

d) The terms "steady state" or "static gain" are given to K_p because for "any step change in the input Δ(input), the resulting change in the output steady state is given by",

$$\Delta(\text{output}) = K_p \Delta(\text{input}) \qquad \text{Eq. (5.10)}$$

Equation 5.10 indicates how sensitive is the system. For example, the same effect in the output stream can be reached by: "A very small change in the input if K_p is large (very sensitive sensor) or "a large change in the input if K_p is small".

For a given P_s, the K_p will be a function of the R_s (Equation 4.57), which is a function of the calibration of the orifice (Equation 4.45). A rule of thumb is the smaller the orifice diameter, the higher R_s (higher orifice resistance to the gas flow), and therefore the higher the K_p (higher pressure drop gain).

5.7.3.3 Sensor design

The data from the slope for each orifice ($1/R_s$) (Appendix F, Table F.13-1), were analyzed using the approach discussed in Section 5.7.3.2 with Equation 4.63. Designs for two sensors are shown in Tables 5.16 and 5.17. Tables 5.18 and 5.19 show the results of response time for a step change to produce a 2942 (Pa) (30 cm of Water) pressure step change for two sensors: sensor 1 (tube diameter 3 inch, 7.62 cm) and sensor 2 (tube diameter 2 inch, 5.08 cm), respectively. (Complete data sets are presented in Appendix F, Table F.20.). Figure 5.49 shows sensor 1, sensor 2 and sensor 3 (sensor 2 modified with a "funnel" of the same opening as sensor 1).

Sensor 1 has been extensively used in plant campaigns (see Chapter 6) and sensor 2 was designed by applying the model to achieve a comparable response time for a tube of smaller diameter. For sensor 2 it is necessary to use a smaller orifice diameter to generate the same pressure change for the same J_g. This can be illustrated with an example: let us chose two orifices that generate a $J_{g\ STD}$ around 1.00 (cm/s), orifice 1.30 (J_g = 1.07 cm/s, Table 5.18) and orifice 0.94 (J_g = 1.07 cm/s, Table 5.19). In these cases, the response time is the same (97 s). This equivalence is approached because as tube diameter is decreased the volume of air passing through the sensor is decreased to produce the same pressure change, thus a smaller orifice must be used. (It can be seen in Tables 5.18 and 5.19 that the smaller the orifice the higher the response time, for the same pressure drop.)

In the second example, consider sensor 1 and sensor 3. As the same gas flow rate will enter both sensors, both require the same orifice (in this example, 1.30). But the configuration in sensor 3 decreases the response time by ca. 50% (97 to 43 s, Tables 5.18 and 5.19, respectively). This is because the ratio of volume of air to slurry in sensor 3 is higher than 1, which reduces the time to reach the new steady state.

The issue considered here is only the tube diameter/orifice selection component of sensor design. As the next Section illustrates, a too small tube diameter, while apparently attractive as it becomes more readily manipulated, runs the risk of biasing the bubble sample. And, the funnel idea while offering decreased response time will probably induce additional frothing through the increase in air/slurry ratio in the tube (Appendix E).

The author recommends the use of sensor design 1.

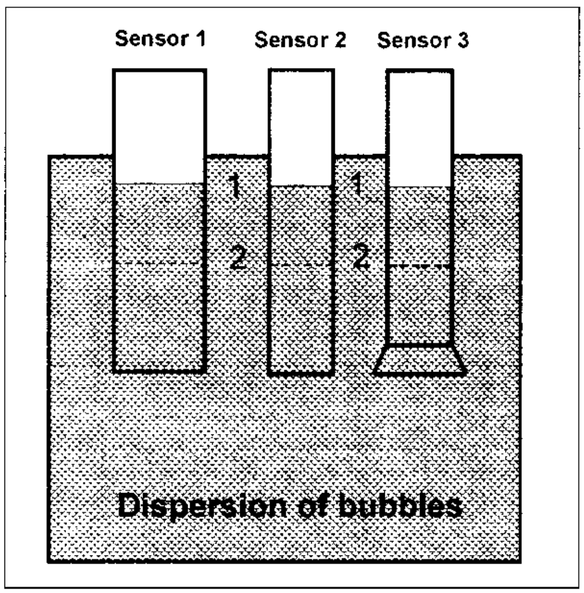

Figure 5.49: Modeling the response time for example 1 and 2.

Table 5.16: Sensor 1 design.

Tube diam. (cm)	7.62
H_l (m)	3
H_p (m)	2
P_s-P_{atm} (Pa)	1373
P_{final}-P_{atm} (Pa)	2942

Table 5.17: Sensor 2 and 3* design.

Tube diam. (cm)	5.08
H_l (m)	3
H_p (m)	2
P_s-P_{atm} (Pa)	1373
P_{final}-P_{atm} (Pa)	2942

* sensor 3 has the same opening as sensor 1.

Table 5.18: Response time calculations for sensor 1 design (Table 5.16).

Orifices	0.70	0.94	1.00	1.30	1.60	2.06
$4\tau_p$ (s)	370	219	189	**97**	76	43
BK (Pa)	1569	1569	1569	1569	1569	1569
J_g (cm/s)	0.28	0.47	0.55	**1.07**	1.36	2.42

Table 5.19: Response time calculations for sensor 2 and 3 design (Table 5.17).

Orifice	0.70	0.94	1.00	1.30	1.60	2.06
$4\tau_p$ (s)	165	**97**	84	**43**	34	19
BK (Pa)	1569	1569	1569	1569	1569	1569
J_g sensor 2 (cm/s)	0.63	**1.07**	1.23	2.42	3.06	5.45
J_g sensor 3 (cm/s)	0.28	**0.47**	0.55	**1.07**	1.36	2.42

5.8 Test of sampling

5.8.1 Introduction

A series of tests was designed to probe bubble sampling by the on-off and continuous techniques. The objective was to study the influence of the tube diameter in the collection of bubbles from a dispersion. For this, a standard instrument is required. A continuous J_g sensor with a tube 4 (inch) (nominal diameter) was selected as a standard (accuracy determined in Section 5.7) and the head of the sensor was adapted with an internal thread to add tubes of different diameter. If an internal concentric tube is installed in the standard J_g sensor, it is possible to measure J_g inside the sampling area of the standard sensor. Comparison between J_g measurements is an indication of the influence of the tube diameter. Figure 5.50 illustrates the concept.

Since bubble size is important in helping interpret the data, it was also measured (using the McGill bubble size analyzer).

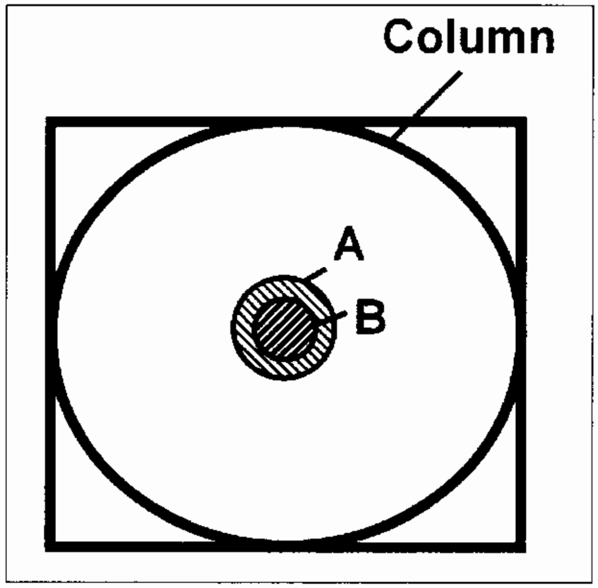

Figure 5.50: Sampling test. A: standard sensor. B: internal sensor.

5.8.2 Experimental setup

A 4 (inch) J_g sensor including on-off and continuous modes was designed (Figure 5.51). The sensor was built with a removable head with half (inch) NPT internal thread to add tubes of different diameter (Figure 5.52). The bottom end of the J_g sensor tubes was machined with a bevel of 60° (Figure 5.53).

Tests were carried out in a 4 (m) high, 50 (cm) diameter column with a Slamjet sparger (Figure 2.13 and 2.14). From experience, it is known that this kind of sparger produces a wide size distribution of bubbles [29] compared to a porous sparger [13].

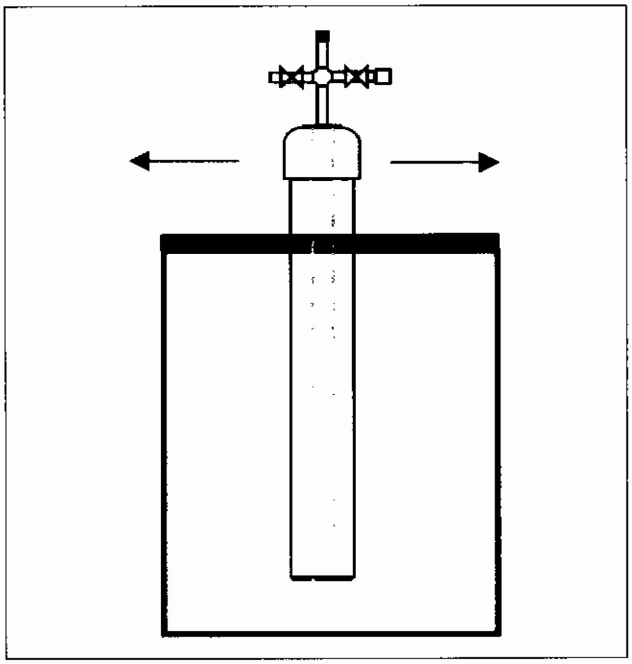

Figure 5.51: Sensor setup. The sensor was installed on a movable plate at the top of a 4 m high, 50 cm diameter column. The dashed lines are the internal J_g sensor.

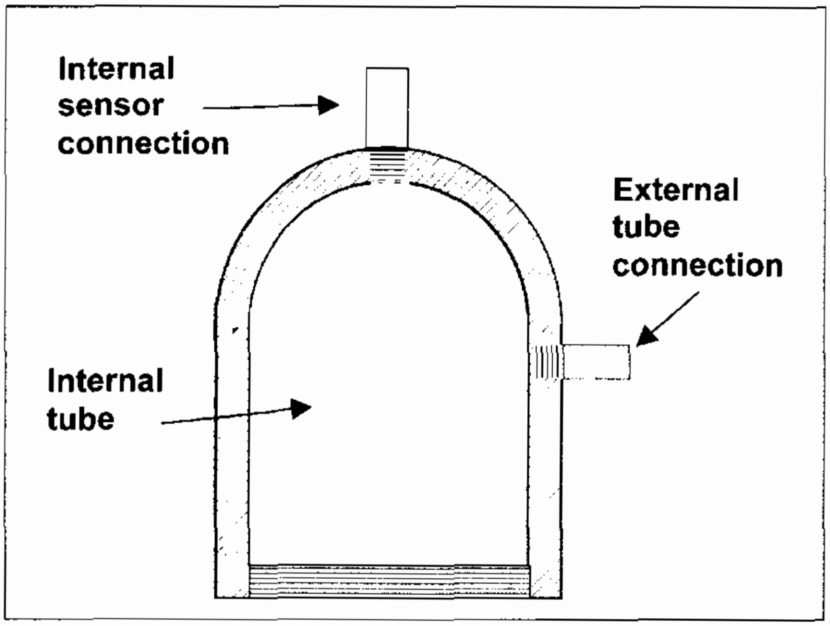

Figure 5.52: Sensor head details.

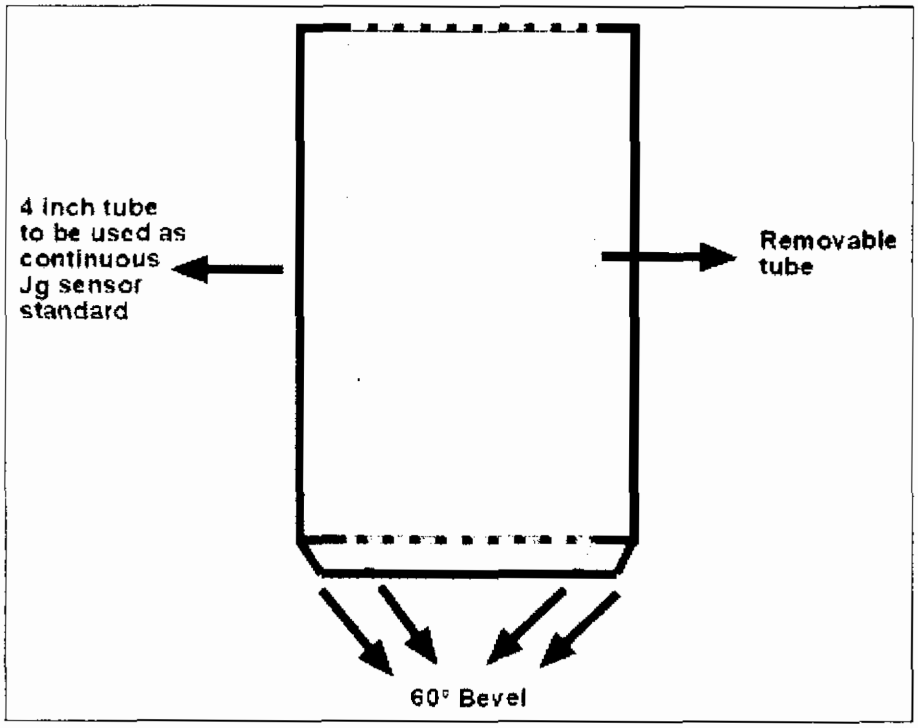

Figure 5.53: J_g sensor: details on base of tube.

The orifices used in the tests are indicated in Appendix F, Table F.22.

5.8.3 Results

The first set of experiments was to identify radial gas distribution. A continuous J_g sensor (tube 4) was located at 5 positions in the column (Figure 5.54). Data was collected for 600 seconds for each location. Figure 5.55 shows the results of this preliminary test. It can be observed that the gas distribution is not even and not symmetrical (although the variations are small). The value of the "escape" J_g (Q_g/A) agrees with the J_g measured by the sensor in locations b, c, d and e. The data are presented in Appendix F, Table F.21.

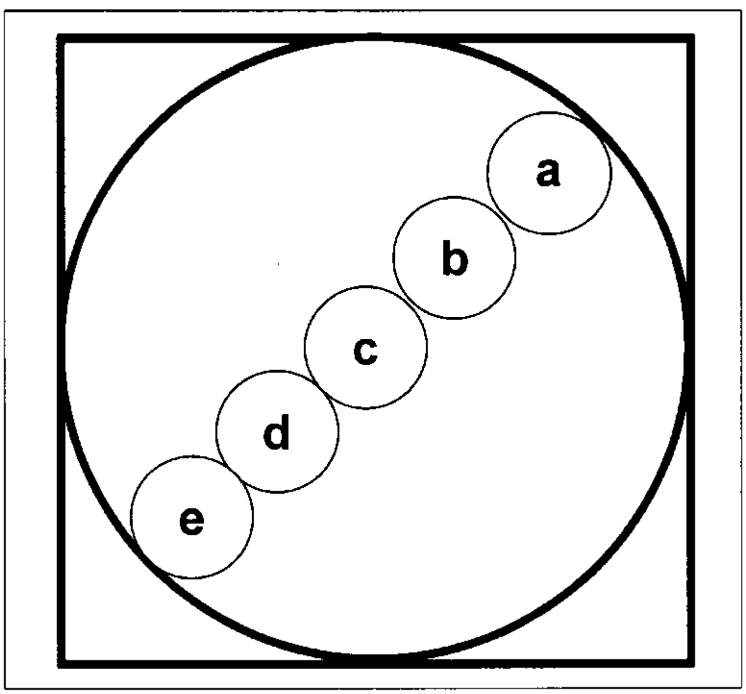

Figure 5.54: Sampling locations.

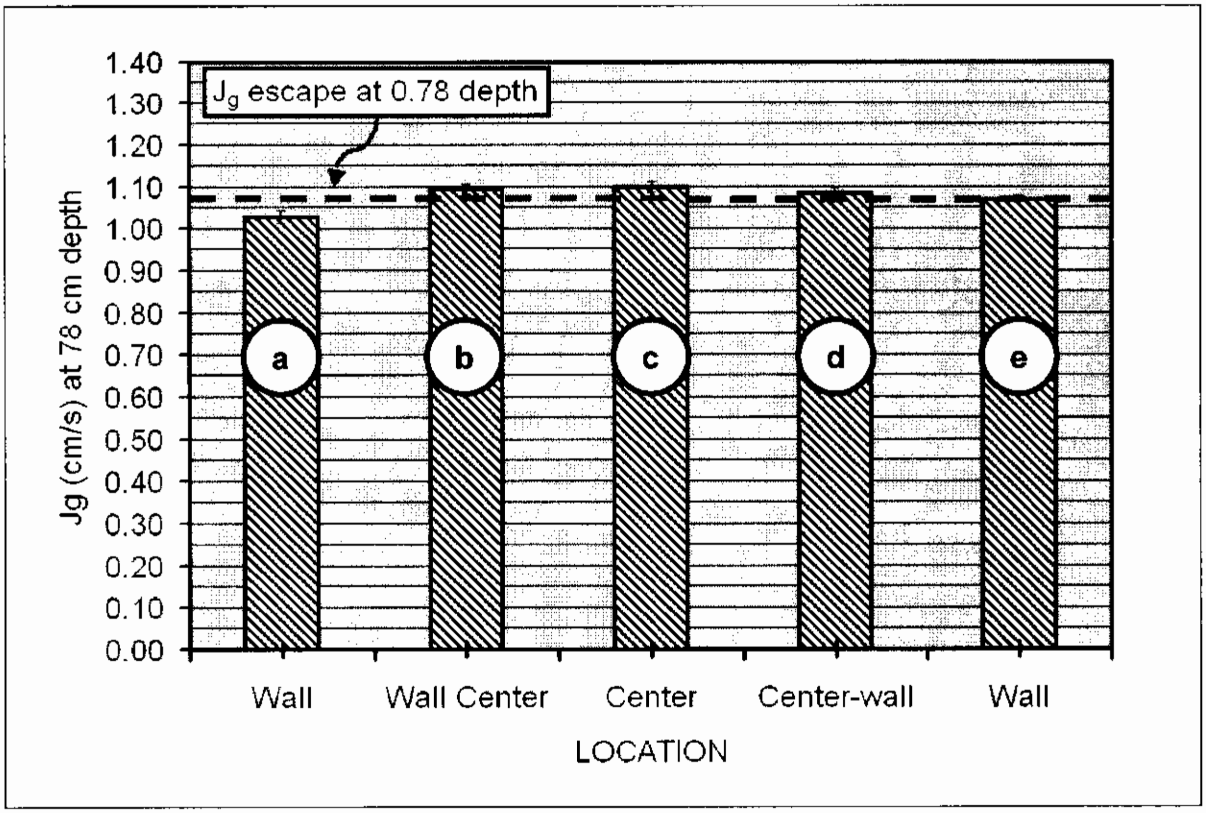

Figure 5.55: Continuous J_g distribution. Letters are the sampling locations as Figure 5.54.

A t-student test was applied to the data (Appendix F, Table F.21) and it was found that a significant difference between the wall location (a) and the center (c).

Based on the previous experiment, the sampling locations chosen were center ("c") and wall ("a"). On-off and continuous J_g measurements were conducted for a High J_g (= 1.75 cm/s) and Low J_g (=0.75 cm/s) with 50 ppm of MIBC. The reason for this range was to generate two different bubble size distributions in the column.

A t-student test was applied to the data (Appendix F, Table F.21) and it was found that a significant difference between the wall location (a) and the center (c).

Based on the previous experiment, the sampling locations chosen were center ("c") and wall ("a"). On-off and continuous J_g measurements were conducted for a High J_g (= 1.75 cm/s) and Low J_g (=0.75 cm/s) with 50 ppm of MIBC. The reason for this range was to generate two different bubble size distributions in the column.

Data was collected for each tube diameter and location for 600 seconds for the continuous J_g, and ten slopes were taken for the on-off J_g. The results are presented in Figures 5.56 and 5.57 (W and C stand for wall and center locations, respectively). The nomenclature is easiest followed with an example: Figure 5.56, "3 W" means tube of 3 (inch) at a wall location, and the values of 1.65 and 1.73 (cm/s) correspond to on-off and continuous J_g, respectively. Complete data sets are presented in Appendix F, Table F.22.

Lines (dots and dashes) in Figures 5.56 and 5.57 represent reference values, the white and black dotted lines represent the J_g measured with the continuous sensor with tube 4 at the center and wall locations respectively. The dashed line is the J_g escape.

Note that the accuracy determined in Section 5.7.2.2 was from –2.40 to -4.20 % and –0.90 to –1.93 % for the continuous technique with tube 3 and 4 respectively. Observed in Figures 5.56 and 5.57 is the good agreement between the two techniques for tubes 3 and 4, and a significant difference for tubes smaller than 3, with the on/off always lower than the continuous. To illustrate, Figure 5.57 shows a difference of 5% in the two techniques for case 4C and when the comparison is between the 4 continuous and 0.5 on/off, the difference went up to 44 %. Statistical t- tests for two samples confirmed the significance of the results (Appendix F, Table F.22).

The conditions are important in the case of tube 2; where Figure 5.56 shows a difference of 13 % between the techniques at the wall and center locations, in Figure 5.57 the difference went up to 20 %. This probably reflects the downward flow of water (J_l) that is generated by the bubbles accumulating in the on-off sensor which tends to exclude some bubbles (this will be discussed in Section 5.8.4). Not only is the gas rate different, so is the bubble size distribution. With the Slamjet, bubbles are generated by shear between the flow of gas and liquid. At J_g = 0.75 (cm/s) the shear is lower than at 1.75 (cm/s) and a wider distribution of bubbles is expected. This seems confirmed in Figure 5.57 (J_g = 0.75 cm/s) with tubes 3 and 4 because J_g at the center, where large bubbles are expected to accumulate, is higher than at the wall; in contrast, in Figure 5.56 (J_g = 1.75 cm/s), a more even distribution is found (the values of J_g are similar at wall and center).

above 3 (inch) is not a factor. (For obvious practical reasons, the smaller tube 3 (7.62 cm diameter) is recommended for field work.).

Tables 5.21 and 5.22 summarise the results of the differences between the continuous and on-off measurements. Good agreement was found between the two sensors for tubes 3 and 4 (compare the differences line by line) despite the wide range in J_g (0.75 to 1.75 cm/s) that may be expected to also involve different bubble size distributions [67]. This may mean there is little influence of the bubble size distribution on the J_g measurement. Deliberate changes in bubble size (using another bubble generator system, for instance) are needed to confirm.

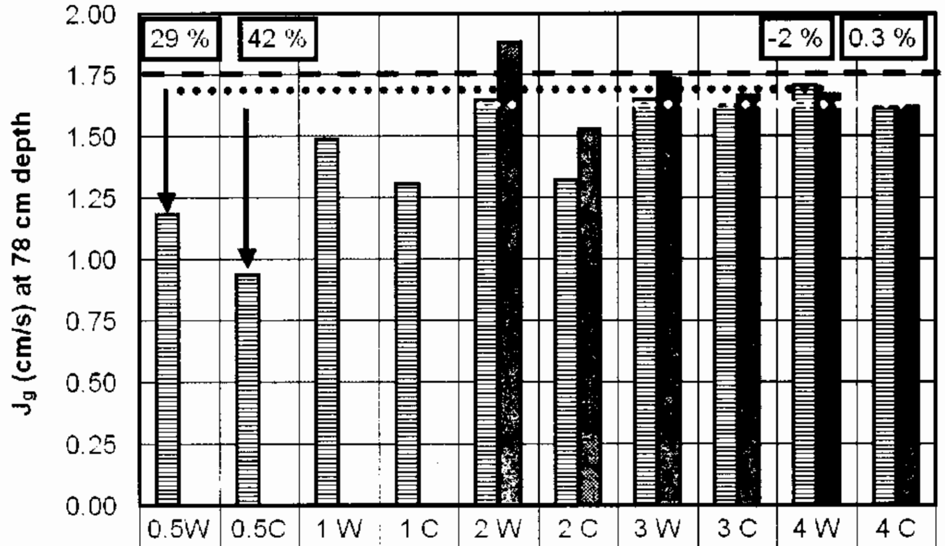

	0.5W	0.5C	1 W	1 C	2 W	2 C	3 W	3 C	4 W	4 C
on\off (cm/s)	1.18	0.94	1.49	1.31	1.64	1.32	1.65	1.62	1.70	1.61
cont. (cm/s)					1.88	1.53	1.73	1.66	1.67	1.62

Figure 5.56: High J_g = 1.75 (cm/s).

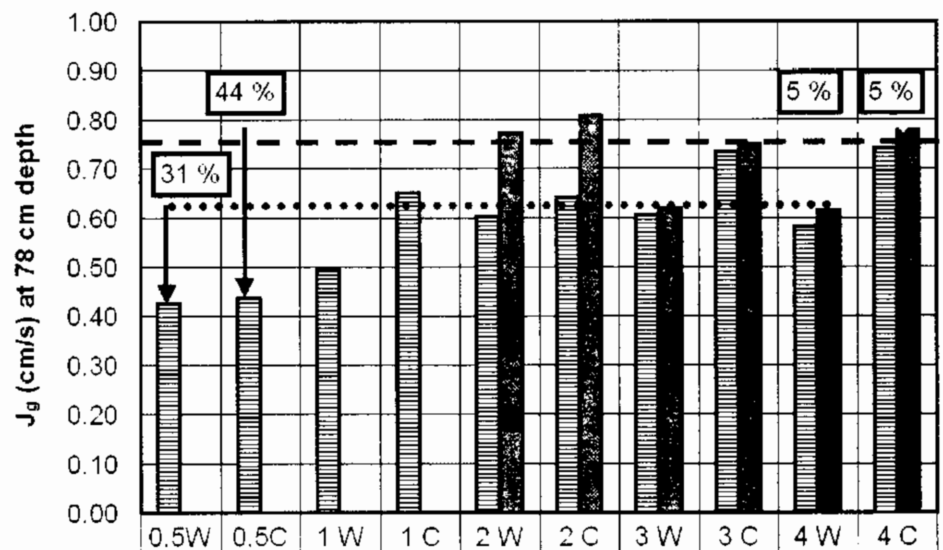

	0.5W	0.5C	1 W	1 C	2 W	2 C	3 W	3 C	4 W	4 C
on\off (cm/s)	0.43	0.44	0.49	0.65	0.60	0.64	0.61	0.73	0.58	0.74
cont. (cm/s)					0.77	0.81	0.62	0.75	0.62	0.78

Figure 5.57: Low J_g = 0.75 (cm/s).

Table 5.21: Difference between continuous and on-off for J_g = 1.75 (cm/s) at 78 (cm) depth and 292.15 (K).

Location	Tube Continuous	Tube On-off	J_g Continuous (cm/s)	J_g On-off (cm/s)	Difference (%)
Center	4	4	1.62	1.61	**0.3**
Center	3	3	1.66	1.62	2.5
Center	2	2	1.53	1.32	13.5
Center	4	1	1.62	1.31	19.2
Center	4	0.5	1.62	0.94	**42.0**
Wall	4	4	1.67	1.70	**2.1**
Wall	3	3	1.73	1.65	4.7
Wall	2	2	1.88	1.64	12.7
Wall	4	1	1.67	1.49	8.1
Wall	4	0.5	1.67	1.18	**29.2**
Tube 2					
Continuous	Wall	Center	1.88	1.53	18.8
On-off	Wall	Center	1.64	1.32	19.5

Table 5.22: Difference between continuous and on-off for J_g = 0.75 (cm/s) at 78 (cm) depth and 292.15 (K).

Location	Tube Continuous	Tube On-off	J_g Continuous (cm/s)	J_g On-off (cm/s)	Difference (%)
Center	4	4	0.78	0.74	**4.7**
Center	3	3	0.75	0.73	2.1
Center	2	2	0.81	0.64	20.5
Center	4	1	0.78	0.65	16.4
Center	4	0.5	0.78	0.44	**43.8**
Wall	4	4	0.62	0.58	**5.3**
Wall	3	3	0.62	0.61	2.3
Wall	2	2	0.77	0.60	22.1
Wall	4	1	0.62	0.49	19.7
Wall	4	0.5	0.62	0.43	**30.8**
Tube 2					
Continuous	Wall	Center	0.77	0.81	4.6
On-off	Wall	Center	0.60	0.64	6.7

5.8.4 Bubble size measurement

The jetting sparger (Slamjet) was chosen for the "sampling" tests because of the wide size range of bubbles generated, which provides a "worst case scenario" (mechanical cells normally generate narrower bubble size distributions).

The present image processing protocol [43,44] does not reliably measure bubbles that exceed 3 (mm) which typically have a shape factor[11] lower than 0.7. The sets of images (Figures 5.58 and 5.59) show two experiments with the same column operating conditions (and thus the same bubble size distribution in the column), but because of the different sampling tube diameter in the bubble analyzer (0.5 and 1 inch located near the wall as in Figure 5.54), the sampling appears biased in tube 0.5, where fewer large bubbles are noted. This corresponds to Figure 5.56, where tube 1W measures a higher J_g than 0.5W.

Bailey [13] discussed the impact of the tube diameter and divided the problem into three groups: bias towards small bubbles, bias against small bubbles, and bias against large bubbles.

The first occurs when a large bubble carries small bubbles in its wake into the sampling tube. This can cause an over estimation of the small bubble population.

The second is caused by the downward liquid flow that hinders small bubbles from entering the tube. Note, the effect may be greater than expected from knowing the average downward superficial velocity (J_l) as at the bottom of the sampling tube the presence of bubbles creates high local interstitial velocities which further counter small bubbles from entering.

---

[11] Shape factor $= 4\pi \text{Area} / \text{Perimeter}^2$

The third case is caused by physical restrictions: The diameter of the tube must be large enough to accommodate the largest bubbles. Using a rule in sampling particles, the opening should be at least 3 times the dimensions of the largest bubble.

In terms of the estimation of J_g, the small bubbles do not contribute as much as the big bubbles. (One large bubble represents the same volume as thousands of small bubbles.) The practical concern is that the tube be wide enough to sample the large bubbles. From Figures 5.56 and 5.57, the 3 (inch) tube appears sufficient.

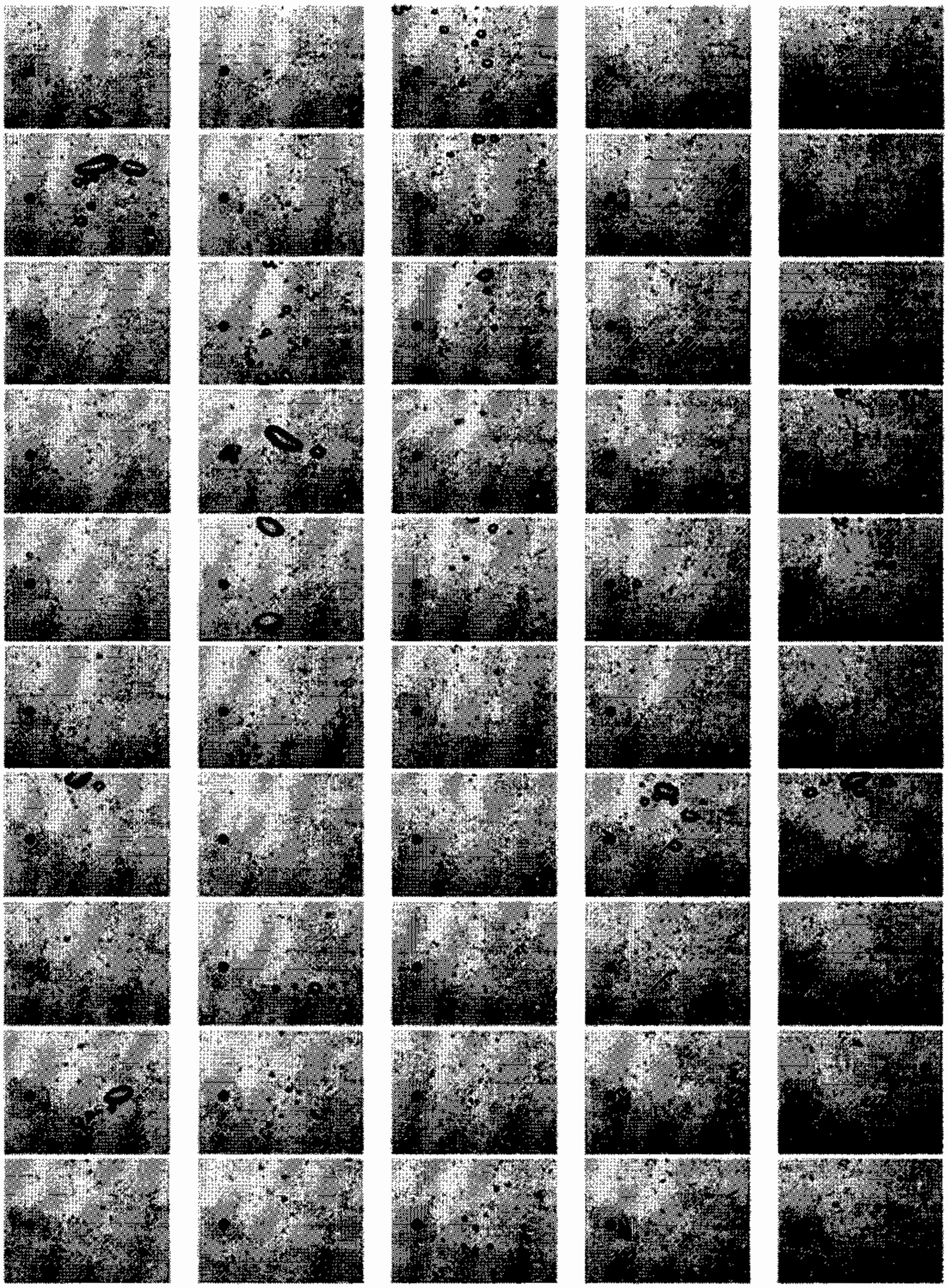

Figure 5.58: Sequence of images (sampling rate 0.5 s per picture) for tube of 0.5 (inch) and $J_{g\,STD}$ = 1.75 (cm/s). Black disk is a 3.05 (mm) standard.

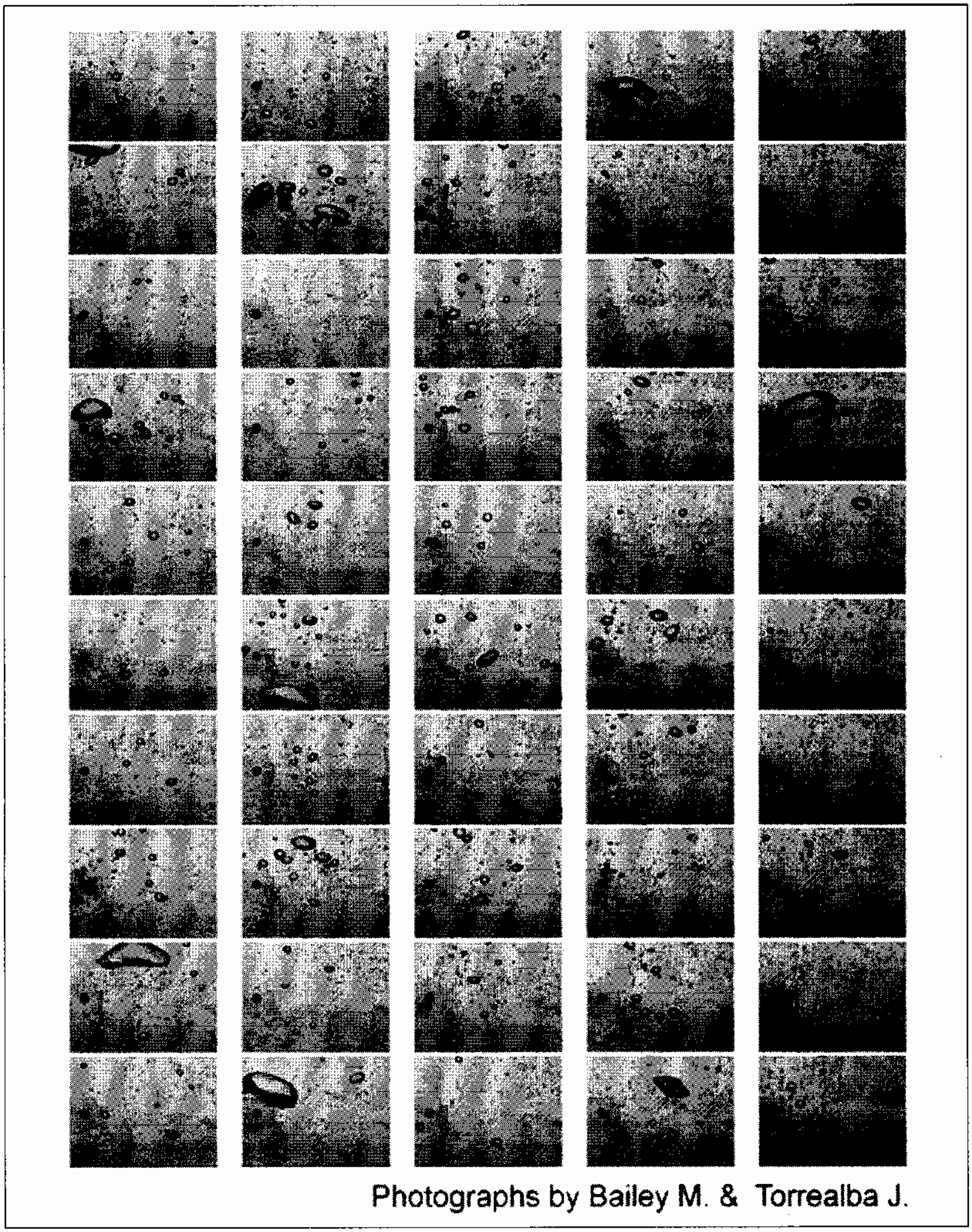

Figure 5.59: Sequence of images (sampling rate 0.5 s per picture) for tube of 1 (inch) and $J_{g\,STD}$ = 1.75 (cm/s). Black disk is a 3.05 (mm) standard.

5.9 Sensitivity analysis for the continuous sensor

A computer sensitivity analysis was conducted for the continuous J_g sensor (Equation 4.40). Figure 5.60 was constructed (data in Appendix F, Table F.29) using the parameters described in Table 5.23.

Table 5.23: Parameters for sensitivity analysis.

Orifice	1.30
Tube diameter (cm)	7.62
P_s (Pa)	104266.78
T (K)	292.15
P_{atm} (Pa)	101325

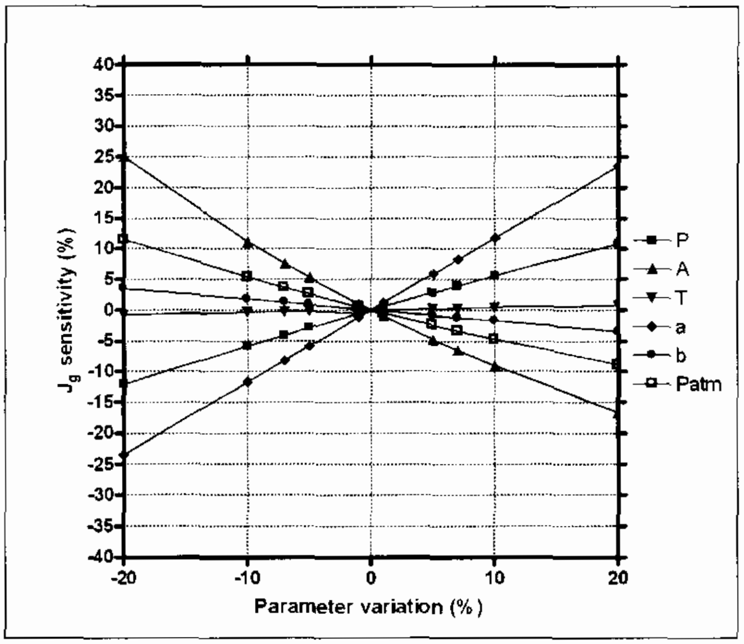

Figure 5.60: Sensitivity analysis for parameters described in Table 5.23.

Figure 5.60 shows the high sensitivity of J_g to the slope coefficient in the calibration, a_{SCMS} (as an example, in Figure 5.16 a 10% change in a_{SCMS} gives almost 12% impact on J_g), and the limited influence of a change in T (as an example, in Figure 5.60 a 20 % change in T gives only 0.72 % impact on FP).

Changes of P_{atm} during data collection normally are small in the range of 5% and the impact of P_{atm} is not considered.

The sensitivity of J_g to a_{SCMS} has an important consequence considering that the reproducibility of a set of 0.94 orifices gave a standard deviation of 8% for a_{SCMS}. The tolerance on the orifices has to be improved.

CHAPTER 6.0
EXPERIENCES WITH THE SENSORS IN PLANT CAMPAIGNS

6.1 Introduction

The on-off and continuous McGill J_g sensors have been used extensively in plant campaigns. The examples range from detecting malfunctioning airflow meters and dart valves [20], to revealing the advantage of setting the distribution of air to cells in a bank, or "J_g profiling" [19].

Figure 6.1 is an example of the impact of profiling. The two parallel 7 cell (Denver 100) banks comprising the final (fourth) Zn cleaner stage at Brunswick Mine were compared, one with J_g increasing from the first to the last cell (the manipulated bank, Row P1, full lines) the other operated normally, i.e., the air set as the operator judged (the control bank, Row P0, dashed lines). The consistent finding was that the manipulated bank with increasing J_g profile outperformed the control bank. This is evident not only because the down-the-bank grade / recovery curves for Row P1 were clustered above those for Row P0 but on each day of the comparison (the same symbol shapes are used) the manipulated bank out did the control bank. The increasing profile was found the best among balanced (all cells with the same air rate) and decreasing. The result was sufficiently clear over several months to convert first the last two cleaning stages to the increasing J_g profile then all four banks, which is the current strategy. The advantage of the increasing profile was traced to control of water recovery and thus entrainment, which is kept low in the first cells where J_g is the lowest.

While it cannot be concluded that an increasing J_g profile fits all situations, clearly demonstrated is the potential metallurgical gain from setting a profile. Establishing a profile with the on/off sensor, however, took the best part of a shift, partly because interactions between cells necessitated constant re-checking. The desirable approach would be to measure gas rate continuously and simultaneously in all cells in the bank. The on/off technique is difficult to refine to meet this challenge. In response, the continuous version was devised.

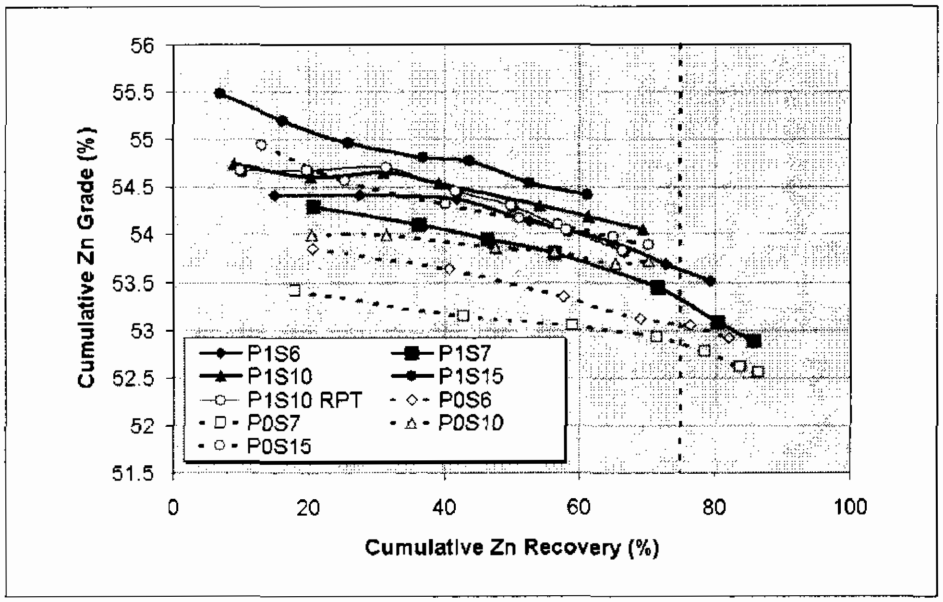

Figure 6.1: Final Zn cleaner stage, Brunswick Mine: comparison of grade / recovery relationships for manipulated row P1 with increasing J_g profile (full lines, closed symbols) with results at corresponding times for control row P0 (dashed lines, open symbols). Note: the vertical dashed line is the target recovery (from Cooper et al. [19]).

To illustrate uses, examples are drawn from plant campaigns in which the author was involved.

6.2 Cell mapping: Northparkes

Northparkes is a gold, copper mine located 27 (km) NW of Parkes, New South Wales, Australia, owned by Rio Tinto, Sumitomo Metal Mining Co. Ltd., and Sumitomo Corporation.

Mapping involves radial and depth measurements, undertaken partly to see how gas is distributed and partly to decide where to install a sensor, for example, for setting J_g profiles down a bank of cells.

Figure 6.2 shows the results of mapping conducted on the second cell (DO-100, Dorr-Oliver nominally 100 m^3) in the Rougher bank at Northparkes mine using the on-off McGill sensor. Data and sensor characteristics are given in Appendix F, Table F.23. The locations are: "1" close to the level controller; "2" half way between the wall and the impeller shaft; "3" close to the impeller and "4" close to the cell wall.

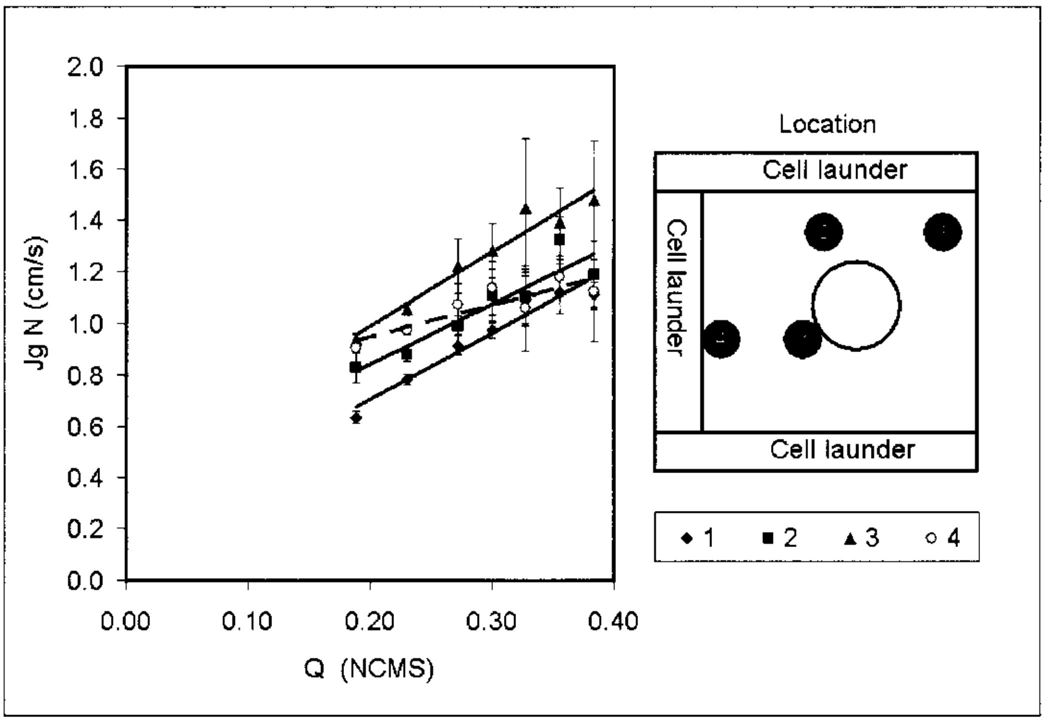

Figure 6.2: Mapping of a flotation cell. NCMS stands for normal cubic meter per second and N stands for normal.

Figure 6.2 reveals information about the distribution of air across the flotation cell. Cell locations 1, 2 and 3 show the same trend but different J_g values, while location 4 (the dashed line in the Figure) has a different slope from the others. The explanation was found in the geometry of the wall, which was angled and restricted bubbles from entering the sensor. (Note, the error bars in the Figure are the standard deviations.)

Another survey with the on-off sensor examined the possible impact of impeller rotation direction. With a set of 4 J_g sensors present, the rotation of the impeller was changed in two Rougher DO-100 cells. An airflow of 0.30 NCMS (setpoint) was delivered to the cells operated at three froth depths a: 0.12, b: 0.14 (setpoint) and c: 0.16 (m). Figures 6.3 and 6.4 show the results of those tests. Sensors characteristics and data are given in Appendix F, Table F.24.

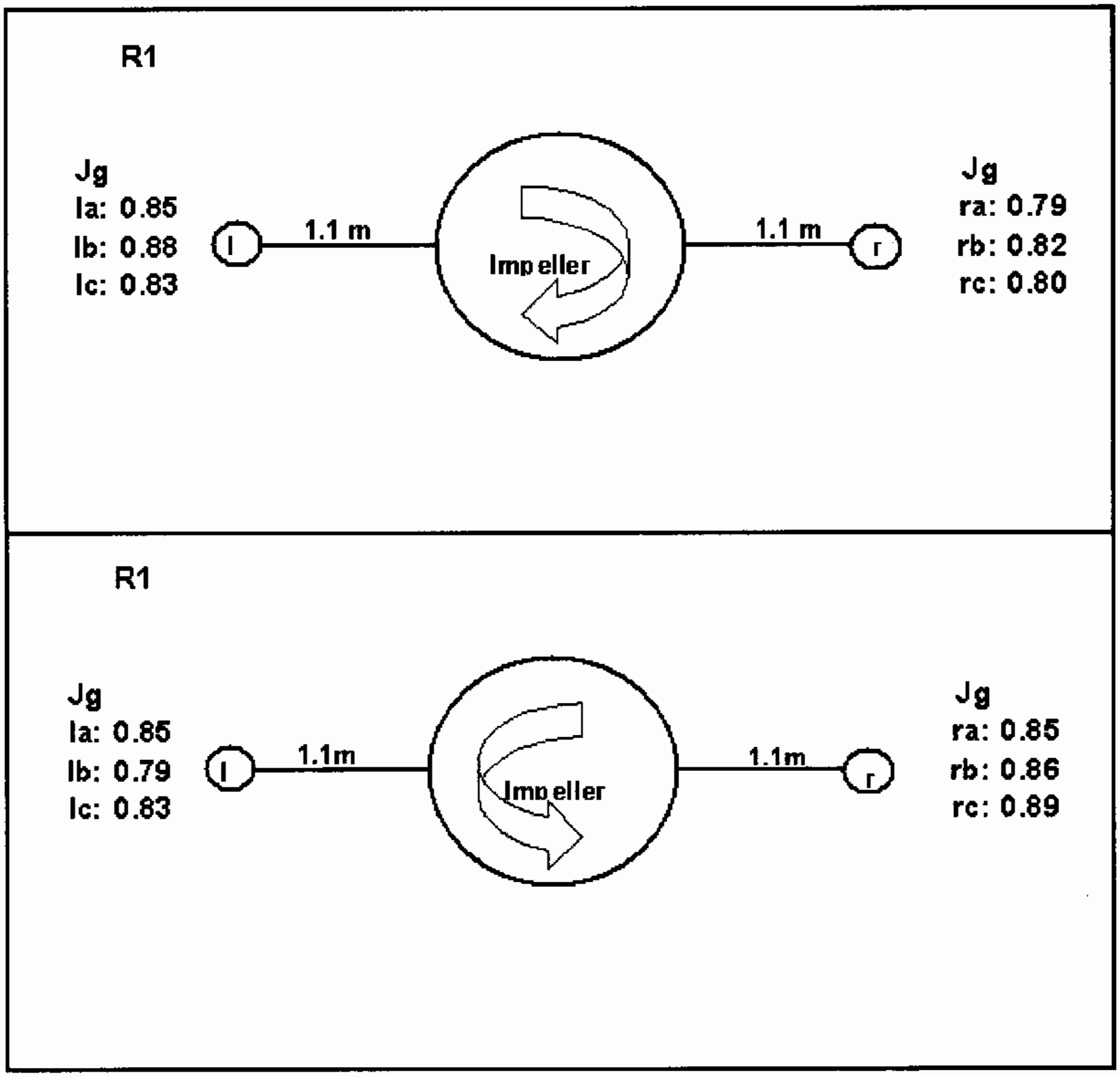

Figure 6.3: Influence of rotation direction in rougher cells R1 and R2 on J_g (cm/s). "l" stands for left, "r" for right, a: 0.12, b: 0.14 and c: 0.16 (m) froth depth. Note that R1 direction is clockwise and R2 is counter-clockwise.

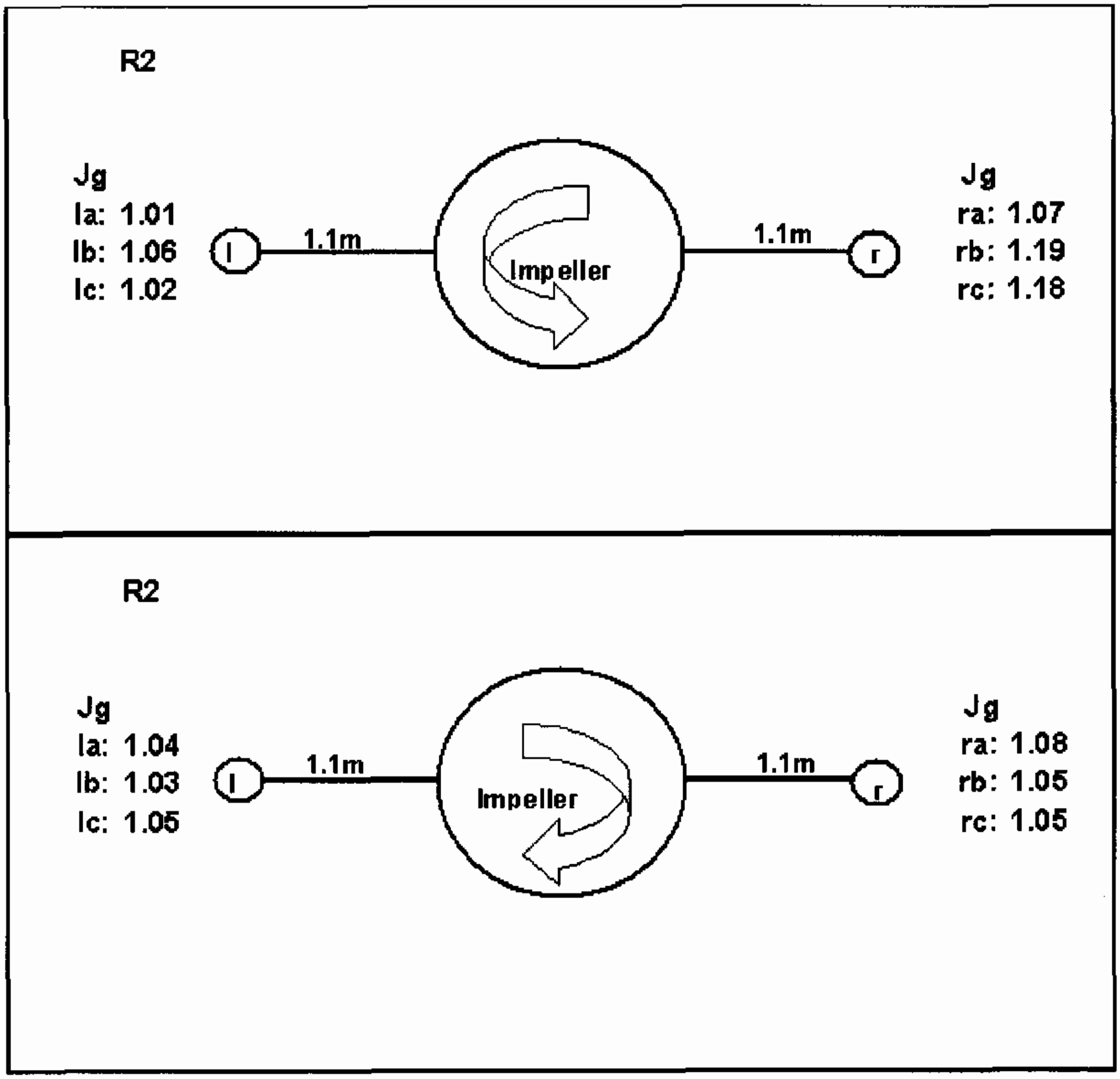

Figure 6.4: Influence of rotation direction in cells R1 and R2 on J_g. "l" stands for left, "r" for right, a: 0.12, b: 0.14 and c: 0.16 (m) froth depth. Note that R1 spin direction is now counter-clockwise and R2 is clockwise.

No major differences were found in the behavior of the cells upon the change of rotation direction, i.e., gas dispersion appears to be independent of the direction of impeller rotation.

Another observation is that the J_g measured in R2 location r were around the values indicated in Figure 6.2 for the similar location 2. These surveys were made several days apart, indicating consistent gas dispersion.

6.3 Troubleshooting: North American Palladium Ltd. Lac des Iles concentrator

North American Palladium Ltd. is Canada's only primary producer of palladium. The Company's Lac des Iles open pit mine, located 85 (km) northwest of Thunder Bay, Ontario, also produces platinum, gold, copper and nickel as by-products.

The circuit includes a row of OK-130 (Outokumpu, nominally 130 m^3) cells each with a froth crowder and individual mass airflow meters [52]. Eight continuous J_g sensors (sensors characteristics and data are given in Appendix F, Table F.25) were connected for simultaneous measurement. To get below the froth crowder (otherwise J_g is dependent on the local cell cross-section area) the sensors were held ca. 1.3 (m) below the froth-pulp interface and 1.6 (m) away from the impeller.

Figure 6.5 shows the J_g trend for three cells, 2, 3 and 4. The signals for cells 2 and 4 were stable over the period, but cell 3 was unexpectedly above the range for the orifice (> 2.5 cm/s). Comparing mass flow meter readings actually indicated a lower value for cell 3 compared to cell 2. The natural reaction was to check the cell 3 sensor, specifically for orifice plugging; but the orifice was clear. A second test was to switch sensors between cells 2 and 3; but this confirmed the high reading. The problem was traced to an incorrectly installed mass flow meter. Once rectified, cell 3 returned to the expected range.

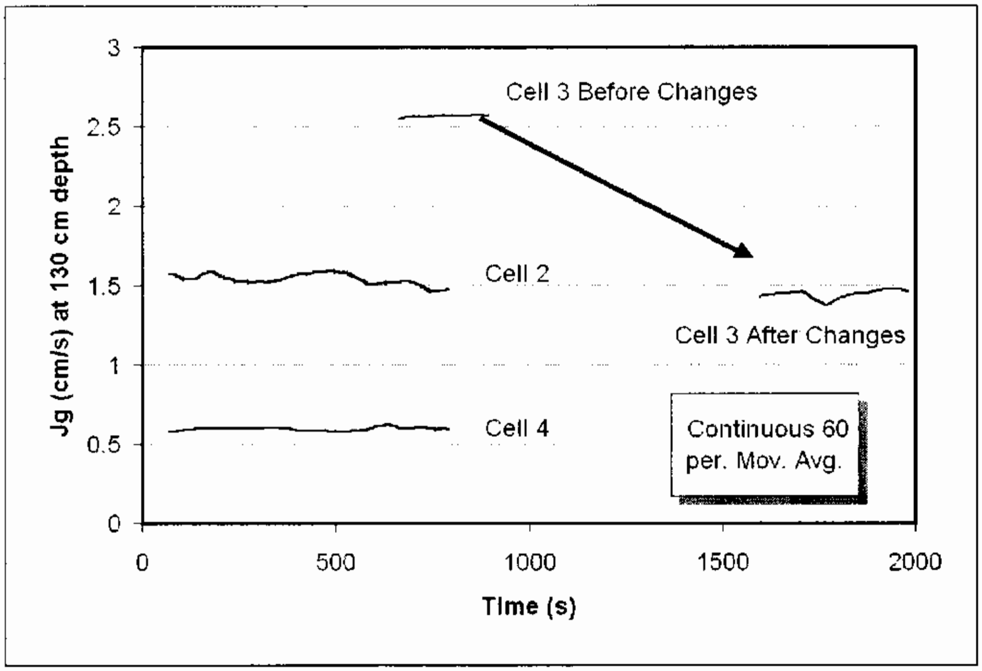

Figure 6.5: Reading for cell 3 before and after changing the mass flow meter compared to cells 2 and 4.

6.4 Cell interactions and orifice plugging: Northparkes

A rougher bank of four DO-100 (Dorr-Oliver, nominally 100 m^3) cells was monitored over extended periods (sensor characteristics and data are given in Appendix F, Table F.26). Cells 1 and 2 are connected to a common airline, as are cells 3 and 4. The sensors were held ca. 61 cm below the froth-pulp interface and 1.0 m away from the impeller.

Figure 6.6 shows the trend in J_g for cells 3 and 4. The signals were stable during the collection period (ca. 6000 s) and revealed that cell 4 received more air than cell 3. This is supported by the readings from the sensor in on/off mode prior to switching to continuous. Figure 6.7 shows the trends for cells 1 and 2. Considering the period ca. 1000 to 2000 seconds, again uneven air distribution is indicated, cell 2 receiving more than cell 1 (which the on/off version confirms). For the two pairs, the cell with higher air rate is the one downstream. It is speculated that bulk density differences may be the cause: with flotation the slurry density downstream is reduced which means a lower back pressure and consequently increased airflow.

Figure 6.7 indicates that after ca. 1000 seconds the signal from sensor 1 started to deviate upwards: the same also occurred for sensor 2 after ca. 6000 seconds. This was traced to froth building in the tube reaching the orifice and eventually depositing solids. This problem can be expected in cells towards the front of a bank where the higher solids loading increases froth stability.

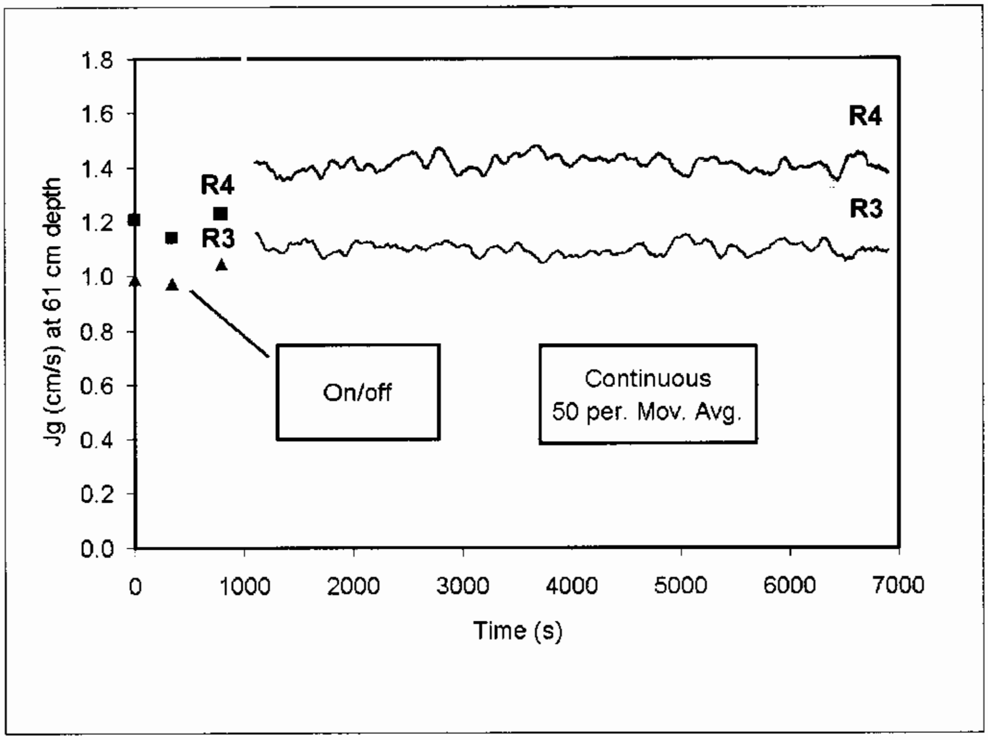

Figure 6.6: On/off and continuous J_g sensor signals for cells 3 and 4.

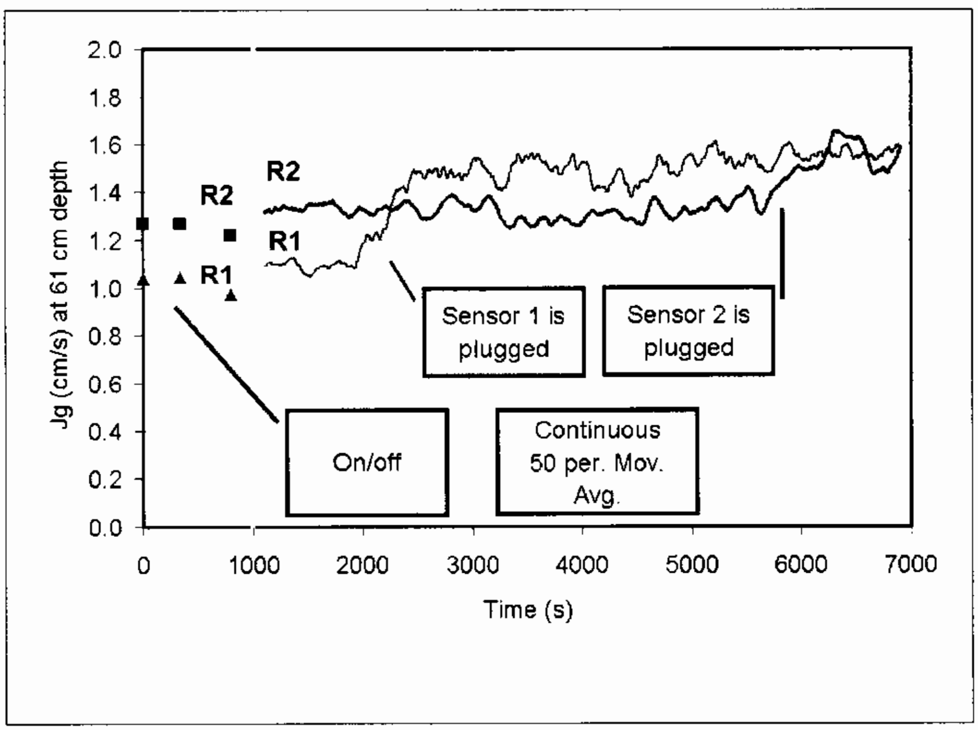

Figure 6.7: On/off and continuous J_g sensor signals for cells 1 and 2.

6.5 Cell interaction and J_g manipulation: INCO's Clarabelle concentrator

The Clarabelle mill is part of INCO Ltd's metallurgical complex centred on Sudbury, some 400 (km) north of Toronto, Ontario. Besides nickel and copper, significant quantities of cobalt, platinum group metals, gold and silver are also recovered. Test work was on a rougher bank of four OK-100 flotation cells (sensor characteristics and data are given in Appendix F, Table F.27). The air distribution system was similar to Northparkes, cells 1 and 2 and cells 3 and 4 sharing a common airline. Four sensors were employed, placed ca. 77.5 (cm) below the froth-pulp interface and 1.0 (m) away from the impeller.

Figure 6.8 shows the J_g trend for cells 1 and 2. Prior to manipulation (point 'a') the air rate in the downstream cell was higher (although not shown, the same was also the case for cells 3 and 4): i.e., the same situation found at Northparkes with presumably the same explanation.

The objective was to manipulate the air valve on cell 2 to give both cells the same J_g. As the valve closed, J_g in cell 2 duly decreased while J_g increased the two equalizing at ca. 1.00 cm/s. Anticipating the same orifice-plugging problem encountered at Northparkes, the sensors were taken off line (points 'b') for inspection. (A water dispersing agent (WD-40) was used to try to extend sensor on-time; applied to the orifice and inside walls of the tube it greatly retarded froth build up.) When, returned they recorded the same steady, equal values of J_g; i.e., the setting was stable. Returning the valve to the initial (point 'c') restored the air rates to the original.

Interaction between cells connected to a common airline is inevitable and was the origin of the tedious iterative procedure to set a J_g profile with a single on/off sensor described at the beginning of the Chapter.

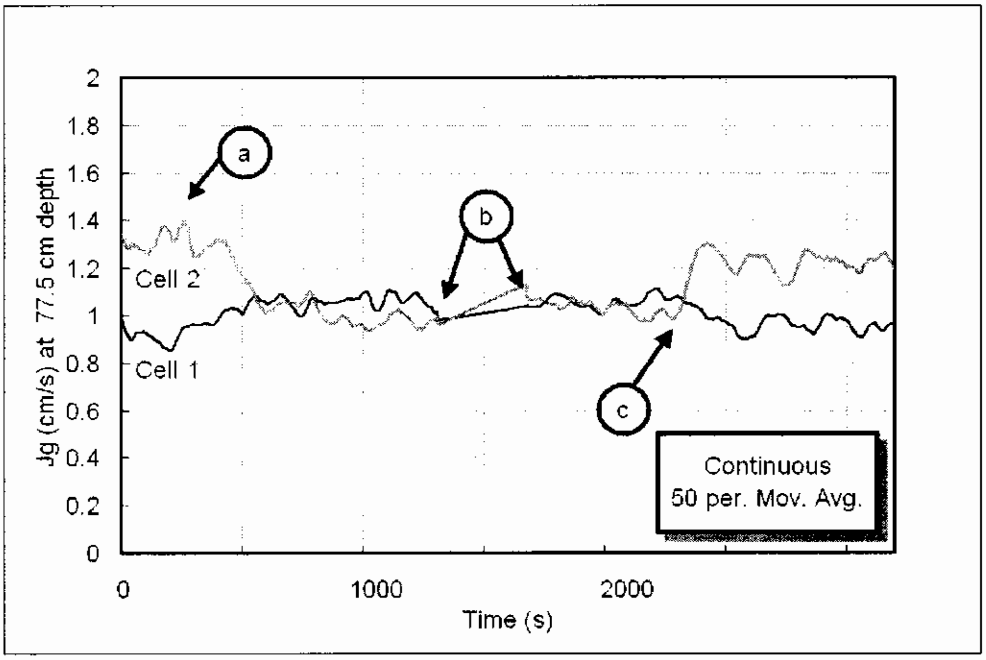

Figure 6.8: Continuous J_g signal for cells 1 and 2.

6.6 Setting a J_g profile: Noranda's Matagami concentrator

The experience indicated the continuous J_g sensor met the needs to simplify setting a profile. A chance to verify opened when invited to contribute to a campaign at Matagami Mines, a gold, copper, zinc producer located 180 km due north of Val d'Or, Quebec.

Setting a profile to the rougher bank of 16 Galigher-Agitair (ca. 4 ft^3) flotation cells was a significant challenge as the units were small and had minimal instrumentation. Eight sensors (sensor characteristics and data are presented in Appendix F, Table F.28) were connected to a frame permitting the sixteen cells to be monitored and manipulated in two blocks (the odd and even cells). Due to depth restrictions (distance from top of froth to bottom of cell was ca. 40 cm), the sensors were held between 20 and 30 (cm) below the froth-pulp interface and 38 (cm) away from the impeller. Delivery of air was regulated using a manual valve on each cell. Inspection showed the valves varied widely in sensitivity.

The approach was to insert the set of sensors in the odd numbered cells, manipulate the air rate, transfer to the even numbered cells, tune those, then return to the odd cells to check. For the eight cells this took about 20 minutes. The whole process, including cleaning the sensors when transferring (WD-40 was again used), took about 80 minutes, a great improvement over the single on/off J_g sensor experiences.

Figure 6.9 illustrates three (of 15) profiles in the campaign: as found, High J_g (target, 0.70 cm/s) and Low J_g (0.40 cm/s). The error band is the standard deviation on readings over 10 minutes. when steady state had been achieved. The "as found" profile appears random (collected for the odd numbered cells when the eight sensor assembly was first inserted), the common experience [19, 20]. The profiles selected were "flat" or "balanced" and this is essentially achieved. The Low shows cells 8 and 15 did not quite conform: for these cells the valve was actually closed completely indicating maintenance is required.

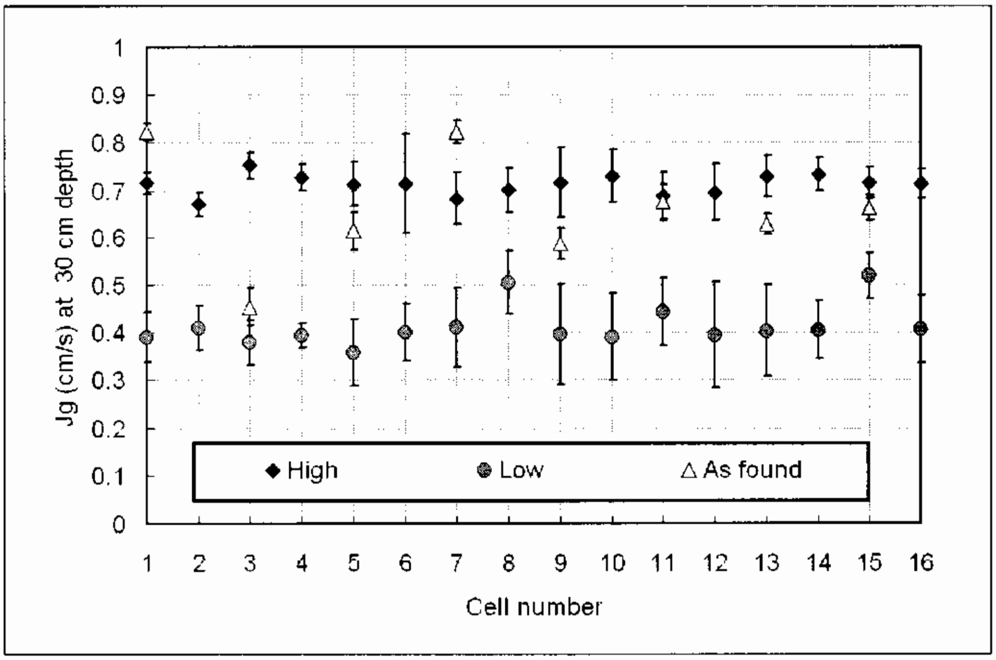

Figure 6.9: Three air profiles set using a multi-unit continuous J_g sensor.

6.7 Conclusions

The J_g sensors introduced in this thesis facilitated troubleshooting cell operation and setting a gas distribution profile to a bank of cells. This opens the way to "gas distribution management".

CHAPTER 7
CONCLUSIONS, FUTURE WORK, AND CLAIMS TO ORIGINAL RESEARCH

7.1 Conclusions

Two novel designs of superficial gas velocity (J_g) sensor based on collecting bubbles by natural buoyancy were the subject of this thesis. The overall conclusion is that robust designs for both sensors were developed incorporating fundamental and practical considerations. The following specific conclusions are drawn:

Chapter 4: Flow model of the gas velocity sensors.

a. The flow equation describing operation of the J_g sensors (continuous and discontinuous) was derived.

b. The location (depth or hydrostatic pressure) for reporting J_g was defined. Two recommended conditions are: standard temperature and pressure (STD) and at the bubble collection point (T, P_l).

c. An error propagation equation were derived for the J_g sensors (continuous and discontinuous). A sensitivity analysis for the J_g sensors (continuous and discontinuous) was conducted. For the McGill on-off technique the most important variable is the bulk density; for the continuous J_g it is calibration parameters for the orifice.

Chapter 5: Sensor validation

d. An accuracy and sampling test set up and procedure were designed.

e. For the continuous J_g sensor using a 3 (inch) tube diameter (7.62 cm): An average correction factor of 1.03 must be applied for the bias error; and, accuracy ranges between – 2.40 to – 4.20 %.

f. A comparison between the discontinuous and continuous techniques indicated a minimum tube diameter of 3 (inch) (7.62 cm) is required.

g. The continuous J_g sensor shows a long response time (e.g., 3 inch diameter sensor with an orifice $1.30, 4\tau_p = 97\,s$) to step changes in flow. The response time can be reduced, using a smaller tube diameter and adding a bubble collecting funnel, but frothing is a likely consequence.

h. An orifice tip made of a brass plug (hex head with NPT thread) was introduced for the continuous sensor. Compared to the original Delrin material, manufacturing time was reduced and the orifice was more robust.

Another improvement is that the orifice was moved from the center of the tip to the bottom to help purge accumulation of liquid in the area ahead of the orifice.

Chapter 6.0: Experience with the sensors in plant campaigns

i. The superficial gas velocity was estimated for the first time using the flow equations derived for the McGill on-off and continuous J_g sensors.

j. Demonstrated benefits for flotation plant operators using the sensors (on-off or continuous) include: troubleshooting plant instrumentation and the setting of J_g profiles to banks.

k. The time taken to set a profile of gas distribution in a bank of flotation cells, using a multi unit continuous sensor compared to a single on-off sensor, is reduced from about a shift to half an hour.

I. The sensors are finding wide application among the sponsoring *companies*.

7.2 Claims to original research

Robust, reliable sensors for measuring superficial gas velocity (J_g) in flotation cells have been developed. The have been characterized in laboratory studies (e.g. accuracy, sampling, sensitivity analysis and dynamic response) and proven practical in numerous plant studies.

For the first time multi-unit J_g sensors with automated data logging facility have been made available. The design lends itself to complete automation in the future.

The governing flow equations to estimate J_g from the sensor output were solved. In the case of the discontinuous sensor, this corrected the prior solutions and reconciled differences between the current and prior art J_g sensors (e.g. the JK sensor)

The sensors are now widely used and are the industry standard for measurement of J_g.

7.3 Future work

7.3.1 Dynamic studies

Dynamic studies of flotation units, e.g., response to step changes in air flow, cell level, etc, are in principle, possible with the continuous J_g sensor now the sensor response time characteristics are known and are ready for more complicated simulations using specific modeling software as Matlab's SIMULINK [4].

7.3.2 Study of frothing in the J_g sensor.

A study to control froth build-up in the continuous sensor should be conducted. Appendix E indicates a device to destroy froths by means of an ultrasonic wave generator. This will be a fundamental step in the integration of the sensor for process control applications.

7.3.3 'Mini' continuous J_g sensor.

The possibility of designing a continuous J_g sensor for laboratory and pilot cells looks feasible. Gas velocity is measured in laboratory cells using an average or "escape" J_g, or if a self-aerated machine using some adaptation of the Denver technique (Section 2.6.2.1). The average J_g tells nothing of local variations and the "Denver technique" depends on the ability of the operator to track the changes in level using a stopwatch.

Using the high precision mass flow meter described in Section 2.7.3 it is possible to have a continuous signal of gas flow and using a tube (of diameter to be selected based on sampling tests) to collect the bubbles in the cell, it may be possible to make a continuous J_g sensor.

The benefits would include:

- For studies where the sampling location is important, for example calculation of bubble surface area flux and bubble size measurement, having a local value of the J_g will give improved appreciation of the distribution of gas in a laboratory flotation cell.

- In the case of flotation pilot plants, the possibility to control gas distribution profile and reproduce the profile of an industrial flotation bank is an advantage that will contribute to the scaling up of the results.

REFERENCES

1. Anon. (1954) Denver Equipment Company. Denver Flotation Cells Handbook, Chapter: Aeration, Flotation Machine Control. pp. 610-611.

2. Anon. (1988) "MFC-13M : Measurement of Fluid Flow Using Orifice, Nozzle, and Venturi". Published by The American Society of Mechanical Engineers. United Engineering Center. New York, N.Y. 10017.

3. Anon, (2001) GL&V Dorr-Oliver Bulletin FLOT-5,. GL&V/Dorr-Oliver Inc. Page 2-3.

4. Anon, (2002) Learning SIMULINK 5. Release 13. The MathWorks, Inc. Third printing, November

5. Anon. (n.d.) MINNOVEX course Notes. Photocopies retrieved February 2003, from Clarabelle Mine, INCO Ltd.

6. Anon. (2003) Canadian Process Technologies Inc. Brochure retrieved March 8, 2004 from http://www.cpti.bc.ca/files/pdf/CPTBrochure.pdf. Page 10.

7. Anon. (2003) ConSep Pty Limited Web page. Information retrieved April 23, 2004, from http://www.consep.com.au/batemanflotationequip.php.

8. Anon. (2003) Defoaming. Information retrieved April 23, 2004 from www.ia.csic.es/ultrasonitww/ potencia/defoaming.htm

9. Anon. (2003) Metso Minerals. Brochure No. 1010-10-01-MP/Sala - English retrieved April 23, 2004, from http://www.metsominerals.com /inetMinerals/MaTobox7.nsf/DocsByID/45609877EA47D58A42256AF6002E 0DF3/$File/Flotation_Machines.pdf.

10. Anon. (2004) Graph Pad Prism 4.0 User's guide. Retrieved March 8, 2004, from www.graphpad.com.

11. Anon. (n.d.) "High Precision Film Flow Meter". STEC CATALOG SF-12. Retrieved March 8, 2004, from http://www.stechoriba.com/sf12.pdf.

12. Anon. (2004.) "MINNOVEX Technologies Inc". Retrieved May 27, 2004, from http://www.minnovex.com/index_html_Netsc.html.

13. Bailey, M. (2004) "Analysis of Bubble Size Distribution Using the McGill Bubble Size Analyzer". Master's Thesis, McGill University, Montreal, Canada.

14. Baker, R. (2003) An Introductory Guide to Flow Measurement. ASME edition. Chapter 4 and Chapter 6. 2003, pp. 49-75 and 117-133.

15. Bezuidenhout, G. (1995) "The Bateman Flotation Machine". Proceedings: XIX International Mineral Processing Congress. San Francisco, Ca, USA, pp. 231-236.

16. Brake, I., Eldridge, G., Luttrell, G., and Yoon, R-H. (1996) "The Design of Industrial Microcell Sparging Systems". Column 96. Edited by Gomez, C.O. and Finch, J.A. Proceedings of International Conference on Column Flotation, Montreal, Quebec. Canada, pp. 13-23.

17. Claridge P.G., Holmes, G.O. and Redfearn M.A. (1989) Operation and Maintenance in Mineral Processing Plants. Special Volume 40. The Canadian Institute of Mining and Metallurgy. Edited by Claridge, P.G. Section 6 Flotation. pp. 265 - 290.

18. Clayton, R., Jameson, G.J. and Manlapig, E.V. (1991) "The Development and Application of the Jameson Cell". Minerals Engineering, Vol 4, Nos 7-11, pp. 925-933.

19. Cooper, M., Scott D., Dahlke, R., Finch J.A. and Gomez C.O. (2004) "Impact of Air Distribution Profile on Banks in a Zn Cleaning Circuit". Proceedings 36st annual meeting of the Canadian Mineral Processors, pp. 525-539.

20. Dahlke, R., Scott, D., Leroux, D., Gomez C.O. and Finch J.A. (2001) "Troubleshooting Flotation Cell Operation Using Gas Velocity Measurements". Proceedings 33st annual meeting of the Canadian Mineral Processors, pp. 359-370.

21. Duan, J., Fornasiero, D. and Ralston J. (2003) "Calculation of the Flotation Rate Constant of Chalcopyrite Particles in an Ore". International Journal of Mineral Processing. 72, pp. 227-237.

22. Fallenius, K. (1976) "Outokumpu Flotation Machines". Flotation A.M. Gaudin Memorial Volume, Edited by Fuerstenau M.C., AIME, New York, Chapter 29, pp. 838 –861.

23. Falutsu, M. (1994) "Direct Measurement of Gas Rate in a Flotation Machine", Minerals Engineering. 7 (12), 1487-1494.

24. Finch J.A. and Hardie, C.A. (1999) "An Example of Innovation from the Waste Management Industry: Deinking Flotation Cells". Minerals Engineering, 12, (5), pp. 467-475.

25. Finch, J.A. (1995) "Column Flotation: A Selected Review - Part IV: Novel Flotation Devices". Minerals Engineering, 8, (6), pp. 587-602.

26. Finch, J.A. and Dobby G.S. (1990) Column Flotation. Pergamon Press, Elmsford, New York, U.S.A.

27. Finch, J.A., Gomez, C.O., Hardie, C., Leichtle, G., Filippone R. and Leroux D. (1999) "Bubble Surface Area Flux: A Parameter to Characterize Flotation Cells". Proceedings 31st annual meeting of the Canadian mineral processors, pp. 199-209.

28. Foreman D. (2001) Personal communication. GL&V/Dorr-Oliver.

29. Gomez, C.O., Hernandez-Aguilar, J.R., McSorley, G., Voigt P. and Finch, J.A. (2003) "Plant experiences in the measurement and interpretation of bubble size distribution in flotation machines". Fifth International Conference Copper 2003 Volume III: Mineral Processing. Edited by Gomez, C. and Barahona, C.A. Canadian Institute of Mining, Metallurgy, and Petroleum, Canada, pp. 225 - 242.

30. Gorain, B.K. (1997) "The Effects of Bubble Surface Area Flux on the Kinetics of Flotation and its Relevance to Scale-Up". PhD. Thesis. Julius Kruttschnitt Mineral research Centre. University of Queensland.

31. Gorain, B.K., Franzidis, J.-P., Ward, K., Johnson, N.W. and Manlapig, E.V. (2000) "Modelling of the Mount Isa Rougher-Scavenger Flotation Circuit Using Size-by-Liberation Data", Minerals and Metallurgical Processing. 17(3): pp. 173-180.

32. Gorain, B. K.; Franzidis, J.-P.; Manlapig, E. V. (1995) "Studies on impeller type, impeller speed and air flow rate in an industrial scale flotation cell. Part 1. Effect on Bubble Size Distribution". Julius Kruttschnitt Mineral Research Centre, University of Queensland, Indooroopilly, Australia. Minerals Engineering 8(6), pp. 615-635.

33. Gorain, B. K.; Franzidis, J.-P.; Manlapig, E. V. (1995) "Studies on impeller type, impeller speed and air flow rate in an industrial scale flotation cell. Part 2. Effect on gas holdup". Julius Kruttschnitt Mineral Research Centre, University of Queensland, Indooroopilly, Australia. Minerals Engineering 8(12), pp. 1557-1570.

34. Gorain, B.K.; Franzidis, J.-P. and Manlapig, E. V. (1996) "Studies on impeller type, impeller speed and air flow rate in an industrial scale flotation cell. Part 3. Effect on superficial gas velocity". Julius Kruttschnitt Mineral Research Centre, University of Queensland, Indooroopilly, Australia. Minerals Engineering 9(6), pp. 639-654.

35. Gorain, B.K.; Franzidis, J.-P. and Manlapig, E.V. (1997) "Studies on impeller type, impeller speed and air flow rate in an industrial scale flotation cell. Part 4. Effect of bubble surface area flux on flotation performance". Julius Kruttschnitt Mineral Res. Centre, Indooroopilly, Australia. Minerals Engineering , 10(4), pp. 367-379.

36. Gorain, B.K.; Napier-Munn, T.J.; Franzidis, J.-P. and Manlapig, E.V. (1998) "Studies on impeller type, impeller speed and air flow rate in an industrial scale flotation cell. Part 5: validation of k-Sb relationship and effect of froth depth". Julius Kruttschnitt Mineral Research Centre, University of Queensland, Indooroopilly, Australia. Minerals Engineering 11(7), pp. 615-626.

37. Gorain, B. K.; Franzidis, J.-P. and Manlapig, E. V. (1997) "The empirical prediction of bubble surface area flux in mechanical flotation cells from cell design and operating data". Julius Kruttschnitt Mineral Research Centre, University of Queensland, Indooroopilly, Australia. Minerals Engineering (1999), 12(3), pp. 309-322.

38. Grau, R.A. and Heiskanen K. (2003) "Gas Dispersion Measurements in a Flotation Cell". Minerals Engineering, 16, pp. 1081-1089.

39. Harbort G., De Bono, S., Carr, D. and Lawson V. (2003) "Jameson Cell Fundamentals – a Revised Perspective". Minerals Engineering. Elsevier Science Ltd., Vol. 16, pp. 1091-1101.

40. Hardie C. (1998) "In-Plant Comparison of Internal and External Spargers for Flotation Column Deinking". Master's Thesis, McGill University, Montreal, Canada.

41. Harris C.C. (1976) "Flotation Machines" Flotation A.M. Gaudin Memorial Volume, Edited by Fuerstenau M.C., AIME, New York, Chapter 27, pp. 753-815.

42. Heiskanen K. (2000) "On the Relationships Between Flotation Rate and Bubble Surface Area Flux". Minerals Engineering, 13(2), pp.141-149.

43. Hernandez-Aguilar, J., Gomez, C.O. and Finch J.A. (2002) "A Technique for the Direct Measurement of Bubble Size Distributions in Industrial Flotation Cells". Proceeding 34th Annual Meeting of the Canadian Mineral Processors, CIM, pp. 389-402.

44. Hernandez-Aguilar, J.R., Coleman, R.G., Gomez, C.O. and Finch J.A. (2004) "A Comparison Between Capillary and Imaging Techniques for Sizing Bubbles in Flotation Systems". Minerals Engineering 17, pp. 53-61.

45. Jameson, G.J. and Allum, P. (1984) "A Survey of Bubble Size in Industrial Flotation Cells". Report for AMIRA Ltd, Australia.

46. Kallionen, J. (1999) "Advances in Application Driven Design for Flotation Cells". Fourth International Conference Copper 99 – Cobre 99 - Volume II: Mineral Processing / Environment, Health And Safety. Edited by Hancock, B. and Pon, M., TMS, Warrendale, Pennsylvania, U.S.A., pp. 29 - 39.

47. Koh, P.T.L., Shwarz, M.P., Zhu, Y. Bourque, P. Peaker, R. and Frazidis, J.P. (2003) "Development of CFD Models of Mineral Flotation Cells". Third International Conference on CFD in the Minerals and Process Industries. Csiro, Melbourne, Australia, pp. 171-176.

48. Kreyszig, E. (1999) Advanced Engineering Mathematics. 8th edition. John Wiley & Sons, Inc. New York, U.S.A., Chapter 5, pp. 250-302.

49. Levenspiel, O. (1984) Engineering Flow and Heat Exchange. Revised Edition. The Plenum Chemical Engineering Series. Series Editor: Dan Luss. Plenum Press New York and London. Chapter 3, pp.43-68.

50. Levenspiel, O. (1984) Engineering Flow and Heat Exchange. Revised Edition. The Plenum Chemical Engineering Series. Series Editor: Dan Luss. Plenum Press New York, U.S.A. Chapter 4, pp. 43-68.

51. Liley, P., Thompson, G. Friend, D.G., Daubert and T. Buck, E. (1999) Chemical Engineers Handbook. Seventh Edition. Edited by Perry, R. and Green D. McGraw-Hill Book Co., New York. Section 2. Physical and Chemical Data, pp. 355-358.

52. Martin, C., Ohrling, T., Olsen, T. and Taggart, P. (2003) "From Tribulation to Triumph – Flotation Improvements at New Lac des Iles Concentrator", Proceedings 35st Annual Meeting of the Canadian Mineral Processors, pp. 13-27.

53. Miller, R. (1996) Flow Measurement Engineering Handbook. Third Edition, McGraw-Hill. New York, U.S.A., Chapter 2, pp. 2.12 to 2.22.

54. Miller, R. (1996) Flow Measurement Engineering Handbook. Third Edition, McGraw-Hill. New York, U.S.A., Chapter 4, pp. 4.17 to 4.25.

55. Miller, R. (1996) Flow Measurement Engineering Handbook. Third Edition, McGraw-Hill. New York, U.S.A. Chapter 6, pp. 6.9.

56. Miller, R. (1996) Flow Measurement Engineering Handbook. Third edition McGraw-Hill. New York, U.S.A. Chapter 9, pp. 9.1 to 9.8.

57. Nesset, J. (2004) Private communication.

58. Peress, J. (2003) "Working with Non-Ideal Gases". CEP magazine. March, pp. 39 – 41.

59. Redlich, O. and Kwong, J. (1949) "On the Thermodynamics of Solutions", Chem. Rev., 44, pp. 233 - 244.

60. Savassi, O.N., Rahal, K.R., Johnson, N.W. and Franzidis, J.P. (1999) "Mass Transfer Across the Pulp-Froth Interface in Industrial Flotation Cells – Part 1: Jg Probe for Measurement of the Air Flow Rate". Transactions of the Institute of Mining and Metallurgy-Section C-Mineral Processing. 108 (Aug.): C99-102.

61. Stephanopoulos, G. (1984) Chemical Process Control, An Introduction to Theory and Practice. Prentice-Hall, Inc. New Jersey, U.S.A., Chapters 6 to 10, pp. 113- 185.

62. Torrealba-Vargas, J., Gomez, C.O. and Finch, J.A. (2003) "Measurement of Gas Velocity in Industrial Flotation Cells". Procedings: XXII International Mineral Processing Congress. Cape Town, South Africa, pp. 1703-1710.

63. Torrealba-Vargas, J., Gomez, C.O. and Finch, J.A. (2002) "Gas Velocity Measurements at Northparkes Mine". Amira P9M Project Flotation 08/02 Research Report.

64. Torrealba-Vargas, J.A., Gomez, C.O. and Finch, J.A. (2004) "Continuous Air Rate Measurement in Flotation Cells: a Step Towards Gas Distribution Management". Minerals Engineering 17 (6), pp. 761-765.

65. Weber, T.W. (1973) An Introduction to Process Dynamics and Control. John Wiley & Sons, inc., New York, U.S.A. Chapters 8 and 9, pp. 157-239.

66. White, F. (1986) Fluid Mechanics. Second Edition. McGraw Hill Book Company. Chapter 3, pp. 166-167.

67. Xu, M. (1991) "Radial Gas Holdup Profile and Mixing in the Collection Zone of Flotation Column". Ph.D. Thesis, McGill University, Montreal, Canada.

68. Yianatos, J., Bergh, L., Condori, P. and Aguilera J. (2001) "Hydrodynamic and Metallurgical Characterization of Industrial Flotation Banks for Control Purposes". Minerals Engineering, 14 (9), pp. 1033-1046.

69. Zheng, X.F. (1990) Amira P9L Final Report. Appendix A: JKMRC Flotation Manual. JKMRC, University of Queensland, Australia.

APPENDIX A
EXAMPLES

A.1 On-off J_g sensor example

The procedure to measure with the on-off J_g sensor was described in Section 4.2.1. The software used to collect the data was JTACQV30. An example of the algorithm used to process the data is presented in Appendix D.1.

Figure A.1 shows an example of raw data. The units for this raw pressure are cm of Water (instead of Pa).

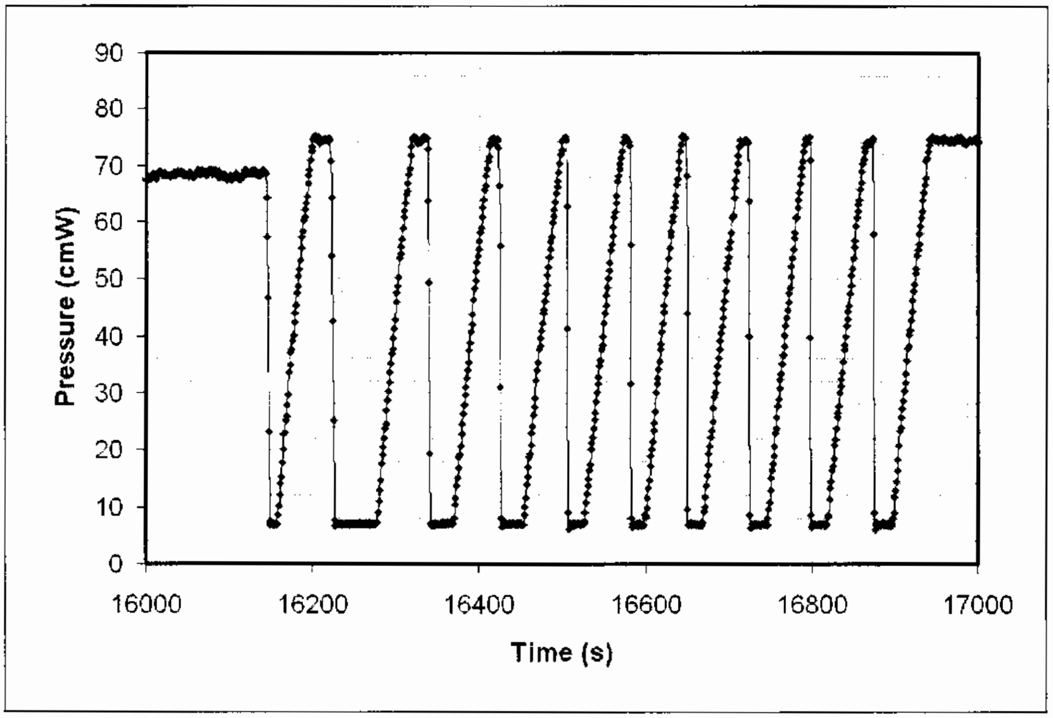

Figure A.1: Raw data from the on-off McGill J_g sensor.

The data is processed as follows: A Low and a High pressure limits for the calculation of the slopes for the pressure variation curve are set in the program based on the visual observation of the raw data. For example, in Figure A.1 the minimum and maximum pressures are approximately 6 and 74 cm of Water then using 10 and 70 as the Low and High limits to filter all the data points that are not part of the pressure variation curve. A threshold of +/- 5 cm of Water is used by the program to trigger the beginning (data in the range of [10-5;10] cm of Water starts the calculation) and ending (data in the range of [70;70+5] cm of Water stops the calculation) of the slope calculation.

Table A.1 shows the results of the raw data processing.

Table A.1: Slopes from Figure A.2.

Test	1	2	3	4	5	6	7	8	9	10	Average	Stdev
$\frac{dP}{dt}$ (cm of Water)/s	1.61	1.64	1.58	1.46	1.51	1.61	1.51	1.52	1.50	1.54	1.54	0.05

Table A.2 shows FP_{McGill} calculated as indicated in Equation 4.23.

Table A.2: FP calculation.

H_p (m)	0.475
H_l (m)	1.25
ρ (kg/m3)	941 ± 25
FP (m/Pa)	1.127E-04

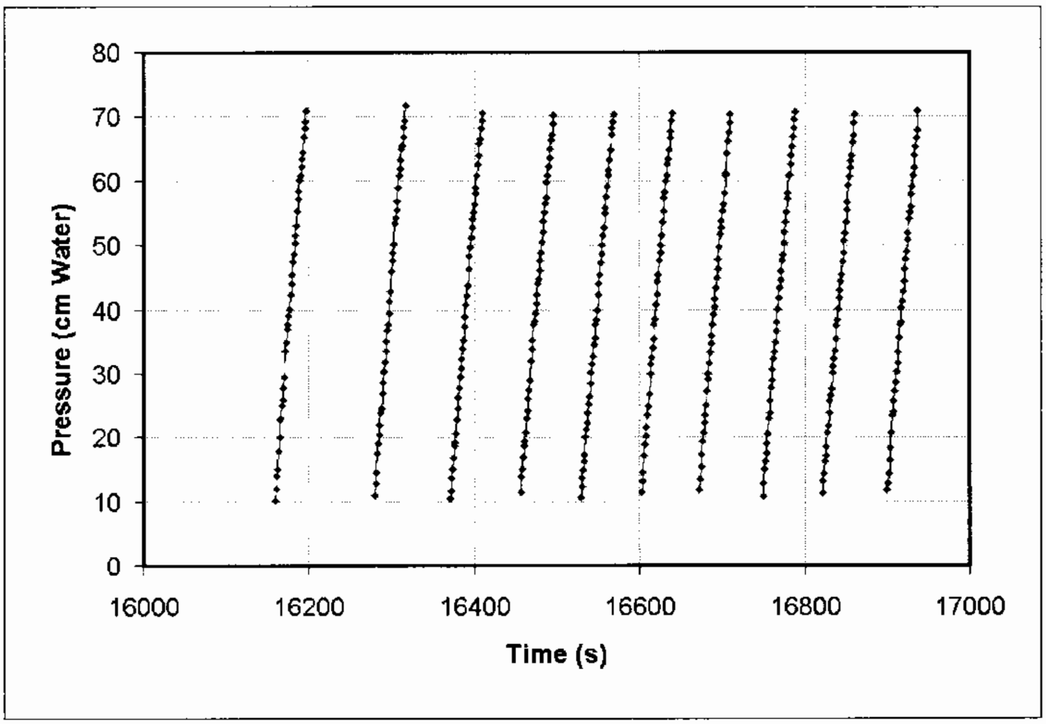

Figure A.2: Filtering of Raw data from Figure A.1.

Table A.3: Example of J_g calculation from the McGill model (Equation 4.23).

$\left(\frac{\partial J_g}{\partial \rho_b}\right)$ **(Eq. 4.65)** **(m^4/sKg)**	$\left(\frac{\partial J_g}{\partial \frac{dP}{dt}}\right)$ **(Eq. 4.66)** **(m/Pa)**	**J_g Stdev (cm/s)**
-1.74E-05	1.13E-04	0.08

Using Equation 4.23,

$$J_g = FP_{McGill} \frac{dP}{dt} \qquad \text{Eq. (F.1)}$$

$$J_g = 0.00113 \left(\frac{m}{Pa}\right) * 1.541 \left(\frac{\text{cm of Water}}{s}\right) * 98.06 \left(\frac{Pa}{\text{cm of Water}}\right) * 100\left(\frac{m}{cm}\right)$$

Eq. (F. 2)

$$J_g = 1.70 \pm 0.08 \text{ (cm/s)} \qquad \text{Eq. (F. 3)}$$

This is the J_g calculated at H_l-H_p = 0.775 (m) (the bottom of the J_g sensor).

A.2 Continuous J_g sensor example

The procedure to measure with the continuous J_g sensor was described in Section 4.2.2. The software used to collect the data was JTACQV30. An example of the algorithm used to process the data is presented in Appendix D.2

Figure A.3 shows an example of the raw data for a continuous J_g sensor. Table A.4 shows the sensor characteristics.

Table A.4: Continuous sensor characteristics.

H_p (m)		190
H_l (m)		360
Orifice 0.94	a_{SCMS} (SCMS $\sqrt{kg/(m^3kPa)}$)	1.56E-5
	b_{SCMS} (SCMS)	-1.93E-6
P_{atm} (Pa)		101325
A (m^2)		4.56E-03

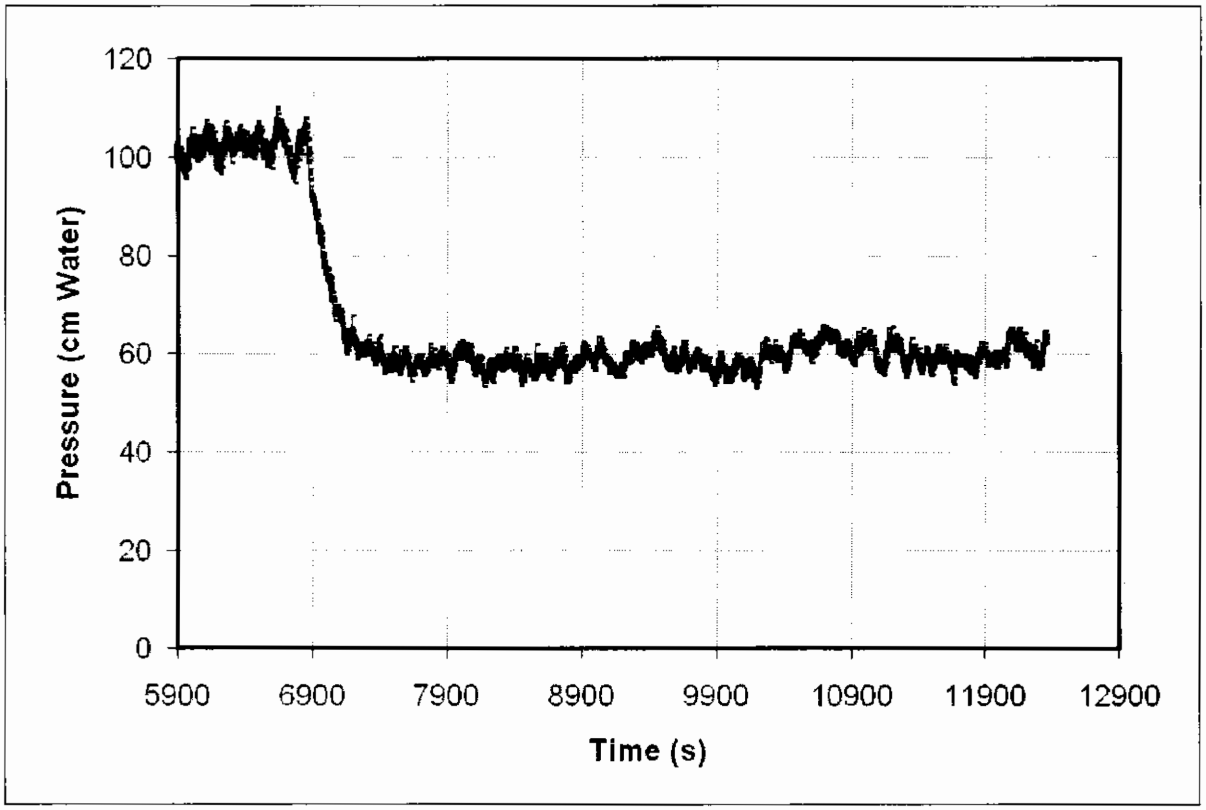

Figure A.3: Raw data from the continuous McGill J_g sensor.

From the raw data a moving average (MA) is calculated as:

$$F_t = \frac{A_t + A_{t-1} + \ldots + A_{t-n+1}}{n} \qquad \text{Eq. (F. 4)}$$

where A_t is the measured value at time t, A_{t-n+1} is the measured value at time t-n+1 and F_t moving average of n values at time t.

The program was set for a time period based on plant experience and analysis in situ of the raw data (in most cases 600 seconds). The MA is used for pressure and pressure standard deviation.

A variable threshold of MA for the standard deviation is set and the steady state is found using a conditional (e.g. MA value <= 0.2). When this conditional is true, the value for the MA for pressure standard deviation is the steady state value for the 600 seconds of data (in Figure A.2 at 8383 s). The value of moving average pressure, P_{MA} is 58.07(cm of Water). The continuous J_g is calculated (orifice 0.94, linear trend I Table 13-3) using Equation 4.40 as follows:

$$J_{g,STD} = \frac{1.55E\text{-}5\sqrt{\frac{58.07*98.06/1000}{1.27}}\text{-}1.93E\text{-}6}{4.56E\text{-}03} = 0.68\ (cm/s) \qquad \text{Eq. (F. 5)}$$

where the density is calculated using Equation 4.37,

$$\rho = \frac{28.8(101325+58.07\bullet 98.06)}{8.314(273.15+19)0.9996} = 1.27\ (kg/m^3) \qquad \text{Eq. (F. 6)}$$

Using Equation 4.41, the J_g at the sampling point (where the pressure is P_l and the temperature, T= 19 C = 292.15 K) is,

$$J_{g,Pl} = 0.68\ \frac{(101325)(273.15+19)}{(101325+(3.60-1.90)98.06+(273.15)} = 0.62(cm/s) \qquad \text{Eq. (F. 7)}$$

This is the J_g calculated at H_l-H_p = 1.70 (m) (the bottom of the J_g sensor).

A.3 Verification test example

Table A.5 shows a typical FP_{McGill} estimation result for the McGill sensor (Equation 4.23). Table A.6 shows the results of the J_g calculation. This result forms part of the verification test (Chapter 5.3.2 and Appendix Table F.3).

Table A.5: Data for J_g calculation in Table F.5.

H_l (m)	H_p (m)	γ	g (m/s)	P_{atm} (Pa)	ρ_{bulk} (kg/m^3)	$\frac{dP}{dt}$ (Pa/s)	FP_{McGill} (from Eq. 4.23) (m/Pa)
3.03	2.42	1.40	9.806	101325	1164.66 ± 127.39	36.58 ± 2.35	1.027E-04

Table A.6: Example of J_g calculation from the McGill model (Equation 4.23).

$\left(\frac{\partial J_g}{\partial \rho_b}\right)$ (Eq. 4.65) (m^4/skg)	$\left(\frac{\partial J_g}{\partial \frac{dP}{dt}}\right)$ (Eq. 4.66) (m/Pa)	J_g (cm/s)	Stdev (cm/s)
-2.781E-06	1.027E-04	0.376	0.035

A.4 Sensitivity analysis example

Table A.7 tabulates the results of the calculation of sensitivity coefficients for the FP_{McGill} equation (from Equation 4.23) derived by neglecting second and third order derivatives.

Table A.7: Example of sensitivity analysis for FP_{McGill} equation derived by neglecting second and third order derivatives. γ =1.40.

Equation	ρ_{bulk} (kg/m^3)	H_l (m)	H_p (m)	FP (m/Pa)	Sensitivity coefficient (%)
4.81	1000	3	2	1.136E-04	$X_{\rho_{bulk}} = -0.91$
4.82	1000	3	2	1.136E-04	$X_{H_p} = -0.06$
4.83	1000	3	2	1.136E-04	$X_{H_l} = 0.15$

A.5 Computer calculated sensitivity coefficients

Table A.8 shows a typical sensitivity analysis for the FP_{McGill} equation (from Equation 4.23). Example: The sensitivity coefficient of FP to H_p (last column and row of Table A.8) is,

$$X_{H_p} = \frac{\%\Delta FP}{\%\Delta H_p} = \frac{\frac{(1.138E-04)-(1.136E-04)}{(1.136E-04)}}{1} = 0.15 \qquad \text{Eq. (F. 8)}$$

Table A.8: Example of sensitivity analysis for FP_{McGill} Equation 4.61. γ =1.40.

ρ_{bulk} (kg/m^3)	H_l (m)	H_p (m)	FP (m/Pa)	Sensitivity coefficient (%)
1000	3	2	1.136E-04	
1010	3	2	1.126E-04	$X_{\rho_{bulk}} = -0.90$
1000	3.03	2	1.135E-04	$X_{H_p} = -0.06$
1000	3	2.02	1.138E-04	$X_{H_l} = 0.15$

A.6 Example of calculation of mass flow

For a set point of 15 SLPM (2.5E-4 SCMS) it takes 37.7 seconds to produce a gauge pressure of 0.85 psi (5883 Pa) and displace a mass of 8.3945 kg of water. The number of moles per minute is,

$$n' = \frac{V[L]*P[Pa]}{R\left[\frac{PaL}{Kmol}\right]*T[K]*t[min]} \quad \text{Eq. (F. 9)}$$

$$n' = \frac{(8.5097*(14.6959+0.853)*\frac{101325}{14.6959})}{8314*(273.15+20)*(37.7/60)} \quad \text{Eq. (F. 10)}$$

$$n' = 0.5950(\frac{mol}{min}) \quad \text{Eq. (F. 11)}$$

Then the number of standard liters per minute is,

$$Q_{SLPM} = \frac{0.5950*8324*273.15}{101325}*0.9996\bullet\frac{1}{1000\bullet 60} \quad \text{Eq. (F. 12)}$$

$$Q_{SCMS} = 2.22E-4(SCMS) \quad \text{Eq. (F. 13)}$$

This value can be found in Appendix F, Table F.1 (shadow data). Also, Table F.1 shows the data fitted with second order polynomials.

A.7 Nomograph reading example

For the parameters given in Tables A.9 and A.10 examples of reading the FP nomograph for McGill and JK sensors (Figures 5.14 and 5.15) are shown in Figures A.4 and A.5.

Table A.9: McGill sensor.

H_l (m)	H_p (m)	ρ_{bulk} (kg/m^3)
3	2	1040

Table A.10: JK sensor.

H_l (m)	H_p (m)	ρ_{bulk} (kg/m^3)	ρ_{sensor} (Calculated for ε_g = 12%) (kg/m3)	H_1 (m)	H_2 (m)
3	2	1040	880	0.50	0.80

From Figures A.4 and A.5 the FP is 0.00012 m/Pa (McGill) and 0.86 (JK). For the given values of $\frac{dP}{dt} = 53.17 \pm 4.22$ (Pa/s) and $\frac{\Delta H}{\Delta t} = 1.17 \pm 0.03$ (cm/s) (Appendix F, Table F.7) then the gas velocity for the McGill and JK sensors is,

McGill: $J_g = 53.17 * 0.000117 \cong 0.64 \pm 0.05$ (cm/s) Eq. (F. 14)

JK: $J_g = 1.17 * 0.86 * 0.64 \cong 0.64 \pm 0.02$ (cm/s) Eq. (F. 15)

It can be observed the good agreement between the two techniques. The differences with the values calculated in 5.3.2 are explained due to differences between the dimensions of sensors in the nomograph (fixed to H_l/H_p: 4/3 and 3/2 and 2/1) and the experimental values (Appendix F, Table F.5).

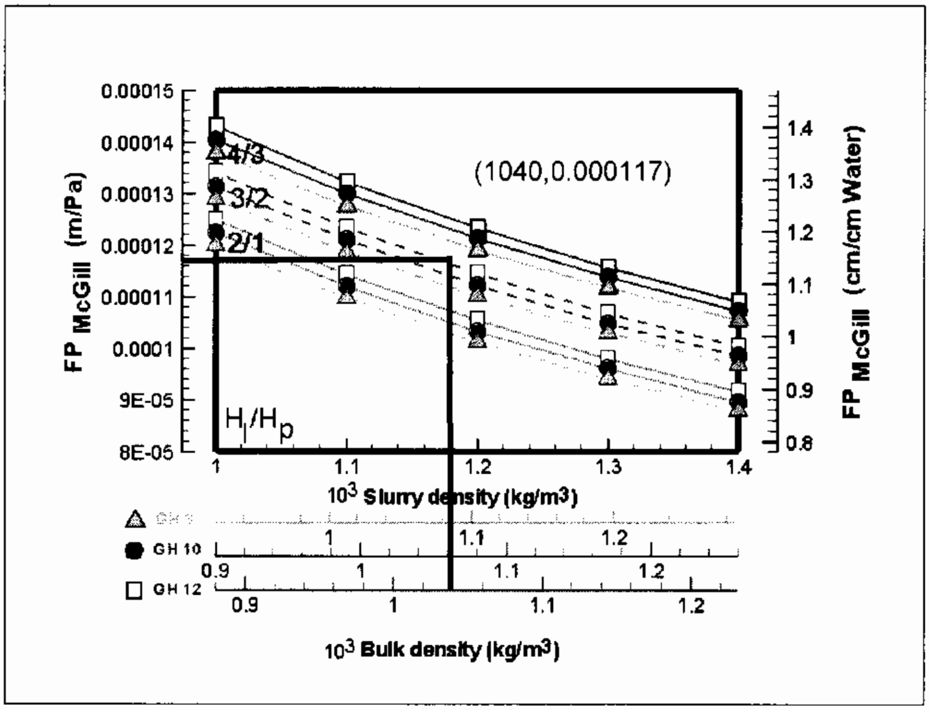

Figure A.4: Nomograph example for McGill on-off sensor.

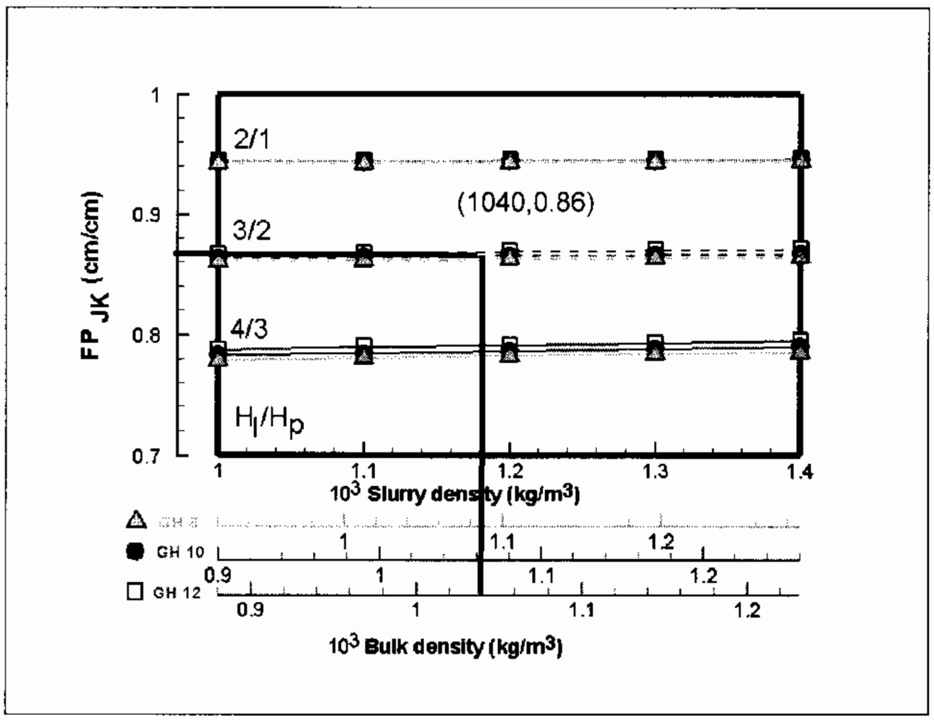

Figure A.5: Nomograph example for JK sensor.

A.8 Mass flow balance example

An example of mass flow balance is shown as follows:

$$q_{KPS,in} = q_{KPS,out1} + q_{KPS,out2} \qquad \text{Eq. (F. 16)}$$

$$\rho = \frac{28.8P_s}{8314 * 292.15} \qquad \text{Eq. (F. 17)}$$

Table A.11 shows the flow balance calculations.

Table A.11: Flow calculations.

Orifices	Orifice$_1$ = 0.70
	Orifice$_2$ = 0.94
$q_{KPS,in}$ (KPS)	$6.96E-5$
$\sqrt{\Delta P_{out1}\rho_{out1}}$ ($\sqrt{kPakg/m^3}$)	$\sqrt{5.838 * 1.277} = 2.730$
$\sqrt{\Delta P_{out2}\rho_{out2}}$ ($\sqrt{kPakg/m^3}$)	$\sqrt{4.551 * 1.262} = 2.397$
Linear (KPS) (coefficients from Appendix F, Table F.13-2)	$q_{KPS,out1} = 1.248E-5 * (2.730) + -6.541E-7 = 3.34E-5$
	$q_{KPS,out2} = 1.446E-5 * (2.397) + 8.889E-7 = 3.55E-5$
Quadratic (KPS) (coefficients from Appendix F, Table F. 13-2)	$q_{KPS,out1} = -4.414E-8 * (2.730)^2 + 1.270E-5 * (2.730) + -9.016E-7 = 3.34E-5$
	$q_{KPS,out2} = -6.778E-7 * (2.397)^2 + 1.788E-5 * (2.397) + -3.079E-6 = 3.59E-5$
Cubic (KPS) (coefficients from Appendix F, Table F.13-2)	$q_{KPS,out1} = -1.909E-7 * (2.730)^3 + 1.375E-6 * (2.730)^2 + 9.358E-6 * (2.730) + 1.564E-6 = 3.35E-5$
	$q_{KPS,out2} = 3.020E-8 * (2.397)^3 - 9.071E-7 * (2.397)^2 + +1.844E-5 * (2.397) - 3.498E-6 = 3.59E-5$

With the data from Table A.11, the bias was calculated as follows (Table A.12):

Table A.12: Results.

Bias error (%)	Mass flow	$\frac{q_{KPS,out1}-(q_{KPS,in}-q_{KPS,out2})}{(q_{KPS,in}-q_{KPS,out2})}*100$
Linear (KPS)	$q_{KPS,out1} = 3.34E-5$	-1.94
	$q_{KPS,out2} = 3.55E-5$	
Quadratic (KPS)	$q_{KPS,out2} = 3.34E-5$	-0.87
	$q_{KPS,out2} = 3.59E-5$	
Cubic (KPS)	$q_{KPS,out1} = 3.35E-5$	-0.74
	$q_{KPS,out2} = 3.59E-5$	

The precision is calculated as

$$\sigma_p = t_{st}\sigma = 2*(-1.94) = -3.88\ (\%) \qquad \text{Eq. (F. 18)}$$

Two tailed student's t values for more than 30 points is 2

Correction factor is calculated as,

$$CF=(1+\frac{-1.94}{100})^{-1} = 1.02 \qquad \text{Eq. (F. 19)}$$

Finally the accuracy is calculated as follows,

$$\text{Accuracy} = \text{Bias} \pm \text{Precision} \qquad \text{Eq. (F. 20)}$$

$$\text{Accuracy} = +(-1.94) \pm 1.02 = -0.92 \text{ to } -2.96\ (\%) \qquad \text{Eq. (F. 21)}$$

APPENDIX B
SOFTWARE MANUAL

JTACQV30-Protocol was written by Jorge Torrealba and Jose Hernandez.

Installation:

1. Create a folder C:\Data\files.
2. Copy Disk\Board, Disk\Control, Disk\Dutec and Disk\JTACQ into the Data folder.
3. The folder tree Must be:

   C:\Data\Files

   C:\Data\Board

   C:\Data\Control

   C:\Data\JTACQ
4. In the Dutec folder run Install 1 and Install 2 , allow the setup to install to its default directory.
5. In the control folder run REGCTRLS, inside REGCTRLS click on register and open TREND.OCX, which should add one item to the list of protocols.

6. The program is now installed, go to the JTACQ folder and click on JTACQV30 to run the data acquisition program.

7. It is recommended that once all the initial parameters have been set up in the program, the files in the control folder should be copied to another location as backup.

Initial setup:

8. Open application by clicking on tool bar. Click on **2PT-Eg** or press enter.

9. Click on **OK** or press enter to acknowledge that this is not a commercial program.

10. Check baseline of pressure transmitter by recording pressure while the valve of the sensor is open.

11. The range can be set either to 127 or 254 depending on the conversion of the transmitter being used, if set to 127 $\mathbf{H_l}$-$\mathbf{H_p}$ cannot be more than 1m.

12. Attach desired orifice, making sure the orifice valve is closed.

13. Click on **1-Begin** to open communications.

14. Record the background pressure with the valves open.

15. Go to sensor configuration to verify the settings and input **ΔL** (the difference in length between the two tubes as installed) for bulk density calculations.

16. The sample option determines the time between samples, in ms, it can be reduced as low as 300 ms with no upper limit. For shallower cells this should be reduced, if the raw data appears to stagger (a step pattern – check this in excel) then the sample time should be increased.

17. The average setting is used to eliminate noise in the measurements; it cannot be set too high for continuous $\mathbf{J_g}$. A safe average to begin with is 2.

18. You should also enter the orifice calibration to be used by clicking on **Change Orifice**. The orifice and calibration used will be saved along with the data.

19. Give a generic name for the group of files to be generated in this experimental test (i.e., "**filename**").

20. **Save** conditions and **close**.

21. Click on **2-Save** to begin data collection.

22. Record time, it is part of the **filename**. (e.g. March 28, 2004, 10:30:15 a.m. = **filename**-28-3-10-30-15.csv)

23. With valves closed, click **Bulk Density** to calculate the bulk density. Record the average maximum pressures $\mathbf{P_1}$ and $\mathbf{P_2}$ and the bulk density (will be used later for **Instant $\mathbf{J_g}$ processing**).

24. **Close** window.

On/off measurement of $\mathbf{J_g}$.

25. To measure J_g using the on/off technique, click on **Record for Instant $\mathbf{J_g}$**, open on/off valve slowly and close in fluid motion. The pressure will drop to zero when the valve is opened and slowly rise with a slope related to J_g once the valve is closed. Ideally, each measurement should have a complete curve (i.e., the maximal pressure is obtained before opening the valve again). Repeat for at least three measurements.

26. Click on **Stop for Instant $\mathbf{J_g}$** followed by **Process**. Enter the values obtained in #19 for bulk density and $\mathbf{P_l}$, $\mathbf{P_{calc}}$ should be half of the $\mathbf{P_l}$ and $\mathbf{H_p}$. In setting the range, the **Low** and **High** values should be at least 5-10 cm shorter than the

actual range observed (i.e., if the slope starts at 0 and ends at 100, a good range would be 10 to 90).

27. Click on **Save Defaults** and **Calculate** on the top section first followed by the bottom section. Record the values of $\mathbf{J_g}$ obtained (A file with the same filename plus "results" is created). **Close** window.

28. The $\mathbf{J_g}$ measurement can be calculated more quickly by only recording half of the slope length for each on-off measurement and then opening the valve form another measurement. When processing the $\mathbf{P_l}$ must be reduced to the new limit of slope, often this must be determined by eye, the range must also be adjusted accordingly and the $\mathbf{P_{calc}}$ must be recalculated. $\mathbf{H_p}$, how ever, remains the same.

Continuous measurement of J_g

29. Verify proper orifice is set-up in program: Click on Sensor Configuration and Change orifice. If is not the proper orifice entered, you will need to close the program and change the orifice settings prior to starting the data collection for the proper orifice to be included in the file. The orifice calibrations can be found in c:\data\board\orifice4.

30. Open valve to orifice and allow for pressure to level out. This can be speed up by opening the on-off valve as well, although this can only be done if the leveling out pressure is know to be in certain range, and care must be taken not to overshoot the leveling pressure.

31. Click on **Mon. Cont.** $\mathbf{J_g}$, **record** $\mathbf{J_g}$ as seen in the middle box. This is the average of the number of readings indicated. Close windows.

32. Verify that orifice is clean and that slurry and froth are not accumulating in the tubes.

APPENDIX C

EQUIPMENT

C.1 Reference for equipment information

Table C.1: List of equipment.

	Brand	References
Data acquisition box: Dutec BIO4, BIO8, BIO16. Baudmaster	Dutec	www.dutec.com
Pressure transmitter	Wika	www.wika.com
Notebook PIII 533 Satellite	Toshiba	www.toshiba.ca
Mass Flow Meters	MKS	www.mks.com
Software		jorge.torrealba@mail.mcgill.ca

APPENDIX D

SOFTWARE

D.1 Algorithm (version Microsoft's Excel 2000 VBA) to process on-off J_g sensor data collected with JTACQV30.

```
'Begin of the subroutine
Sub Jg_SLOPES_Clasic()
number = 1
Dim rws As Single
ReDim LTR(36)
ReDim LTRB(36)
LTR(2) = "b"
LTR(3) = "c"
LTR(4) = "d"
LTR(5) = "e"
LTR(6) = "f"
LTR(7) = "g"
LTR(8) = "h"
LTR(9) = "i"
'1 Channel 1
LTR(10) = "k"
LTRB(10) = "l"
'2 Channel 2
LTR(11) = "m"
LTRB(11) = "n"
'3 Channel 3
LTR(12) = "o"
LTRB(12) = "p"
'4 Channel 4
LTR(13) = "q"
LTRB(13) = "r"
'5 Channel 5
LTR(14) = "s"
LTRB(14) = "t"
'6 Channel 6
LTR(15) = "u"
LTRB(15) = "v"
'7 Channel 7
LTR(16) = "w"
LTRB(16) = "x"
'8 Channel 8
```

```
LTR(17) = "y"
LTRB(17) = "z"
'the rest of the variables can be activated if 16 channels are used'
LTR(18) = "ab"
LTR(19) = "ac"
LTR(20) = "ad"
LTR(21) = "ae"
LTR(22) = "af"
LTR(23) = "ag"
LTR(24) = "ah"
LTR(25) = "ai"
LTR(26) = "aj"
LTR(27) = "ak"
LTR(28) = "al"
LTR(29) = "am"
LTR(30) = "an"
LTR(31) = "ao"
LTR(32) = "ap"
LTR(33) = "aq"
LTR(34) = "ar"
LTR(35) = "as"
'Reads the active sheet and the number of lines
Worksheets(ActiveSheet.Name).Activate
c = Range("a1").End(xlDown).Address
A = "a1:" & c
Range(A).Select
 areaCount = Selection.Areas.Count
i = 1
 For Each A In Selection.Areas
rws = A.Rows.Count
i = i + 1
Next A
Dim rw As Integer
Dim columna As Integer
rw = 6
Dim value As Single
ReDim myarray(rws, 9)
ReDim cord(1000, 2)
myarray(1, 1) = Cells(1, 6).value
myarray(1, 2) = Cells(1, 7).value
'myarray(1, 3) = Cells(1, 8).Value
'Reads the data in an array
T = 0
For f = 2 To rws
myarray(f, 1) = Cells(f, 1).value
Next f
For c = 2 To 9
codecheck = 0
T = 0
scnd = 0
For f = 2 To rws
myarray(f, c) = Cells(f, c).value
 'beginning of the filtering
If myarray(f, c) > 10 And T = 0 Then
If myarray(f, c) < 15 And myarray(f, c) > 10 Then
beg = f
```

```
T = 1
scnd = 1
End If
End If
If myarray(f, c) > 70 And scnd = 1 Then
If myarray(f, c) < 75 And myarray(f, c) > 70 Then
endd = f
cont = 0
T = 0
second = 0
index = index + 1
cord(index, 1) = begg
cord(index, 2) = endd
'Copy the range of data
A = "a" & cord(index, 1) & ":a" & cord(index, 2)
b = LTR(c) & cord(index, 1) & ":" & LTR(c) & cord(index, 2)
Worksheets(ActiveSheet.Name).Range(A).Copy
row1 = 6 + row2
row2 = cord(index, 2) - cord(index, 1) + 6 + row2
If (row2) > 0 Then
Worksheets(ActiveSheet.Name).Range(LTR(c + 8) & rw1 & ":" & LTR(c + 8) & rw2).PasteSpecial
Worksheets(ActiveSheet.Name).Range(b).Copy
Worksheets(ActiveSheet.Name).Range(LTRB(c + 8) & rw1 & ":" & LTRB(c + 8) &
rw2).PasteSpecial
Worksheets(ActiveSheet.Name).Range("ac4").value = "slope"
Worksheets(ActiveSheet.Name).Range(LTR(18) & rw).value = rw - 5
Worksheets(ActiveSheet.Name).Range(LTR(c + 17) & rw).Formula = "=+Slope(" & LTRB(c + 8) &
rw1 & ":" & LTRB(c + 8) & rw2 & "," & LTR(c + 8) & rw1 & ":" & LTR(c + 8) & rw2 & ")"
Worksheets(ActiveSheet.Name).Range("al4").value = "rsq"
Worksheets(ActiveSheet.Name).Range(LTR(27) & rw).value = rw - 5
Worksheets(ActiveSheet.Name).Range(LTR(c + 26) & rw).Formula = "=+rsq(" & LTRB(c + 8) &
rw1 & ":" & LTRB(c + 8) & rw2 & "," & LTR(c + 8) & rw1 & ":" & LTR(c + 8) & rw2 & ")"
rw = rw + 1
Dim check
For check = rw2 To rw1 Step -1
'                           change the limits for the slope calculation
If Worksheets(ActiveSheet.Name).Range(LTRB(c + 8) & check).value < 70 Then
If Worksheets(ActiveSheet.Name).Range(LTRB(c + 8) & check).value < 12 Then
Worksheets(ActiveSheet.Name).Range(LTRB(c + 8) & check & ":" & LTRB(c + 8) & rw1).Clear
check = rw1
codigocheck = 1
End If
End If
Next check
codigocheck = 0
T = 0
scnd = 0
End If
End If
End If
Next f
rw2 = 0
rw = 6
Next c
'Load integer values into first column of MyArray
 For i = 1 To rws
```

```
 myarray(i, 0) = i
 Next i
End Sub
```

D.2 Algorithm (version Microsoft's Excel 2000 VBA) to process continuous J_g sensor data collected with JTACQV30.

This version was designed to read 8 channels.

```
Sub average_cont()
Dim i, j As Single
ReDim LTR(16)
ReDim LTRo(16)
Dim rws As Single
Dim r(), myRange As Range
ReDim r(8)
Dim v() As Single
Dim va() As String
ReDim v(200)
ReDim va(200)
Dim pfile As String
Dim pfiletww As String
Dim files() As Single
Dim filea() As String
ReDim files(200)
ReDim filea(200)
Dim onn As Single
Dim tww As Single
Dim P$
pfile = ActiveSheet.Name
pfile = ActiveWorkbook.Name
LTR(1) = "b"
LTR(2) = "c"
LTR(3) = "d"
LTR(4) = "e"
LTR(5) = "f"
LTR(6) = "g"
LTR(7) = "h"
LTR(8) = "i"
LTR(9) = "j"
LTR(10) = "k"
LTR(11) = "l"
LTR(12) = "m"
LTR(13) = "n"
LTR(14) = "o"
LTR(15) = "p"
LTR(16) = "q"
LTRo(1) = "e"
LTRo(2) = "f"
LTRo(3) = "g"
LTRo(4) = "h"
LTRo(5) = "i"
```

```
LTRo(6) = "j"
LTRo(7) = "k"
LTRo(8) = "l"
LTRo(9) = "m"
LTRo(10) = "n"
LTRo(11) = "o"
LTRo(12) = "p"
LTRo(13) = "q"
LTRo(14) = "r"
LTRo(15) = "s"
LTRo(16) = "t"
Worksheets(ActiveSheet.Name).Activate
 c = Range("A3").End(xlDown).Address
A = "A3:" & c
e = Range(c).Row
Range(A).Select
areaCount = Selection.Areas.Count
i = 3
For Each d In Selection.Areas
rws = d.Rows.Count
i = i + 1
filea(i) = Worksheets(ActiveSheet.Name).Range("A" & i).value
Next d
file$ = ActiveSheet.Name
rws = rws + 2
For j = 3 To (rws)
Range("d" & j).Select
onn = ActiveCell.value
Range("e" & j).Select
tww = ActiveCell.value
Range("a" & j).Select
pfiletww = ActiveCell.value
solt = Match_cont(j, onn, tww, pfile, pfiletww)
Next j
End Sub
Function Match_cont(j As Single, beg As Single, en As Single, FO As String, FD As String) As String
Dim value As String
Dim cell As String
Dim lnine As Single
Dim ax As Single
Dim bx As Single
Dim area As Single
Dim onn As Single
Dim tww As Single
he = FO
FO = ActiveSheet.Name
Range("F" & j).Select
Act = "=MATCH(" & beg & ",'[" & FD & ".xls]" & FD & "'!R9C1:R65000C1,1)"
ActiveCell.FormulaR1C1 = "=+9+MATCH(" & beg & ",'[" & FD & ".xls]" & FD & "'!R9C1:R65000C1,1)"
onn = ActiveCell.value
Range("g" & j).Select
ACT2 = "=+9+MATCH(" & en & ",'[" & FD & ".xls]" & FD & "'!R9C1:R65000C1,1)"
ActiveCell.FormulaR1C1 = ACT2
tww = ActiveCell.value
```

```
Range("c" & j).Select
value = ActiveCell.value
If value = "C1" Then
cell = "C10"
cell = "C6"
Else
If value = "C2" Then
cell = "C11"
cell = "C7"
Else
If value = "C3" Then
cell = "C12"
cell = "C8"
Else
If value = "C4" Then
cell = "C13"
cell = "C9"
Else
GoTo scp:
If value = "C5" Then
cell = "C14"
cell = "C10"
Else
If value = "C6" Then
cell = "C15"
cell = "C10"
Else
If value = "C7" Then
cell = "C16"
cell = "C10"
Else
If value = "C8" Then
cell = "C17"
cell = "C10"
Else
If value = "C9" Then
cell = "C18"
Else
cell = "C19"
End If
End If
End If
End If
End If
End If
End If
End If
End If
scp:
Range("h" & j).Select
Act3 = "=+average('[" & FD & ".xls]" & FD & "'!R" & onn & cell & ":R" & tww & cell & ")"
ActiveCell.FormulaR1C1 = Act3
Range("i" & j).Select
Act3 = "=+stdev('[" & FD & ".xls]" & FD & "'!R" & onn & cell & ":R" & tww & cell & ")"
ActiveCell.FormulaR1C1 = Act3
Range("j" & j).Select
```

```
Act3 = "=+sum(R" & j & "C5" & "-R" & j & "C4" & ")"
ActiveCell.FormulaR1C1 = Act3
Range("k" & j).Select
Inine = ActiveCell.value
Range("O" & j).Select
area = ActiveCell.value
Range("p" & j).Select
baseline = ActiveCell.value
If Inine = 2.06 Then
Range("r" & 3).Select
ax = ActiveCell.value
Range("s" & 3).Select
bx = ActiveCell.value
Else
If Inine = 1.6 Then
Range("r" & 4).Select
ax = ActiveCell.value
Range("s" & 4).Select
bx = ActiveCell.value
Else
If Inine = 1.3 Then
Range("r" & 5).Select
ax = ActiveCell.value
Range("s" & 5).Select
bx = ActiveCell.value
Else
If Inine = 0.94 Then
Range("r" & 6).Select
ax = ActiveCell.value
Range("s" & 6).Select
bx = ActiveCell.value
Else
Range("r" & 7).Select
ax = ActiveCell.value
Range("s" & 7).Select
bx = ActiveCell.value
End If
End If
End If
End If
solt = Jgpaste_cont(j, Inine, onn, tww, ax, bx, value, FO, FD, area, baseline)
Windows(FO & ".xls").Activate
End Function
Function Jgpaste_cont(P As Single, Inine As Single, beg As Single, en As Single, ax As Single,
bx As Single, value As String, FO As String, FD As String, area As Single, baseline As Single)
Dim LTR() As String
ReDim LTR(16)
LTR(1) = "R"
LTR(2) = "S"
LTR(3) = "T"
LTR(4) = "U"
LTR(5) = "V"
LTR(6) = "W"
LTR(7) = "X"
LTR(8) = "Y"
LTR(9) = "Z"
```

```
LTR(10) = "AA"
LTR(11) = "AB"
LTR(12) = "AC"
LTR(13) = "AD"
LTR(14) = "AE"
LTR(15) = "AF"
LTR(16) = "AG"
Dim cell As String
If value = "C1" Then
cell = "C10"
cell = "C6"
i = 1
ACT2 = LTR(i)
Else
If value = "C2" Then
cell = "C11"
cell = "C7"
i = 2
ACT2 = LTR(i)
Else
If value = "C3" Then
cell = "C12"
cell = "C8"
i = 3
ACT2 = LTR(i)
Else
If value = "C4" Then
cell = "C13"
cell = "C9"
i = 4
ACT2 = LTR(i)
Else
GoTo scp2:
If value = "C5" Then
cell = "C14"
i = 5
ACT2 = LTR(i)
Else
If value = "C6" Then
cell = "C15"
i = 6
ACT2 = LTR(i)
Else
If value = "C7" Then
cell = "C16"
i = 7
ACT2 = LTR(i)
Else
If value = "C8" Then
cell = "C17"
i = 8
ACT2 = LTR(i)
Else
If value = "C9" Then
cell = "C18"
i = 9
```

```
ACT2 = LTR(i)
Else
cell = "C19"
i = 10
ACT2 = LTR(i)
End If
End If
End If
End If
End If
End If
End If
End If
End If
scp2:
Windows(FD & ".xls").Activate
ActiveSheet.Name = FD
j = P
If lnine = 2.06 Then
Range("r" & 3).Select
ActiveCell.value = ax
Range("s" & 3).Select
ActiveCell.value = bx
Range("T" & 3).Select
ActiveCell.value = baseline
Range("u" & 3).Select
ActiveCell.value = area
Else
If lnine = 1.6 Then
Range("r" & 4).Select
ActiveCell.value = ax
Range("s" & 4).Select
ActiveCell.value = bx
Range("T" & 4).Select
ActiveCell.value = baseline
Range("u" & 4).Select
ActiveCell.value = area
Else
If lnine = 1.3 Then
Range("r" & 5).Select
ActiveCell.value = ax
Range("s" & 5).Select
ActiveCell.value = bx
Range("T" & 5).Select
ActiveCell.value = baseline
Range("u" & 5).Select
ActiveCell.value = area
Else
If lnine = 0.94 Then
Range("r" & 6).Select
ActiveCell.value = ax
Range("s" & 6).Select
ActiveCell.value = bx
Range("T" & 6).Select
ActiveCell.value = baseline
Range("u" & 6).Select
```

```
ActiveCell.value = area
Else
Range("r" & 7).Select
ActiveCell.value = ax
Range("s" & 7).Select
ActiveCell.value = bx
Range("T" & 7).Select
ActiveCell.value = baseline
Range("u" & 7).Select
ActiveCell.value = area
End If
End If
End If
End If
j = beg
If lnine = 2.06 Then
Act3 = "=+sum(+sqrt(R" & j & cell & "-R3C20)*R3C18+R3C19)*1000/60/R3C21"
Else
If lnine = 1.6 Then
Act3 = "=+sum(+sqrt(R" & j & cell & "-R4C20)*R4C18+R4C19)*1000/60/R4C21"
Else
If lnine = 1.3 Then
Act3 = "=+sum(+sqrt(R" & j & cell & "-R5C20)*R5C18+R5C19)*1000/60/R5C21"
Else
If lnine = 0.94 Then
Act3 = "=+sum(+sqrt(R" & j & cell & "-R6C20)*R6C18+R6C19)*1000/60/R6C21"
Else
Act3 = "=+sum(+sqrt(R" & j & cell & "-R7C20)*R7C18+R7C19)*1000/60/R7C21"
End If
End If
End If
End If
'back to the file activated
Windows(FD & ".xls").Activate
ActiveSheet.Name = FD
Range(LTR(i) & j).Select
ActiveCell.FormulaR1C1 = Act3
If lnine = 2.06 Then
Act3 = "=+SUM(+SQRT(RC[-8]-2)*R3C18+R3C19)*1000/60/R4C21"
Else
If lnine = 1.6 Then
Act3 = "=+SUM(+SQRT(RC[-8]-2)*R4C18+R4C19)*1000/60/R4C21"
Else
If lnine = 1.3 Then
Act3 = "=+SUM(+SQRT(RC[-8]-2)*R5C18+R5C19)*1000/60/R4C21"
Else
If lnine = 0.94 Then
Act3 = "=+SUM(+SQRT(RC[-8]-2)*R6C18+R6C19)*1000/60/R4C21"
Else
Act3 = "=+SUM(+SQRT(RC[-8]-2)*R7C18+R7C19)*1000/60/R4C21"
End If
End If
End If
End If
Range(LTR(i) & j).Select
Selection.Copy
```

```
Range(LTR(i) & j & ":" & LTR(i) & en).Select
ActiveSheet.Paste
cell = "C" & i + 8 + 9
aver = ave_cont(P, cell, beg, en, FO, FD)
scp:
End Function
Function ave_cont(j As Single, cell As String, onn As Single, tww As Single, FO As String, FD As
String) As Single
'*******************************************************************
'                    average & stdev calculation
'*******************************************************************
Windows(FO & ".xls").Activate
Range("M" & j).Select
Act3 = "=+average('[" & FD & ".xls]" & FD & "'!R" & onn & cell & ":R" & tww & cell & ")"
ActiveCell.FormulaR1C1 = Act3

Range("N" & j).Select
Act3 = "=+stdev('[" & FD & ".xls]" & FD & "'!R" & onn & cell & ":R" & tww & cell & ")"
ActiveCell.FormulaR1C1 = Act3
Windows(FD & ".xls").Activate
End Function

Function namefile() As String
'*******************************************************************
'                  ActivieWorkbook name
'*******************************************************************
namefile = ActiveWorkbook.Name
End Function
Function namesheet() As String
'*******************************************************************
'                     Sheet name
*******************************************************************
namesheet = ActiveSheet.Name
End Function
Sub put_names()
i = ActiveCell.Row
j = ActiveCell.Column
namefile
namesheet
Range("k" & i).Select
ActiveCell.value = namefile
Range("k" & i + 1).Select
ActiveCell.value = namesheet
End Sub
Sub put_values_Q_P_T()
Dim i As Single
Worksheets(ActiveSheet.Name).Activate
c = Range("A3").End(xlDown).Address
A = "A3:" & c
e = Range(c).Row
Range(A).Select
areaCount = Selection.Areas.Count
i = 3 'start
rws = e
i = i + 1
For Row = 3 To rws
```

```
Range("f" & Row).Select
i = Row
j = ActiveCell.Column
Range("b" & i).Select
namedirectory = ActiveCell.value
Range("c" & i).Select
nf = ActiveCell.value
Range("d" & i).Select
ns = ActiveCell.value
Range("e" & i).Select
nr = ActiveCell.value
Range("f" & i).Select
Act3 = "=+('" & namedirectory & "[" & nf & "]" & ns & "'!R" & nr & "C3)"
ActiveCell.FormulaR1C1 = Act3
Range("g" & i).Select
Act3 = "=+('" & namedirectory & "[" & nf & "]" & ns & "'!R" & nr & "c2)"
ActiveCell.FormulaR1C1 = Act3
Range("h" & i).Select
Act3 = "=+('" & namedirectory & "[" & nf & "]" & ns & "'!R" & nr & "c1)"
ActiveCell.FormulaR1C1 = Act3
Next Row
End Sub
```

D3 Serial cable

A serial cable can be made it with a three wires cable (up to 10 m) and 2 D9 male and female serial connectors. The actual configuration (as July 2004) uses a standard straight through 9-pin to 9-pin RS232 cable, and the connections are:

Pin2 goes to Pin2, Pin 3 goes to Pin3, and Pin 5 goes to Pin5.

APPENDIX E
FROTHING CONTROL

Froth build up inside the sensor is a normal phenomenon. Particularly in the presence of solids the froth stability can be such that the height builds eventually reaching the top of the sensor and plugging the orifice. A mean to control the froth was sought.

Conventional froth control methods are based on thermal, chemical, electrical and mechanical effects.

A mechanical based attempt was the acceleration and anticipated collapse of the froth by means of smaller diameter insert and a reservoir (to collect the froth) before the orifice. This method is popular in the oil industry, especially with foams of large bubbles; but in our case there little delay in the production of a stable froth. A longer tube sensor was tried, but this only delayed without solving and led to an unwieldy device. A third mechanical method, ultrasonic froth destruction is yet an untried possibility [8]. A chemical approach, using a water dispersing product, WD-40, sprayed over the internal walls of the sensor tube before insertion in the cell, gave desired increased time for measurement, but was discarded as an option due to the potential contamination of the process.

All the alternatives tried above are ways to delay froth buildup. If the buildup cannot be eliminated then the approach must consider two step procedures: data acquisition followed by tube cleaning. Froth buildup typically takes around 15- 30 minutes during which data can be collected. A cleaning step could comprise a solenoid valve activating compressed air to eject the froth-slurry from the sensor. As compressed air is available at plant sites and normally the pressure required is lower than 9.8 (kPa) (100 cm of Water), this may be a practical solution. Cleaning will take less than a minute and the sensor will be ready for another data acquisition step.

APPENDIX F
DATA TABLES

Table F.1: Mass Flow meter calibration data.

Q Setpoint in (SCMS)	Q Actual in (SCMS)	M Water (kg)	t (s)	P (Pa)	M Water/t (kg/min)	n' (mol/min)	Q calculated (SCMS)
5 LPM Mass flow meter calibration.							
8.33E-06	8.17E-06	6.079	708	4903	0.52	0.022	8.40E-06
1.67E-05	1.65E-05	6.071	357	4903	1.02	0.044	1.66E-05
3.33E-05	3.32E-05	6.063	180	4903	2.02	0.088	3.29E-05
4.17E-05	4.15E-05	6.080	146	4903	2.51	0.109	4.09E-05
5.00E-05	4.98E-05	6.075	121	4903	3.01	0.131	4.91E-05
6.67E-05	6.65E-05	6.110	91	4903	4.03	0.176	6.56E-05
8.33E-05	8.32E-05	6.082	72	4903	5.06	0.221	8.25E-05
30 LPM Mass flow meter calibration.							
5.00E-05	5.03E-05	8.500	239	5883	2.13	0.094	3.51E-05
8.33E-05	8.37E-05	8.499	130	5883	3.94	0.173	6.48E-05
1.67E-04	1.67E-04	8.498	58	5883	8.81	0.387	1.45E-04
2.50E-04	**2.50E-04**	**8.500**	**38**	**5883**	**13.53**	**0.595**	**2.22E-04**
3.33E-04	3.34E-04	8.561	28	5883	18.34	0.807	3.02E-04
4.17E-04	4.17E-04	8.585	22	5883	23.31	1.025	3.83E-04
5.00E-04	5.00E-04	8.744	19	5883	27.76	1.221	4.56E-04
200 LPM Mass flow meter calibration.							
1.67E-04	1.66E-04	14.538	229	8618	3.81	0.1718	6.42E-05
3.33E-04	3.32E-04	14.927	62	9307	14.45	0.6557	2.45E-04
5.00E-04	4.98E-04	20.905	50	12409	25.09	1.1706	4.38E-04
6.67E-04	6.65E-04	21.533	35	12754	36.91	1.7278	6.46E-04
8.33E-04	8.33E-04	24.337	30	8618	48.67	2.1956	8.21E-04
1.00E-03	9.99E-04	34.282	38	15856	54.13	2.6026	9.73E-04
1.17E-03	1.16E-03	27.381	24	14822	68.45	3.2622	1.22E-03
1.67E-03	1.66E-03	33.276	20	12065	99.83	4.6444	1.74E-03
2.50E-03	2.50E-03	39.644	15	17580	158.57	7.7364	2.89E-03
3.33E-03	3.33E-03	47.731	13	20682	220.30	11.0282	4.12E-03
Second order polynomials.							
Mass flow meter	**Equation**						
5 LPM	$Q_{SCMS} = 301.56\,(Q_{SCMS\text{-}IN})^2 + 0.96\,(Q_{SCMS\text{-}IN}) + 6.43E\text{-}7$, $R^2=0.99999$						
30 LPM	$Q_{SCMS} = -21.78\,(Q_{SCMS\text{-}IN})^2 + 0.95\,(Q_{SCMS\text{-}IN}) - 1.40E\text{-}5$, $R^2=0.99991$						
200 LPM	$Q_{SCMS} = 82.61\,(Q_{SCMS\text{-}IN})^2 + 0.98\,(Q_{SCMS\text{-}IN}) - 7.73E\text{-}5$, $R^2=0.99954$						

Table F.2: Pressure transmitter calibration.

Calibration pressure transducer (PT) 6A.	
Pressure water displaced (Pa)	**Pressure gauge PT (Pa)**
1510.12	1421.87
2647.62	2520.14
3628.22	3569.38
4540.18	4432.31
5510.97	5520.78
6511.18	6442.54
7442.75	7344.69
8393.94	8325.29
9345.12	9266.67
10345.33	10237.46
Calibration pressure transducer (PT) 4A.	
Pressure water displaced (Pa)	**Pressure gauge PT (Pa)**
1519.93	1833.72
2294.60	2588.78
2961.41	3285.01
3961.62	4363.67
4912.81	5295.24
5932.63	6246.42
6923.04	7236.83
7923.25	8246.85
8854.82	9296.09
1519.93	1833.72
2294.60	2588.78

Table F.3: Laboratory verification.

Results for Equations 4.30 and 4.33b verification.									
Real		**JKMRC**							
		(Test 292.15 K)		**Eq 4.33b**		**Eq 4.30**			
						γ=1		**γ=1.4**	
J_g STD (cm/s)	**Stdev (cm/s)**	**dH/dt (cm/dt)**	**Stdev (cm/s)**	**J_g STD (cm/s)**	**Stdev (cm/s)**	**J_g STD (cm/s)**	**Stdev (cm/s)**	**J_g STD (cm/s)**	**Stdev (cm/s)**
0.765	0.0005	0.7682	0.0007	0.713	0.001	0.760	0.000	0.744	0.0000
1.012	0.0005	1.0286	0.0035	0.955	0.003	1.018	0.0006	0.996	0.0006
1.259	0.0005	1.2887	0.0033	1.196	0.003	1.275	0.0006	1.248	0.0006
1.506	0.0005	1.5625	0.0037	1.450	0.003	1.546	0.0006	1.513	0.0006
1.752	0.0005	1.8138	0.0038	1.684	0.003	1.795	0.0006	1.756	0.0006
1.990	0.0005	2.0690	0.0124	1.920	0.010	2.048	0.0006	2.003	0.0006

Comparison between the two techniques using McGill model (T=292.15 K).		
Real	**JKMRC Eq. 4.30**	**McGill Eq. 4.23**

J_g STD (cm/s)	Stdev (cm/s)	γ=1 (Eq. 4.32)		γ=1.4 (Eq.4.30)		dP/dt (cm/s)	Stdev (cm/s)	γ=1 (Eq.4.25)		γ=1.4 (Eq.4.23)	
		J_g STD (cm/s)	Stdev (cm/s)	J_g STD (cm/s)	Stdev (cm/s)			J_g STD (cm/s)	Stdev (cm/s)	J_g STD (cm/s)	Stdev (cm/s)
0.765	0.0005	0.760	0.000	0.744	0.000	66.37	0.065	0.728	0.000	0.756	0.001
1.012	0.0005	1.018	0.001	0.996	0.001	88.91	0.266	0.975	0.001	1.013	0.003
1.259	0.0005	1.275	0.001	1.248	0.001	111.29	0.058	1.220	0.003	1.267	0.001
1.506	0.0005	1.546	0.001	1.513	0.001	136.24	0.473	1.493	0.001	1.552	0.005
1.752	0.0005	1.795	0.001	1.756	0.001	157.96	0.565	1.731	0.005	1.799	0.006
1.990	0.0005	2.048	0.001	2.003	0.001	179.22	0.319	1.965	0.006	2.041	0.004

Table F.4: Results from the plant comparison (Northparkes).

Parameter		McGill	JK
H_l (m)		2.00	2.33
H_P (m)		1.50	1.63
H_1 (m)			0.145
H_2 (m)			0.415
Water density (kg/m^3)			1000
Gas holdup (%)		10	10
ρ_{bulk} (kg/m^3) *		1130	1130
ρ_s (kg/m^3)		1130	900
Function P (m / Pa)	Function P (dimensionless)	1.04E-04	8.57E-01
dP/dt (Pa/s)	dH/dt (m/s)	107.92	1.52·10-2
J_g' (cm/s)		1.12	1.35
Tube diameter (m)		0.10	4.2·10-2
Tip diameter (m)			4.8·10-2
Nozzle factor			0.875
J_g (m/s)		1.12	1.14
Depth difference J_g correction from 0.70 to 0.50 (m), J_g		1.12	1.16
Difference		3.6 %	
* Estimated from measurements taken 6 days later			

Table F.5: Results from the plant comparison (Red Dog).

Cell flow rate	McGill				JK Their data		JK			
SCMS	4.23 (cm/s)	Stdev (cm/s)	4.25 (cm/s)	Stdev (cm/s)	4.33b (cm/s)	Stdev (cm/s)	4.30 (cm/s)	Stdev (cm/s)	4.32 (cm/s)	Stdev (cm/s)
4.48E-02	**0.376**	**0.035**	**0.402**	**0.044**	**0.467**	**0.034**	**0.488**	**0.052**	**0.495**	**0.052**
6.13E-02	0.600	0.080	0.639	0.082	0.581	0.013	0.601	0.021	0.609	0.021
7.79E-02	0.673	0.078	0.716	0.079	0.645	0.027	0.667	0.041	0.676	0.042
9.44E-02	0.838	0.111	0.890	0.113	0.747	0.011	0.771	0.018	0.780	0.018

Table F.6: Bulk density.

	P_1		P_2		P_2-P_1		ρ_{bulk}	
day	(Pa)	Stdev (Pa)	(Pa)	Stdev (Pa)	(Pa)	Stdev (Pa)	(kg/m^3)	Stdev (kg/m^3)
A	23854.71	235.32	7041.72	123.31	16812.99	200.42	1143.04	13.63
B	23177.67	407.87	6691.38	278.22	16486.29	298.25	1120.83	20.28
C	18715.39	1514.34	4876.57	1350.63	13838.82	684.86	940.84	46.56
D	23295.72	274.12	6818.87	120.94	16476.85	246.00	1120.19	16.72
E	22712.61	613.43	6260.73	127.09	16451.88	600.12	1118.49	40.80

Table F.7: FP nomograph data.

Tube	Gas Holdup (%)						
H_l/H_p		12		10		8	
3/2	ρ_{slurry} (kg/m^3)	FP JK Eq.(4.32)	FP McGill Eq.(4.25)	FP JK Eq.(4.32)	FP McGill Eq.(4.25)	FP JK Eq.(4.32)	FP McGill Eq.(4.25)
	1400	0.871	1.00E-04	0.868	9.85E-05	0.865	9.67E-05
	1300	0.870	1.07E-04	0.867	1.05E-04	0.864	1.03E-04
	1200	0.869	1.14E-04	0.866	1.12E-04	0.863	1.10E-04
	1100	0.868	1.23E-04	0.865	1.21E-04	0.862	1.19E-04
	1000	0.867	1.34E-04	0.864	1.31E-04	0.861	1.29E-04
2/1							
	1400	0.947	9.16E-05	0.946	8.97E-05	0.945	8.80E-05
	1300	0.946	9.80E-05	0.945	9.60E-05	0.944	9.41E-05
	1200	0.946	1.06E-04	0.945	1.03E-04	0.944	1.01E-04
	1100	0.945	1.14E-04	0.944	1.12E-04	0.943	1.10E-04
	1.00	0.945	1.25E-04	0.944	1.22E-04	0.943	1.20E-04
4/3							
	1400	0.795	1.09E-04	0.790	1.07E-04	0.786	1.06E-04
	1300	0.793	1.16E-04	0.789	1.14E-04	0.785	1.12E-04
	1200	0.791	1.23E-04	0.787	1.21E-04	0.783	1.19E-04
	1100	0.790	1.32E-04	0.785	1.30E-04	0.781	1.28E-04
	1000	0.788	1.43E-04	0.784	1.41E-04	0.779	1.38E-04

Table F.8: Sensitivity analysis for Equation 4.25.

H_l/H_p= 3/2 (m/m)		
Percentage of parameter variation	Percentage of variation of FP due to	Percentage of variation of FP due to
	ρ_{bulk}	H_P
ρ_{bulk} = 1000 (kg/m^3)		
1	-0.85	0.18
2	-1.69	0.35
4	-3.32	0.71
8	-6.40	1.43
10	-7.86	1.80

15	-11.28	2.72
20	-14.43	3.66
40	-24.80	7.60
50	-28.97	9.68
	ρ_{bulk} = 1200 (kg/m^3)	
1	-0.84	0.21
2	-1.66	0.42
4	-3.26	0.84
8	-6.27	1.69
10	-7.70	2.13
15	-11.06	3.22
20	-14.15	4.34
40	-24.34	9.08
50	-28.44	11.61
	ρ_{bulk} = 800 (kg/m^3)	
1	-0.87	0.14
2	-1.73	0.29
4	-3.40	0.58
8	-6.55	1.16
10	-8.04	1.46
15	-11.54	2.20
20	-14.75	2.96
40	-25.33	6.10
50	-29.58	7.74
	H_l/H_p = 2/1 (m/m)	
Percentage of parameter variation	**Percentage of variation of FP due to**	**Percentage of variation of FP due to**
	ρ_{bulk}	**H_P**
	ρ_{bulk} = 1000 (kg/m^3)	
1	-0.92	0.09
2	-1.82	0.18
4	-3.56	0.35
8	-6.86	0.71
10	-8.42	0.89
15	-12.09	1.34
20	-15.46	1.80
40	-26.53	3.66
50	-30.97	4.62
	ρ_{bulk} = 1200 (kg/m^3)	
1	-0.91	0.10
2	-1.80	0.21
4	-3.52	0.42
8	-6.79	0.84
10	-8.33	1.05
15	-11.96	1.59
20	-15.29	2.13
40	-26.26	4.34
50	-30.66	5.49
	ρ_{bulk} = 800 (kg/m^3)	

1	-0.93	0.07
2	-1.84	0.14
4	-3.61	0.29
8	-6.95	0.58
10	-8.53	0.72
15	-12.24	1.09
20	-15.64	1.46
40	-26.84	2.96
50	-31.33	3.73

Table F.9: Adiabatic gas expansion factor, Y_1.

ΔP	P_{f1}	P_{f2}	Y_1 (dimensionless)					
			Orifices (mm)					
(Pa)	(Pa)	(Pa)	0.70	0.94	1.30	1.60	2.06	3.00
0	101325	101325						
980.6	102305.6	101325	0.995	0.995	0.995	0.995	0.995	0.993
1961.2	103286.3	101325	0.990	0.990	0.990	0.990	0.989	0.988
2941.8	104266.9	101325	0.985	0.985	0.985	0.985	0.984	0.983
3922.4	105247.6	101325	0.980	0.980	0.980	0.980	0.979	0.978
4903	106228.2	101325	0.975	0.975	0.975	0.975	0.975	0.973
5883.6	107208.8	101325	0.970	0.970	0.970	0.970	0.970	0.969
6864.2	108189.5	101325	0.965	0.965	0.965	0.965	0.965	0.964
7844.8	109170.1	101325	0.961	0.961	0.961	0.961	0.960	0.959
8825.4	110150.7	101325	0.956	0.956	0.956	0.956	0.956	0.955
9806	111131.4	101325	0.952	0.952	0.952	0.951	0.951	0.950
10786.6	112112	101325	0.947	0.947	0.947	0.947	0.947	0.946
11767.2	113092.7	101325	0.943	0.943	0.943	0.943	0.942	0.941
12747.8	114073.3	101325	0.938	0.938	0.938	0.938	0.938	0.937

Table F.10: 1.30 orifice calibration in a horizontal (H) and vertical (V) setup.

Vertical						
T (K)	P (cm of Water)	P (kPa)	Q (SLPM)	ρ (kg/m^3)	$\sqrt{\frac{\Delta P}{\rho}}$ (kPa*m^3/kg)$^{0.5}$	Q (SCMS)
294.34	103.34	10.13	6.31	1.31	2.78	1.05E-04
294.40	88.79	8.71	5.83	1.30	2.59	9.73E-05
294.53	75.05	7.36	5.36	1.28	2.40	8.93E-05
294.53	63.05	6.18	4.89	1.27	2.21	8.15E-05
294.56	52.14	5.11	4.42	1.25	2.02	7.36E-05
294.57	42.46	4.16	3.94	1.24	1.83	6.57E-05
294.59	33.85	3.32	3.46	1.23	1.64	5.76E-05
294.55	26.34	2.58	2.98	1.22	1.45	4.97E-05
294.57	19.81	1.94	2.51	1.22	1.26	4.19E-05
294.53	14.35	1.41	2.04	1.21	1.08	3.40E-05
P_{atm} = 101596 (Pa)						

Horizontal						
292.61	101.91	9.99	6.31	1.32	2.75	1.05E-04
292.09	87.55	8.59	5.83	1.31	2.57	9.73E-05
292.21	74.23	7.28	5.36	1.29	2.38	8.94E-05
292.71	62.57	6.14	4.88	1.27	2.20	8.14E-05
293.03	51.94	5.09	4.42	1.26	2.01	7.36E-05
293.28	42.50	4.17	3.93	1.25	1.83	6.56E-05
293.46	33.61	3.30	3.45	1.24	1.63	5.76E-05
293.59	26.23	2.57	2.98	1.23	1.45	4.97E-05
293.68	19.65	1.93	2.51	1.22	1.26	4.19E-05
293.81	14.26	1.40	2.04	1.21	1.07	3.40E-05
P_{atm} = 101596 (Pa)						

Table F.11: 1.60 and 3.00 orifices calibration in a horizontal setup, with short (S) and long (L) nipple.

1.60 orifice						
L						
T (K)	P (cm of Water)	P (kPa)	Q (SLPM)	ρ (kg/m^3)	$\sqrt{\frac{\Delta P}{\rho}}$ ($(kPa*m^3/kg)^{0.5}$)	Q (SCMS)
294.36	114.21	11.20	10.58	1.33	2.91	2.06E-04
294.34	105.02	10.30	10.10	1.31	2.80	1.96E-04
294.28	95.37	9.35	9.63	1.30	2.68	1.86E-04
294.28	85.93	8.43	9.15	1.29	2.55	1.76E-04
294.28	77.01	7.55	8.68	1.28	2.43	1.67E-04
294.28	69.09	6.78	8.21	1.27	2.31	1.57E-04
294.28	60.81	5.96	7.74	1.26	2.17	1.48E-04
294.28	53.59	5.26	7.26	1.26	2.05	1.38E-04
294.28	47.46	4.65	6.79	1.25	1.93	1.29E-04
294.28	40.59	3.98	6.31	1.24	1.79	1.20E-04
294.28	34.85	3.42	5.84	1.23	1.66	1.10E-04
294.22	29.85	2.93	5.36	1.23	1.54	1.01E-04
294.20	24.69	2.42	4.89	1.22	1.41	9.24E-05
294.15	20.42	2.00	4.41	1.22	1.28	8.35E-05
294.15	16.54	1.62	3.94	1.21	1.16	7.46E-05
294.15	13.36	1.31	3.46	1.21	1.04	6.58E-05
294.09	10.19	1.00	2.98	1.21	0.91	5.72E-05
294.09	7.86	0.77	2.51	1.20	0.80	4.88E-05
P_{atm} = 101325 (Pa)						
S						
299.46	114.37	11.22	10.58	1.30	2.93	2.06E-04
299.46	106.52	10.45	10.10	1.29	2.84	1.96E-04
299.49	96.31	9.44	9.63	1.28	2.71	1.86E-04
299.53	86.05	8.44	9.15	1.27	2.58	1.76E-04
299.53	77.85	7.63	8.68	1.26	2.46	1.67E-04
299.53	69.05	6.77	8.21	1.25	2.33	1.57E-04

299.53	61.44	6.03	7.74	1.24	2.20	1.48E-04
299.58	54.02	5.30	7.26	1.23	2.07	1.38E-04
299.64	47.31	4.64	6.79	1.23	1.94	1.29E-04
299.65	41.19	4.04	6.32	1.22	1.82	1.20E-04
299.65	35.11	3.44	5.84	1.21	1.69	1.11E-04
299.65	29.73	2.92	5.36	1.21	1.55	1.01E-04
299.65	25.00	2.45	4.89	1.20	1.43	9.24E-05
299.65	20.51	2.01	4.42	1.20	1.30	8.35E-05
299.51	16.53	1.62	3.94	1.19	1.17	7.47E-05
299.20	13.20	1.29	3.46	1.19	1.04	6.59E-05
298.78	10.09	0.99	2.98	1.19	0.91	5.72E-05
298.42	7.78	0.76	2.51	1.19	0.80	4.88E-05
P_{atm} = 102096 (Pa)						
3.00 Orifice						
L						
T (K)	**P (cm of Water)**	**P (kPa)**	**Q (SLPM)**	**ρ (kg/m^3)**	**$\sqrt{\frac{\Delta P}{\rho}}$ $(kPa/m^3*kg)^{0.5}$**	**Q (SCMS)**
293.15	69.22	6.79	27.47	1.28	2.30	4.58E-04
293.15	60.88	5.97	25.61	1.27	2.17	4.27E-04
293.15	53.10	5.21	23.75	1.26	2.03	3.96E-04
293.15	45.12	4.42	21.87	1.25	1.88	3.65E-04
293.15	37.89	3.72	20.00	1.24	1.73	3.33E-04
293.15	31.57	3.10	18.12	1.24	1.58	3.02E-04
293.15	24.76	2.43	16.23	1.23	1.41	2.71E-04
293.15	19.01	1.86	14.35	1.22	1.24	2.39E-04
293.15	14.00	1.37	12.46	1.21	1.06	2.08E-04
P_{atm} = 101325 (Pa)						
S						
293.15	69.62	6.83	27.50	1.28	2.31	4.58E-04
293.15	61.02	5.98	25.61	1.27	2.17	4.27E-04
293.15	52.73	5.17	23.74	1.26	2.03	3.96E-04
293.15	44.76	4.39	21.86	1.25	1.87	3.65E-04
293.15	37.59	3.69	19.99	1.24	1.72	3.33E-04
293.15	30.97	3.04	18.12	1.23	1.57	3.02E-04
293.15	24.74	2.43	16.24	1.23	1.41	2.71E-04
293.15	18.77	1.84	14.35	1.22	1.23	2.39E-04
P_{atm} = 102096 (Pa)						

Table F.12: Orifice calibration data.

Test	T (K)	P (cm of Water)	P (kPa)	Q (LPM)	Qcal (LPM)	Q (SCMS)
Orifice	**0.70**					
1	295.15	102.14	10.02	2.09	2.07	3.45E-05
	295.15	88.14	8.64	1.94	1.92	3.20E-05

	295.15	76.06	7.46	1.79	1.77	2.95E-05
	295.15	64.82	6.36	1.64	1.63	2.71E-05
	295.15	55.54	5.45	1.49	1.48	2.47E-05
	295.15	44.75	4.39	1.34	1.33	2.22E-05
	295.15	36.15	3.54	1.19	1.19	1.98E-05
	295.15	28.41	2.79	1.04	1.04	1.74E-05
	295.15	21.50	2.11	0.89	0.90	1.50E-05
	295.15	15.16	1.49	0.74	0.75	1.26E-05
2	295.15	101.78	9.98	2.09	2.07	3.45E-05
	295.15	87.90	8.62	1.94	1.92	3.20E-05
	295.15	75.78	7.43	1.79	1.77	2.95E-05
	295.15	64.48	6.32	1.64	1.63	2.71E-05
	295.15	55.37	5.43	1.49	1.48	2.47E-05
	295.15	44.75	4.39	1.34	1.33	2.22E-05
	295.15	36.10	3.54	1.19	1.19	1.98E-05
	295.15	28.41	2.79	1.04	1.04	1.74E-05
	295.15	21.50	2.11	0.89	0.90	1.50E-05
	295.15	15.16	1.49	0.74	0.75	1.26E-05
3	295.15	100.86	9.89	2.09	2.07	3.44E-05
	295.15	88.06	8.64	1.94	1.92	3.20E-05
	295.15	75.83	7.44	1.79	1.77	2.95E-05
	295.15	64.42	6.32	1.64	1.63	2.71E-05
	295.15	55.33	5.43	1.49	1.48	2.47E-05
	295.15	44.75	4.39	1.34	1.33	2.22E-05
	295.15	36.10	3.54	1.19	1.19	1.98E-05
	295.15	28.41	2.79	1.04	1.04	1.74E-05
	295.15	21.50	2.11	0.89	0.90	1.50E-05
	295.15	15.16	1.49	0.74	0.75	1.26E-05
Average	295.15	101.59	9.96	2.09	2.07	3.44E-05
	295.15	88.03	8.63	1.94	1.92	3.20E-05
	295.15	75.89	7.44	1.79	1.77	2.95E-05
	295.15	64.57	6.33	1.64	1.63	2.71E-05
	295.15	55.41	5.43	1.49	1.48	2.47E-05
	295.15	44.75	4.39	1.34	1.33	2.22E-05
	295.15	36.12	3.54	1.19	1.19	1.98E-05
	295.15	28.41	2.79	1.04	1.04	1.74E-05
	295.15	21.50	2.11	0.89	0.90	1.50E-05
	295.15	15.16	1.49	0.74	0.75	1.26E-05
	0.94					
1	295.15	101.69	9.97	2.49	2.46	4.10E-05
	295.15	81.95	8.04	2.24	2.21	3.69E-05
	295.15	64.80	6.35	1.99	1.97	3.28E-05
	295.15	49.82	4.89	1.74	1.72	2.87E-05
	295.15	37.05	3.63	1.49	1.48	2.47E-05
	295.15	26.13	2.56	1.24	1.24	2.06E-05
	295.15	17.54	1.72	0.99	0.99	1.66E-05
2	295.15	101.69	9.97	2.49	2.46	4.10E-05
	295.15	81.87	8.03	2.24	2.21	3.69E-05
	295.15	64.61	6.34	1.99	1.97	3.28E-05
	295.15	49.82	4.89	1.74	1.72	2.87E-05
	295.15	37.05	3.63	1.49	1.48	2.47E-05
	295.15	26.10	2.56	1.24	1.24	2.06E-05
	295.15	17.59	1.72	0.99	0.99	1.66E-05
3	295.15	101.71	9.97	2.49	2.46	4.10E-05
	295.15	81.87	8.03	2.24	2.21	3.69E-05

	295.15	64.58	6.33	1.99	1.97	3.28E-05
	295.15	49.82	4.89	1.74	1.72	2.87E-05
	295.15	37.09	3.64	1.49	1.48	2.47E-05
	295.15	26.10	2.56	1.24	1.24	2.06E-05
	295.15	17.54	1.72	0.99	0.99	1.66E-05
Average	295.15	101.70	9.97	2.49	2.46	4.10E-05
	295.15	81.90	8.03	2.24	2.21	3.69E-05
	295.15	64.66	6.34	1.99	1.97	3.28E-05
	295.15	49.82	4.89	1.74	1.72	2.87E-05
	295.15	37.07	3.63	1.49	1.48	2.47E-05
	295.15	26.11	2.56	1.24	1.24	2.06E-05
	295.15	17.55	1.72	0.99	0.99	1.66E-05
				1.00		
1	293.15	107.08	10.50	5.26	4.17	6.95E-05
	293.15	96.10	9.42	5.01	3.93	6.56E-05
	293.15	85.29	8.36	4.75	3.69	6.15E-05
	293.15	75.29	7.38	4.51	3.46	5.76E-05
	293.15	66.05	6.48	4.26	3.22	5.37E-05
	293.15	57.36	5.62	4.01	2.98	4.97E-05
	293.15	49.32	4.84	3.76	2.75	4.58E-05
	293.15	42.34	4.15	3.52	2.51	4.19E-05
	293.15	35.07	3.44	3.27	2.27	3.79E-05
	293.15	28.80	2.82	3.02	2.04	3.40E-05
	293.15	23.09	2.26	2.76	1.79	2.99E-05
	293.15	18.60	1.82	2.51	1.56	2.59E-05
	293.15	13.57	1.33	2.26	1.32	2.20E-05
2	293.15	106.91	10.48	5.26	4.17	6.95E-05
	293.15	95.92	9.41	5.01	3.94	6.56E-05
	293.15	85.15	8.35	4.76	3.69	6.15E-05
	293.15	75.12	7.37	4.51	3.46	5.76E-05
	293.15	65.92	6.46	4.26	3.22	5.37E-05
	293.15	57.23	5.61	4.01	2.98	4.97E-05
	293.15	49.22	4.83	3.76	2.75	4.58E-05
	293.15	42.37	4.15	3.52	2.51	4.19E-05
	293.15	35.07	3.44	3.26	2.27	3.79E-05
	293.15	28.80	2.82	3.02	2.04	3.40E-05
	293.15	23.09	2.26	2.76	1.79	2.99E-05
	293.15	18.57	1.82	2.51	1.56	2.59E-05
	293.15	13.57	1.33	2.26	1.32	2.20E-05
3	293.15	106.82	10.48	5.26	4.17	6.95E-05
	293.15	95.89	9.40	5.01	3.94	6.56E-05
	293.15	85.10	8.35	4.76	3.69	6.16E-05
	293.15	75.05	7.36	4.51	3.46	5.76E-05
	293.15	65.88	6.46	4.26	3.22	5.37E-05
	293.15	57.24	5.61	4.01	2.98	4.97E-05
	293.15	49.19	4.82	3.76	2.75	4.58E-05
	293.15	42.37	4.15	3.52	2.51	4.19E-05
	293.15	35.06	3.44	3.27	2.27	3.79E-05
	293.15	28.75	2.82	3.02	2.04	3.40E-05
	293.15	23.09	2.26	2.76	1.79	2.99E-05
	293.15	18.57	1.82	2.51	1.56	2.59E-05
	293.15	13.57	1.33	2.26	1.32	2.20E-05
Average	293.15	106.94	10.49	5.26	4.17	6.95E-05
	293.15	95.97	9.41	5.01	3.94	6.56E-05
	293.15	85.18	8.35	4.76	3.69	6.15E-05

	293.15	75.15	7.37	4.51	3.46	5.76E-05
	293.15	65.95	6.47	4.26	3.22	5.37E-05
	293.15	57.28	5.62	4.01	2.98	4.97E-05
	293.15	49.24	4.83	3.76	2.75	4.58E-05
	293.15	42.36	4.15	3.52	2.51	4.19E-05
	293.15	35.07	3.44	3.27	2.27	3.79E-05
	293.15	28.78	2.82	3.02	2.04	3.40E-05
	293.15	23.09	2.26	2.76	1.79	2.99E-05
	293.15	18.58	1.82	2.51	1.56	2.59E-05
	293.15	13.57	1.33	2.26	1.32	2.20E-05
				1.08		
1	293.15	101.14	9.92	6.01	4.88	8.14E-05
	293.15	81.95	8.04	5.52	4.42	7.36E-05
	293.15	65.98	6.47	5.02	3.94	6.56E-05
	293.15	51.42	5.04	4.51	3.46	5.76E-05
	293.15	39.27	3.85	4.01	2.98	4.97E-05
	293.15	28.67	2.81	3.52	2.51	4.19E-05
2	293.15	100.98	9.90	6.01	4.89	8.14E-05
	293.15	81.95	8.04	5.52	4.42	7.36E-05
	293.15	65.90	6.46	5.01	3.94	6.56E-05
	293.15	51.42	5.04	4.51	3.46	5.77E-05
	293.15	39.27	3.85	4.01	2.98	4.97E-05
	293.15	28.61	2.81	3.52	2.51	4.19E-05
3	293.15	101.03	9.91	6.01	4.89	8.15E-05
	293.15	81.95	8.04	5.52	4.42	7.36E-05
	293.15	65.93	6.47	5.02	3.94	6.56E-05
	293.15	51.41	5.04	4.51	3.46	5.76E-05
	293.15	39.26	3.85	4.01	2.98	4.97E-05
	293.15	28.61	2.81	3.52	2.51	4.19E-05
Average	293.15	101.05	9.91	6.01	4.89	8.14E-05
	293.15	81.95	8.04	5.52	4.42	7.36E-05
	293.15	65.93	6.47	5.01	3.94	6.56E-05
	293.15	51.42	5.04	4.51	3.46	5.76E-05
	293.15	39.27	3.85	4.01	2.98	4.97E-05
	293.15	28.63	2.81	3.52	2.51	4.19E-05
				1.18		
1	293.15	97.89	9.60	6.51	5.35	8.92E-05
	293.15	82.03	8.04	6.01	4.88	8.14E-05
	293.15	67.49	6.62	5.51	4.41	7.36E-05
	293.15	55.54	5.45	5.01	3.94	6.56E-05
	293.15	42.37	4.15	4.51	3.46	5.76E-05
	293.15	32.45	3.18	4.01	2.98	4.97E-05
	293.15	23.41	2.30	3.52	2.51	4.19E-05
2	293.15	112.70	11.05	7.01	5.83	9.72E-05
	293.15	98.34	9.64	6.51	5.36	8.93E-05
	293.15	82.03	8.04	6.01	4.89	8.14E-05
	293.15	67.35	6.61	5.52	4.42	7.36E-05
	293.15	55.50	5.44	5.02	3.94	6.57E-05
	293.15	42.37	4.15	4.51	3.46	5.77E-05
	293.15	32.45	3.18	4.01	2.98	4.97E-05
	293.15	23.41	2.30	3.52	2.51	4.19E-05
3	293.15	112.60	11.04	7.01	5.83	9.72E-05
	293.15	98.24	9.63	6.51	5.36	8.93E-05
	293.15	82.03	8.04	6.01	4.89	8.14E-05
	293.15	67.28	6.60	5.52	4.42	7.36E-05

	293.15	55.51	5.44	5.02	3.94	6.57E-05
	293.15	42.37	4.15	4.51	3.46	5.76E-05
	293.15	32.45	3.18	4.01	2.98	4.97E-05
	293.15	23.41	2.30	3.52	2.51	4.19E-05
Average	293.15	112.65	11.05	7.01	5.83	9.72E-05
	293.15	98.16	9.63	6.51	5.36	8.93E-05
	293.15	82.03	8.04	6.01	4.88	8.14E-05
	293.15	67.37	6.61	5.52	4.41	7.36E-05
	293.15	55.51	5.44	5.02	3.94	6.56E-05
	293.15	42.37	4.15	4.51	3.46	5.76E-05
	293.15	32.45	3.18	4.01	2.98	4.97E-05
	293.15	23.41	2.30	3.52	2.51	4.19E-05
				1.30		
1	292.15	100.91	9.90	7.52	6.31	1.05E-04
	292.15	85.44	8.38	7.01	5.83	9.72E-05
	292.15	71.96	7.06	6.51	5.36	8.93E-05
	292.15	60.22	5.90	6.01	4.89	8.15E-05
	292.15	49.59	4.86	5.52	4.42	7.36E-05
	292.15	40.15	3.94	5.02	3.94	6.57E-05
	292.15	32.45	3.18	4.51	3.46	5.77E-05
	292.15	24.76	2.43	4.01	2.98	4.97E-05
	292.15	18.57	1.82	3.52	2.51	4.19E-05
	292.15	13.57	1.33	3.02	2.04	3.40E-05
2	292.15	100.42	9.85	7.52	6.31	1.05E-04
	292.15	85.44	8.38	7.01	5.83	9.72E-05
	292.15	72.04	7.06	6.51	5.36	8.94E-05
	292.15	60.22	5.90	6.01	4.89	8.15E-05
	292.15	49.54	4.86	5.51	4.41	7.35E-05
	292.15	40.15	3.94	5.02	3.94	6.57E-05
	292.15	32.45	3.18	4.51	3.45	5.76E-05
	292.15	24.76	2.43	4.01	2.98	4.97E-05
	292.15	18.57	1.82	3.52	2.51	4.19E-05
	292.15	13.57	1.33	3.02	2.04	3.40E-05
3	292.15	100.48	9.85	7.51	6.31	1.05E-04
	292.15	85.35	8.37	7.01	5.83	9.72E-05
	292.15	71.88	7.05	6.51	5.36	8.94E-05
	292.15	60.14	5.90	6.01	4.88	8.14E-05
	292.15	49.43	4.85	5.52	4.42	7.36E-05
	292.15	40.15	3.94	5.01	3.93	6.56E-05
	292.15	32.45	3.18	4.51	3.46	5.77E-05
	292.15	24.76	2.43	4.01	2.98	4.97E-05
	292.15	18.57	1.82	3.52	2.51	4.19E-05
	292.15	13.57	1.33	3.02	2.04	3.40E-05
Average	292.15	100.60	9.87	7.52	6.31	1.05E-04
	292.15	85.41	8.38	7.01	5.83	9.72E-05
	292.15	71.96	7.06	6.51	5.36	8.93E-05
	292.15	60.19	5.90	6.01	4.89	8.14E-05
	292.15	49.52	4.86	5.51	4.41	7.35E-05
	292.15	40.15	3.94	5.02	3.94	6.57E-05
	292.15	32.45	3.18	4.51	3.46	5.76E-05
	292.15	24.76	2.43	4.01	2.98	4.97E-05
	292.15	18.57	1.82	3.52	2.51	4.19E-05
	292.15	13.57	1.33	3.02	2.04	3.40E-05
				1.35		
1	293.15	79.21	7.77	9.01	7.73	1.29E-04

	293.15	72.46	7.11	8.51	7.25	1.21E-04
	293.15	63.15	6.19	8.01	6.78	1.13E-04
	293.15	55.54	5.45	7.52	6.31	1.05E-04
	293.15	46.49	4.56	7.01	5.83	9.72E-05
	293.15	39.09	3.83	6.51	5.36	8.93E-05
	293.15	32.45	3.18	6.01	4.89	8.14E-05
	293.15	26.50	2.60	5.52	4.42	7.36E-05
	293.15	21.50	2.11	5.01	3.94	6.56E-05
	293.15	16.65	1.63	4.51	3.46	5.76E-05
2	293.15	72.22	7.08	8.51	7.25	1.21E-04
	293.15	63.02	6.18	8.01	6.79	1.13E-04
	293.15	55.54	5.45	7.52	6.31	1.05E-04
	293.15	46.41	4.55	7.01	5.83	9.72E-05
	293.15	38.98	3.82	6.51	5.36	8.93E-05
	293.15	32.45	3.18	6.01	4.89	8.15E-05
	293.15	26.50	2.60	5.52	4.42	7.36E-05
	293.15	21.36	2.09	5.02	3.94	6.56E-05
	293.15	16.55	1.62	4.51	3.46	5.76E-05
3	293.15	72.06	7.07	8.51	7.25	1.21E-04
	293.15	62.91	6.17	8.01	6.78	1.13E-04
	293.15	55.52	5.44	7.52	6.31	1.05E-04
	293.15	46.33	4.54	7.01	5.83	9.72E-05
	293.15	38.80	3.80	6.51	5.36	8.93E-05
	293.15	32.45	3.18	6.01	4.89	8.15E-05
	293.15	26.42	2.59	5.52	4.42	7.36E-05
	293.15	21.43	2.10	5.02	3.94	6.57E-05
	293.15	16.59	1.63	4.51	3.46	5.77E-05
Average	293.15	72.25	7.08	8.51	7.25	1.21E-04
	293.15	63.03	6.18	8.01	6.78	1.13E-04
	293.15	55.53	5.45	7.52	6.31	1.05E-04
	293.15	46.41	4.55	7.01	5.83	9.72E-05
	293.15	38.96	3.82	6.51	5.36	8.93E-05
	293.15	32.45	3.18	6.01	4.89	8.15E-05
	293.15	26.48	2.60	5.52	4.42	7.36E-05
	293.15	21.43	2.10	5.02	3.94	6.56E-05
	293.15	16.60	1.63	4.51	3.46	5.76E-05
				1.40		
1	293.15	93.03	9.12	9.01	7.74	1.29E-04
	293.15	81.93	8.03	8.51	7.25	1.21E-04
	293.15	71.21	6.98	8.01	6.78	1.13E-04
	293.15	61.56	6.04	7.52	6.31	1.05E-04
	293.15	52.60	5.16	7.01	5.83	9.72E-05
	293.15	44.03	4.32	6.51	5.36	8.93E-05
	293.15	36.60	3.59	6.01	4.89	8.14E-05
	293.15	29.76	2.92	5.52	4.42	7.36E-05
	293.15	23.82	2.34	5.02	3.94	6.57E-05
	293.15	18.57	1.82	4.51	3.46	5.76E-05
2	293.15	92.17	9.04	9.01	7.73	1.29E-04
	293.15	81.82	8.02	8.51	7.25	1.21E-04
	293.15	71.16	6.98	8.01	6.78	1.13E-04
	293.15	61.48	6.03	7.52	6.31	1.05E-04
	293.15	52.60	5.16	7.01	5.83	9.72E-05
	293.15	44.05	4.32	6.51	5.36	8.93E-05
	293.15	36.58	3.59	6.01	4.89	8.14E-05
	293.15	29.75	2.92	5.52	4.42	7.36E-05

	293.15	23.85	2.34	5.02	3.94	6.57E-05
	293.15	18.57	1.82	4.51	3.46	5.76E-05
3	293.15	92.43	9.06	9.01	7.73	1.29E-04
	293.15	81.81	8.02	8.51	7.25	1.21E-04
	293.15	71.13	6.98	8.01	6.78	1.13E-04
	293.15	61.48	6.03	7.52	6.31	1.05E-04
	293.15	52.60	5.16	7.01	5.83	9.72E-05
	293.15	44.03	4.32	6.51	5.36	8.93E-05
	293.15	36.58	3.59	6.01	4.89	8.15E-05
	293.15	29.75	2.92	5.52	4.42	7.36E-05
	293.15	23.82	2.34	5.02	3.94	6.57E-05
	293.15	18.57	1.82	4.51	3.46	5.77E-05
Average	293.15	92.55	9.08	9.01	7.73	1.29E-04
	293.15	81.85	8.03	8.51	7.25	1.21E-04
	293.15	71.17	6.98	8.01	6.78	1.13E-04
	293.15	61.51	6.03	7.52	6.31	1.05E-04
	293.15	52.60	5.16	7.01	5.83	9.72E-05
	293.15	44.04	4.32	6.51	5.36	8.93E-05
	293.15	36.58	3.59	6.01	4.89	8.14E-05
	293.15	29.76	2.92	5.52	4.42	7.36E-05
	293.15	23.83	2.34	5.02	3.94	6.57E-05
	293.15	18.57	1.82	4.51	3.46	5.76E-05
			1.45			
1	293.15	101.51	9.95	11.51	10.10	1.68E-04
	293.15	92.88	9.11	11.01	9.63	1.60E-04
	293.15	84.28	8.26	10.51	9.15	1.52E-04
	293.15	75.91	7.44	10.01	8.68	1.45E-04
	293.15	68.16	6.68	9.51	8.20	1.37E-04
	293.15	61.24	6.01	9.02	7.74	1.29E-04
	293.15	54.17	5.31	8.51	7.25	1.21E-04
	293.15	48.06	4.71	8.01	6.78	1.13E-04
	293.15	42.19	4.14	7.52	6.31	1.05E-04
	293.15	37.34	3.66	7.01	5.84	9.73E-05
	293.15	31.88	3.13	6.51	5.36	8.93E-05
	293.15	27.33	2.68	6.01	4.89	8.15E-05
	293.15	24.27	2.38	5.52	4.42	7.36E-05
	293.15	19.68	1.93	5.02	3.94	6.57E-05
	293.15	16.57	1.62	4.51	3.46	5.77E-05
2	293.15	102.43	10.04	11.51	10.10	1.68E-04
	293.15	93.15	9.13	11.02	9.63	1.61E-04
	293.15	84.40	8.28	10.51	9.15	1.52E-04
	293.15	76.10	7.46	10.01	8.68	1.45E-04
	293.15	68.36	6.70	9.51	8.20	1.37E-04
	293.15	61.23	6.00	9.02	7.74	1.29E-04
	293.15	54.25	5.32	8.51	7.26	1.21E-04
	293.15	48.06	4.71	8.01	6.78	1.13E-04
	293.15	42.30	4.15	7.52	6.31	1.05E-04
	293.15	37.91	3.72	7.01	5.83	9.72E-05
	293.15	31.88	3.13	6.51	5.36	8.93E-05
	293.15	27.51	2.70	6.01	4.89	8.15E-05
	293.15	24.27	2.38	5.52	4.42	7.36E-05
	293.15	19.82	1.94	5.02	3.94	6.57E-05
	293.15	16.65	1.63	4.51	3.46	5.76E-05
3	293.15	102.40	10.04	11.51	10.10	1.68E-04
	293.15	93.18	9.14	11.02	9.63	1.61E-04

	293.15	84.40	8.28	10.51	9.15	1.53E-04
	293.15	76.22	7.47	10.01	8.68	1.45E-04
	293.15	68.41	6.71	9.51	8.20	1.37E-04
	293.15	61.26	6.01	9.02	7.74	1.29E-04
	293.15	54.33	5.33	8.51	7.25	1.21E-04
	293.15	48.06	4.71	8.01	6.78	1.13E-04
	293.15	42.47	4.16	7.52	6.31	1.05E-04
	293.15	37.94	3.72	7.01	5.83	9.72E-05
	293.15	31.88	3.13	6.51	5.36	8.93E-05
	293.15	27.61	2.71	6.01	4.89	8.14E-05
	293.15	24.27	2.38	5.52	4.42	7.36E-05
	293.15	19.88	1.95	5.02	3.94	6.57E-05
	293.15	16.65	1.63	4.51	3.46	5.77E-05
Average	293.15	102.11	10.01	11.51	10.10	1.68E-04
	293.15	93.07	9.13	11.01	9.63	1.60E-04
	293.15	84.36	8.27	10.51	9.15	1.52E-04
	293.15	76.08	7.46	10.01	8.68	1.45E-04
	293.15	68.31	6.70	9.51	8.20	1.37E-04
	293.15	61.24	6.01	9.02	7.74	1.29E-04
	293.15	54.25	5.32	8.51	7.26	1.21E-04
	293.15	48.06	4.71	8.01	6.78	1.13E-04
	293.15	42.32	4.15	7.52	6.31	1.05E-04
	293.15	37.73	3.70	7.01	5.84	9.73E-05
	293.15	31.88	3.13	6.51	5.36	8.93E-05
	293.15	27.48	2.70	6.01	4.89	8.15E-05
	293.15	19.79	1.94	5.02	3.94	6.57E-05
	293.15	16.62	1.63	4.51	3.46	5.77E-05
1.60						
1	292.15	113.40	11.12	12.01	10.57	1.76E-04
	292.15	106.88	10.48	11.51	10.10	1.68E-04
	292.15	97.10	9.52	11.02	9.63	1.61E-04
	292.15	87.45	8.58	10.51	9.15	1.52E-04
	292.15	78.70	7.72	10.01	8.68	1.45E-04
	292.15	70.14	6.88	9.51	8.20	1.37E-04
	292.15	62.20	6.10	9.02	7.74	1.29E-04
	292.15	55.54	5.45	8.51	7.26	1.21E-04
	292.15	47.92	4.70	8.01	6.79	1.13E-04
	292.15	42.03	4.12	7.52	6.31	1.05E-04
	292.15	35.74	3.50	7.01	5.83	9.72E-05
	292.15	30.19	2.96	6.51	5.36	8.93E-05
	292.15	25.31	2.48	6.01	4.89	8.15E-05
	292.15	20.95	2.05	5.52	4.42	7.36E-05
	292.15	17.24	1.69	5.01	3.94	6.56E-05
2	292.15	113.00	11.08	12.01	10.57	1.76E-04
	292.15	106.04	10.40	11.51	10.10	1.68E-04
	292.15	96.23	9.44	11.01	9.63	1.60E-04
	292.15	86.68	8.50	10.51	9.15	1.53E-04
	292.15	77.96	7.64	10.01	8.68	1.45E-04
	292.15	69.81	6.85	9.51	8.21	1.37E-04
	292.15	62.06	6.09	9.01	7.73	1.29E-04
	292.15	55.54	5.45	8.51	7.25	1.21E-04
	292.15	47.68	4.68	8.01	6.78	1.13E-04
	292.15	41.47	4.07	7.52	6.31	1.05E-04
	292.15	35.54	3.49	7.01	5.83	9.72E-05
	292.15	30.10	2.95	6.51	5.36	8.93E-05

	292.15	25.22	2.47	6.01	4.89	8.15E-05
	292.15	20.94	2.05	5.52	4.42	7.36E-05
	292.15	17.06	1.67	5.01	3.94	6.56E-05
3	292.15	112.88	11.07	12.02	10.58	1.76E-04
	292.15	105.91	10.39	11.51	10.10	1.68E-04
	292.15	96.02	9.42	11.02	9.63	1.61E-04
	292.15	86.60	8.49	10.51	9.15	1.52E-04
	292.15	77.90	7.64	10.01	8.68	1.45E-04
	292.15	69.73	6.84	9.51	8.20	1.37E-04
	292.15	61.94	6.07	9.02	7.74	1.29E-04
	292.15	55.54	5.45	8.51	7.26	1.21E-04
	292.15	47.70	4.68	8.01	6.78	1.13E-04
	292.15	41.41	4.06	7.52	6.31	1.05E-04
	292.15	35.54	3.49	7.01	5.83	9.72E-05
	292.15	30.07	2.95	6.51	5.36	8.93E-05
	292.15	25.20	2.47	6.01	4.89	8.15E-05
	292.15	20.94	2.05	5.52	4.42	7.36E-05
	292.15	17.16	1.68	5.01	3.94	6.56E-05
Average	292.15	106.28	10.42	11.51	10.10	1.68E-04
	292.15	96.45	9.46	11.01	9.63	1.60E-04
	292.15	86.91	8.52	10.51	9.15	1.52E-04
	292.15	78.18	7.67	10.01	8.68	1.45E-04
	292.15	69.90	6.85	9.51	8.20	1.37E-04
	292.15	62.07	6.09	9.02	7.74	1.29E-04
	292.15	55.54	5.45	8.51	7.26	1.21E-04
	292.15	47.77	4.68	8.01	6.78	1.13E-04
	292.15	41.64	4.08	7.52	6.31	1.05E-04
	292.15	35.61	3.49	7.01	5.83	9.72E-05
	292.15	30.12	2.95	6.51	5.36	8.93E-05
	292.15	25.24	2.48	6.01	4.89	8.15E-05
	292.15	20.94	2.05	5.52	4.42	7.36E-05
	292.15	17.15	1.68	5.01	3.94	6.56E-05
	292.15	13.57	1.33	4.51	3.46	5.76E-05
				1.80		
1	293.15	93.45	9.16	19.51	17.65	2.94E-04
	293.15	83.59	8.20	18.50	16.71	2.78E-04
	293.15	74.15	7.27	17.51	15.77	2.63E-04
	293.15	65.29	6.40	16.50	14.82	2.47E-04
	293.15	56.80	5.57	15.51	13.89	2.31E-04
	293.15	48.97	4.80	14.51	12.94	2.16E-04
	293.15	42.28	4.15	13.52	12.00	2.00E-04
	293.15	34.99	3.43	12.51	11.05	1.84E-04
	293.15	28.80	2.82	11.51	10.11	1.68E-04
	293.15	23.25	2.28	10.51	9.16	1.53E-04
	293.15	18.57	1.82	9.51	8.21	1.37E-04
	293.15	13.81	1.35	8.51	7.26	1.21E-04
2	293.15	83.59	8.20	18.51	16.71	2.79E-04
	293.15	74.34	7.29	17.52	15.77	2.63E-04
	293.15	65.55	6.43	16.51	14.83	2.47E-04
	293.15	57.17	5.61	15.51	13.89	2.31E-04
	293.15	49.27	4.83	14.51	12.94	2.16E-04
	293.15	42.34	4.15	13.51	12.00	2.00E-04
	293.15	35.30	3.46	12.51	11.05	1.84E-04
	293.15	29.17	2.86	11.51	10.11	1.68E-04
	293.15	23.51	2.31	10.51	9.16	1.53E-04

	293.15	18.57	1.82	9.51	8.21	1.37E-04
	293.15	14.11	1.38	8.51	7.26	1.21E-04
3	293.15	82.99	8.14	19.48	17.62	2.94E-04
	293.15	83.09	8.15	18.50	16.70	2.78E-04
	293.15	74.10	7.27	17.51	15.77	2.63E-04
	293.15	65.22	6.40	16.50	14.82	2.47E-04
	293.15	56.82	5.57	15.51	13.88	2.31E-04
	293.15	49.03	4.81	14.51	12.94	2.16E-04
	293.15	42.34	4.15	13.51	12.00	2.00E-04
	293.15	35.02	3.43	12.51	11.05	1.84E-04
	293.15	28.90	2.83	11.51	10.10	1.68E-04
	293.15	23.33	2.29	10.51	9.16	1.53E-04
	293.15	18.57	1.82	9.51	8.21	1.37E-04
	293.15	13.89	1.36	8.51	7.26	1.21E-04
Average	293.15	88.22	8.65	19.49	17.64	2.94E-04
	293.15	83.42	8.18	18.51	16.71	2.78E-04
	293.15	74.19	7.28	17.51	15.77	2.63E-04
	293.15	65.35	6.41	16.51	14.82	2.47E-04
	293.15	56.93	5.58	15.51	13.89	2.31E-04
	293.15	49.09	4.81	14.51	12.94	2.16E-04
	293.15	42.32	4.15	13.51	12.00	2.00E-04
	293.15	35.10	3.44	12.51	11.05	1.84E-04
	293.15	28.96	2.84	11.51	10.11	1.68E-04
	293.15	23.36	2.29	10.51	9.16	1.53E-04
	293.15	18.57	1.82	9.51	8.21	1.37E-04
	293.15	13.94	1.37	8.51	7.26	1.21E-04
			2.06			
1	293.15	101.79	9.98	19.52	17.65	2.94E-04
	293.15	97.11	9.52	19.01	17.18	2.86E-04
	293.15	92.01	9.02	18.51	16.71	2.78E-04
	293.15	86.92	8.52	18.01	16.24	2.71E-04
	293.15	82.03	8.04	17.51	15.77	2.63E-04
	293.15	77.24	7.58	17.01	15.30	2.55E-04
	293.15	72.43	7.10	16.51	14.82	2.47E-04
	293.15	67.75	6.64	16.01	14.35	2.39E-04
	293.15	63.63	6.24	15.51	13.89	2.31E-04
	293.15	59.14	5.80	15.01	13.42	2.24E-04
	293.15	55.56	5.44	14.51	12.94	2.16E-04
	293.15	50.87	4.99	14.01	12.46	2.08E-04
	293.15	47.12	4.62	13.52	12.00	2.00E-04
	293.15	43.50	4.27	13.01	11.52	1.92E-04
	293.15	39.88	3.91	12.51	11.05	1.84E-04
	293.15	36.58	3.59	12.02	10.58	1.76E-04
2	293.15	101.94	10.00	19.51	17.65	2.94E-04
	293.15	96.90	9.50	19.01	17.18	2.86E-04
	293.15	91.60	8.98	18.52	16.72	2.79E-04
	293.15	86.58	8.49	18.01	16.24	2.71E-04
	293.15	81.95	8.04	17.52	15.78	2.63E-04
	293.15	76.91	7.54	17.02	15.31	2.55E-04
	293.15	72.25	7.09	16.51	14.83	2.47E-04
	293.15	67.62	6.63	16.01	14.35	2.39E-04
	293.15	63.34	6.21	15.51	13.89	2.31E-04
	293.15	59.07	5.79	15.02	13.42	2.24E-04
	293.15	55.57	5.45	14.51	12.94	2.16E-04
	293.15	50.87	4.99	14.01	12.47	2.08E-04

	293.15	47.10	4.62	13.52	12.00	2.00E-04
	293.15	43.48	4.26	13.01	11.52	1.92E-04
	293.15	39.91	3.91	12.51	11.05	1.84E-04
3	293.15	102.02	10.01	19.52	17.66	2.94E-04
	293.15	96.94	9.51	19.01	17.18	2.86E-04
	293.15	91.69	8.99	18.51	16.71	2.79E-04
	293.15	86.58	8.49	18.01	16.24	2.71E-04
	293.15	81.95	8.04	17.52	15.78	2.63E-04
	293.15	76.93	7.54	17.01	15.30	2.55E-04
	293.15	72.19	7.08	16.51	14.83	2.47E-04
	293.15	67.65	6.63	16.01	14.36	2.39E-04
	293.15	63.36	6.21	15.52	13.89	2.31E-04
	293.15	59.10	5.80	15.02	13.42	2.24E-04
	293.15	55.54	5.45	14.51	12.94	2.16E-04
	293.15	50.85	4.99	14.01	12.47	2.08E-04
	293.15	47.16	4.63	13.51	12.00	2.00E-04
	293.15	43.47	4.26	13.02	11.53	1.92E-04
	293.15	39.91	3.91	12.52	11.05	1.84E-04
Average	293.15	96.98	9.51	19.01	17.18	2.86E-04
	293.15	91.77	9.00	18.51	16.71	2.79E-04
	293.15	86.69	8.50	18.01	16.24	2.71E-04
	293.15	81.98	8.04	17.52	15.78	2.63E-04
	293.15	77.02	7.55	17.02	15.30	2.55E-04
	293.15	72.29	7.09	16.51	14.83	2.47E-04
	293.15	67.68	6.64	16.01	14.35	2.39E-04
	293.15	63.44	6.22	15.51	13.89	2.31E-04
	293.15	59.11	5.80	15.02	13.42	2.24E-04
	293.15	55.55	5.45	14.51	12.94	2.16E-04
	293.15	50.87	4.99	14.01	12.47	2.08E-04
	293.15	47.13	4.62	13.52	12.00	2.00E-04
	293.15	43.48	4.26	13.01	11.53	1.92E-04
	293.15	39.90	3.91	12.51	11.05	1.84E-04
	293.15	36.58	3.59	12.02	10.58	1.76E-04
				3.00		
1	293.15	67.82	6.65	29.98	27.45	4.57E-04
	293.15	60.14	5.90	28.01	25.61	4.27E-04
	293.15	53.31	5.23	26.01	23.74	3.96E-04
	293.15	45.30	4.44	24.01	21.87	3.65E-04
	293.15	38.00	3.73	22.02	20.00	3.33E-04
	293.15	31.83	3.12	20.01	18.11	3.02E-04
	293.15	24.76	2.43	18.01	16.23	2.71E-04
	293.15	19.04	1.87	16.02	14.35	2.39E-04
	293.15	14.06	1.38	14.01	12.46	2.08E-04
2	293.15	69.94	6.86	30.00	27.47	4.58E-04
	293.15	61.27	6.01	27.99	25.60	4.27E-04
	293.15	53.00	5.20	26.01	23.75	3.96E-04
	293.15	45.02	4.41	24.02	21.88	3.65E-04
	293.15	37.85	3.71	22.02	20.00	3.33E-04
	293.15	31.42	3.08	20.02	18.12	3.02E-04
	293.15	24.76	2.43	18.01	16.23	2.71E-04
	293.15	18.97	1.86	16.02	14.36	2.39E-04
	293.15	13.97	1.37	14.01	12.46	2.08E-04
3	293.15	69.89	6.85	30.02	27.48	4.58E-04
	293.15	61.25	6.01	28.02	25.62	4.27E-04
	293.15	52.98	5.20	26.02	23.75	3.96E-04

	293.15	45.03	4.42	24.00	21.86	3.64E-04
	293.15	37.81	3.71	22.01	20.00	3.33E-04
	293.15	31.45	3.08	20.01	18.12	3.02E-04
	293.15	24.76	2.43	18.02	16.24	2.71E-04
	293.15	19.02	1.87	16.01	14.35	2.39E-04
	293.15	13.97	1.37	14.01	12.46	2.08E-04
Average	293.15	69.22	6.79	30.00	27.47	4.58E-04
	293.15	60.88	5.97	28.01	25.61	4.27E-04
	293.15	53.10	5.21	26.02	23.75	3.96E-04
	293.15	45.12	4.42	24.01	21.87	3.64E-04
	293.15	37.89	3.72	22.02	20.00	3.33E-04
	293.15	31.57	3.10	20.01	18.12	3.02E-04
	293.15	24.76	2.43	18.01	16.23	2.71E-04
	293.15	19.01	1.86	16.02	14.35	2.39E-04
	293.15	14.00	1.37	14.01	12.46	2.08E-04
				3.00-L		
1	293.15	61.09	5.99	28.01	25.61	4.27E-04
	293.15	52.89	5.19	26.01	23.74	3.96E-04
	293.15	44.78	4.39	24.00	21.86	3.64E-04
	293.15	37.69	3.70	22.01	19.99	3.33E-04
	293.15	30.99	3.04	20.01	18.12	3.02E-04
	293.15	24.76	2.43	18.02	16.24	2.71E-04
	293.15	18.81	1.84	16.01	14.35	2.39E-04
2	293.15	69.69	6.83	30.05	27.51	4.59E-04
	293.15	61.05	5.99	28.02	25.62	4.27E-04
	293.15	52.70	5.17	26.03	23.76	3.96E-04
	293.15	44.75	4.39	24.01	21.87	3.64E-04
	293.15	37.55	3.68	22.02	20.00	3.33E-04
	293.15	31.02	3.04	20.01	18.11	3.02E-04
	293.15	24.76	2.43	18.01	16.23	2.71E-04
	293.15	18.75	1.84	16.02	14.36	2.39E-04
3	293.15	69.54	6.82	30.01	27.48	4.58E-04
	293.15	60.93	5.97	28.00	25.60	4.27E-04
	293.15	52.62	5.16	25.99	23.73	3.95E-04
	293.15	44.75	4.39	24.01	21.86	3.64E-04
	293.15	37.53	3.68	22.00	19.99	3.33E-04
	293.15	30.89	3.03	20.01	18.12	3.02E-04
	293.15	24.72	2.42	18.01	16.24	2.71E-04
	293.15	18.75	1.84	16.01	14.35	2.39E-04
Average	293.15	69.62	6.83	30.03	27.50	4.58E-04
	293.15	61.02	5.98	28.01	25.61	4.27E-04
	293.15	52.73	5.17	26.01	23.74	3.96E-04
	293.15	44.76	4.39	24.01	21.86	3.64E-04
	293.15	37.59	3.69	22.01	19.99	3.33E-04
	293.15	30.97	3.04	20.01	18.12	3.02E-04
	293.15	24.74	2.43	18.01	16.24	2.71E-04
	293.15	18.77	1.84	16.01	14.35	2.39E-04

Table F.13: Orifices calibration candidate equations.

13-1: Mass flow rate in kg per second versus square rot of pressure drop.						
		a	**b**	**c**	**d**	**R^2**
0.70	**L**	4.36E-07				0.99622
	L	4.62E-07	-1.96E-06			0.99967
	Q	3.67E-10	4.11E-07	-3.40E-07		0.99985
	C	-7.79E-12	1.99E-09	3.05E-07	1.88E-06	0.99988
0.94	**L**	5.28E-07				0.99945
	L	5.37E-07	-7.30E-07			0.99980
	Q	-4.37E-10	5.99E-07	-2.74E-06		0.99998
	C	2.22E-12	-9.09E-10	6.31E-07	-3.43E-06	0.99998
1.00	**L**	8.52E-07				0.99220
	L	9.31E-07	-5.93E-06			0.99992
	Q	-2.31E-11	9.34E-07	-6.03E-06		0.99992
	C	-6.29E-12	1.29E-09	8.48E-07	-4.25E-06	0.99993
1.08	**L**	1.05E-06				0.99743
	L	1.10E-06	-4.08E-06			0.99973
	Q	-1.14E-09	1.27E-06	-1.04E-05		0.99993
	C	-4.60E-11	9.37E-09	4.89E-07	8.42E-06	0.99998
1.18	**L**	1.16E-06				0.99598
	L	1.23E-06	-5.73E-06			0.99940
	Q	1.24E-09	1.04E-06	1.10E-06		0.99966
	C	3.96E-11	-7.86E-09	1.72E-06	-1.48E-05	0.99973
1.30	**L**	1.35E-06				0.99262
	L	1.46E-06	-8.24E-06			0.99916
	Q	-2.29E-09	1.77E-06	-1.78E-05		0.99993
	C	-1.49E-11	7.49E-10	1.57E-06	-1.39E-05	0.99994
1.35	**L**	1.85E-06				0.99963
	L	1.85E-06	1.58E-07			0.99963
	Q	-1.42E-09	2.02E-06	-5.07E-06		0.99972
	C	1.15E-10	-2.29E-08	3.32E-06	-3.03E-05	0.99980
1.40	**L**	1.74E-06				0.99987
	L	1.73E-06	7.84E-07			0.99992
	Q	-6.64E-10	1.82E-06	-2.18E-06		0.99995
	C	5.02E-11	-1.10E-08	2.51E-06	-1.69E-05	0.99998
1.45	**L**	2.12E-06				0.98736
	L	2.37E-06	-1.88E-05			0.99908
	Q	-3.93E-09	2.92E-06	-3.69E-05		0.99989
	C	3.33E-11	-1.09E-08	3.39E-06	-4.68E-05	0.99990
1.60	**L**	2.12E-06				0.99929
	L	2.16E-06	-3.39E-06			0.99977
	Q	-1.45E-09	2.36E-06	-9.72E-06		0.99992
	C	3.49E-11	-8.71E-09	2.84E-06	-1.96E-05	0.99994
1.80	**L**	4.01E-06				0.99682
	L	3.86E-06	1.06E-05			0.99840
	Q	6.23E-09	3.04E-06	3.54E-05		0.99902
	C	2.89E-10	-5.03E-08	6.57E-06	-3.42E-05	0.99931
2.06	**L**	3.77E-06				0.99988
	L	3.75E-06	1.52E-06			0.99990
	Q	1.78E-09	3.47E-06	1.23E-05		0.99993
	C	1.36E-12	1.46E-09	3.50E-06	1.17E-05	0.99993
3.00	**L**	7.08E-06				0.99889

	L	7.08E-06	-5.11E-09			0.99889
	Q	1.77E-08	4.97E-06	5.94E-05		0.99991
	C	6.57E-11	5.87E-09	5.64E-06	4.69E-05	0.99991
3.00-L	**L**	7.09E-06				0.99944
	L	7.12E-06	-1.77E-06			0.99946
	Q	1.37E-08	5.39E-06	5.03E-05		0.99995
	C	-2.43E-10	5.95E-08	2.59E-06	1.06E-04	0.99996
13-2: Mass flow rate in kg per second versus square rot of pressure drop multiplied by air density.						
		a	**b**	**c**	**d**	**R^2**
0.70	**L**	1.22E-05				0.99942
	L	1.25E-05	-6.54E-07			0.99984
	Q	-4.41E-08	1.27E-05	-9.02E-07		0.99984
	C	-1.91E-07	1.38E-06	9.36E-06	1.56E-06	0.99988
0.94	**L**	1.48E-05				0.99856
	L	1.45E-05	8.89E-07			0.99912
	Q	-6.78E-07	1.79E-05	-3.08E-06		0.99998
	C	3.02E-08	-9.07E-07	1.84E-05	-3.50E-06	0.99999
1.00	**L**	2.38E-05				0.99710
	L	2.50E-05	-3.26E-06			0.99962
	Q	-6.35E-07	2.82E-05	-6.86E-06		0.99992
	C	-1.59E-07	5.55E-07	2.54E-05	-4.79E-06	0.99993
1.08	**L**	2.92E-05				0.99915
	L	2.91E-05	1.06E-07			0.99916
	Q	-1.58E-06	3.78E-05	-1.12E-05		0.99993
	C	-8.66E-07	5.53E-06	1.89E-05	5.13E-06	0.99998
1.18	**L**	3.24E-05				0.99955
	L	3.27E-05	-1.04E-06			0.99968
	Q	2.35E-08	3.26E-05	-8.75E-07		0.99968
	C	6.75E-07	-5.56E-06	4.74E-05	-1.34E-05	0.99973
1.30	**L**	3.76E-05				0.99605
	L	3.93E-05	-4.34E-06			0.99800
	Q	-2.61E-06	5.20E-05	-1.83E-05		0.99993
	C	-2.84E-07	-5.34E-07	4.72E-05	-1.49E-05	0.99994
1.35	**L**	5.21E-05				0.99804
	L	5.03E-05	4.11E-06			0.99934
	Q	-2.19E-06	6.00E-05	-6.01E-06		0.99972
	C	2.32E-06	-1.76E-05	9.29E-05	-2.86E-05	0.99981
1.40	**L**	4.88E-05				0.99725
	L	4.66E-05	5.70E-06			0.99959
	Q	-1.61E-06	5.46E-05	-3.48E-06		0.99995
	C	9.20E-07	-8.43E-06	7.08E-05	-1.57E-05	0.99998
1.45	**L**	5.93E-05				0.99310
	L	6.36E-05	-1.16E-05			0.99795
	Q	-4.40E-06	8.58E-05	-3.75E-05		0.99988
	C	6.66E-07	-9.42E-06	9.78E-05	-4.67E-05	0.99990
1.60	**L**	5.90E-05				0.99879
	L	5.80E-05	2.71E-06			0.99912
	Q	-2.45E-06	7.02E-05	-1.10E-05		0.99992
	C	6.02E-07	-6.96E-06	8.08E-05	-1.89E-05	0.99994
1.80	**L**	1.12E-04				0.99289

	L	1.05E-04	1.99E-05			0.99892
	Q	2.18E-06	9.44E-05	3.10E-05		0.99906
	C	5.53E-06	-3.65E-05	1.80E-04	-2.93E-05	0.99932
2.06	L	1.05E-04				0.99615
	L	9.93E-05	1.73E-05			0.99989
	Q	-1.42E-06	1.07E-04	6.34E-06		0.99993
	C	-1.95E-07	2.32E-07	1.03E-04	1.05E-05	0.99993
3.00	L	2.00E-04				0.99848
	L	1.94E-04	1.33E-05			0.99945
	Q	8.93E-06	1.56E-04	5.10E-05		0.99991
	C	2.75E-07	7.18E-06	1.60E-04	4.86E-05	0.99991
3.00-L	L	2.00E-04				0.99881
	L	1.94E-04	1.39E-05			0.99979
	Q	5.70E-06	1.68E-04	4.10E-05		0.99994
	C	-5.60E-06	4.32E-05	8.73E-05	9.80E-05	0.99996
13-3: Volumetric rate (SCMS) versus square rot of pressure drop divided by air density.						
		a	**b**	**c**	**d**	**R^2**
0.70	L	1.21E-05				0.98955
	L	1.33E-05	-2.62E-06			0.99894
	Q	8.77E-07	9.94E-06	4.33E-07		0.99987
	C	-1.74E-07	1.89E-06	8.07E-06	1.53E-06	0.99988
0.94	L	1.46E-05				0.99628
	L	1.55E-05	-1.93E-06			0.99997
	Q	9.84E-08	1.52E-05	-1.57E-06		0.99998
	C	1.84E-07	-9.94E-07	1.72E-05	-2.82E-06	0.99999
1.00	L	2.37E-05				0.98395
	L	2.70E-05	-6.85E-06			0.99963
	Q	9.55E-07	2.33E-05	-3.55E-06		0.99993
	C	-6.06E-08	1.31E-06	2.26E-05	-3.17E-06	0.99993
1.08	L	2.91E-05				0.99051
	L	3.22E-05	-6.77E-06			0.99994
	Q	3.82E-08	3.20E-05	-6.61E-06		0.99994
	C	-1.75E-06	1.12E-05	8.86E-06	9.05E-06	0.99998
1.18	L	3.25E-05				0.98737
	L	3.62E-05	-8.47E-06			0.99853
	Q	2.81E-06	2.43E-05	3.56E-06		0.99963
	C	2.00E-06	-9.94E-06	5.05E-05	-1.38E-05	0.99972
1.30	L	3.75E-05				0.98607
	L	4.22E-05	-9.66E-06			0.99982
	Q	-9.68E-07	4.59E-05	-1.28E-05		0.99993
	C	-4.43E-07	1.54E-06	4.14E-05	-1.03E-05	0.99994
1.35	L	5.10E-05				0.99859
	L	5.27E-05	-3.16E-06			0.99971
	Q	1.81E-07	5.21E-05	-2.63E-06		0.99971
	C	4.65E-06	-2.42E-05	9.35E-05	-2.54E-05	0.99980
1.40	L	4.83E-05				0.99860
	L	5.00E-05	-3.53E-06			0.99986
	Q	1.06E-06	4.59E-05	2.12E-07		0.99993
	C	2.34E-06	-1.25E-05	7.12E-05	-1.49E-05	0.99998
1.45	L	5.89E-05				0.97824
	L	6.87E-05	-2.06E-05			0.99974

	Q	-1.77E-06	7.57E-05	-2.70E-05		0.99988
	C	1.59E-06	-1.11E-05	9.31E-05	-3.74E-05	0.99990
1.60	**L**	5.90E-05				0.99607
	L	6.27E-05	-7.74E-06			0.99987
	Q	6.70E-07	6.01E-05	-5.46E-06		0.99990
	C	1.83E-06	-9.89E-06	7.95E-05	-1.66E-05	0.99994
1.80	**L**	1.11E-04				0.99745
	L	1.11E-04	4.15E-07			0.99746
	Q	1.02E-05	7.32E-05	3.27E-05		0.99895
	C	1.22E-05	-5.65E-05	1.90E-04	-3.23E-05	0.99928
2.06	**L**	1.05E-04				0.99706
	L	1.11E-04	-1.26E-05			0.99966
	Q	6.57E-06	8.18E-05	1.85E-05		0.99992
	C	1.19E-06	-1.30E-06	9.89E-05	6.34E-06	0.99993
3.00	**L**	1.95E-04				0.99711
	L	2.01E-04	-1.10E-05			0.99807
	Q	2.46E-05	1.18E-04	5.50E-05		0.99991
	C	5.20E-06	-1.68E-06	1.61E-04	3.27E-05	0.99991
3.00-L	**L**	1.96E-04				0.99740
	L	2.03E-04	-1.44E-05			0.99891
	Q	2.11E-05	1.28E-04	4.92E-05		0.99995
	C	-7.30E-06	5.98E-05	6.17E-05	8.67E-05	0.99996

Table F.14: Reproducibility.

Test	**T (K)**	**P (cm of Water)**	**P (kPa)**	**Q (LPM)**	**ρ (kg/m³)**	$\sqrt{\frac{\Delta P}{\rho}}$ **(kPa*m³/kg)$^{0.5}$**	**Q (SCMS)**
0.94-1	293.15	100.49	9.86	3.15	1.32	2.73	5.25E-05
	293.15	83.50	8.19	2.85	1.30	2.51	4.76E-05
	293.15	67.88	6.66	2.56	1.28	2.28	4.26E-05
	293.15	54.04	5.30	2.26	1.26	2.05	3.77E-05
	293.15	41.78	4.10	1.97	1.25	1.81	3.28E-05
	293.15	31.03	3.04	1.68	1.24	1.57	2.79E-05
	293.15	21.93	2.15	1.38	1.23	1.32	2.31E-05
	293.15	14.48	1.42	1.09	1.22	1.08	1.82E-05
	293.15	14.49	1.42	1.09	1.22	1.08	1.82E-05
	293.15	8.64	0.85	0.80	1.21	0.84	1.34E-05
0.94-2	290.15	83.50	8.19	3.15	1.31	2.50	5.25E-05
	290.15	69.06	6.77	2.85	1.29	2.29	4.76E-05
	290.15	55.89	5.48	2.56	1.28	2.07	4.26E-05
	290.15	44.18	4.33	2.26	1.27	1.85	3.77E-05
	290.15	34.06	3.34	1.97	1.25	1.63	3.28E-05
	290.15	25.64	2.51	1.68	1.24	1.42	2.79E-05
	290.15	18.38	1.80	1.38	1.23	1.21	2.31E-05
	290.15	12.27	1.20	1.09	1.23	0.99	1.82E-05
	290.15	12.27	1.20	1.09	1.23	0.99	1.82E-05
	290.15	7.48	0.73	0.80	1.22	0.77	1.34E-05
0.94-3	290.15	99.21	9.73	3.15	1.33	2.70	5.25E-05

	290.15	82.02	8.04	2.85	1.31	2.48	4.76E-05
	290.15	66.67	6.54	2.56	1.29	2.25	4.26E-05
	290.15	52.89	5.19	2.26	1.28	2.02	3.77E-05
	290.15	40.67	3.99	1.97	1.26	1.78	3.28E-05
	290.15	29.90	2.93	1.68	1.25	1.53	2.79E-05
	290.15	21.00	2.06	1.38	1.24	1.29	2.31E-05
	290.15	13.86	1.36	1.09	1.23	1.05	1.82E-05
0.94-4	290.15	71.58	7.02	3.15	1.30	2.33	5.25E-05
	290.15	59.79	5.86	2.85	1.28	2.14	4.76E-05
	290.15	49.08	4.81	2.56	1.27	1.95	4.26E-05
	290.15	39.39	3.86	2.26	1.26	1.75	3.77E-05
	290.15	30.75	3.02	1.97	1.25	1.55	3.28E-05
	290.15	23.11	2.27	1.68	1.24	1.35	2.79E-05
	290.15	16.63	1.63	1.38	1.23	1.15	2.31E-05
0.94-5	290.15	84.46	8.28	3.15	1.31	2.51	5.25E-05
	290.15	70.21	6.89	2.85	1.30	2.31	4.76E-05
	290.15	57.25	5.61	2.56	1.28	2.09	4.26E-05
	290.15	45.74	4.49	2.26	1.27	1.88	3.77E-05
	290.15	35.45	3.48	1.97	1.25	1.66	3.28E-05
	290.15	26.47	2.60	1.68	1.24	1.44	2.79E-05
	290.15	18.76	1.84	1.38	1.24	1.22	2.31E-05
	290.15	12.27	1.20	1.09	1.23	0.99	1.82E-05
	290.15	12.27	1.20	1.09	1.23	0.99	1.82E-05
0.94-6	290.15	110.05	10.79	3.15	1.34	2.84	5.25E-05
	290.15	91.06	8.93	2.85	1.32	2.60	4.76E-05
	290.15	73.83	7.24	2.56	1.30	2.36	4.26E-05
	290.15	58.44	5.73	2.26	1.28	2.11	3.77E-05
	290.15	44.80	4.39	1.97	1.27	1.86	3.28E-05
	290.15	32.88	3.22	1.68	1.25	1.60	2.79E-05
	290.15	22.77	2.23	1.38	1.24	1.34	2.31E-05
	290.15	14.43	1.42	1.09	1.23	1.07	1.82E-05
0.94-7	290.15	93.58	9.18	3.15	1.32	2.63	5.25E-05
	290.15	77.81	7.63	2.85	1.30	2.42	4.76E-05
	290.15	63.52	6.23	2.56	1.29	2.20	4.26E-05
	290.15	50.43	4.95	2.26	1.27	1.97	3.77E-05
	290.15	38.91	3.82	1.97	1.26	1.74	3.28E-05
	290.15	28.87	2.83	1.68	1.25	1.51	2.79E-05
	290.15	20.28	1.99	1.38	1.24	1.27	2.31E-05
	290.15	13.19	1.29	1.09	1.23	1.03	1.82E-05
0.94-8	290.15	101.21	9.93	3.15	1.33	2.73	5.25E-05
	290.15	84.14	8.25	2.85	1.31	2.51	4.76E-05
	290.15	68.43	6.71	2.56	1.29	2.28	4.26E-05
	290.15	54.35	5.33	2.26	1.28	2.04	3.77E-05
	290.15	41.70	4.09	1.97	1.26	1.80	3.28E-05
	290.15	30.74	3.01	1.68	1.25	1.55	2.79E-05
	290.15	21.36	2.10	1.38	1.24	1.30	2.31E-05
	290.15	13.70	1.34	1.09	1.23	1.05	1.82E-05
	290.15	13.70	1.34	1.09	1.23	1.05	1.82E-05

0.94-X	290.15	64.63	6.34	2.75	1.29	2.22	4.59E-05
	290.15	56.02	5.49	2.56	1.28	2.07	4.26E-05
	290.15	48.36	4.74	2.36	1.27	1.93	3.94E-05
	290.15	41.01	4.02	2.16	1.26	1.79	3.61E-05
	290.15	28.38	2.78	1.77	1.25	1.49	2.95E-05
	290.15	14.18	1.39	1.19	1.23	1.06	1.98E-05
	290.15	10.71	1.05	0.99	1.23	0.93	1.66E-05
0.94-Y	290.15	70.50	6.91	2.75	1.30	2.31	4.58E-05
	290.15	61.25	6.01	2.55	1.29	2.16	4.25E-05
	290.15	52.66	5.16	2.36	1.28	2.01	3.93E-05
	290.15	44.85	4.40	2.16	1.27	1.86	3.60E-05
	290.15	31.24	3.06	1.77	1.25	1.57	2.95E-05
	290.15	16.01	1.57	1.19	1.23	1.13	1.98E-05
	290.15	12.02	1.18	0.99	1.23	0.98	1.65E-05
1.30							
1.30-1	292.15	91.60	8.98	6.78	1.31	2.62	1.13E-04
	292.15	79.37	7.78	6.31	1.30	2.45	1.05E-04
	292.15	67.93	6.66	5.83	1.28	2.28	9.72E-05
	292.15	47.79	4.6	4.89	1.26	1.93	8.15E-05
	292.15	31.47	3.09	3.94	1.24	1.58	6.56E-05
	292.15	18.89	1.85	2.99	1.23	1.23	4.98E-05
1.30-2	290.15	88.00	8.63	6.79	1.32	2.56	1.13E-04
	290.15	76.32	7.48	6.31	1.30	2.40	1.05E-04
	290.15	65.39	6.41	5.83	1.29	2.23	9.72E-05
	290.15	46.03	4.51	4.89	1.27	1.89	8.15E-05
	290.15	30.26	2.97	3.94	1.25	1.54	6.57E-05
	290.15	18.22	1.79	2.99	1.23	1.20	4.98E-05
1.30-3	290.15	94.96	9.31	6.78	1.32	2.65	1.13E-04
	290.15	82.38	8.08	6.31	1.31	2.48	1.05E-04
	290.15	59.96	5.88	5.36	1.28	2.14	8.93E-05
	290.15	50.27	4.93	4.89	1.27	1.97	8.15E-05
	290.15	33.50	3.29	3.94	1.25	1.62	6.57E-05
	290.15	20.36	2.00	2.99	1.24	1.27	4.98E-05
	290.15	15.13	1.48	2.51	1.23	1.10	4.19E-05
	290.15	15.13	1.48	2.51	1.23	1.10	4.19E-05
	290.15	10.73	1.05	2.13	1.23	0.93	3.55E-05
1.30-4	290.15	98.42	9.65	6.79	1.33	2.70	1.13E-04
	290.15	85.44	8.38	6.31	1.31	2.53	1.05E-04
	290.15	62.22	6.10	5.36	1.29	2.18	8.94E-05
	290.15	52.17	5.12	4.89	1.27	2.00	8.15E-05
	290.15	35.02	3.43	3.94	1.25	1.65	6.56E-05
	290.15	21.39	2.10	2.99	1.24	1.30	4.98E-05
	290.15	16.00	1.57	2.51	1.23	1.13	4.19E-05
	290.15	16.00	1.57	2.51	1.23	1.13	4.19E-05
1.30-5	290.15	84.46	8.28	2.21	1.31	2.51	3.68E-05
	290.15	70.21	6.89	1.92	1.30	2.31	3.20E-05
	290.15	57.25	5.61	1.63	1.28	2.09	2.72E-05
	290.15	45.74	4.47	1.35	1.27	1.88	2.25E-05
	290.15	35.45	3.48	1.06	1.25	1.66	1.77E-05

	290.15	26.47	2.60	0.78	1.24	1.44	1.29E-05
	290.15	18.76	1.84	0.49	1.24	1.22	8.18E-06
	290.15	12.27	1.20	0.20	1.23	0.99	3.41E-06
	290.15	12.27	1.20	0.20	1.23	0.99	3.41E-06
1.30-6	290.15	124.20	12.18	7.54	1.36	2.99	1.26E-04
	290.15	104.91	10.29	6.79	1.34	2.77	1.13E-04
	290.15	90.92	8.92	6.31	1.32	2.60	1.05E-04
	290.15	65.88	6.46	5.36	1.29	2.24	8.94E-05
	290.15	55.11	5.40	4.89	1.28	2.06	8.15E-05
	290.15	36.77	3.61	3.94	1.26	1.69	6.56E-05
	290.15	22.28	2.19	2.98	1.24	1.33	4.97E-05
	290.15	16.54	1.62	2.51	1.23	1.15	4.19E-05
	290.15	16.56	1.62	2.51	1.23	1.15	4.19E-05
1.30-7	290.15	123.88	12.15	7.53	1.36	2.99	1.26E-04
	290.15	101.80	9.98	6.78	1.33	2.74	1.13E-04
	290.15	88.57	8.69	6.31	1.32	2.57	1.05E-04
	290.15	64.56	6.33	5.35	1.29	2.22	8.92E-05
	290.15	54.08	5.30	4.88	1.28	2.04	8.14E-05
	290.15	36.07	3.54	3.94	1.26	1.68	6.57E-05
	290.15	21.97	2.15	2.99	1.24	1.32	4.98E-05
	290.15	16.32	1.60	2.51	1.23	1.14	4.19E-05
	290.15	16.32	1.60	2.51	1.23	1.14	4.19E-05
1.30-8	290.15	115.22	11.30	7.54	1.35	2.89	1.26E-04
	290.15	93.91	9.21	6.78	1.32	2.64	1.13E-04
	290.15	81.51	7.99	6.31	1.31	2.47	1.05E-04
	290.15	59.12	5.80	5.35	1.28	2.13	8.92E-05
	290.15	49.46	4.85	4.89	1.27	1.95	8.15E-05
	290.15	32.93	3.23	3.93	1.25	1.61	6.56E-05
	290.15	19.97	1.96	2.99	1.24	1.26	4.98E-05
	290.15	14.75	1.45	2.51	1.23	1.08	4.19E-05
	290.15	14.73	1.45	2.51	1.23	1.08	4.19E-05
	290.15	13.02	1.28	2.36	1.23	1.02	3.94E-05
1.30-X	290.15	113.14	11.10	6.78	1.35	2.87	1.13E-04
	290.15	97.99	9.61	6.31	1.33	2.69	1.05E-04
	290.15	70.74	6.94	5.35	1.30	2.31	8.92E-05
	290.15	59.07	5.79	4.89	1.28	2.13	8.15E-05
	290.15	39.19	3.84	3.94	1.26	1.75	6.57E-05
	290.15	23.81	2.33	2.98	1.24	1.37	4.97E-05
	290.15	17.67	1.73	2.51	1.23	1.18	4.19E-05
1.30-L	290.15	117.03	11.48	5.83	1.35	2.92	9.72E-05
	290.15	83.11	8.15	4.88	1.31	2.49	8.14E-05
	290.15	55.49	5.44	3.94	1.28	2.06	6.56E-05
	290.15	33.78	3.31	2.98	1.25	1.63	4.97E-05
	290.15	25.12	2.46	2.51	1.24	1.41	4.19E-05
	290.15	25.12	2.46	2.51	1.24	1.41	4.19E-05
	290.15	17.76	1.74	2.22	1.23	1.19	3.71E-05
1.60							
1.60-1	292.15	117.63	11.54	9.62	1.34	2.93	1.60E-04
	292.15	95.01	9.32	8.67	1.32	2.66	1.45E-04

	292.15	75.07	7.36	7.73	1.29	2.39	1.29E-04
	292.15	57.63	5.65	6.78	1.27	2.11	1.13E-04
	292.15	42.73	4.19	5.83	1.25	1.83	9.72E-05
	292.15	30.18	2.96	4.89	1.24	1.54	8.15E-05
	292.15	20.12	1.97	3.94	1.23	1.27	6.56E-05
	292.15	20.12	1.97	3.94	1.23	1.27	6.56E-05
1.60-2	291.15	99.67	9.77	9.63	1.33	2.72	1.61E-04
	291.15	80.62	7.91	8.68	1.30	2.46	1.45E-04
	291.15	63.88	6.26	7.74	1.28	2.21	1.29E-04
	291.15	49.14	4.82	6.78	1.27	1.95	1.13E-04
	291.15	36.55	3.58	5.83	1.25	1.69	9.72E-05
	291.15	25.93	2.54	4.89	1.24	1.43	8.15E-05
	291.15	17.35	1.70	3.94	1.23	1.18	6.57E-05
	291.15	17.33	1.70	3.94	1.23	1.18	6.57E-05
	291.15	13.68	1.34	3.75	1.23	1.05	6.25E-05
1.60-3	290.15	100.96	9.90	10.58	1.33	2.73	1.76E-04
	290.15	83.41	8.18	9.63	1.31	2.50	1.61E-04
	290.15	67.72	6.64	8.68	1.29	2.27	1.45E-04
	290.15	53.78	5.27	7.73	1.28	2.03	1.29E-04
	290.15	41.40	4.06	6.78	1.26	1.79	1.13E-04
	290.15	30.74	3.01	5.83	1.25	1.55	9.72E-05
	290.15	21.70	2.13	4.89	1.24	1.31	8.15E-05
	290.15	14.56	1.43	3.94	1.23	1.08	6.57E-05
1.60-4	290.15	85.78	8.41	9.63	1.31	2.53	1.61E-04
	290.15	69.51	6.82	8.68	1.29	2.29	1.45E-04
	290.15	55.14	5.41	7.74	1.28	2.06	1.29E-04
	290.15	42.56	4.17	6.79	1.26	1.82	1.13E-04
	290.15	31.67	3.11	5.83	1.25	1.58	9.72E-05
	290.15	22.44	2.20	4.89	1.24	1.33	8.15E-05
	290.15	14.94	1.47	3.94	1.23	1.09	6.56E-05
1.60-5	290.15	100.18	9.82	10.57	1.33	2.72	1.76E-04
	290.15	82.92	8.13	9.63	1.31	2.49	1.61E-04
	290.15	67.15	6.59	8.68	1.29	2.26	1.45E-04
	290.15	53.19	5.22	7.74	1.28	2.02	1.29E-04
	290.15	40.88	4.01	6.78	1.26	1.78	1.13E-04
	290.15	30.41	2.98	5.83	1.25	1.55	9.72E-05
	290.15	21.41	2.10	4.89	1.24	1.30	8.15E-05
	290.15	14.32	1.40	3.94	1.23	1.07	6.57E-05
1.60-6	290.15	100.80	9.89	10.57	1.33	2.72	1.76E-04
	290.15	83.27	8.17	9.63	1.31	2.50	1.61E-04
	290.15	67.39	6.61	8.68	1.29	2.26	1.45E-04
	290.15	53.36	5.23	7.74	1.28	2.03	1.29E-04
	290.15	40.81	4.00	6.79	1.26	1.78	1.13E-04
	290.15	30.29	2.97	5.83	1.25	1.54	9.72E-05
	290.15	21.62	2.12	4.89	1.24	1.31	8.15E-05
	290.15	14.49	1.42	3.94	1.23	1.07	6.57E-05
1.60-7	290.15	100.23	9.83	10.58	1.33	2.72	1.76E-04
	290.15	82.92	8.13	9.63	1.31	2.49	1.61E-04

	290.15	67.18	6.59	8.68	1.29	2.26	1.45E-04
	290.15	53.27	5.22	7.74	1.28	2.02	1.29E-04
	290.15	40.99	4.02	6.79	1.26	1.79	1.13E-04
	290.15	30.44	2.99	5.83	1.25	1.55	9.72E-05
	290.15	21.46	2.10	4.89	1.24	1.30	8.15E-05
	290.15	14.27	1.40	3.94	1.23	1.07	6.57E-05
1.60-8	290.15	121.85	11.95	10.57	1.36	2.97	1.76E-04
	290.15	100.64	9.87	9.63	1.33	2.72	1.60E-04
	290.15	81.41	7.98	8.68	1.31	2.47	1.45E-04
	290.15	64.41	6.32	7.74	1.29	2.21	1.29E-04
	290.15	49.56	4.86	6.78	1.27	1.96	1.13E-04
	290.15	36.86	3.62	5.83	1.26	1.70	9.72E-05
	290.15	26.06	2.56	4.89	1.24	1.43	8.15E-05
	290.15	17.28	1.70	3.94	1.23	1.17	6.56E-05
	290.15	13.68	1.34	3.46	1.23	1.04	5.77E-05
	290.15	13.70	1.34	3.46	1.23	1.05	5.77E-05
1.60-X	290.15	90.09	8.83	9.63	1.32	2.59	1.60E-04
	290.15	72.94	7.15	8.68	1.30	2.35	1.45E-04
	290.15	57.87	5.67	7.74	1.28	2.10	1.29E-04
	290.15	44.56	4.37	6.79	1.27	1.86	1.13E-04
	290.15	33.13	3.25	5.84	1.25	1.61	9.73E-05
	290.15	23.46	2.30	4.89	1.24	1.36	8.15E-05
	290.15	15.54	1.52	3.94	1.23	1.11	6.57E-05
			2.06				
2.06-1	293.15	93.37	9.16	17.65	1.31	2.64	2.94E-04
	293.15	88.42	8.67	17.17	1.30	2.58	2.78E-04
	293.15	83.49	8.19	16.71	1.30	2.51	2.71E-04
	293.15	78.78	7.73	16.24	1.29	2.44	2.63E-04
	293.15	74.15	7.27	15.77	1.29	2.38	2.55E-04
	293.15	69.73	6.84	15.29	1.28	2.31	2.47E-04
	293.15	65.21	6.40	14.82	1.28	2.24	2.39E-04
	293.15	61.06	5.99	14.35	1.27	2.17	2.31E-04
	293.15	56.80	5.57	13.89	1.27	2.10	2.23E-04
	293.15	52.84	5.18	13.41	1.26	2.03	2.16E-04
	293.15	48.95	4.80	12.94	1.26	1.95	2.08E-04
	293.15	45.37	4.45	12.46	1.25	1.88	2.00E-04
	293.15	42.37	4.15	11.99	1.25	1.82	1.92E-04
	293.15	38.60	3.79	11.52	1.25	1.74	1.84E-04
	293.15	35.07	3.44	11.05	1.24	1.66	1.76E-04
	293.15	32.45	3.18	10.57	1.24	1.60	1.68E-04
	293.15	29.17	2.86	10.11	1.23	1.52	1.60E-04
	293.15	26.18	2.57	9.63	1.23	1.44	1.53E-04
	293.15	23.58	2.31	9.15	1.23	1.37	1.45E-04
	293.15	21.19	2.08	8.68	1.23	1.30	1.37E-04
	293.15	18.65	1.83	8.21	1.22	1.22	1.29E-04
2.06-2	292.15	76.35	7.49	15.30	1.29	2.41	2.55E-04
	292.15	58.52	5.74	13.41	1.27	2.12	2.23E-04
	292.15	35.97	3.53	10.58	1.25	1.68	1.76E-04

	292.15	24.09	2.36	8.68	1.23	1.38	1.45E-04
	292.15	21.44	2.10	8.21	1.23	1.31	1.37E-04
	292.15	16.71	1.64	7.26	1.22	1.16	1.21E-04
	292.15	16.71	1.64	7.26	1.22	1.16	1.21E-04
2.06-3	292.15	71.10	6.97	15.29	1.29	2.33	2.55E-04
	292.15	54.51	5.34	13.41	1.27	2.05	2.23E-04
	292.15	33.55	3.29	10.58	1.24	1.63	1.76E-04
	292.15	22.39	2.20	8.68	1.23	1.34	1.45E-04
	292.15	19.97	1.96	8.21	1.23	1.26	1.37E-04
	292.15	15.60	1.53	7.26	1.22	1.12	1.21E-04
	292.15	15.60	1.53	7.26	1.22	1.12	1.21E-04
2.06-4	292.15	101.66	9.97	17.65	1.32	2.74	2.94E-04
	292.15	76.46	7.50	15.30	1.29	2.41	2.55E-04
	292.15	58.63	5.75	13.41	1.27	2.12	2.24E-04
	292.15	36.24	3.55	10.58	1.25	1.69	1.76E-04
	292.15	24.23	2.38	8.68	1.23	1.39	1.45E-04
	292.15	21.68	2.13	8.20	1.23	1.31	1.37E-04
	292.15	16.95	1.66	7.26	1.22	1.16	1.21E-04
2.06-5	292.15	72.89	7.15	15.30	1.29	2.35	2.55E-04
	292.15	55.79	5.47	13.41	1.27	2.08	2.24E-04
	292.15	34.40	3.37	10.58	1.25	1.65	1.76E-04
	292.15	23.03	2.26	8.68	1.23	1.35	1.45E-04
	292.15	20.52	2.01	8.21	1.23	1.28	1.37E-04
	292.15	16.05	1.57	7.26	1.22	1.13	1.21E-04
2.06-6	292.15	100.12	9.82	17.65	1.32	2.73	2.94E-04
	292.15	75.32	7.39	15.30	1.29	2.39	2.55E-04
	292.15	57.71	5.66	13.42	1.27	2.11	2.24E-04
	292.15	35.42	3.47	10.58	1.25	1.67	1.76E-04
	292.15	23.68	2.32	8.68	1.23	1.37	1.45E-04
	292.15	21.08	2.07	8.20	1.23	1.30	1.37E-04
	292.15	16.43	1.61	7.26	1.22	1.15	1.21E-04
2.06-7	292.2	95.50	9.37	15.29	1.32	2.67	2.55E-04
	292.2	73.04	7.16	13.41	1.29	2.36	2.24E-04
	292.2	44.92	4.41	10.58	1.26	1.87	1.76E-04
	292.2	29.93	2.94	8.68	1.24	1.54	1.45E-04
	292.2	26.74	2.62	8.20	1.24	1.46	1.37E-04
	292.2	20.84	2.04	7.26	1.23	1.29	1.21E-04
2.06-8	292.15	76.35	7.49	15.30	1.29	2.41	2.55E-04
	292.15	58.52	5.74	13.41	1.27	2.12	2.23E-04
	292.15	35.97	3.53	10.58	1.25	1.68	1.76E-04
	292.15	24.09	2.36	8.68	1.23	1.38	1.45E-04
	292.15	21.44	2.10	8.21	1.23	1.31	1.37E-04
	292.15	16.71	1.64	7.26	1.22	1.16	1.21E-04
	292.15	16.71	1.64	7.26	1.22	1.16	1.21E-04
2.06-X	293.15	101.79	9.98	17.64	1.32	2.75	2.94E-04
	293.15	97.11	9.52	17.18	1.31	2.69	2.86E-04
	293.15	92.01	9.02	16.70	1.31	2.63	2.78E-04
	293.15	86.92	8.52	16.23	1.30	2.56	2.71E-04

	293.15	82.03	8.04	15.77	1.30	2.49	2.63E-04
	293.15	77.24	7.57	15.29	1.29	2.42	2.55E-04
	293.15	72.43	7.10	14.82	1.28	2.35	2.47E-04
	293.15	67.75	6.64	14.35	1.28	2.28	2.39E-04
	293.15	63.63	6.24	13.88	1.27	2.21	2.31E-04
	293.15	59.14	5.80	13.41	1.27	2.14	2.23E-04
	293.15	55.56	5.45	12.94	1.27	2.07	2.16E-04
	293.15	50.87	4.99	12.46	1.26	1.99	2.08E-04
	293.15	47.12	4.62	12.00	1.26	1.92	2.00E-04
	293.15	43.50	4.27	11.52	1.25	1.85	1.92E-04
	293.15	39.88	3.91	11.04	1.25	1.77	1.84E-04
	293.15	36.58	3.59	10.58	1.24	1.70	1.76E-04
2.06-Y	293.15	93.45	9.16	17.65	1.31	2.65	2.94E-04
	293.15	83.59	8.20	16.70	1.30	2.51	2.78E-04
	293.15	74.15	7.27	15.77	1.29	2.38	2.63E-04
	293.15	65.29	6.40	14.82	1.28	2.24	2.47E-04
	293.15	56.80	5.57	13.88	1.27	2.10	2.31E-04
	293.15	48.97	4.80	12.93	1.26	1.95	2.16E-04
	293.15	42.28	4.15	12.00	1.25	1.82	2.00E-04
	293.15	34.99	3.43	11.05	1.24	1.66	1.84E-04
	293.15	28.80	2.82	10.10	1.23	1.51	1.68E-04
	293.15	23.25	2.28	9.15	1.23	1.36	1.53E-04
	293.15	18.57	1.82	8.20	1.22	1.22	1.37E-04
	293.15	13.81	1.35	7.26	1.22	1.05	1.21E-04

Averages						
		Slope	**Intercept**	**CI 95%**	**Lower**	**Upper**
0.94	**Average**	2.14E-05	-4.05E-06		2.00E-05	2.29E-05
	Stdev	1.76E-06	8.70E-07			
	% Stdev	8.2	-21			
1.3	**Average**	4.55E-05	-8.12E-06		4.49E-05	4.61E-05
	Stdev	6.65E-07	1.50E-06			
	% Stdev	1.5	-18			
1.6	**Average**	6.39E-05	-5.92E-06		6.06E-05	6.72E-05
	Stdev	3.93E-06	8.06E-07			
	% Stdev	6.1	-14			
2.06	**Average**	1.08E-04	-4.94E-06		1.04E-04	1.12E-04
	Stdev	4.22E-06	4.66E-06			
	% Stdev	3.9	-94			

Table F.15: Orifices tip dimensions.

Nominal diameter (mm)	d (mm)						L (cm)	l (cm)
	d1	**d2**	**d3**	**d4**	**Average**	**Stdev**		
0.7	0.79	0.70	0.79	0.72	0.750	0.005	3.040	2.146
0.94-X	0.840	0.880	0.750	0.870	0.835	0.059	3.080	2.150
0.94-Y	0.780	0.740	0.760	0.860	0.785	0.053	3.084	2.054
1.00	0.680	0.689	0.689	0.672	0.683	0.008	3.024	3.006

1.08	0.880	0.820	0.830	0.897	0.857	0.038	3.022	2.146
1.18	0.940	0.880	0.840	0.896	0.889	0.041	3.034	2.146
1.30-X	1.180	1.180	1.220	1.120	1.175	0.041	3.008	2.148
1.30-Y	1.210	1.210	1.180	1.130	1.183	0.038	3.084	2.072
1.30-L	1.390	1.310	1.350	1.370	1.355	0.034	3.018	0.000
1.35	1.210	1.250	1.280	1.280	1.255	0.033	3.036	1.990
1.40	1.280	1.286	1.320	1.240	1.282	0.033	3.030	2.098
1.45	1.320	1.280	1.287	1.301	1.297	0.018	2.940	1.898
1.60-X	1.380	1.380	1.360	1.430	1.388	0.030	3.168	2.150
1.60-Y	1.390	1.390	1.340	1.340	1.365	0.029	3.054	2.090
1.80	1.900	1.870	1.840	1.970	1.895	0.056	3.000	2.154
2.06-X	1.830	1.860	1.880	1.900	1.868	0.030	3.014	2.152
2.06-Y	1.870	1.890	1.900	1.740	1.850	0.074	3.006	2.160
3.00	3.280	3.310	3.290	3.200	3.270	0.048	3.060	0.000
				Set 1 (0.94)				
1	0.88	0.82	0.83	0.77	0.83	0.0451	3.008	2.330
2	0.92	0.92	0.95	0.95	0.94	0.0173	3.070	2.038
3	0.93	0.86	0.93	0.91	0.91	0.0330	3.080	2.040
4	0.90	0.90	0.86	0.87	0.88	0.0176	3.060	2.056
5	0.81	0.74	0.78	0.79	0.78	0.0288	3.066	2.030
6	0.80	0.84	0.83	0.84	0.83	0.0184	3.068	2.052
7	0.78	0.82	0.83	0.83	0.81	0.0259	3.010	2.314
8	0.82	0.91	0.88	0.86	0.87	0.0365	3.008	2.320
Average							3.040	2.199
Stdev							0.031	0.168
				Set 2 (1.30)				
1	1.2100	1.2100	1.2000	1.2400	1.2150	0.0173	1.2100	1.2100
2	1.2100	1.1900	1.2200	1.1200	1.1850	0.0451	1.2100	1.1900
3	1.3400	1.3200	1.3400	1.2600	1.3150	0.0379	1.3400	1.3200
4	1.2000	1.2600	1.2200	1.2400	1.2300	0.0258	1.2000	1.2600
5	1.5400	1.6100	1.5000	1.4900	1.5350	0.0545	1.5400	1.6100
6	1.2600	1.1400	1.2600	1.2200	1.2200	0.0566	1.2600	1.1400
7	1.1400	1.2300	1.0400	1.1600	1.1425	0.0785	1.1400	1.2300
8	1.2800	1.3100	1.2300	1.2200	1.2600	0.0424	1.2800	1.3100
Average							3.038	2.283
Stdev							0.031	0.165
				Set 3 (1.60)				
1	1.4000	1.1700	1.2700	1.3200	1.2900	0.0963	3.010	2.354
2	1.3800	1.4800	1.3000	1.4500	1.4025	0.0802	3.010	2.290
3	1.5100	1.5200	1.4800	1.3900	1.4750	0.0592	3.058	2.084
4	1.5100	1.4100	1.3900	1.4600	1.4425	0.0538	3.020	2.052
5	1.4300	1.4300	1.3700	1.4000	1.4075	0.0287	3.058	2.030
6	1.4300	1.4700	1.3700	1.4700	1.4350	0.0473	3.050	2.110
7	1.5000	1.5600	1.5600	1.5600	1.5450	0.0300	3.070	2.086
8	1.3800	1.2400	1.3000	1.3000	1.3050	0.0574	3.006	2.354
Average							3.030	2.212
Stdev							0.026	0.151
				Set 4 (2.06)				
1	1.9900	1.9300	1.9460	1.8800	1.9365	0.0454	3.004	2.158
2	2.0030	1.9660	1.9330	1.9400	1.9605	0.0317	3.012	2.188

3	1.8660	1.8240	1.7550	1.8520	1.8243	0.0494	3.016	2.124
4	1.9320	1.8960	1.8170	1.9520	1.8993	0.0595	3.006	2.174
5	1.7900	1.7600	1.7660	1.7810	1.7743	0.0137	3.018	2.150
6	1.3400	1.2500	1.2300	1.3600	1.2950	0.0645	3.008	2.080
7	1.4100	1.2800	1.4000	1.4300	1.3800	0.0678	2.984	2.170
Average							3.007	2.149
Stdev							0.011	0.037
Orifice	**0.94**		**1.30**		**1.60**		**2.06**	
	Length	**$(d/D)^4$**	**Length**	**$(d/D)^4$**	**Length**	**$(d/D)^4$**	**Length**	**$(d/D)^4$**
1	0.678	1.78E-05	0.636	8.38E-05	0.656	1.06E-04	0.846	4.50E-04
2	1.032	2.94E-05	0.570	7.58E-05	0.720	1.49E-04	0.846	5.41E-04
3	1.040	2.61E-05	0.870	1.15E-04	0.974	1.82E-04	0.824	5.68E-04
4	1.004	2.32E-05	1.010	8.80E-05	0.968	1.66E-04	0.892	4.26E-04
5	1.036	1.42E-05	0.940	2.13E-04	1.028	1.51E-04	0.832	5.00E-04
6	1.016	1.80E-05	0.686	8.52E-05	0.940	1.63E-04	0.868	3.81E-04
7	0.696	1.68E-05	0.958	6.55E-05	0.984	2.19E-04	0.928	1.08E-04
8	0.688	2.17E-05	0.694	9.69E-05	0.652	1.11E-04	0.814	1.39E-04

Table F.16: Orifice-B.

Nominal diameter (mm)	**d (mm)**						**L (mm)**	**l (mm)**
	d1	**d2**	**d3**	**d4**	**Average**	**Stdev**		
0.94	0.91	0.92	0.91	0.95	0.92	0.02	2.450	1.412
1.30	1.26	1.32	1.28	1.31	1.29	0.03	2.448	1.344

Table F.17: Accuracy.

Tube 3											
Q_{in}		**T**		**P_{out1}**		**ρ_{out1}**		**P_{out2}**		**ρ_{out2}**	
Avg (kg/s)	**Stdev (kg/s)**	**Avg (K)**	**Stdev (K)**	**Avg (kPa)**	**Stdev (kPa)**	**Avg (kg/m^3)**	**Stdev (kg/m^3)**	**Avg (kPa)**	**Stdev (kPa)**	**Avg (kg/m^3)**	**Stdev (kg/m^3)**
O_{out1} = 0.70 and O_{out2} = 0.94											
6.96E-05	8.3E-07	289.15	0.0E+00	2.11	3.9E-03	1.24	4.7E-03	8.63	3.7E-07	1.32	4.5E-07
6.75E-05	8.3E-07	289.15	0.0E+00	1.98	3.8E-03	1.24	4.6E-03	8.10	4.8E-03	1.31	5.8E-03
6.54E-05	8.3E-07	289.15	0.0E+00	1.86	3.7E-03	1.24	4.5E-03	7.60	6.0E-03	1.31	7.3E-03
6.33E-05	8.3E-07	289.15	0.0E+00	1.76	5.0E-03	1.24	6.0E-03	7.11	0.0E+00	1.30	0.0E+00
6.11E-05	8.3E-07	289.15	0.0E+00	1.72	5.3E-08	1.24	6.5E-08	6.66	3.0E-03	1.29	3.7E-03
5.90E-05	8.3E-07	289.15	0.0E+00	1.55	2.4E-03	1.23	2.9E-03	6.19	3.9E-03	1.29	4.7E-03
5.69E-05	8.3E-07	289.15	0.0E+00	1.47	2.9E-03	1.23	3.5E-03	5.73	3.5E-03	1.28	4.3E-03
5.48E-05	8.3E-07	289.15	0.0E+00	1.39	0.0E+00	1.23	0.0E+00	5.33	8.5E-03	1.28	1.0E-02
5.27E-05	8.3E-07	289.15	0.0E+00	1.31	3.7E-03	1.23	4.5E-03	4.94	1.5E-07	1.27	1.8E-07
5.06E-05	8.3E-07	289.15	0.0E+00	1.23	7.1E-08	1.23	8.6E-08	4.50	0.0E+00	1.27	0.0E+00
O_{out1} = 0.70 and O_{out2} = 1.60											
1.86E-04	1.8E-05	291.83	1.7E-02	11.36	4.0E-07	1.35	1.2E-03	4.16	1.9E-07	1.26	1.1E-03
1.76E-04	1.8E-05	291.65	0.0E+00	10.84	1.0E-02	1.34	1.2E-02	3.64	2.9E-03	1.26	3.5E-03
1.66E-04	1.8E-05	291.53	0.0E+00	10.39	1.0E-01	1.34	1.2E-01	3.14	3.3E-03	1.25	3.9E-03

1.55E-04	1.8E-05	291.49	3.1E-02	9.32	9.4E-03	1.33	1.2E-02	2.73	7.9E-03	1.25	9.7E-03
1.45E-04	1.8E-05	291.46	0.0E+00	8.73	1.6E-02	1.32	1.9E-02	2.34	0.0E+00	1.24	0.0E+00
1.35E-04	1.8E-05	291.46	0.0E+00	7.69	8.5E-03	1.31	1.0E-02	2.05	1.0E-02	1.24	1.2E-02
O_{out1} = 1.30 and O_{out2} = 2.06											
3.88E-04	1.8E-05	291.21	0.0E+00	5.94	1.3E-01	1.28	1.5E-01	5.63	2.9E-03	1.27	3.5E-03
3.68E-04	1.8E-05	291.21	0.0E+00	5.46	1.1E-01	1.27	1.3E-01	5.02	9.4E-03	1.27	1.1E-02
3.48E-04	1.8E-05	291.09	0.0E+00	4.96	1.0E-01	1.27	1.2E-01	4.44	7.0E-03	1.26	8.4E-03
3.28E-04	1.8E-05	291.08	1.9E-02	4.51	1.0E-01	1.26	1.2E-01	3.89	5.3E-03	1.25	6.5E-03
3.07E-04	1.8E-05	291.04	2.7E-02	4.04	1.1E-01	1.25	1.3E-01	3.38	2.9E-03	1.25	4.0E-03
2.87E-04	1.8E-05	291.03	0.0E+00	3.57	9.4E-02	1.25	1.1E-01	2.93	5.8E-03	1.24	7.0E-03
2.67E-04	1.8E-05	291.00	3.0E-02	3.19	9.0E-02	1.24	1.1E-01	2.48	2.9E-03	1.24	4.1E-03
O_{out1} = 1.60 and O_{out2} = 2.06											
5.29E-04	1.8E-05	291.21	0.0E+00	4.25	1.9E-02	1.26	2.3E-02	10.39	8.6E-03	1.33	1.0E-02
5.08E-04	1.8E-05	291.09	0.0E+00	3.88	2.7E-02	1.25	3.3E-02	9.68	1.3E-02	1.32	1.6E-02
4.89E-04	1.8E-05	291.12	5.5E-02	3.69	1.3E-02	1.25	1.6E-02	8.89	9.5E-03	1.31	1.2E-02
4.68E-04	1.8E-05	291.09	1.8E-02	3.32	2.8E-02	1.25	3.4E-02	8.20	3.9E-03	1.30	4.9E-03
4.48E-04	1.8E-05	291.09	0.0E+00	3.08	9.3E-08	1.24	1.1E-07	7.52	9.8E-03	1.30	1.2E-02
4.28E-04	1.8E-05	291.09	0.0E+00	2.73	1.7E-02	1.24	2.0E-02	6.93	1.0E-02	1.29	1.2E-02
4.08E-04	1.8E-05	291.10	3.4E-02	2.47	1.2E-02	1.24	1.5E-02	6.32	6.8E-03	1.28	8.6E-03
Tube 4											
O_{out1} = 0.70 and O_{out2} = 0.94											
9.53E-05	8.27E-07	290.28	0.E+00	10.70	6.7E-02	1.34	8.2E-02	7.72	4.8E-02	1.30	5.9E-02
9.20E-05	8.32E-07	290.28	0.E+00	9.33	2.2E-03	1.32	2.7E-03	7.73	8.7E-03	1.30	1.1E-02
8.88E-05	8.32E-07	290.34	0.E+00	8.71	3.9E-03	1.31	4.7E-03	7.27	1.1E-02	1.29	1.3E-02
8.56E-05	8.27E-07	290.34	0.E+00	8.17	2.9E-03	1.31	3.5E-03	6.75	2.1E-03	1.29	2.6E-03
8.24E-05	8.40E-07	290.28	0.E+00	7.65	3.5E-03	1.30	4.3E-03	6.27	4.9E-03	1.28	5.9E-03
7.92E-05	8.37E-07	290.28	0.E+00	7.14	3.7E-03	1.29	4.4E-03	5.80	4.9E-03	1.28	6.0E-03
7.60E-05	8.33E-07	290.28	0.E+00	6.66	3.2E-03	1.29	3.9E-03	5.30	3.6E-03	1.27	4.3E-03
7.28E-05	8.27E-07	290.46	0.E+00	6.22	1.1E-02	1.28	1.3E-02	4.94	2.1E-03	1.27	2.6E-03
6.96E-05	8.27E-07	290.46	0.E+00	5.84	7.5E-08	1.28	9.1E-08	4.55	3.6E-03	1.26	4.3E-03
6.64E-05	8.38E-07	290.44	0.E+00	5.32	1.3E-02	1.27	1.5E-02	4.05	4.0E-03	1.26	4.9E-03
6.32E-05	8.36E-07	290.34	0.E+00	4.94	3.3E-03	1.27	4.0E-03	3.70	8.5E-03	1.25	1.0E-02
6.01E-05	8.27E-07	290.46	0.E+00	4.55	3.0E-07	1.26	3.6E-07	3.38	0.0E+00	1.25	0.0E+00
5.69E-05	8.27E-07	290.46	0.E+00	4.19	3.6E-03	1.26	4.3E-03	3.06	2.1E-07	1.24	2.5E-07
5.37E-05	8.34E-07	290.34	0.E+00	3.83	2.0E-03	1.25	2.4E-03	2.75	3.5E-03	1.24	4.3E-03
5.06E-05	8.27E-07	290.33	0.E+00	3.47	5.5E-03	1.25	6.6E-03	2.35	2.0E-02	1.24	2.4E-02
4.74E-05	8.27E-07	290.30	0.E+00	3.17	1.5E-03	1.25	1.9E-03	2.03	3.0E-03	1.23	3.6E-03
4.43E-05	8.27E-07	290.34	0.E+00	2.82	3.6E-03	1.24	4.3E-03	1.70	3.8E-03	1.23	4.6E-03
4.11E-05	8.27E-07	290.34	0.E+00	2.59	2.0E-03	1.24	2.4E-03	1.47	3.2E-03	1.23	3.9E-03
3.80E-05	8.27E-07	290.51	0.E+00	2.28	5.1E-03	1.23	6.1E-03	1.22	4.5E-03	1.22	5.4E-03
O_{out1} = 1.30 and O_{out2} = 1.60											
2.67E-04	1.79E-05	290.15	0.E+00	8.38	1.6E-02	1.31	1.9E-02	4.63	6.6E-03	1.26	8.0E-03
2.57E-04	1.79E-05	290.15	0.E+00	7.78	1.7E-02	1.30	2.1E-02	4.24	3.1E-02	1.26	3.8E-02
2.47E-04	1.79E-05	290.15	0.E+00	7.20	6.1E-03	1.29	7.3E-03	3.86	6.5E-03	1.25	7.9E-03
2.37E-04	1.79E-05	290.15	0.E+00	6.64	1.5E-02	1.29	1.8E-02	3.52	9.2E-03	1.25	1.1E-02
2.27E-04	1.79E-05	290.15	0.E+00	6.10	1.2E-02	1.28	1.4E-02	3.21	6.9E-03	1.25	8.4E-03
2.16E-04	1.79E-05	290.15	0.E+00	5.70	6.0E-03	1.28	7.2E-03	2.90	6.7E-03	1.24	8.1E-03
2.06E-04	1.79E-05	290.15	0.E+00	5.11	1.3E-02	1.27	1.6E-02	2.63	2.8E-03	1.24	3.4E-03
1.96E-04	1.79E-05	290.15	0.E+00	4.66	4.3E-03	1.26	5.2E-03	2.32	9.8E-03	1.24	1.2E-02
1.86E-04	1.79E-05	290.15	0.E+00	4.23	7.4E-03	1.26	8.9E-03	2.07	6.9E-03	1.23	8.3E-03
1.76E-04	1.79E-05	290.15	0.E+00	3.81	8.2E-03	1.25	9.9E-03	1.84	5.0E-03	1.23	6.1E-03
1.66E-04	1.79E-05	290.15	0.E+00	3.46	0.0E+00	1.25	0.0E+00	1.60	5.9E-03	1.23	7.2E-03
1.55E-04	1.79E-05	290.15	0.E+00	3.07	1.1E-02	1.25	1.3E-02	1.38	3.9E-03	1.23	4.7E-03

O_{out1} = 1.30 and O_{out2} = 1.60											
2.29E-04	1.79E-05	290.42	6.E-02	6.40	1.3E-02	1.28	1.6E-02	3.36	2.5E-02	1.25	3.1E-02
2.27E-04	1.79E-05	290.39	6.E-02	6.30	8.2E-03	1.28	1.1E-02	3.22	2.3E-03	1.25	5.3E-03
2.24E-04	1.79E-05	290.42	6.E-02	6.18	5.5E-03	1.28	8.1E-03	3.16	1.6E-02	1.25	2.0E-02
2.22E-04	1.79E-05	290.34	2.E-02	6.07	8.1E-03	1.28	9.9E-03	3.10	1.1E-02	1.24	1.3E-02
2.20E-04	1.79E-05	290.40	6.E-02	5.98	8.6E-03	1.28	1.1E-02	3.04	6.9E-03	1.24	9.5E-03
2.18E-04	1.79E-05	290.37	6.E-02	5.86	1.2E-02	1.28	1.5E-02	2.98	5.1E-03	1.24	7.4E-03
2.16E-04	1.79E-05	290.40	6.E-02	5.77	1.1E-02	1.28	1.4E-02	2.91	1.1E-02	1.24	1.4E-02
2.14E-04	1.79E-05	290.46	0.E+00	5.72	3.0E-03	1.28	3.6E-03	2.86	0.0E+00	1.24	0.0E+00
2.12E-04	1.79E-05	290.38	6.E-02	5.65	4.2E-02	1.28	5.1E-02	2.80	1.2E-02	1.24	1.5E-02
2.10E-04	1.79E-05	290.44	5.E-02	5.49	1.3E-02	1.27	1.6E-02	2.75	6.8E-03	1.24	9.0E-03
2.08E-04	1.79E-05	290.41	6.E-02	5.38	1.5E-02	1.27	1.9E-02	2.69	1.5E-02	1.24	1.8E-02
2.06E-04	1.79E-05	290.42	6.E-02	5.30	1.3E-02	1.27	1.7E-02	2.63	1.3E-03	1.24	4.5E-03
2.04E-04	1.79E-05	290.44	4.E-02	5.19	1.2E-02	1.27	1.5E-02	2.63	2.9E-03	1.24	4.7E-03
2.02E-04	1.79E-05	290.46	0.E+00	5.09	9.9E-03	1.27	1.2E-02	2.53	2.5E-02	1.24	3.0E-02
2.00E-04	1.79E-05	290.46	1.E-02	5.02	3.9E-03	1.27	4.8E-03	2.46	6.1E-03	1.24	7.5E-03
1.98E-04	1.79E-05	290.46	0.E+00	4.93	5.8E-03	1.27	7.0E-03	2.41	7.5E-03	1.24	9.1E-03
1.96E-04	1.79E-05	290.46	0.E+00	4.82	3.0E-03	1.26	3.6E-03	2.37	3.9E-03	1.24	4.8E-03
1.94E-04	1.79E-05	290.46	0.E+00	4.73	1.3E-02	1.26	1.6E-02	2.31	1.4E-07	1.23	1.7E-07
1.92E-04	1.79E-05	290.47	1.E-02	4.63	1.3E-02	1.26	1.6E-02	2.25	6.5E-03	1.23	7.9E-03
1.90E-04	1.79E-05	290.46	0.E+00	4.56	1.2E-02	1.26	1.5E-02	2.19	9.7E-03	1.23	1.2E-02
1.88E-04	1.79E-05	290.46	0.E+00	4.44	1.1E-02	1.26	1.3E-02	2.15	1.1E-02	1.23	1.3E-02
1.86E-04	1.79E-05	290.46	7.E-03	4.43	3.6E-03	1.26	4.4E-03	2.09	4.9E-03	1.23	5.9E-03
1.84E-04	1.79E-05	290.46	0.E+00	4.28	8.0E-03	1.26	9.7E-03	2.03	8.4E-03	1.23	1.0E-02
1.82E-04	1.79E-05	290.46	0.E+00	4.20	8.7E-03	1.26	1.1E-02	2.03	2.0E-07	1.23	2.5E-07
1.80E-04	1.79E-05	290.47	1.E-02	4.09	7.6E-03	1.26	9.2E-03	2.02	1.1E-02	1.23	1.3E-02
1.78E-04	1.79E-05	290.46	8.E-03	4.04	1.5E-02	1.26	1.8E-02	1.90	6.3E-03	1.23	7.6E-03
1.76E-04	1.80E-05	290.46	0.E+00	3.93	9.5E-03	1.25	1.1E-02	1.85	4.8E-03	1.23	5.8E-03
1.74E-04	1.79E-05	290.47	2.E-02	3.85	1.0E-02	1.25	1.2E-02	1.82	6.3E-03	1.23	7.7E-03
1.72E-04	1.79E-05	290.46	0.E+00	3.77	1.0E-02	1.25	1.2E-02	1.77	3.4E-03	1.23	4.1E-03
1.70E-04	1.79E-05	290.51	3.E-02	3.70	1.6E-02	1.25	2.0E-02	1.70	9.6E-03	1.23	1.2E-02
1.68E-04	1.79E-05	290.49	3.E-02	3.61	1.1E-02	1.25	1.3E-02	1.68	1.9E-02	1.23	2.3E-02
1.66E-04	1.79E-05	290.51	3.E-02	3.52	9.7E-03	1.25	1.2E-02	1.61	5.3E-03	1.23	6.7E-03
1.64E-04	1.79E-05	290.46	1.E-02	3.46	0.0E+00	1.25	7.7E-04	1.55	8.7E-03	1.23	1.1E-02
1.62E-04	1.79E-05	290.50	3.E-02	3.46	3.0E-03	1.25	4.3E-03	1.54	3.2E-03	1.23	4.4E-03
1.60E-04	1.79E-05	290.46	1.E-02	3.37	9.7E-03	1.25	1.2E-02	1.54	3.4E-03	1.23	4.1E-03
1.58E-04	1.79E-05	290.47	1.E-02	3.24	9.3E-03	1.25	1.1E-02	1.46	3.2E-02	1.22	3.9E-02
1.55E-04	1.79E-05	290.51	3.E-02	3.15	9.4E-03	1.24	1.2E-02	1.39	2.4E-03	1.22	3.4E-03
O_{out1} = 2.06 and O_{out2} = 2.06											
5.89E-04	1.75E-05	290.78	2.E-02	5.43	4.1E-02	1.27	4.9E-02	6.30	5.6E-02	1.28	6.7E-02
5.79E-04	1.75E-05	290.80	3.E-02	5.42	5.5E-07	1.27	2.2E-03	6.26	6.6E-07	1.28	2.2E-03
5.69E-04	1.76E-05	290.83	2.E-02	5.42	5.5E-07	1.27	1.8E-03	6.26	6.6E-07	1.28	1.8E-03
5.59E-04	1.76E-05	290.84	0.E+00	5.42	5.5E-07	1.27	6.7E-07	6.26	6.6E-07	1.28	8.0E-07
5.49E-04	1.76E-05	290.84	0.E+00	5.42	5.5E-07	1.27	6.7E-07	6.26	6.6E-07	1.28	8.0E-07
5.39E-04	1.76E-05	290.84	2.E-02	5.42	5.5E-07	1.27	1.5E-03	6.26	6.6E-07	1.28	1.5E-03
5.29E-04	1.77E-05	290.88	6.E-02	5.35	2.7E-01	1.27	3.3E-01	6.18	2.8E-01	1.28	3.4E-01
5.19E-04	1.77E-05	290.95	4.E-02	4.16	5.4E-02	1.26	6.5E-02	5.01	6.9E-02	1.27	8.3E-02
5.09E-04	1.77E-05	290.88	6.E-02	3.93	4.0E-02	1.25	4.8E-02	4.84	5.5E-02	1.26	6.6E-02
4.99E-04	1.77E-05	290.96	0.E+00	3.79	4.8E-02	1.25	5.8E-02	4.65	4.0E-02	1.26	4.9E-02
4.89E-04	1.77E-05	290.96	0.E+00	3.66	3.6E-02	1.25	4.4E-02	4.42	3.0E-02	1.26	3.7E-02
4.79E-04	1.77E-05	290.96	0.E+00	3.45	3.5E-02	1.25	4.2E-02	4.33	3.0E-02	1.26	3.7E-02
4.69E-04	1.77E-05	290.96	0.E+00	3.29	2.8E-02	1.25	3.4E-02	4.11	3.0E-02	1.26	3.6E-02
4.59E-04	1.78E-05	290.97	1.E-02	3.12	5.1E-02	1.24	6.2E-02	3.99	6.4E-02	1.25	7.7E-02

4.49E-04	1.78E-05	291.03	0.E+00	3.03	4.4E-02	1.24	5.4E-02	3.73	5.0E-02	1.25	6.0E-02
4.39E-04	1.78E-05	291.21	0.E+00	2.88	5.3E-03	1.24	6.4E-03	3.62	2.0E-02	1.25	2.4E-02
4.28E-04	1.77E-05	291.28	1.E-02	2.79	6.6E-02	1.24	8.0E-02	3.44	4.0E-02	1.25	4.9E-02
4.18E-04	1.78E-05	291.28	1.E-02	2.59	3.6E-02	1.24	4.4E-02	3.36	3.5E-02	1.25	4.2E-02
4.08E-04	1.78E-05	291.28	0.E+00	2.44	3.1E-02	1.23	3.8E-02	3.17	3.1E-02	1.24	3.7E-02
3.98E-04	1.78E-05	291.28	0.E+00	2.36	1.5E-02	1.23	1.8E-02	2.97	1.6E-02	1.24	2.0E-02
3.88E-04	1.78E-05	291.27	1.E-02	2.16	3.4E-02	1.23	4.1E-02	2.88	3.9E-02	1.24	4.7E-02
3.78E-04	1.78E-05	291.21	0.E+00	2.03	3.1E-02	1.23	3.8E-02	2.75	1.7E-02	1.24	2.1E-02
3.68E-04	1.78E-05	291.21	0.E+00	1.91	2.4E-02	1.23	2.9E-02	2.62	2.6E-02	1.24	3.1E-02
O_{out1} = 2.06 and O_{out2} = 2.06											
5.89E-04	1.75E-05	291.46	0.E+00	5.49	3.1E-02	1.27	3.7E-02	6.22	3.3E-02	1.28	4.0E-02
5.87E-04	1.75E-05	291.36	5.E-02	5.51	4.9E-02	1.27	5.9E-02	6.13	5.3E-02	1.28	6.3E-02
5.85E-04	1.75E-05	291.34	0.E+00	5.45	5.2E-02	1.27	6.2E-02	6.12	5.2E-02	1.28	6.3E-02
5.83E-04	1.75E-05	291.31	3.E-02	5.38	2.7E-02	1.27	3.3E-02	6.10	4.0E-02	1.28	4.8E-02
5.81E-04	1.76E-05	291.30	3.E-02	5.36	2.1E-02	1.27	2.6E-02	6.07	4.7E-02	1.28	5.7E-02
5.79E-04	1.76E-05	291.30	3.E-02	5.36	2.1E-02	1.27	2.5E-02	6.01	5.3E-02	1.28	6.4E-02
5.77E-04	1.75E-05	291.34	1.E-02	5.35	5.5E-03	1.27	6.7E-03	5.96	5.1E-02	1.28	6.1E-02
5.75E-04	1.75E-05	291.37	6.E-02	5.33	3.2E-02	1.27	3.8E-02	5.92	4.8E-02	1.28	5.9E-02
5.73E-04	1.75E-05	291.44	5.E-02	5.31	4.9E-02	1.27	5.9E-02	5.88	5.9E-02	1.27	7.1E-02
5.71E-04	1.76E-05	291.46	0.E+00	5.27	7.3E-02	1.27	8.8E-02	5.83	5.3E-02	1.27	6.3E-02
5.69E-04	1.76E-05	291.50	3.E-02	5.18	7.1E-02	1.27	8.6E-02	5.81	4.4E-02	1.27	5.3E-02
5.67E-04	1.76E-05	291.49	3.E-02	5.11	4.1E-02	1.27	5.0E-02	5.79	4.1E-02	1.27	4.9E-02
5.65E-04	1.76E-05	291.50	3.E-02	5.03	4.6E-02	1.26	5.6E-02	5.79	6.4E-02	1.27	7.7E-02
5.63E-04	1.76E-05	291.53	0.E+00	5.00	2.9E-02	1.26	3.5E-02	5.74	3.7E-02	1.27	4.4E-02
5.61E-04	1.76E-05	291.53	7.E-03	4.97	4.3E-02	1.26	5.2E-02	5.71	5.0E-02	1.27	6.1E-02
5.59E-04	1.76E-05	291.53	7.E-03	4.93	4.2E-02	1.26	5.1E-02	5.67	4.2E-02	1.27	5.0E-02
5.57E-04	1.76E-05	291.56	3.E-02	4.93	3.7E-02	1.26	4.4E-02	5.63	1.4E-02	1.27	1.7E-02
5.55E-04	1.76E-05	291.59	7.E-03	4.91	3.4E-02	1.26	4.1E-02	5.58	5.3E-02	1.27	6.4E-02
5.53E-04	1.77E-05	291.57	3.E-02	4.87	3.6E-02	1.26	4.4E-02	5.54	5.9E-02	1.27	7.1E-02
5.51E-04	1.77E-05	291.59	0.E+00	4.82	6.3E-02	1.26	7.6E-02	5.53	9.2E-02	1.27	1.1E-01
5.49E-04	1.76E-05	291.59	0.E+00	4.77	3.0E-02	1.26	3.6E-02	5.51	5.7E-02	1.27	6.9E-02
5.47E-04	1.76E-05	291.60	2.E-02	4.75	3.9E-02	1.26	4.8E-02	5.44	4.6E-02	1.27	5.6E-02
5.45E-04	1.76E-05	291.65	7.E-03	4.69	3.1E-02	1.26	3.8E-02	5.43	4.1E-02	1.27	5.0E-02
5.43E-04	1.76E-05	291.63	3.E-02	4.71	3.8E-02	1.26	4.6E-02	5.34	4.2E-02	1.27	5.0E-02
5.41E-04	1.76E-05	291.63	3.E-02	4.65	3.4E-02	1.26	4.1E-02	5.34	4.6E-02	1.27	5.5E-02
5.39E-04	1.77E-05	291.65	7.E-03	4.64	3.7E-02	1.26	4.4E-02	5.28	4.6E-02	1.27	5.6E-02
5.37E-04	1.76E-05	291.65	7.E-03	4.62	4.3E-02	1.26	5.2E-02	5.23	4.7E-02	1.27	5.6E-02
5.35E-04	1.76E-05	291.65	2.E-02	4.59	5.8E-02	1.26	6.9E-02	5.20	5.5E-02	1.27	6.7E-02
5.33E-04	1.77E-05	291.65	0.E+00	4.54	4.2E-02	1.26	5.1E-02	5.18	4.3E-02	1.27	5.2E-02
5.31E-04	1.76E-05	291.62	3.E-02	4.46	2.9E-02	1.26	3.5E-02	5.19	4.2E-02	1.27	5.1E-02
5.29E-04	1.76E-05	291.63	3.E-02	4.47	1.8E-02	1.26	2.2E-02	5.11	2.6E-02	1.26	3.1E-02
5.27E-04	1.76E-05	291.60	3.E-02	4.44	3.2E-02	1.26	3.8E-02	5.08	3.9E-02	1.26	4.7E-02

Table F.18: Accuracy fitting analysis.

Tube 3						
Linear						
Q_{in}		**Q_{out1}**		**Q_{out2}**		**Error**
Avg (kg/s)	**Stdev (kg/s)**	**Avg (kg/s)**	**Stdev (kg/s)**	**Avg (kg/s)**	**Stdev (kg/s)**	**(%)**
O_{out1} = 0.70 and O_{out2} = 0.94						
6.96E-05	8.27E-07	1.95E-05	1.85E-08	4.96E-05	1.05E-12	-2.75
6.75E-05	8.27E-07	1.89E-05	1.88E-08	4.79E-05	1.39E-08	-3.55

6.54E-05	8.27E-07	1.82E-05	1.86E-08	4.64E-05	1.80E-08	-4.05
6.33E-05	8.27E-07	1.77E-05	2.60E-08	4.48E-05	0.00E+00	-4.22
6.11E-05	8.27E-07	1.75E-05	2.82E-13	4.33E-05	9.63E-09	-1.98
5.90E-05	8.27E-07	1.66E-05	1.31E-08	4.17E-05	1.27E-08	-4.45
5.69E-05	8.27E-07	1.61E-05	1.65E-08	4.00E-05	1.21E-08	-4.66
5.48E-05	8.27E-07	1.56E-05	0.00E+00	3.86E-05	3.02E-08	-3.57
5.27E-05	8.27E-07	1.51E-05	2.25E-08	3.71E-05	5.55E-13	-3.10
5.06E-05	8.34E-07	1.47E-05	4.40E-13	3.54E-05	0.00E+00	-3.39
O_{out1} = 0.70 and O_{out2} = 1.60						
1.86E-04	1.79E-05	4.82E-05	2.22E-08	1.36E-04	1.09E-07	-3.94
1.76E-04	1.79E-05	4.70E-05	2.20E-08	1.27E-04	8.87E-08	-3.91
1.66E-04	1.79E-05	4.59E-05	2.30E-07	1.18E-04	1.08E-07	-4.22
1.55E-04	1.79E-05	4.32E-05	4.34E-08	1.10E-04	3.23E-07	-5.19
1.45E-04	1.79E-05	4.17E-05	3.91E-08	1.02E-04	0.00E+00	-4.33
1.35E-04	1.79E-05	3.89E-05	2.19E-08	9.52E-05	4.12E-07	-2.94
O_{out1} = 1.30 and O_{out2} = 2.06						
3.88E-04	1.78E-05	1.04E-04	1.17E-06	2.83E-04	7.06E-08	-0.93
3.68E-04	1.78E-05	9.92E-05	1.03E-06	2.68E-04	2.42E-07	-1.10
3.48E-04	1.78E-05	9.41E-05	1.01E-06	2.52E-04	1.92E-07	-1.48
3.28E-04	1.79E-05	8.93E-05	1.05E-06	2.37E-04	1.95E-07	-1.79
3.07E-04	1.79E-05	8.41E-05	1.16E-06	2.21E-04	1.83E-07	-2.36
2.87E-04	1.79E-05	7.87E-05	1.10E-06	2.07E-04	1.93E-07	-2.13
2.67E-04	1.79E-05	7.39E-05	1.11E-06	1.91E-04	1.84E-07	-2.49
O_{out1} = 1.60 and O_{out2} = 2.06						
5.29E-04	1.77E-05	1.37E-04	5.45E-07	3.87E-04	1.59E-07	-3.60
5.08E-04	1.78E-05	1.31E-04	8.12E-07	3.73E-04	2.57E-07	-3.65
4.89E-04	1.78E-05	1.27E-04	5.31E-07	3.57E-04	5.74E-07	-3.42
4.68E-04	1.77E-05	1.21E-04	9.19E-07	3.42E-04	1.85E-07	-4.26
4.48E-04	1.78E-05	1.16E-04	3.07E-12	3.27E-04	2.11E-07	-3.78
4.28E-04	1.75E-05	1.09E-04	5.95E-07	3.14E-04	2.22E-07	-4.00
4.08E-04	1.78E-05	1.04E-04	4.76E-07	3.00E-04	3.21E-07	-3.77
Quadratic						
Q_{in}		**Q_{out1}**		**Q_{out2}**		**Error**
Avg (kg/s)	**Stdev (kg/s)**	**Avg (kg/s)**	**Stdev (kg/s)**	**Avg (kg/s)**	**Stdev (kg/s)**	**(%)**
O_{out1} = 0.70 and O_{out2} = 0.94						
6.96E-05	8.27E-07	1.95E-05	3.47E-08	4.95E-05	5.88E-12	-3.40
6.75E-05	8.27E-07	1.89E-05	3.35E-08	4.79E-05	7.50E-08	-3.64
6.54E-05	8.27E-07	1.82E-05	3.17E-08	4.65E-05	9.30E-08	-3.67
6.33E-05	8.27E-07	1.77E-05	4.24E-08	4.50E-05	0.00E+00	-3.40
6.11E-05	8.27E-07	1.75E-05	4.54E-13	4.35E-05	4.54E-08	-0.76
5.90E-05	8.27E-07	1.66E-05	1.96E-08	4.20E-05	5.69E-08	-2.97
5.69E-05	8.27E-07	1.61E-05	2.38E-08	4.04E-05	5.12E-08	-2.95
5.48E-05	8.27E-07	1.56E-05	0.00E+00	3.89E-05	1.21E-07	-1.68
5.27E-05	8.27E-07	1.51E-05	3.02E-08	3.74E-05	2.11E-12	-1.12
5.06E-05	8.34E-07	1.46E-05	5.71E-13	3.57E-05	0.00E+00	-1.48
O_{out1} = 0.70 and O_{out2} = 1.60						
1.86E-04	1.79E-05	4.81E-05	1.63E-08	1.37E-04	8.62E-08	-1.49
1.76E-04	1.79E-05	4.69E-05	1.58E-07	1.28E-04	2.53E-07	-1.79
1.66E-04	1.79E-05	4.58E-05	1.60E-06	1.19E-04	2.69E-07	-2.72
1.55E-04	1.79E-05	4.32E-05	1.45E-07	1.10E-04	6.30E-07	-4.41
1.45E-04	1.79E-05	4.17E-05	2.36E-07	1.02E-04	0.00E+00	-4.55
1.35E-04	1.79E-05	3.89E-05	1.19E-07	9.47E-05	7.17E-07	-4.24

O_{out1} = 1.30 and O_{out2} = 2.06						
3.88E-04	1.78E-05	1.05E-04	4.98E-06	2.84E-04	3.00E-07	0.43
3.68E-04	1.78E-05	1.00E-04	4.14E-06	2.68E-04	9.36E-07	0.39
3.48E-04	1.78E-05	9.55E-05	3.80E-06	2.52E-04	6.71E-07	0.00
3.28E-04	1.79E-05	9.08E-05	3.70E-06	2.36E-04	4.92E-07	-0.49
3.07E-04	1.79E-05	8.55E-05	3.78E-06	2.21E-04	2.83E-07	-1.42
2.87E-04	1.79E-05	7.99E-05	3.28E-06	2.06E-04	4.80E-07	-1.77
2.67E-04	1.79E-05	7.49E-05	3.06E-06	1.90E-04	2.60E-07	-2.97
O_{out1} = 1.60 and O_{out2} = 2.06						
5.29E-04	1.77E-05	1.38E-04	1.82E-06	3.86E-04	1.09E-06	-3.25
5.08E-04	1.78E-05	1.32E-04	2.49E-06	3.72E-04	1.67E-06	-3.14
4.89E-04	1.78E-05	1.28E-04	1.21E-06	3.56E-04	1.22E-06	-2.73
4.68E-04	1.77E-05	1.22E-04	2.44E-06	3.42E-04	4.79E-07	-3.55
4.48E-04	1.78E-05	1.17E-04	7.68E-12	3.28E-04	1.13E-06	-3.06
4.28E-04	1.75E-05	1.10E-04	1.34E-06	3.14E-04	1.11E-06	-3.47
4.08E-04	1.78E-05	1.04E-04	9.22E-07	3.00E-04	7.69E-07	-3.47

Cubic						
Q_{in}		**Q_{out1}**		**Q_{out2}**		**Error**
Avg (kg/s)	**Stdev (kg/s)**	**Avg (kg/s)**	**Stdev (kg/s)**	**Avg (kg/s)**	**Stdev (kg/s)**	**(%)**
O_{out1} = 0.70 and O_{out2} = 0.94						
6.96E-05	8.27E-07	1.95E-05	3.39E-08	4.95E-05	5.88E-12	-3.04
6.75E-05	8.27E-07	1.89E-05	3.27E-08	4.80E-05	7.49E-08	-3.23
6.54E-05	8.27E-07	1.82E-05	3.08E-08	4.65E-05	9.29E-08	-3.17
6.33E-05	8.27E-07	1.77E-05	4.10E-08	4.50E-05	0.00E+00	-2.81
6.11E-05	8.27E-07	1.75E-05	4.38E-13	4.36E-05	4.53E-08	-0.11
5.90E-05	8.27E-07	1.66E-05	1.88E-08	4.20E-05	5.67E-08	-2.11
5.69E-05	8.27E-07	1.62E-05	2.27E-08	4.04E-05	5.10E-08	-1.94
5.48E-05	8.27E-07	1.57E-05	0.00E+00	3.90E-05	1.21E-07	-0.49
5.27E-05	8.27E-07	1.52E-05	2.86E-08	3.75E-05	2.10E-12	0.29
5.06E-05	8.34E-07	1.48E-05	5.38E-13	3.58E-05	0.00E+00	0.14
O_{out1} = 0.70 and O_{out2} = 1.60						
1.86E-04	1.79E-05	4.78E-05	1.50E-08	1.37E-04	8.27E-08	-1.90
1.76E-04	1.79E-05	4.67E-05	1.47E-07	1.28E-04	2.44E-07	-1.87
1.66E-04	1.79E-05	4.57E-05	1.50E-06	1.19E-04	2.64E-07	-2.56
1.55E-04	1.79E-05	4.32E-05	1.40E-07	1.10E-04	6.28E-07	-3.98
1.45E-04	1.79E-05	4.17E-05	2.31E-07	1.02E-04	0.00E+00	-4.11
1.35E-04	1.79E-05	3.90E-05	1.19E-07	9.48E-05	7.51E-07	-3.84
O_{out1} = 1.30 and O_{out2} = 2.06						
3.88E-04	1.78E-05	1.05E-04	5.00E-06	2.84E-04	2.99E-07	0.50
3.68E-04	1.78E-05	1.01E-04	4.16E-06	2.68E-04	9.34E-07	0.43
3.48E-04	1.78E-05	9.55E-05	3.83E-06	2.52E-04	6.69E-07	0.01
3.28E-04	1.79E-05	9.08E-05	3.72E-06	2.36E-04	4.92E-07	-0.50
3.07E-04	1.79E-05	8.55E-05	3.81E-06	2.21E-04	2.83E-07	-1.43
2.87E-04	1.79E-05	7.98E-05	3.30E-06	2.06E-04	4.81E-07	-1.76
2.67E-04	1.79E-05	7.48E-05	3.07E-06	1.90E-04	2.61E-07	-2.88
O_{out1} = 1.60 and O_{out2} = 2.06						
5.29E-04	1.77E-05	1.38E-04	1.74E-06	3.86E-04	1.10E-06	-3.23
5.08E-04	1.78E-05	1.32E-04	2.40E-06	3.72E-04	1.68E-06	-3.04
4.89E-04	1.78E-05	1.29E-04	1.17E-06	3.56E-04	1.22E-06	-2.60
4.68E-04	1.77E-05	1.22E-04	2.37E-06	3.42E-04	4.80E-07	-3.37
4.48E-04	1.78E-05	1.17E-04	7.53E-12	3.28E-04	1.13E-06	-2.86

4.28E-04	1.75E-05	1.10E-04	1.33E-06	3.14E-04	1.11E-06	-3.26
4.08E-04	1.78E-05	1.04E-04	9.35E-07	3.00E-04	7.68E-07	-3.28
Tube 4						
Linear						
Qin		**Q_{out1}**		**Q_{out2}**		**Error**
Avg (kg/s)	**Stdev (kg/s)**	**Avg (kg/s)**	**Stdev (kg/s)**	**Avg (kg/s)**	**Stdev (kg/s)**	**(%)**
O_{out1} = 0.70 and O_{out2} = 0.94						
9.53E-05	8.27E-07	4.65E-05	1.49E-07	4.67E-05	1.44E-07	-4.18
9.20E-05	8.32E-07	4.31E-05	5.27E-09	4.68E-05	2.60E-08	-4.74
8.88E-05	8.32E-07	4.15E-05	9.45E-09	4.53E-05	3.26E-08	-4.64
8.56E-05	8.27E-07	4.01E-05	7.17E-09	4.35E-05	6.72E-09	-4.64
8.24E-05	8.40E-07	3.87E-05	9.15E-09	4.19E-05	1.61E-08	-4.46
7.92E-05	8.37E-07	3.73E-05	9.77E-09	4.03E-05	1.68E-08	-4.28
7.60E-05	8.33E-07	3.59E-05	8.91E-09	3.84E-05	1.27E-08	-4.34
7.28E-05	8.27E-07	3.46E-05	3.02E-08	3.70E-05	7.78E-09	-3.27
[redacted]						
6.64E-05	8.38E-07	3.18E-05	3.87E-08	3.35E-05	1.62E-08	-3.50
6.32E-05	8.36E-07	3.06E-05	1.04E-08	3.20E-05	3.59E-08	-2.18
6.01E-05	8.27E-07	2.92E-05	9.90E-13	3.06E-05	0.00E+00	-0.88
5.69E-05	8.27E-07	2.80E-05	1.23E-08	2.91E-05	9.49E-13	0.74
5.37E-05	8.34E-07	2.67E-05	7.13E-09	2.76E-05	1.71E-08	2.21
5.06E-05	8.27E-07	2.53E-05	2.05E-08	2.55E-05	1.06E-07	1.12
4.74E-05	8.27E-07	2.41E-05	6.00E-09	2.38E-05	1.69E-08	2.08
4.43E-05	8.27E-07	2.27E-05	1.48E-08	2.18E-05	2.33E-08	0.94
4.11E-05	8.27E-07	2.17E-05	8.62E-09	2.03E-05	2.14E-08	4.31
3.80E-05	8.27E-07	2.03E-05	2.33E-08	1.85E-05	3.26E-08	4.51
O_{out1} = 1.30 and O_{out2} = 1.60						
2.67E-04	1.79E-05	1.26E-04	1.22E-07	1.43E-04	1.82E-07	1.47
2.57E-04	1.79E-05	1.21E-04	1.39E-07	1.37E-04	8.90E-07	0.51
2.47E-04	1.79E-05	1.16E-04	5.06E-08	1.30E-04	1.95E-07	-0.61
2.37E-04	1.79E-05	1.11E-04	1.29E-07	1.24E-04	2.88E-07	-1.41
2.27E-04	1.79E-05	1.05E-04	1.05E-07	1.19E-04	2.26E-07	-2.13
2.16E-04	1.79E-05	1.02E-04	5.55E-08	1.13E-04	2.28E-07	-1.73
2.06E-04	1.79E-05	9.57E-05	1.26E-07	1.07E-04	1.00E-07	-3.18
1.96E-04	1.79E-05	9.10E-05	4.37E-08	1.01E-04	3.73E-07	-4.22
1.86E-04	1.79E-05	8.64E-05	7.92E-08	9.54E-05	2.77E-07	-4.61
1.76E-04	1.79E-05	8.15E-05	9.26E-08	9.00E-05	2.14E-07	-4.97
1.66E-04	1.79E-05	7.73E-05	0.00E+00	8.41E-05	2.71E-07	-5.30
1.55E-04	1.79E-05	7.25E-05	1.35E-07	7.83E-05	1.91E-07	-5.99
O_{out1} = 1.30 and O_{out2} = 1.60						
2.29E-04	1.79E-05	1.08E-04	2.26E-07	1.22E-04	8.81E-07	1.20
2.27E-04	1.79E-05	1.07E-04	2.11E-07	1.19E-04	3.79E-07	-0.33
2.24E-04	1.79E-05	1.06E-04	2.01E-07	1.18E-04	6.47E-07	-0.35
2.22E-04	1.79E-05	1.05E-04	8.94E-08	1.17E-04	3.68E-07	-0.57
2.20E-04	1.79E-05	1.04E-04	2.12E-07	1.16E-04	4.36E-07	-0.54
2.18E-04	1.79E-05	1.03E-04	2.08E-07	1.14E-04	3.72E-07	-0.62
2.16E-04	1.79E-05	1.02E-04	2.17E-07	1.13E-04	5.13E-07	-1.05
2.14E-04	1.79E-05	1.02E-04	2.76E-08	1.12E-04	0.00E+00	-0.53
2.12E-04	1.79E-05	1.01E-04	4.31E-07	1.11E-04	5.33E-07	-0.27
2.10E-04	1.79E-05	9.95E-05	1.93E-07	1.10E-04	3.68E-07	-1.10
2.08E-04	1.79E-05	9.85E-05	2.32E-07	1.09E-04	6.27E-07	-1.10
2.06E-04	1.79E-05	9.76E-05	2.17E-07	1.07E-04	3.27E-07	-1.13

2.04E-04	1.79E-05	9.65E-05	1.75E-07	1.07E-04	2.61E-07	-0.23
2.02E-04	1.79E-05	9.55E-05	9.69E-08	1.05E-04	9.05E-07	-1.32
2.00E-04	1.79E-05	9.48E-05	5.63E-08	1.04E-04	2.39E-07	-1.46
1.98E-04	1.79E-05	9.39E-05	5.73E-08	1.03E-04	2.82E-07	-1.54
1.96E-04	1.79E-05	9.27E-05	3.03E-08	1.02E-04	1.49E-07	-1.37
1.94E-04	1.79E-05	9.17E-05	1.31E-07	1.01E-04	5.23E-12	-1.73
1.92E-04	1.79E-05	9.07E-05	1.42E-07	9.95E-05	2.61E-07	-2.09
1.90E-04	1.79E-05	8.99E-05	1.27E-07	9.80E-05	3.82E-07	-2.35
1.88E-04	1.79E-05	8.86E-05	1.16E-07	9.72E-05	4.33E-07	-2.50
1.86E-04	1.79E-05	8.85E-05	4.25E-08	9.59E-05	1.99E-07	-1.76
1.84E-04	1.79E-05	8.68E-05	8.55E-08	9.45E-05	3.41E-07	-2.86
1.82E-04	1.79E-05	8.60E-05	9.40E-08	9.44E-05	8.27E-12	-1.70
1.80E-04	1.79E-05	8.47E-05	9.04E-08	9.42E-05	4.51E-07	-1.02
1.78E-04	1.79E-05	8.42E-05	1.66E-07	9.15E-05	2.66E-07	-2.40
1.76E-04	1.80E-05	8.29E-05	1.05E-07	9.03E-05	2.03E-07	-3.04
1.74E-04	1.79E-05	8.20E-05	1.25E-07	8.96E-05	2.85E-07	-2.61
1.72E-04	1.79E-05	8.10E-05	1.14E-07	8.83E-05	1.49E-07	-2.78
1.70E-04	1.79E-05	8.02E-05	1.96E-07	8.65E-05	4.42E-07	-3.55
1.68E-04	1.79E-05	7.92E-05	1.46E-07	8.59E-05	8.45E-07	-3.10
1.66E-04	1.79E-05	7.81E-05	1.32E-07	8.44E-05	2.69E-07	-3.91
1.64E-04	1.79E-05	7.73E-05	2.52E-08	8.28E-05	4.05E-07	-4.42
1.62E-04	1.79E-05	7.73E-05	8.18E-08	8.23E-05	1.96E-07	-2.54
1.60E-04	1.79E-05	7.62E-05	1.18E-07	8.23E-05	1.63E-07	-1.50
1.58E-04	1.79E-05	7.46E-05	1.17E-07	8.03E-05	1.55E-06	-3.45
1.55E-04	1.79E-05	7.35E-05	1.30E-07	7.85E-05	1.55E-07	-4.49
O_{out1} = 2.06 and O_{out2} = 2.06						
5.19E-04	1.77E-05	2.44E-04	1.54E-06	2.72E-04	1.80E-06	-0.77
5.09E-04	1.77E-05	2.38E-04	1.22E-06	2.68E-04	1.50E-06	-1.30
4.99E-04	1.77E-05	2.34E-04	1.42E-06	2.62E-04	1.08E-06	-1.22
4.89E-04	1.77E-05	2.30E-04	1.08E-06	2.56E-04	8.36E-07	-1.33
4.79E-04	1.77E-05	2.23E-04	1.07E-06	2.53E-04	8.40E-07	-0.87
4.69E-04	1.77E-05	2.18E-04	8.95E-07	2.47E-04	8.45E-07	-1.53
4.59E-04	1.78E-05	2.13E-04	1.66E-06	2.43E-04	1.84E-06	-1.04
4.49E-04	1.78E-05	2.10E-04	1.46E-06	2.35E-04	1.48E-06	-1.38
4.39E-04	1.78E-05	2.05E-04	1.78E-07	2.32E-04	6.09E-07	-0.89
4.28E-04	1.77E-05	2.02E-04	2.28E-06	2.26E-04	1.25E-06	-0.18
4.18E-04	1.78E-05	1.95E-04	1.29E-06	2.24E-04	1.10E-06	0.10
4.08E-04	1.78E-05	1.90E-04	1.15E-06	2.17E-04	9.81E-07	-0.57
3.98E-04	1.78E-05	1.87E-04	5.62E-07	2.11E-04	5.39E-07	-0.29
3.88E-04	1.78E-05	1.79E-04	1.32E-06	2.07E-04	1.30E-06	-0.87
3.78E-04	1.78E-05	1.74E-04	1.25E-06	2.03E-04	5.87E-07	-0.37
3.68E-04	1.78E-05	1.70E-04	9.93E-07	1.98E-04	9.01E-07	-0.08
O_{out1} = 2.06 and O_{out2} = 2.06						
5.89E-04	1.75E-05	2.80E-04	7.66E-07	3.03E-04	7.72E-07	-2.01
5.87E-04	1.75E-05	2.80E-04	1.26E-06	3.01E-04	1.29E-06	-1.92
5.85E-04	1.75E-05	2.79E-04	1.28E-06	3.01E-04	1.23E-06	-1.93
5.83E-04	1.75E-05	2.77E-04	7.14E-07	3.00E-04	9.74E-07	-1.94
5.81E-04	1.76E-05	2.77E-04	5.77E-07	3.00E-04	1.13E-06	-1.61
5.79E-04	1.76E-05	2.76E-04	5.65E-07	2.98E-04	1.28E-06	-1.56
5.77E-04	1.75E-05	2.76E-04	1.74E-07	2.97E-04	1.22E-06	-1.32
5.75E-04	1.75E-05	2.76E-04	8.97E-07	2.96E-04	1.23E-06	-1.08
5.73E-04	1.75E-05	2.75E-04	1.27E-06	2.95E-04	1.46E-06	-1.02
5.71E-04	1.76E-05	2.74E-04	1.84E-06	2.94E-04	1.26E-06	-1.11

5.69E-04	1.76E-05	2.72E-04	1.83E-06	2.93E-04	1.08E-06	-1.41
5.67E-04	1.76E-05	2.70E-04	1.09E-06	2.92E-04	1.01E-06	-1.55
5.65E-04	1.76E-05	2.68E-04	1.22E-06	2.93E-04	1.55E-06	-1.55
5.63E-04	1.76E-05	2.67E-04	7.45E-07	2.91E-04	8.83E-07	-1.59
5.61E-04	1.76E-05	2.66E-04	1.13E-06	2.91E-04	1.22E-06	-1.51
5.59E-04	1.76E-05	2.65E-04	1.10E-06	2.89E-04	1.01E-06	-1.49
5.57E-04	1.76E-05	2.65E-04	9.77E-07	2.88E-04	4.10E-07	-1.23
5.55E-04	1.76E-05	2.65E-04	9.01E-07	2.87E-04	1.30E-06	-1.12
5.53E-04	1.77E-05	2.64E-04	9.70E-07	2.86E-04	1.47E-06	-1.17
5.51E-04	1.77E-05	2.62E-04	1.67E-06	2.86E-04	2.26E-06	-1.02
5.49E-04	1.76E-05	2.61E-04	7.93E-07	2.85E-04	1.40E-06	-1.05
5.47E-04	1.76E-05	2.60E-04	1.06E-06	2.83E-04	1.16E-06	-1.14
5.45E-04	1.76E-05	2.59E-04	8.37E-07	2.83E-04	1.03E-06	-1.09
5.43E-04	1.76E-05	2.59E-04	1.03E-06	2.81E-04	1.07E-06	-1.03
5.41E-04	1.76E-05	2.58E-04	9.37E-07	2.81E-04	1.17E-06	-0.83
5.39E-04	1.77E-05	2.58E-04	9.81E-07	2.79E-04	1.17E-06	-0.81
5.37E-04	1.76E-05	2.57E-04	1.16E-06	2.78E-04	1.18E-06	-0.68
5.35E-04	1.76E-05	2.56E-04	1.56E-06	2.77E-04	1.41E-06	-0.57
5.33E-04	1.77E-05	2.55E-04	1.15E-06	2.77E-04	1.10E-06	-0.55
5.31E-04	1.76E-05	2.53E-04	8.08E-07	2.77E-04	1.09E-06	-0.49
5.29E-04	1.76E-05	2.53E-04	5.34E-07	2.75E-04	6.94E-07	-0.46
5.27E-04	1.76E-05	2.52E-04	8.81E-07	2.74E-04	1.02E-06	-0.40
Quadratic						
Q_{in}		**Q_{out1}**		**Q_{out2}**		**Error**
Avg (kg/s)	**Stdev (kg/s)**	**Avg (kg/s)**	**Stdev (kg/s)**	**Avg (kg/s)**	**Stdev (kg/s)**	**(%)**
O_{out1} = 0.70 and O_{out2} = 0.94						
9.53E-05	8.27E-07	4.65E-05	1.08E-06	4.68E-05	7.54E-07	-4.14
9.20E-05	8.32E-07	4.31E-05	3.41E-08	4.68E-05	1.36E-07	-4.65
8.88E-05	8.32E-07	4.15E-05	5.78E-08	4.54E-05	1.64E-07	-4.33
8.56E-05	8.27E-07	4.01E-05	4.16E-08	4.38E-05	3.21E-08	-4.12
8.24E-05	8.40E-07	3.87E-05	5.03E-08	4.22E-05	7.28E-08	-3.76
7.92E-05	8.37E-07	3.73E-05	5.07E-08	4.06E-05	7.19E-08	-3.44
7.60E-05	8.33E-07	3.59E-05	4.36E-08	3.88E-05	5.10E-08	-3.40
7.28E-05	8.27E-07	3.46E-05	1.40E-07	3.74E-05	2.97E-08	-2.26
[redacted]						
6.64E-05	8.38E-07	3.18E-05	1.57E-07	3.38E-05	5.33E-08	-2.53
6.32E-05	8.36E-07	3.06E-05	3.96E-08	3.23E-05	1.10E-07	-1.29
6.01E-05	8.27E-07	2.93E-05	3.51E-12	3.08E-05	0.00E+00	-0.11
5.69E-05	8.27E-07	2.80E-05	4.05E-08	2.92E-05	2.53E-12	1.30
5.37E-05	8.34E-07	2.67E-05	2.18E-08	2.76E-05	4.19E-08	2.45
5.06E-05	8.27E-07	2.54E-05	5.78E-08	2.54E-05	2.32E-07	0.77
4.74E-05	8.27E-07	2.42E-05	1.56E-08	2.35E-05	3.34E-08	1.07
4.43E-05	8.27E-07	2.27E-05	3.51E-08	2.14E-05	4.08E-08	-0.94
4.11E-05	8.27E-07	2.17E-05	1.90E-08	1.97E-05	3.42E-08	1.44
3.80E-05	8.27E-07	2.03E-05	4.65E-08	1.77E-05	4.69E-08	0.35
O_{out1} = 1.30 and O_{out2} = 1.60						
2.67E-04	1.79E-05	1.25E-04	6.39E-07	1.44E-04	6.55E-07	2.14
2.57E-04	1.79E-05	1.21E-04	6.98E-07	1.38E-04	2.96E-06	1.61
2.47E-04	1.79E-05	1.16E-04	2.44E-07	1.32E-04	5.95E-07	0.80
2.37E-04	1.79E-05	1.11E-04	5.90E-07	1.25E-04	8.07E-07	0.23
2.27E-04	1.79E-05	1.07E-04	4.55E-07	1.20E-04	5.85E-07	-0.35
2.16E-04	1.79E-05	1.03E-04	2.30E-07	1.14E-04	5.39E-07	0.03

2.06E-04	1.79E-05	9.71E-05	4.87E-07	1.08E-04	2.18E-07	-1.49
1.96E-04	1.79E-05	9.25E-05	1.58E-07	1.01E-04	7.29E-07	-2.84
1.86E-04	1.79E-05	8.78E-05	2.67E-07	9.48E-05	4.92E-07	-3.63
1.76E-04	1.79E-05	8.28E-05	2.90E-07	8.91E-05	3.47E-07	-4.53
1.66E-04	1.79E-05	7.85E-05	0.00E+00	8.26E-05	3.97E-07	-5.63
1.55E-04	1.79E-05	7.34E-05	3.62E-07	7.63E-05	2.53E-07	-7.31
O_{out1} = 1.30 and O_{out2} = 1.60						
2.29E-04	1.79E-05	1.09E-04	5.18E-07	1.22E-04	2.17E-06	2.99
2.27E-04	1.79E-05	1.08E-04	3.53E-07	1.20E-04	3.54E-07	1.38
2.24E-04	1.79E-05	1.07E-04	2.60E-07	1.19E-04	1.39E-06	1.40
2.22E-04	1.79E-05	1.06E-04	3.19E-07	1.17E-04	8.94E-07	1.19
2.20E-04	1.79E-05	1.05E-04	3.67E-07	1.16E-04	6.43E-07	1.22
2.18E-04	1.79E-05	1.04E-04	4.82E-07	1.15E-04	4.90E-07	1.15
2.16E-04	1.79E-05	1.04E-04	4.38E-07	1.14E-04	9.11E-07	0.70
2.14E-04	1.79E-05	1.03E-04	1.15E-07	1.13E-04	0.00E+00	1.21
2.12E-04	1.79E-05	1.02E-04	1.61E-06	1.11E-04	9.73E-07	1.45
2.10E-04	1.79E-05	1.01E-04	5.00E-07	1.10E-04	5.82E-07	0.62
2.08E-04	1.79E-05	9.98E-05	5.84E-07	1.09E-04	1.20E-06	0.61
2.06E-04	1.79E-05	9.90E-05	5.26E-07	1.08E-04	2.74E-07	0.54
2.04E-04	1.79E-05	9.79E-05	4.74E-07	1.08E-04	2.92E-07	1.50
2.02E-04	1.79E-05	9.69E-05	3.73E-07	1.06E-04	1.90E-06	0.29
2.00E-04	1.79E-05	9.62E-05	1.50E-07	1.04E-04	4.70E-07	0.09
1.98E-04	1.79E-05	9.53E-05	2.16E-07	1.03E-04	5.69E-07	-0.04
1.96E-04	1.79E-05	9.41E-05	1.12E-07	1.02E-04	2.97E-07	0.10
1.94E-04	1.79E-05	9.32E-05	4.80E-07	1.01E-04	1.02E-11	-0.34
1.92E-04	1.79E-05	9.21E-05	4.91E-07	9.93E-05	4.83E-07	-0.78
1.90E-04	1.79E-05	9.13E-05	4.51E-07	9.77E-05	7.11E-07	-1.14
1.88E-04	1.79E-05	9.00E-05	4.06E-07	9.68E-05	7.95E-07	-1.36
1.86E-04	1.79E-05	8.99E-05	1.33E-07	9.54E-05	3.53E-07	-0.71
1.84E-04	1.79E-05	8.82E-05	2.92E-07	9.39E-05	5.98E-07	-1.93
1.82E-04	1.79E-05	8.74E-05	3.16E-07	9.38E-05	1.45E-11	-0.78
1.80E-04	1.79E-05	8.61E-05	2.74E-07	9.36E-05	7.80E-07	-0.14
1.78E-04	1.79E-05	8.56E-05	5.41E-07	9.07E-05	4.40E-07	-1.76
1.76E-04	1.80E-05	8.42E-05	3.38E-07	8.94E-05	3.31E-07	-2.55
1.74E-04	1.79E-05	8.33E-05	3.65E-07	8.86E-05	4.41E-07	-2.21
1.72E-04	1.79E-05	8.23E-05	3.55E-07	8.72E-05	2.35E-07	-2.53
1.70E-04	1.79E-05	8.15E-05	5.69E-07	8.53E-05	6.57E-07	-3.50
1.68E-04	1.79E-05	8.04E-05	3.84E-07	8.46E-05	1.27E-06	-3.18
1.66E-04	1.79E-05	7.93E-05	3.42E-07	8.29E-05	3.66E-07	-4.19
1.64E-04	1.79E-05	7.84E-05	2.11E-08	8.12E-05	5.78E-07	-4.91
1.62E-04	1.79E-05	7.84E-05	1.21E-07	8.07E-05	2.33E-07	-3.12
1.60E-04	1.79E-05	7.73E-05	3.34E-07	8.07E-05	2.27E-07	-2.18
1.58E-04	1.79E-05	7.56E-05	3.17E-07	7.85E-05	2.12E-06	-4.44
1.55E-04	1.79E-05	7.44E-05	3.23E-07	7.65E-05	1.74E-07	-5.75
O_{out1} = 2.06 and O_{out2} = 2.06						
5.19E-04	1.77E-05	2.44E-04	5.03E-06	2.73E-04	6.82E-06	-0.53
5.09E-04	1.77E-05	2.38E-04	3.69E-06	2.68E-04	5.37E-06	-1.12
4.99E-04	1.77E-05	2.33E-04	4.36E-06	2.63E-04	3.88E-06	-1.07
4.89E-04	1.77E-05	2.29E-04	3.23E-06	2.57E-04	2.89E-06	-1.22
4.79E-04	1.77E-05	2.23E-04	3.03E-06	2.54E-04	2.85E-06	-0.83
4.69E-04	1.77E-05	2.18E-04	2.44E-06	2.47E-04	2.75E-06	-1.56
4.59E-04	1.78E-05	2.12E-04	4.33E-06	2.44E-04	5.84E-06	-1.14
4.49E-04	1.78E-05	2.09E-04	3.74E-06	2.36E-04	4.45E-06	-1.57

4.39E-04	1.78E-05	2.04E-04	4.37E-07	2.32E-04	1.78E-06	-1.17
4.28E-04	1.77E-05	2.01E-04	5.45E-06	2.26E-04	3.49E-06	-0.55
4.18E-04	1.78E-05	1.94E-04	2.91E-06	2.24E-04	3.02E-06	-0.40
4.08E-04	1.78E-05	1.88E-04	2.47E-06	2.17E-04	2.58E-06	-1.23
3.98E-04	1.78E-05	1.86E-04	1.18E-06	2.11E-04	1.34E-06	-1.08
3.88E-04	1.78E-05	1.77E-04	2.58E-06	2.07E-04	3.16E-06	-1.87
3.78E-04	1.78E-05	1.72E-04	2.33E-06	2.03E-04	1.38E-06	-1.55
3.68E-04	1.78E-05	1.68E-04	1.78E-06	1.98E-04	2.03E-06	-1.47
O_{out1} = 2.06 and O_{out2} = 2.06						
5.89E-04	1.75E-05	2.80E-04	3.19E-06	3.04E-04	3.55E-06	-1.72
5.87E-04	1.75E-05	2.80E-04	5.03E-06	3.02E-04	5.60E-06	-1.63
5.85E-04	1.75E-05	2.79E-04	5.31E-06	3.01E-04	5.57E-06	-1.64
5.83E-04	1.75E-05	2.77E-04	2.77E-06	3.01E-04	4.26E-06	-1.65
5.81E-04	1.76E-05	2.77E-04	2.19E-06	3.00E-04	5.00E-06	-1.31
5.79E-04	1.76E-05	2.77E-04	2.13E-06	2.99E-04	5.63E-06	-1.25
5.77E-04	1.75E-05	2.76E-04	5.68E-07	2.98E-04	5.37E-06	-1.01
5.75E-04	1.75E-05	2.76E-04	3.25E-06	2.97E-04	5.11E-06	-0.77
5.73E-04	1.75E-05	2.75E-04	4.97E-06	2.95E-04	6.21E-06	-0.71
5.71E-04	1.76E-05	2.74E-04	7.39E-06	2.94E-04	5.51E-06	-0.80
5.69E-04	1.76E-05	2.72E-04	7.22E-06	2.94E-04	4.60E-06	-1.10
5.67E-04	1.76E-05	2.70E-04	4.18E-06	2.93E-04	4.26E-06	-1.25
5.65E-04	1.76E-05	2.68E-04	4.65E-06	2.93E-04	6.65E-06	-1.25
5.63E-04	1.76E-05	2.67E-04	2.88E-06	2.92E-04	3.80E-06	-1.29
5.61E-04	1.76E-05	2.66E-04	4.33E-06	2.91E-04	5.22E-06	-1.21
5.59E-04	1.76E-05	2.65E-04	4.19E-06	2.90E-04	4.31E-06	-1.19
5.57E-04	1.76E-05	2.65E-04	3.63E-06	2.89E-04	1.44E-06	-0.93
5.55E-04	1.76E-05	2.65E-04	3.42E-06	2.88E-04	5.45E-06	-0.81
5.53E-04	1.77E-05	2.64E-04	3.58E-06	2.87E-04	6.06E-06	-0.86
5.51E-04	1.77E-05	2.62E-04	6.24E-06	2.87E-04	9.44E-06	-0.71
5.49E-04	1.76E-05	2.61E-04	2.94E-06	2.86E-04	5.84E-06	-0.75
5.47E-04	1.76E-05	2.60E-04	3.88E-06	2.84E-04	4.72E-06	-0.84
5.45E-04	1.76E-05	2.59E-04	3.06E-06	2.84E-04	4.22E-06	-0.79
5.43E-04	1.76E-05	2.59E-04	3.72E-06	2.82E-04	4.25E-06	-0.74
5.41E-04	1.76E-05	2.58E-04	3.34E-06	2.81E-04	4.67E-06	-0.53
5.39E-04	1.77E-05	2.58E-04	3.56E-06	2.80E-04	4.68E-06	-0.51
5.37E-04	1.76E-05	2.57E-04	4.19E-06	2.79E-04	4.69E-06	-0.39
5.35E-04	1.76E-05	2.56E-04	5.59E-06	2.78E-04	5.57E-06	-0.28
5.33E-04	1.77E-05	2.55E-04	4.11E-06	2.77E-04	4.36E-06	-0.27
5.31E-04	1.76E-05	2.53E-04	2.75E-06	2.78E-04	4.25E-06	-0.21
5.29E-04	1.76E-05	2.53E-04	1.77E-06	2.75E-04	2.60E-06	-0.18
5.27E-04	1.76E-05	2.52E-04	3.03E-06	2.74E-04	3.89E-06	-0.12
Cubic						
Q_{in}		**Q_{out1}**		**Q_{out2}**		**Error**
Avg (kg/s)	**Stdev (kg/s)**	**Avg (kg/s)**	**Stdev (kg/s)**	**Avg (kg/s)**	**Stdev (kg/s)**	**(%)**
O_{out1} = 0.70 and O_{out2} = 0.94						
9.53E-05	8.27E-07	4.63E-05	1.01E-06	4.68E-05	7.54E-07	-4.56
9.20E-05	8.32E-07	4.31E-05	3.29E-08	4.68E-05	1.36E-07	-4.73
8.88E-05	8.32E-07	4.15E-05	5.65E-08	4.54E-05	1.64E-07	-4.30
8.56E-05	8.27E-07	4.02E-05	4.10E-08	4.38E-05	3.20E-08	-4.03
8.24E-05	8.40E-07	3.88E-05	5.00E-08	4.22E-05	7.27E-08	-3.63
7.92E-05	8.37E-07	3.73E-05	5.07E-08	4.06E-05	7.18E-08	-3.28
7.60E-05	8.33E-07	3.60E-05	4.39E-08	3.88E-05	5.09E-08	-3.24

7.28E-05	8.27E-07	3.47E-05	1.41E-07	3.74E-05	2.96E-08	-2.11
[redacted]						
6.64E-05	8.38E-07	3.18E-05	1.59E-07	3.38E-05	5.32E-08	-2.44
6.32E-05	8.36E-07	3.06E-05	4.02E-08	3.23E-05	1.10E-07	-1.25
6.01E-05	8.27E-07	2.92E-05	3.56E-12	3.08E-05	0.00E+00	-0.13
5.69E-05	8.27E-07	2.80E-05	4.10E-08	2.93E-05	2.53E-12	1.22
5.37E-05	8.34E-07	2.67E-05	2.20E-08	2.76E-05	4.19E-08	2.31
5.06E-05	8.27E-07	2.53E-05	5.82E-08	2.54E-05	2.32E-07	0.56
4.74E-05	8.27E-07	2.41E-05	1.57E-08	2.35E-05	3.35E-08	0.80
4.43E-05	8.27E-07	2.26E-05	3.50E-08	2.13E-05	4.10E-08	-1.27
4.11E-05	8.27E-07	2.16E-05	1.89E-08	1.97E-05	3.44E-08	1.08
3.80E-05	8.27E-07	2.03E-05	4.58E-08	1.77E-05	4.73E-08	-0.02
O_{out1} = 1.30 and O_{out2} = 1.60						
2.67E-04	1.79E-05	1.25E-04	6.32E-07	1.44E-04	6.29E-07	2.23
2.57E-04	1.79E-05	1.21E-04	6.94E-07	1.38E-04	2.84E-06	1.78
2.47E-04	1.79E-05	1.16E-04	2.43E-07	1.32E-04	5.72E-07	1.04
2.37E-04	1.79E-05	1.12E-04	5.92E-07	1.26E-04	7.81E-07	0.51
2.27E-04	1.79E-05	1.07E-04	4.57E-07	1.20E-04	5.71E-07	-0.05
2.16E-04	1.79E-05	1.03E-04	2.32E-07	1.14E-04	5.33E-07	0.33
2.06E-04	1.79E-05	9.72E-05	4.91E-07	1.08E-04	2.19E-07	-1.23
1.96E-04	1.79E-05	9.25E-05	1.59E-07	1.01E-04	7.47E-07	-2.65
1.86E-04	1.79E-05	8.77E-05	2.69E-07	9.50E-05	5.15E-07	-3.54
1.76E-04	1.79E-05	8.27E-05	2.92E-07	8.91E-05	3.71E-07	-4.58
1.66E-04	1.79E-05	7.84E-05	0.00E+00	8.25E-05	4.36E-07	-5.86
1.55E-04	1.79E-05	7.33E-05	3.63E-07	7.60E-05	2.87E-07	-7.78
O_{out1} = 1.30 and O_{out2} = 1.60						
2.29E-04	1.79E-05	1.09E-04	5.20E-07	1.23E-04	2.11E-06	3.29
2.27E-04	1.79E-05	1.08E-04	3.54E-07	1.20E-04	3.46E-07	1.69
2.24E-04	1.79E-05	1.07E-04	2.62E-07	1.19E-04	1.36E-06	1.71
2.22E-04	1.79E-05	1.06E-04	3.21E-07	1.18E-04	8.76E-07	1.50
2.20E-04	1.79E-05	1.06E-04	3.69E-07	1.16E-04	6.32E-07	1.53
2.18E-04	1.79E-05	1.04E-04	4.84E-07	1.15E-04	4.83E-07	1.46
2.16E-04	1.79E-05	1.04E-04	4.41E-07	1.14E-04	9.01E-07	1.01
2.14E-04	1.79E-05	1.03E-04	1.16E-07	1.13E-04	0.00E+00	1.51
2.12E-04	1.79E-05	1.03E-04	1.62E-06	1.12E-04	9.67E-07	1.75
2.10E-04	1.79E-05	1.01E-04	5.03E-07	1.10E-04	5.80E-07	0.91
2.08E-04	1.79E-05	9.99E-05	5.88E-07	1.09E-04	1.20E-06	0.89
2.06E-04	1.79E-05	9.90E-05	5.29E-07	1.08E-04	2.75E-07	0.81
2.04E-04	1.79E-05	9.80E-05	4.78E-07	1.08E-04	2.94E-07	1.77
2.02E-04	1.79E-05	9.69E-05	3.76E-07	1.06E-04	1.92E-06	0.55
2.00E-04	1.79E-05	9.63E-05	1.51E-07	1.04E-04	4.76E-07	0.33
1.98E-04	1.79E-05	9.53E-05	2.17E-07	1.03E-04	5.79E-07	0.18
1.96E-04	1.79E-05	9.41E-05	1.13E-07	1.02E-04	3.03E-07	0.31
1.94E-04	1.79E-05	9.32E-05	4.83E-07	1.01E-04	1.05E-11	-0.14
1.92E-04	1.79E-05	9.21E-05	4.95E-07	9.94E-05	4.97E-07	-0.61
1.90E-04	1.79E-05	9.13E-05	4.55E-07	9.78E-05	7.37E-07	-1.00
1.88E-04	1.79E-05	9.00E-05	4.09E-07	9.69E-05	8.26E-07	-1.23
1.86E-04	1.79E-05	8.99E-05	1.34E-07	9.55E-05	3.69E-07	-0.60
1.84E-04	1.79E-05	8.82E-05	2.94E-07	9.40E-05	6.28E-07	-1.86
1.82E-04	1.79E-05	8.74E-05	3.18E-07	9.39E-05	1.52E-11	-0.71
1.80E-04	1.79E-05	8.61E-05	2.75E-07	9.37E-05	8.20E-07	-0.08
1.78E-04	1.79E-05	8.55E-05	5.44E-07	9.07E-05	4.68E-07	-1.76
1.76E-04	1.80E-05	8.42E-05	3.40E-07	8.94E-05	3.54E-07	-2.58

1.74E-04	1.79E-05	8.32E-05	3.67E-07	8.86E-05	4.73E-07	-2.27
1.72E-04	1.79E-05	8.23E-05	3.57E-07	8.72E-05	2.53E-07	-2.63
1.70E-04	1.79E-05	8.14E-05	5.72E-07	8.52E-05	7.15E-07	-3.65
1.68E-04	1.79E-05	8.03E-05	3.86E-07	8.45E-05	1.38E-06	-3.35
1.66E-04	1.79E-05	7.92E-05	3.44E-07	8.28E-05	4.02E-07	-4.41
1.64E-04	1.79E-05	7.83E-05	2.12E-08	8.10E-05	6.40E-07	-5.19
1.62E-04	1.79E-05	7.83E-05	1.21E-07	8.05E-05	2.59E-07	-3.43
1.60E-04	1.79E-05	7.72E-05	3.35E-07	8.05E-05	2.52E-07	-2.50
1.58E-04	1.79E-05	7.55E-05	3.18E-07	7.82E-05	2.38E-06	-4.84
1.55E-04	1.79E-05	7.43E-05	3.24E-07	7.62E-05	1.97E-07	-6.22
O_{out1} = 2.06 and O_{out2} = 2.06						
5.19E-04	1.77E-05	2.44E-04	5.02E-06	2.73E-04	6.83E-06	-0.53
5.09E-04	1.77E-05	2.38E-04	3.68E-06	2.68E-04	5.38E-06	-1.10
4.99E-04	1.77E-05	2.33E-04	4.36E-06	2.63E-04	3.88E-06	-1.05
4.89E-04	1.77E-05	2.29E-04	3.23E-06	2.57E-04	2.89E-06	-1.19
4.79E-04	1.77E-05	2.23E-04	3.03E-06	2.54E-04	2.86E-06	-0.79
4.69E-04	1.77E-05	2.18E-04	2.44E-06	2.47E-04	2.75E-06	-1.51
4.59E-04	1.78E-05	2.12E-04	4.33E-06	2.44E-04	5.84E-06	-1.08
4.49E-04	1.78E-05	2.09E-04	3.75E-06	2.36E-04	4.45E-06	-1.50
4.39E-04	1.78E-05	2.04E-04	4.38E-07	2.32E-04	1.79E-06	-1.08
4.28E-04	1.77E-05	2.01E-04	5.46E-06	2.26E-04	3.50E-06	-0.45
4.18E-04	1.78E-05	1.94E-04	2.92E-06	2.24E-04	3.03E-06	-0.28
4.08E-04	1.78E-05	1.89E-04	2.48E-06	2.18E-04	2.58E-06	-1.10
3.98E-04	1.78E-05	1.86E-04	1.19E-06	2.11E-04	1.34E-06	-0.94
3.88E-04	1.78E-05	1.78E-04	2.59E-06	2.07E-04	3.16E-06	-1.69
3.78E-04	1.78E-05	1.73E-04	2.35E-06	2.03E-04	1.38E-06	-1.36
3.68E-04	1.78E-05	1.68E-04	1.79E-06	1.98E-04	2.02E-06	-1.25
O_{out1} = 2.06 and O_{out2} = 2.06						
5.89E-04	1.75E-05	2.80E-04	3.18E-06	3.04E-04	3.55E-06	-1.74
5.87E-04	1.75E-05	2.80E-04	5.02E-06	3.02E-04	5.61E-06	-1.65
5.85E-04	1.75E-05	2.79E-04	5.29E-06	3.01E-04	5.57E-06	-1.66
5.83E-04	1.75E-05	2.77E-04	2.76E-06	3.01E-04	4.26E-06	-1.67
5.81E-04	1.76E-05	2.77E-04	2.18E-06	3.00E-04	5.00E-06	-1.33
5.79E-04	1.76E-05	2.77E-04	2.13E-06	2.99E-04	5.64E-06	-1.28
5.77E-04	1.75E-05	2.76E-04	5.66E-07	2.98E-04	5.37E-06	-1.03
5.75E-04	1.75E-05	2.76E-04	3.24E-06	2.97E-04	5.11E-06	-0.79
5.73E-04	1.75E-05	2.75E-04	4.96E-06	2.95E-04	6.22E-06	-0.73
5.71E-04	1.76E-05	2.74E-04	7.37E-06	2.94E-04	5.51E-06	-0.81
5.69E-04	1.76E-05	2.72E-04	7.20E-06	2.94E-04	4.60E-06	-1.12
5.67E-04	1.76E-05	2.70E-04	4.17E-06	2.93E-04	4.26E-06	-1.26
5.65E-04	1.76E-05	2.68E-04	4.64E-06	2.93E-04	6.65E-06	-1.27
5.63E-04	1.76E-05	2.67E-04	2.87E-06	2.92E-04	3.80E-06	-1.31
5.61E-04	1.76E-05	2.66E-04	4.32E-06	2.91E-04	5.23E-06	-1.22
5.59E-04	1.76E-05	2.65E-04	4.18E-06	2.90E-04	4.31E-06	-1.21
5.57E-04	1.76E-05	2.65E-04	3.63E-06	2.89E-04	1.44E-06	-0.94
5.55E-04	1.76E-05	2.65E-04	3.41E-06	2.88E-04	5.46E-06	-0.83
5.53E-04	1.77E-05	2.64E-04	3.58E-06	2.87E-04	6.07E-06	-0.88
5.51E-04	1.77E-05	2.62E-04	6.23E-06	2.87E-04	9.45E-06	-0.73
5.49E-04	1.76E-05	2.61E-04	2.93E-06	2.86E-04	5.85E-06	-0.76
5.47E-04	1.76E-05	2.60E-04	3.87E-06	2.84E-04	4.72E-06	-0.85
5.45E-04	1.76E-05	2.59E-04	3.05E-06	2.84E-04	4.23E-06	-0.80
5.43E-04	1.76E-05	2.59E-04	3.71E-06	2.82E-04	4.26E-06	-0.75
5.41E-04	1.76E-05	2.58E-04	3.33E-06	2.81E-04	4.68E-06	-0.54

5.39E-04	1.77E-05	2.58E-04	3.55E-06	2.80E-04	4.69E-06	-0.52
5.37E-04	1.76E-05	2.57E-04	4.18E-06	2.79E-04	4.70E-06	-0.39
5.35E-04	1.76E-05	2.56E-04	5.57E-06	2.78E-04	5.57E-06	-0.29
5.33E-04	1.77E-05	2.55E-04	4.10E-06	2.77E-04	4.37E-06	-0.27
5.31E-04	1.76E-05	2.53E-04	2.75E-06	2.78E-04	4.25E-06	-0.21
5.29E-04	1.76E-05	2.53E-04	1.76E-06	2.75E-04	2.60E-06	-0.18
5.27E-04	1.76E-05	2.52E-04	3.02E-06	2.74E-04	3.90E-06	-0.12

Table 3

t-Test: Two-Sample Assuming Unequal Variances				t-Test: Two-Sample Assuming Unequal Variances		
	Variable 1	Variable 2			Variable 1	Variable 2
Mean	-3.30	-2.43		Mean	-2.43	-2.07
Variance	1.18	1.97		Variance	1.97	2.09
Observations	30	30		Observations	30	30
Hypothesized Mean Difference 0				Hypothesized Mean Difference 0		
df	55			df	58	
t Stat	**-2.70**			**t Stat**	**-0.98**	
P(T<=t) one-tail	0.00464			P(T<=t) one-tail	0.16666	
t Critical one-tail	1.67			t Critical one-tail	1.67	
P(T<=t) two-tail	0.0093			P(T<=t) two-tail	0.3333	
t Critical two-tail	**2.00**			**t Critical two-tail**	**2.00**	
Reject Hypothesis (|t Stat|>t critical, is true) Mean bias calculated from linear and quadratic equations are significant different				**Accept Hypothesis (|t Stat|>t critical is false) Mean bias calculated from quadratic and linear equations are not significant different**		

Table 4

z-Test: Two Sample for Means				z-Test: Two Sample for Means		
	Variable 1	Variable 2			Variable 1	Variable 2
Mean	-1.42	-0.97		Mean	-0.97	-0.93
Known Variance	2.69	2.71		Known Variance	2.71	3.01
Observations	113	113		Observations	113	113
Hypothesized Mean Difference 0				Hypothesized Mean Difference 0		
z	**-2.02**			**z**	**-0.19**	
P(Z<=z) one-tail	0.0219			P(Z<=z) one-tail	0.42434	
z Critical one-tail	**1.64**			**z Critical one-tail**	**1.64**	
P(Z<=z) two-tail	0.04382			P(Z<=z) two-tail	0.84869	
Reject Hypothesis (|z Stat|>z critical, is true) Mean bias calculated from linear and quadratic equations are significant different				**Accept Hypothesis (|z Stat|>z critical is false) Mean bias calculated from quadratic and linear equations are not significant different**		

Table F.19: Modeling data.

Parameter	1.30-X	1.30-L	1.30-B	0.94-X	0.94-B
Results from a non-linear fitting					
BK (Pa)	946	1774	759	1771	1940
C_e (kg/Pa)	2.44E-02	1.46E-02	2.05E-02	9.89E-03	9.94E-03
τ_p (s)	41.05	68.40	48.69	101.10	100.60
Results from model Equation 4.59					
H_l-H_p (m)	1.0				
ρ (kg/m^3)	1.35				
V (m^3)	2.28E-03				
A (m^2)	4.56E-03				
γ	1.40				
P (Pa)	1.06E+05				
ρ_{bulk} (kg/m^3)	8.80E+02			9.40E+02	
C_e (kg/Pa)	7.35E-07	7.35E-07	7.35E-07	6.90E-07	6.90E-07
P_s-P_{atm} (Pa)	1451.29	2647.62	1500.32	3549.77	4285.22
P_{final}-P_{atm} (Pa)	2519.16	4149.90	2302.45	5323.68	6275.84
R_s (Pa$^{0.5}$s/kg)	7.42E+05	9.29E+05	6.75E+05	1.35E+06	1.25E+06
τ_p (s)	41.61	70.31	38.44	111.32	112.64
K_p (Pa)	5.66E+07	1.91E+08	1.05E+08	3.23E+08	3.27E+08
B	1.89E-05	7.86E-06	7.67E-06	5.50E-06	6.10E-06
BK_p (Pa)	1068	1502	802	1774	1991

Table F.20: Modeling data.

Results from sensor 1 design							
H_l-H_p (m)	1.00						
ρ_{air}(kg/m^3)	1.35						
V (m^3)	2.28E-03						
A (m^2)	4.56E-03						
γ	1.40						
P (Pa)	107205						
ρ_{bulk}(kg/m^3)	1200						
C_e (kg/Pa)	5.45E-07						
P_s-P_{atm} (Pa)	1372.84						
P_{final}-P_{atm} (Pa)	2941.80						
Orifices (mm)	0.70	0.94	1.00	1.30	1.60	1.80	2.06

R_s ($Pa^{0.5}s/kg$)	2.29E+06	1.35E+06	1.17E+06	5.98E+05	4.73E+05	2.49E+05	2.65E+05
τ_p(s)	92.60	54.69	47.37	24.13	19.08	10.07	10.70
$4\tau_p$(s)	370	219	189	**97**	76	40	43
K (Pa)	1.70E+08	1.00E+08	8.69E+07	4.43E+07	3.50E+07	1.85E+07	1.96E+07
B	9.23E-06	1.56E-05	1.80E-05	3.54E-05	4.48E-05	8.49E-05	7.99E-05
BK (Pa)	1569	1569	1569	1569	1569	1569	1569
J_g STD (cm/s)	0.28	0.47	0.55	**1.07**	1.36	2.57	2.42
Results from sensor 2 and 3 design							
H_l-H_p (m)	1.00						
ρ (kg/m^3)	1.35						
V (m^3)	1.01E-03						
A sensor 2 (m^2)	2.03E-03						
A sensor 3 (m^2)	4.56E-03						
	1.40						
P (Pa)	107205						
ρ_{bulk}(kg/m^3)	1200						
C_e (kg/Pa)	2.42E-07						
P_s-P_{atm} (Pa)	1372.84						
P_{final}-P_{atm} (Pa)	2941.80						
Orifices (mm)	0.70	0.94	1.00	1.30	1.60	1.80	2.06
R_s ($Pa^{0.5}s/kg$)	2.29E+06	1.35E+06	1.17E+06	5.98E+05	4.73E+05	2.49E+05	2.65E+05
τ_p (s)	41.15	24.31	21.05	10.73	8.48	4.48	4.76
$4\tau_p$ (s)	165	**97**	84	**43**	34	18	19
K_p (Pa)	1.70E+08	1.00E+08	8.69E+07	4.43E+07	3.50E+07	1.85E+07	1.96E+07
B	9.23E-06	1.56E-05	1.80E-05	3.54E-05	4.48E-05	8.49E-05	7.99E-05
BK_p (Pa)	1569	1569	1569	1569	1569	1569	1569
J_g STD Sensor 2 (cm/s)	0.63	1.07	1.23	2.42	3.06	5.79	5.45
J_g STD Sensor 3 (cm/s)	0.28	0.47	0.55	**1.07**	1.36	2.57	2.42

Table F.21: Mapping.

Location		**J_g STD (cm/s)**	
	Nominally	**Avg**	**Stdev**
W	**1**	1.03	0.013
W-C	**2**	1.09	0.013
C	**3**	1.10	0.012
C-W	**4**	1.08	0.011
W	**5**	1.07	0.007

t-Test: Two-Sample Assuming Equal Variances			
	Variable 1	Variable 2	
Mean	1.02	1.10	
Variance	2.33E-04	1.46E-04	
Observations	901	701	
Pooled Variance	1.95E-04		
Hypothesized Mean Difference	0		
df	1600		
t Stat	-103.95		
P(T<=t) one-tail	0		
t Critical one tail	1.65		
P(T<=t) two tail			
t Critical two tail	1.96		
Reject Hypothesis (|t Stat|>t critical, is true) Mean bias calculated from wall and center are significant different.			

Table F.22: Sampling.

Continuous J_g sensor													
Location	A (cm^2)	P (cm Water)		P (kPa)		ρ (kg/m^3)		$\sqrt{\frac{\Delta P}{\rho}}$ $(kPa/kg/m^3)^{0.5}$		Orif (mm)	J_g STD (cm/s)	J_g (cm/s) at 78 cm depth and 292.15 (K)	
		Avg	Stdev	Avg	Stdev	Avg	Stdev	Avg	Stdev		Avg	Avg	Stdev
Gas delivered $J_{g\ STD}$=1.75 (cm/s)													
4W	81.07	68.11	0.74	6.68	0.07	1.28	0.01	2.28	0.02	1.60	1.67	1.67	0.02
4C	81.07	64.07	0.95	6.28	0.09	1.28	0.01	2.22	0.03	1.60	1.62	1.62	0.02
3W	45.60	56.84	1.21	5.57	0.12	1.27	0.01	2.10	0.03	1.30	1.73	1.73	0.03
3C	45.60	53.00	1.01	5.20	0.10	1.26	0.01	2.03	0.03	1.30	1.67	1.66	0.03
2W	20.27	35.36	1.37	3.47	0.13	1.24	0.01	1.67	0.04	1.00	1.88	1.88	0.06
2C	20.27	24.73	0.94	2.43	0.09	1.23	0.01	1.40	0.03	1.00	1.53	1.53	0.05
Gas delivered $J_{g\ STD}$ =0.75 (cm/s)													
4W	81.07	25.18	1.10	2.47	0.11	1.23	0.01	1.42	0.04	1.30	0.62	0.62	0.02
4C	81.07	37.99	0.79	3.73	0.08	1.25	0.01	1.73	0.03	1.30	0.78	0.78	0.01
3W	45.60	71.76	0.74	7.04	0.07	1.29	0.01	2.34	0.02	0.94	0.75	0.75	0.01
3C	45.60	49.01	0.91	4.81	0.09	1.26	0.01	1.95	0.03	0.94	0.62	0.62	0.01
2W	20.27	25.75	0.88	2.53	0.09	1.23	0.01	1.43	0.03	0.70	0.81	0.81	0.02
2C	20.27	23.81	0.56	2.33	0.06	1.23	0.01	1.38	0.02	0.70	0.78	0.77	0.02

On-off sensor												
Gas delivered J_g =1.75 (cm/s), J_g (cm/s) measured at 78 (cm) depth, 292.15 (K)												
Jg	1	2	3	4	5	6	7	8	9	10	Avg	Stdev
4W	1.78	1.79	1.73	1.61	1.66	1.76	1.68	1.67	1.66	1.70	1.70	0.06
4C	1.60	1.60	1.67	1.56	1.66	1.59	1.58	1.61	1.59	1.66	1.61	0.04
3W	1.64	1.59	1.66	1.64	1.64	1.64	1.69	1.69	1.61	1.65	1.65	0.03
3C	1.57	1.63	1.63	1.65	1.62	1.65	1.62	1.56	1.63	1.65	1.62	0.03
2W	1.71	1.70	1.57	1.67	1.62	1.68	1.65	1.61	1.67	1.54	1.64	0.06
2C	1.25	1.38	1.22	1.30	1.32	1.32	1.32	1.39	1.31	1.40	1.32	0.06
1W	1.51	1.51	1.52	1.53	1.51	1.50	1.45	1.44	1.50	1.38	1.49	0.05

1C	1.36	1.32	1.25	1.29	1.29	1.29	1.33	1.32	1.27	1.34	1.31	0.03
0.5W	1.14	1.14	1.20	1.24	1.10	1.28	1.21	1.20	1.11	1.18	1.18	0.06
0.5C	0.95	0.99	0.89	0.92	0.95	0.96	0.88	0.97	1.02	0.94	0.95	0.04
R^2												
4W	0.9968	0.9980	0.9989	0.9982	0.9996	0.9978	0.9992	0.9992	0.9995	0.9985	0.9988	0.0007
4C	0.9986	0.9986	0.9955	0.9990	0.9976	0.9972	0.9987	0.9986	0.9988	0.9975	0.9979	0.0011
3W	0.9989	0.9993	0.9988	0.9986	0.9990	0.9991	0.9964	0.9987	0.9995	0.9992	0.9987	0.0009
3C	0.9975	0.9969	0.9983	0.9956	0.9979	0.9987	0.9967	0.9967	0.9981	0.9970	0.9973	0.0010
2W	0.9995	0.9994	0.9994	0.9962	0.9982	0.9992	0.9989	0.9995	0.9986	0.9981	0.9986	0.0010
2C	0.9960	0.9969	0.9974	0.9981	0.9973	0.9969	0.9976	0.9978	0.9981	0.9973	0.9975	0.0005
1W	0.9989	0.9992	0.9988	0.9987	0.9982	0.9987	0.9987	0.9991	0.9977	0.9994	0.9987	0.0005
1C	0.9977	0.9948	0.9973	0.9969	0.9961	0.9984	0.9959	0.9975	0.9966	0.9981	0.9969	0.0011
0.5W	0.9990	0.9992	0.9983	0.9987	0.9983	0.9990	0.9967	0.9977	0.9987	0.9992	0.9984	0.0008
0.5C	0.9976	0.9973	0.9959	0.9960	0.9980	0.9971	0.9985	0.9968	0.9948	0.9957	0.9967	0.0012
On-off sensor												
Gas delivered J_g =0.75 (cm/s), J_g (cm/s) measured at 78 (cm) depth and 292.15 (K)												
	1	**2**	**3**	**4**	**5**	**6**	**7**	**8**	**9**	**10**	**Avg**	**Stdev**
4W	0.60	0.57	0.58	0.59	0.59	0.58	0.58	0.57	0.58	0.61	0.59	0.01
4C	0.78	0.74	0.75	0.73	0.72	0.72	0.76	0.74	0.73	0.74	0.74	0.02
3W	0.62	0.61	0.60	0.58	0.62	0.63	0.61	0.60			0.61	0.02
3C	0.73	0.71	0.74	0.78	0.75	0.74	0.71	0.71	0.78	0.75	0.74	0.03
2W	0.61	0.59	0.60	0.58	0.59	0.58	0.62	0.65	0.61	0.61	0.60	0.02
2C	0.64	0.62	0.64	0.63	0.65	0.65	0.62	0.61	0.65	0.70	0.64	0.02
1W	0.51	0.53	0.49	0.48	0.46	0.50	0.52	0.49	0.50	0.50	0.50	0.02
1C	0.66	0.65	0.65	0.64	0.72	0.62	0.67	0.67	0.64	0.65	0.66	0.03
0.5W	0.40	0.47	0.41	0.44	0.44	0.41	0.40	0.45	0.43	0.42	0.43	0.02
0.5C	0.46	0.43	0.46	0.42	0.46	0.44	0.43	0.43	0.43	0.42	0.44	0.02
R^2												
4W	0.9982	0.9988	0.9994	0.9990	0.9995	0.9995	0.9994	0.9993	0.9992	0.9988	0.9991	0.0004
4C	0.9985	0.9981	0.9964	0.9990	0.9993	0.9990	0.9986	0.9990	0.9980	0.9986	0.9985	0.0008
3W	0.9988	0.9983	0.9988	0.9978	0.9971	0.9972	0.9974	0.9987	0.9988	0.9989	0.9982	0.0007
3C	0.9992	0.9989	0.9987	0.9992	0.9970	0.9986	0.9987	0.9982			0.9986	0.0007
2W	0.9988	0.9990	0.9993	0.9987	0.9990	0.9984	0.9986	0.9987	0.9990	0.9992	0.9989	0.0003
2C	0.9979	0.9977	0.9988	0.9988	0.9964	0.9985	0.9977	0.9980	0.9982	0.9977	0.9980	0.0007
1W	0.9977	0.9992	0.9981	0.9964	0.9984	0.9987	0.9982	0.9982	0.9971	0.9943	0.9976	0.0014
1C	0.9980	0.9990	0.9951	0.9987	0.9982	0.9971	0.9989	0.9982	0.9982	0.9978	0.9979	0.0011
0.5W	0.9990	0.9974	0.9986	0.9991	0.9985	0.9994	0.9988	0.9992	0.9982	0.9984	0.9987	0.0006
0.5C	0.9940	0.9980	0.9987	0.9984	0.9985	0.9980	0.9988	0.9984	0.9985	0.9983	0.9980	0.0014

Tube	**4**			**3**			**2**		
Technique And Location	**Avg (cm/s)**	**Stdev (cm/s)**	**points**	**Avg (cm/s)**	**Stdev (cm/s)**	**points**	**Avg (cm/s)**	**Stdev (cm/s)**	**points**
On-Off-HW	1.70	0.0522	10	1.65	0.0282	8	1.64	0.0508	10
Continuous-HW	1.67	0.0182	300	1.73	0.0311	501	1.88	0.0589	300
On-Off-HC	1.61	0.0346	10	1.62	0.0275	10	1.32	0.0515	10
Continuous-HC	1.62	0.0212	300	1.66	0.0276	300	1.53	0.0485	300
On-Off-LW	0.58	0.0123	10	0.61	0.0161	10	0.60	0.0192	10
Continuous-LW	0.62	0.0217	300	0.62	0.00953	509	0.77	0.0154	416
On-Off-LW	0.58	0.0123	10	0.61	0.0161	10	0.60	0.0192	10

Continuous-LW	0.62	0.0217	300	0.62	0.00953	509	0.77	0.0154	416

Continuous			
t-test, two tail, two samples	**Tube**	**3**	**2**
HW	**4**	no signif.	significative
HC	**4**	no signif.	significative
LW	**4**	no signif.	significative
LC	**4**	no signif.	significative
On-Off			
t-test, two tail, two samples	**Tube**	**3**	**2**
HW	**4**	no signif.	significative
HC	**4**	no signif.	significative
LW	**4**	no signif.	significative
LC	**4**	no signif.	significative

Table F.23: Mapping Northparkes.

	J_g Normal conditions (cm/s)							
Q	**1**		**2**		**3**		**4**	
(NCMS)	**Avg (cm/s)**	**Stdev (cm/s)**	**Avg (cm/s)**	**Stdev (cm/s)**	**Avg (cm/s)**	**Stdev (cm/s)**	**Avg (cm/s)**	**Stdev (cm/s)**
0.19	0.63	0.02	0.83	0.06	0.94	0.02	0.91	0.05
0.23	0.78	0.02	0.88	0.02	1.06	0.02	0.98	0.02
0.27	0.92	0.04	0.99	0.04	1.22	0.11	1.07	0.08
0.30	0.98	0.03	1.11	0.10	1.28	0.11	1.14	0.10
0.33	1.09	0.10	1.10	0.11	1.45	0.27	1.06	0.17
0.36	1.12	0.08	1.32	0.09	1.40	0.13	1.18	0.07
0.38	1.11	0.05	1.19	0.13	1.48	0.23	1.13	0.19

Table F.24: Rotation Northparkes.

CCW								
Level	**Slope (cm of Water/s)**				**R^2**			
	R1r	**R1l**	**R2r**	**R2l**	**R1r**	**R1l**	**R2r**	**R2l**
120 (mm)								
1	0.81	0.82	1.11	1.03	0.9959	0.9937	0.9963	0.9897
2	0.73	0.83	0.99	1.00	0.9959	0.9968	0.9954	0.9946
3	0.81	0.86	1.08	0.98	0.9965	0.9952	0.9862	0.9941
Average	0.78	0.84	1.06	1.00	0.9961	0.9952	0.9926	0.9928
Stdev	0.05	0.02	0.06	0.02	0.0003	0.0015	0.0056	0.0027
140 (mm)								
1	0.90	0.85	1.24	1.00	0.9933	0.9937	0.9951	0.9920
2	0.85	0.87	1.25	1.07	0.9926	0.9962	0.9987	0.9927
3	0.72	0.85	1.10	1.01	0.9927	0.9920	0.9955	0.9972
4	0.78	0.90	1.14	1.13	0.9969	0.9963	0.9977	0.9954
Average	0.81	0.87	1.18	1.05	0.9939	0.9946	0.9968	0.9944
Stdev	0.08	0.02	0.07	0.06	0.0020	0.0021	0.0017	0.0024
160 (mm)								

1	0.81	0.82	1.22	0.95	0.9958	0.9937	0.9977	0.9893
2	0.79	0.83	1.15	1.00	0.9958	0.9957	0.9977	0.9894
3	0.80	0.82	1.05	1.04	0.9957	0.9933	0.9871	0.9951
4	0.75	0.82	1.25	1.07	0.9955	0.9932	0.9973	0.9933
Average	0.79	0.82	1.17	1.01	0.9957	0.9940	0.9950	0.9918
Stdev	0.03	0.00	0.09	0.05	0.0001	0.0012	0.0052	0.0029
CW								
	Slope (cm of Water/s)				**R^2**			
	R1r	**R1l**	**R2r**	**R2l**	**R1r**	**R1l**	**R2r**	**R2l**
120 (mm)								
1	0.90	0.85	1.14	1.05	0.9943	0.9933	0.9960	0.9950
2	0.78	0.80	1.06	1.04	0.9963	0.9837	0.9978	0.9911
3	0.84	0.74	1.00	0.98	0.9967	0.9916	0.9975	0.9923
4		0.81	0.97	0.98		0.9880	0.9982	0.9886
5			1.20	1.07			0.9958	0.9932
Average	0.84	0.80	1.07	1.02	0.9958	0.9891	0.9971	0.9920
Stdev	0.06	0.06	0.07	0.04	0.0013	0.0051	0.0010	0.0020
140 (mm)								
1	0.81	0.77	1.09	0.95	0.9962	0.9932	0.9958	0.9932
2	0.82	0.78	1.06	1.04	0.9960	0.9906	0.9982	0.9908
3	0.80	0.78	1.01	1.05	0.9969	0.9915	0.9979	0.9904
4	0.87	0.72	1.00	1.01	0.9974	0.9929	0.9956	0.9945
5	0.93	0.83	1.06	1.08	0.9977	0.9893	0.9977	0.9900
6	0.89	0.79	0.99	1.00	0.9966	0.9934	0.9964	0.9894
Average	0.85	0.78	1.03	1.02	0.9968	0.9918	0.9969	0.9914
Stdev	0.05	0.04	0.04	0.05	0.0007	0.0016	0.0011	0.0020
160 (mm)								
1	0.87	0.86	1.07	1.20	0.9967	0.9910	0.9970	0.9890
2	0.92	0.80	1.06	0.94	0.9960	0.9938	0.9972	0.9876
3	0.84	0.82	0.98	0.98	0.9964	0.9886	0.9960	0.9932
Average	0.88	0.83	1.04	1.04	0.9964	0.9911	0.9967	0.9900
Stdev	0.04	0.03	0.05	0.14	0.0004	0.0026	0.0007	0.0029

J_g (cm/s)					
FP (cm/cm of Water)		1.01	1.01	1.01	1.01
Level (mm)		**1**	**2**	**3**	**4**
CCW	**120**	0.79	0.84	0.83	0.79
CCW	**140**	0.82	1.07	1.18	1.04
CCW	**160**	0.80	1.01	1.02	1.03
CW	**120**	0.85	0.88	0.81	0.83
CW	**140**	0.86	1.19	1.08	1.05
CW	**160**	0.89	1.06	1.03	1.05

Table F.25: LDI data.

H_l-H_p = 1.13 (m)								
T = 292.2 (K)								
Area = 0.005 (m^2)								
Calibration used		a				b		
Orifice (mm) 0.94		8.21E-04				9.24E-05		
Orifice (mm) 1.30		2.22E-03				-1.05E-04		
Cell	C2		C3				C4	
			Before		After			
	Avg	Stdev	Avg	Stdev	Avg	Stdev	Avg	Stdev
P (cm of Water)	42.39	2.44	115.49	2.49	37.43	1.78	39.50	2.26
P (kPa)	4.16	0.24	11.32	0.24	3.67	0.17	3.87	0.22
Orifice (mm)	1.30		1.30		1.30		0.94	
$J_{g\ STD}$ (cm/s)	1.62	0.36	2.70	0.36	1.52	0.30	0.62	0.18
J_g (cm/s) at 292.15 K 130 cm depth and 1000 (kg/m^3) Bulk density (estimated)	1.54	0.34	2.56	0.34	1.44	0.29	0.59	0.17

Table F.26: Northparkes data.

H_l-H_p = 1.00 (m)								
T = 292.15 (K)								
Area = 0.0081 (m^2)								
On-off								
Cell number	J_g (cm/s)							
	R1		R2		R3		R4	
1	1.04		1.27		0.99		1.21	
2	1.04		1.27		0.97		1.14	
3	0.97		1.22		1.05		1.23	
Average	1.02		1.25		1.00		1.19	
Stdev	0.04		0.03		0.04		0.05	
Continuous								
Rougher cell number	R1		R2		R3		R4	
	Avg (cm/s)	Stdev (cm/s)	Avg (cm/s)	Stdev (cm/s)	Avg (cm/s)	Stdev (cm/s)	Avg (cm/s)	Stdev (cm/s)
P (cm of Water)	18.54	1.45	26.54	2.03	18.46	1.31	30.46	2.18
P (kPa)	1.82	0.14	2.60	0.20	1.81	0.13	2.99	1.99
Orifice (mm)	1.60		1.60		1.60		1.60	
Calibration used is a=6.3729E-5 , b=0								
$J_{g\ STD}$ (cm/s)	1.06	0.30	1.27	0.35	1.06	0.28	1.36	1.11
J_g (cm/s) at 292.15 K, 61 (cm) depth and 1130 (kg/m^3) bulk density T=303.15 (K)	1.10	0.31	1.32	0.37	1.10	0.29	1.41	1.15

Table F.27: INCO data.

H_l-H_p 1.13(m)					
T 292.15 (K)					
Area 0.00456 (m^2)					
Cell number		C1		C2	
		Avg (cm/s)	Stdev (cm/s)	Avg (cm/s)	Stdev (cm/s)
Orifice (mm)		1.30		1.30	
$J_{g\ STD}$ (cm/s)	a	0.91	0.03	1.28	0.08
	b	1.06	0.04	1.03	0.05
	c	0.96	0.04	1.22	0.06
J_g corrected (cm/s) at 292.15 (K) 77.5 cm depth and 1000 (kg/m^3) bulk density. T=292.15 (K)	a	0.91	0.03	1.28	0.08
	b	1.05	0.04	1.02	0.05
	c	0.95	0.04	1.21	0.06

Table F.28: Matagami data.

H_l-H_p = 1.13 (m)								
T = 292.15 (K)								
Area = 4.56E-03 (m^2)								
As found profile								
Cell	C1		C3		C5		C7	
P Average (cm of Water)	10.94	0.46	6.28	0.54	7.35	0.78	11.46	0.59
P (kPa)	1.07	0.05	0.62	0.05	0.72	0.08	1.12	0.06
Orifice (mm)	1.30				1.30			
$J_{g\ Std}$ (cm/s)	0.82	0.02	0.45	0.04	0.61	0.04	0.82	0.02
J_g (cm/s) at 283.15 K 30 cm depth	0.82	0.02	0.45	0.04	0.61	0.04	0.82	0.02
Cell	C9		C11		C13		C15	
P Average (cm of Water)	6.81	0.59	8.58	0.77	7.58	0.44	8.31	0.55
P (kPa)	0.67	0.06	0.84	0.08	0.74	0.04	0.82	0.05
Orifice	1.30				0.94			

(mm)								
J_g Std (cm/s)	0.58	0.03	0.67	0.04	0.62	0.02	0.66	0.03
J_g (cm/s) at 283.15 K 30 cm depth	0.59	0.03	0.68	0.04	0.63	0.02	0.66	0.03

High J_g profile																
Cell	C1		C2		C3		C4		C5		C6		C7		C8	
P Average (cm of Water)	9.96	1.80	9.27	0.91	11.38	0.56	9.30	1.31	10.62	1.62	8.26	1.52	9.24	1.25	9.98	1.42
P (kPa)	0.98	0.18	0.91	0.09	1.12	0.06	0.91	0.13	1.04	0.16	0.81	0.15	0.91	0.12	0.98	0.14
Orifice	1.30								1.30							
J_g (cm/s)	0.71	0.02	0.67	0.02	0.75	0.03	0.72	0.03	0.71	0.05	0.71	0.10	0.68	0.05	0.70	0.05
J_g (cm/s) at 283.15 K 30 cm depth	0.72	0.02	0.67	0.02	0.75	0.03	0.73	0.03	0.71	0.05	0.71	0.11	0.68	0.06	0.70	0.05
Cell	C9		C10		C11		C12		C13		C14		C15		C16	
P Average (cm of Water)	10.08	1.81	10.79	1.71	9.46	1.09	9.68	1.51	11.19	0.90	10.79	1.26	9.89	0.75	10.28	1.35
P (kPa)	0.99	0.18	1.06	0.17	0.93	0.11	0.95	0.15	1.10	0.09	1.06	0.12	0.97	0.07	1.01	0.13
Orifice (mm)	1.30								1.30							
J_g (cm/s)	0.71	0.07	0.73	0.05	0.68	0.05	0.69	0.06	0.72	0.04	0.73	0.03	0.71	0.03	0.71	0.03
J_g (cm/s) at 283.15 K and 30 cm depth	0.72	0.07	0.73	0.06	0.69	0.05	0.70	0.06	0.73	0.04	0.73	0.03	0.72	0.03	0.72	0.03

Low J_g profile																
Cell	C1		C2		C3		C4		C5		C6		C7		C8	
P Average (cm of Water)	4.94	0.48	4.97	0.28	4.61	0.63	4.29	0.33	4.43	0.94	4.22	0.77	4.85	1.13	6.09	1.07

P (kPa)	*0.48*	*0.05*	*0.49*	*0.03*	*0.45*	*0.06*	*0.42*	*0.03*	*0.43*	*0.09*	*0.41*	*0.08*	*0.48*	*0.11*	*0.60*	*0.10*
Orifice (mm)	0.94		0.94		0.94		0.94		0.94		0.94		0.94		0.94	
J_g (cm/s)	0.39	0.05	0.41	0.05	0.38	0.05	0.39	0.03	0.36	0.07	0.40	0.06	0.41	0.08	0.50	0.07
J_g (cm/s) at 283.15 K 30 cm depth	0.39	0.05	0.41	0.05	0.38	0.05	0.39	0.03	0.36	0.07	0.40	0.06	0.41	0.08	0.50	0.07
Cell	**C9**		**C10**		**C11**		**C12**		**C13**		**C14**		**C15**		**C16**	
P Average (cm of Water)	4.42	1.29	4.71	0.96	4.99	0.92	4.56	1.17	4.57	1.32	4.25	0.79	6.07	0.79	4.37	0.86
P (kPa)	0.43	0.13	0.46	0.09	0.49	0.09	0.45	0.11	0.45	0.13	0.42	0.08	0.60	0.08	0.43	0.08
Orifice (mm)	0.94		0.94		0.94		0.94		0.94		0.94		0.94		0.94	
J_g (cm/s)	0.39	0.11	0.39	0.09	0.44	0.07	0.39	0.11	0.40	0.10	0.40	0.06	0.52	0.05	0.40	0.07
J_g (cm/s) at 283.15K 30 cm depth	*0.40*	*0.11*	*0.39*	*0.09*	*0.44*	*0.07*	*0.39*	*0.11*	*0.40*	*0.10*	*0.41*	*0.06*	*0.52*	*0.05*	*0.41*	*0.07*